ISSN 2221-7754

МІНІСТЕРСТВО ОСВІТИ І НАУКИ, МОЛОДІ ТА СПОРТУ УКРАЇНИ

ВІСНИК

ХАРКІВСЬКОГО НАЦІОНАЛЬНОГО УНІВЕРСИТЕТУ

імені В.Н. Каразіна

№ 1017

серія: фізична

«Ядра, частинки, поля»

Заснована у 1998 р.

Випуск **3** /55/

присвячується 50-річчю заснування фізико-технічного факультету Харківського національного університету

The Journal of Kharkiv National University

№ 1017

physical series

«Nuclei, Particles, Fields»

Issue **3** /55/

issue is dedicated to the 50th anniversary of the physical-technical department of Kharkiv national university

Харків

2012

DESCRIPTION AND PURPOSE OF THE JOURNAL

The Journal of Kharkov National University (Physical series "Nuclei, Particles, Fields") is a journal covering elementary particles physics, nuclear physics, plasma physics and technologies, solid state physics and radiation physics. The Journal publishes research articles, short communications, review articles and book reviews.
Issues per year – 4.

EDITORIAL BOARD

Editor-in-Chief - Zalubovsky I.I., Corresponding member of Ukrainian National Academy of Science, D.Sc., Professor
Deputy Chief Editor - Azarenkov N.A., Academician of Ukrainian National Academy of Science, D.Sc., Professor
Executive Secretary - Girnyk S.A., PhD

Adamenko I.N., D.Sc., Professor, Kharkiv national university named V.N. Karazin
Berezhnoy Yu.A., D.Sc., Professor, Kharkiv national university named V.N. Karazin
Bizyukov A.A., D.Sc., Professor, Kharkiv national university named V.N. Karazin
Budagov Yu.A., D.Sc., Laboratory of nuclear problems, Joint Institute of Nuclear Research, Dubna, Russia
Duplij S.A., D.Sc., Kharkiv national university named V.N. Karazin
Garkusha I.E., D.Sc., Professor, Director of Institute of Plasma Physics NSC "Kharkov Institute of Physics and Technology"
Girka I.A., D.Sc., Professor, Kharkiv national university named V.N. Karazin
Khodusov V.D., D.Sc., Professor, Kharkiv national university named V.N. Karazin
Kondratenko A.N., D.Sc., Professor, Kharkiv national university named V.N. Karazin
Lazurik V.T., D.Sc., Kharkiv national university V.N. Karazin
Merenkov M.P., D.Sc., NSC "Kharkov Institute of Physics and Technology"
Jean-Marie Noterdaeme, PhD., Professor, Max Planck Institute for Plasma Physics, Germany and Universiteit Gent, Belgium
Ostrikov K., D.Sc., Founding Leader, Plasma Nanoscience Centre Australia (PNCA), CEO Science Leader, CSIRO Materials Science and Engineering, Clayton, Australia
Peletminsky S.V., Academician of Ukrainian National Academy of Science, D.Sc., Professor, NSC "Kharkov Institute of Physics and Technology"
Slyusarenko Yu.V., Corresponding member of Ukrainian National Academy of Science, D.Sc., Professor, NSC "Kharkov Institute of Physics and Technology"
Smolyakov A., D.Sc., Professor, Department of Physics and Engineering Physics, University of Saskatchewan, Canada
Shul'ga N.F., Academician of Ukrainian National Academy of Science, D.Sc., Professor, NSC "Kharkov Institute of Physics and Technology"
Tkachenko V.I., D.Sc., Professor, Director "Renewable Energy Sources and Sustainable Technology" Science and Production Establishment, NSC "Kharkov Institute of Physics and Technology"
Tolok V.T., Corresponding member of Ukrainian National Academy of Science, D.Sc., Professor, NPTC, Ministry of Education and Science of Ukraine
Tovstiak V.V., D.Sc., Professor, Kharkiv national university named V.N. Karazin

Editorial office address
High Technology Institute
Kharkov National University named V.N. Karazin
Kurchatov av., 31, office 402, Kharkiv, 61108, Ukraine
Phone: +38-057-335-18-33
E-mail: visnyk@pht.univer.kharkov.ua
Web-page: http://www-nuclear.univer.kharkov.ua

ПРОФІЛЬ ЖУРНАЛУ ТА МЕТА ВИДАННЯ

"Вісник Харківського національного університету" (серія: фізична «Ядра, частинки, поля») є збірником наукових робіт з фізики елементарних частинок, ядерної фізики, фізики плазми та плазмових технологій, фізики твердого тіла та радіаційної фізики. Журнал публікує наукові статті, короткі повідомлення, оглядові статті та рецензії на книги.
Періодичність випуску збірника – 4 рази на рік.

Затверджено до друку рішенням Вченої ради Харківського національного університету імені В.Н. Каразіна (протокол № 9 від 28 вересня 2012 р.)

РЕДАКЦІЙНА КОЛЕГІЯ

Головний редактор – Залюбовський І.І. – чл.-кор. НАН України, д. ф.-м. наук, професор
Заступник головного редактора – Азарєнков М.О. – академік НАН України, д. ф.-м. наук, професор
Відповідальний секретар – Гірник С.А. – к. ф.-м. наук

Адаменко І.М. – д. ф.-м. наук, професор, ХНУ ім. В.Н. Каразіна
Бережной Ю.А. – д. ф.-м. наук, професор, ХНУ ім. В.Н. Каразіна
Бізюков О.А. – д. ф.-м. наук, професор, ХНУ ім. В.Н. Каразіна
Будагов Ю.А. – д. ф.-м. наук, професор, Лабораторія ядерних проблем ім. В.П. Джелєпова, ОІЯД м.Дубна, Росія
Дуплій С.А. – д. ф.-м. наук, член Американської і Европейської физичної спілки, член Ассоціації математичної фізики, ХНУ імені В.Н. Каразіна
Гаркуша І.Є. – д. ф.-м. наук, професор, директор Інституту фізики плазми ННЦ ХФТІ
Гірка І.О. – д. ф.-м. наук, професор, ХНУ ім. В.Н. Каразіна
Кондратенко А.М. – д. ф.-м. наук, професор, ХНУ ім. В.Н. Каразіна
Лазурик В.Т. – д. ф.-м. наук, професор, ХНУ ім. В.Н. Каразіна
Меренков М.П. – д. ф.-м. наук, ННЦ ХФТІ
Жан-Мари Нотердам – доктор, професор, Інститут фізики Макса-Планка Німеччина, Університет м. Гент, Бельгія
Остриков К. – д. ф.-м. наук, професор, Головний виконавчий директор та науковий співробітник Організації Співдружності з наукових і промислових досліджень (CSIRO), Клайтон, Австралія
Пелетмінський С.В. – акад. НАН України, д. ф.-м. наук, професор, ННЦ ХФТІ
Слюсаренко Ю.В. – чл.-кор. НАН України, д. ф.-м. наук, професор, ННЦ ХФТІ
Смоляков А. – д. ф.-м. наук, професор, факультет фізики та інженерної фізики, Саскачеванський університет, Канада
Ткаченко В.І. д. ф.-м. наук, професор, директор Науково-виробничого комплексу "Відновлювані джерела енергії та ресурсозберігаючі технології", ННЦ ХФТІ
Товстяк В.В. – д. ф.-м. наук, професор, ХНУ ім. В.Н. Каразіна
Толок В.Т. – чл.-кор. НАН України, д. ф.-м. наук, професор, НФТЦ МОН, НАНУ
Ходусов В.Д. – д. ф.-м. наук, професор, ХНУ ім. В.Н. Каразіна
Шульга М.Ф. – академік НАН України, д. ф.-м. наук, професор, ННЦ ХФТІ

Адреса редакції
Інститут високих технологій
Харківський національний університет імені В.Н. Каразіна
пр. Курчатова, 31, кімната 402, Харків, 61108 Україна
Телефон: +380-57-335-18-33
E-mail: visnyk@pht.univer.kharkov.ua
Web-сторінка: http://www-nuclear.univer.kharkov.ua

Усі статті прорецензовано.
Свідоцтво про державну реєстрацію КВ № 11825-696 ПР від 4.10.2006.

© Харківський національний університет імені В.Н. Каразіна, оформлення, 2012

CONTENTS

Reviews

N.A. Azarenkov, I.M. Neklyudov, V.N. Voyevodin
Reactor materials-modern status **4**

V.M. Kuklin
On new representations of well-known physical phenomena **19**

S.A. Duplij
Polyadic systems, representations and quantum groups **28**

Articles

Yu.M. Poluektov, V.N. Savchenko
On theory of spectrum of hydrogen-like atoms **60**

V.A. Rudakov
On physical parameters of the demonstration stellarator-reactor operating in the mode of self-supported thermonuclear reaction **66**

A.A. Zakharchenko
Determination of sensitivity of semiconductor detectors of gamma-radiation **75**

A.N. Dovbnya, V.V. Zakutin, N.G. Reshetnyak
Direct-action accelerator based on the magnetron gun with a secondary-emission cathode and its applications in radio-technologies **85**

V.T. Lazurik, V.M. Lazurik, G.F. Popov, Yu.V. Rogov, G.E. Sarukhanian
Integration of computational methods in spectrometry of electron beams **90**

V.A. Lisovskiy, V.A. Derevyanko, E.P. Artushenko, V.D. Yegorenkov
Stratification of the positive column of a DC discharge in nitrogen **95**

Z.F. Nazyrov, N.N. Zavgorodnya, R.V. Vovk, K.A. Kotvitskaya
Effect of high-pressure-induced structural relaxation on evolution of the temperature dependence pseudogap in $HoBa_2Cu_3O_{7-\delta}$ single crystals **102**

I.S. Guk, S.G. Kononenko, F.A. Peev, A.S. Tarasenko
The basic summaries of working out of recirculator SALO magnetooptical system **107**

N.A. Azarenkov, V.G. Rudychev, S.A. Pismenetskiy, Y.V. Rudychev, P.S. Badzym, S.I. Shapar, O.V. Vystavna
Solid and liquid waste processing and reducing of personnel doses **117**

V.G. Kirichenko, O.V. Kovalenko, T.A. Kovalenko, Yu.I. Gofman
Nuclear gamma-resonance observation in conditions of combined linear and transverse Doppler shifts and features of relativistic theory **123**

B.V. Borts, S.F. Skoromnaya, V.I. Tkachenko
Formation of associates from nanosized complexes of uranium in the water - supercritical carbon dioxide system **128**

Yu.A. Kirochkin, A.Yu. Kirochkin
Once again about advantages of the new method of electromagnetic isotopes separation **135**

A.V. Karpukhin, I.N. Kudryavtsev, A.V. Borisov, D.I. Gritsiv
High-speed communication networks chaotic behavior analysis of data systems **138**

I. Marushchenko, N.A. Azarenkov
On efficiency of collisional energy exchange of electrons and ions in relativistic plasmas **146**

ЗМІСТ

Огляди

Н.А. Азаренков, І.М. Неклюдов, В.Н. Воеводін
Матеріали для реакторів-сучасний статус **4**

В.М. Куклін
Про нові описи добре відомих фізичних явищ **19**

С.А. Дуплій
Поліадичні системи, представлення і квантові групи **28**

Статті

Ю.М. Полуектов, В.М. Савченко
До теорії спектра водньоподібних атомів **60**

В.А. Рудаков
Про фізичні параметри демонстраційного реактора-стеларатора, який діє в режимі термоядерної реакції із самопідтриманням **66**

О.О. Захарченко
Визначення чутливості напівпровідникових детекторів гамма-випромінювання **75**

А.М. Довбня, В.В. Закутін, М.Г. Решетняк
Прискорювач прямої дії на основі магнетронної гармати з вторинноеміссійним катодом та його застосування в радіаційних технологіях **85**

В.Т. Лазурик, В.М. Лазурик, Г.Ф. Попов, Ю.В. Рогов, Г.Е. Саруханян
Інтегрування обчислювальних методів у спектрометрію електронних пучків **90**

В.О. Лісовський, В.О. Дерев'янко, К.П. Артюшенко, В.Д. Єгоренков
Стратифікация позитивного стовпа розряду постійного струму в азоті **95**

З.Ф. Назиров, Н.М. Завгородня, Р.В. Вовк, К.А. Котвицька
Вплив індукованої високим тиском структурної релаксації на еволюцію температурної залежності псевдощілини монокристалів $HoBa_2Cu_3O_{7-\delta}$ **102**

І.С. Гук, С.Г. Кононенко, Ф.А. Пеєв, О.С. Тарасенко
Основні підсумки розробки магнітооптичної системи рециркулятора SALO **107**

М.А. Азаренков, В.Г. Рудичев, С.А. Письменецкий, Е.В. Рудичев, П.С. Бадзим, С.І. Шапарь, О.В. Виставна
Переробка твердих і рідких відходів та зменшення доз персоналу **117**

В.Г. Кіріченко, О.В. Коваленко, Т.О. Коваленко, Ю.Й. Гофман
Особливості спостереження ядерного гамма-резонансу обертових об'єктів та розширена теорія відносності **123**

Б.В. Борц, С.Ф. Скоромна, В.І. Ткаченко
Утворення ассоциатів із нанорозмірних комплексів урану в системі вода - надкритичний діоксид вуглецю **128**

Ю.О. Кірочкін, О.Ю. Кірочкін
Ще раз про переваги нового метода електромагнітного розділення ізотопів **135**

О.В. Карпухін, І.М. Кудрявцев, О.В. Борисов, Д.І. Гриців
Вивчення хаотичної поведінки високошвидкісних мереж зв'язку інформаційних систем **138**

І.М. Марущенко, М.О. Азарєнков
Про ефективність обміну енергією при зіткненнях електронів та іонів у релятивістській плазмі **146**

UDC 621.039:531

REACTOR MATERIALS-MODERN STATUS

N.A. Azarenkov*, I.M. Neklyudov, V.N. Voyevodin****
**Kharkiv National University of V.N.Karazin*
4, sq. Svobody, Kharkov, 61022, Ukraine
***National Science Center "Kharkov Institute of Physics and technology"*
1, Akademicheskaya str., 61108, Kharkov, Ukraine
E-mail: voyev@kipt.kharkov.ua
Received 19 August 2012, accepted 14 September 2012

This paper presents short description of modern status of reactor materials for nuclear. The fast growing energy demand and concerns about climate changes require nuclear energy to play a role among other energy sources to satisfy future energy needs of mankind. Exactly core materials behaviour provides safe and economy exploitation of nuclear power plants. Metals and alloys used in nuclear service serve in very challenging environments involving high temperatures and stresses, as well as exposure to high irradiation doses. Problems of radiation resistance of materials for exploitation reactors and reactors of next generation are described.
KEY WORDS: nuclear energetic, radiation resistant materials, radiation defects, impurities, reactors on thermal neutrons, fast reactors.

МАТЕРИАЛЫ ДЛЯ РЕАКТОРОВ – СОВРЕМЕННЫЙ СТАТУС
Н.А. Азаренков*, И.М. Неклюдов, В.Н. Воеводин**
**Харьковский национальный университет имени В.Н. Каразина*
Украина, 61022, г. Харьков, пл. Свободы 4
***Национальный Научный Центр «Харьковский Физико-технический институт»*
Украина , 61108, Харьков, ул. Академическая 1
Данная статья представляет краткое описание современного состояния реакторных материалов для ядерной энергетики. Быстро растущий спрос на энергию и озабоченности по поводу изменения климата требуют от ядерной энергетики играть важную роль среди других источников энергии для удовлетворения будущих потребностей всего человечества в энергии. Именно основное поведение материалов обеспечивает безопасную и экономичную эксплуатацию атомных электростанций. Металлы и сплавы, используемые в ядерной отрасли, работают в очень сложных условиях при наличии высоких температур и напряжений, а также воздействии высоких доз облучений. В данной статье также описаны проблемы радиационной стойкости материалов при эксплуатации реакторов в наше время, а также реакторов следующего поколения.
КЛЮЧЕВЫЕ СЛОВА: ядерная энергетика, радиационно-стойкие материалы, радиационные дефекты, примеси, реакторы на тепловых нейтронах, реакторы на быстрых нейтронах.

МАТЕРІАЛИ ДЛЯ РЕАКТОРІВ-СУЧАСНИЙ СТАТУС
Н.А. Азаренков *, І.М. Неклюдов, В.Н. Воеводін **
** Харківський національний університет імені В.Н.Каразіна,*
Україна, 61022, м. Харків, пл. Свободи 4
*** Національний Науковий Центр "Харківський Фізико-технічний інститут»,*
Україна, 61108, Харків, вул. Академічна 1
Дана стаття являє короткий опис сучасного стану реакторних матеріалів для ядерної енергетики. Швидко зростаючий попит на енергію і заклопотаність з приводу зміни клімату вимагають від ядерної енергетики відігравати важливу роль серед інших джерел енергії для задоволення майбутніх потреб всього людства в енергії. Саме основна поведінка матеріалів забезпечує безпечну і економічну експлуатацію атомних електростанцій. Метали і сплави, які використовуються в ядерній галузі, працюють в дуже складних умовах при наявності високих температур і напружень, а також впливі високих доз опромінень. У даній статті також описані проблеми радіаційної стійкості матеріалів реакторів, що експлуатуються в наш час, а також реакторів наступного покоління.
КЛЮЧОВІ СЛОВА: ядерна енергетика, радіаційно-стійкі матеріали, радіаційні дефекти, домішки, реактори на теплових нейтронах, реактори на швидких нейтронах.

Today's nuclear power is the more real in the world that possesses the humanity for the production and supply of low cost electrical and thermal power for distant prospective with guarantee of nuclear, physical, ecological and technical safety in amounts corresponding with society needs.

Three factors emphasize on the nuclear power – exhausting of hydrocarbon resources, environmental contamination, necessity to control the power safety [1].

According to the data of IAEA more than 500 nuclear power units of research and other reactors are now in operation. In spite of Fukushima accident nuclear energetic at the world is developing stable and consequently.

It is just the behavior of structural materials of operated and developed reactors that determines the safe and economical operation of nuclear power stations.

Materials of operating and designed fission reactors may be divided on three groups:

- fuel materials – nuclear fuel: uranium, plutonium, thorium and their alloys.

© AzarenkovN.A. , NeklyudovI.M. , VoyevodinV.N. , 2012

- structural materials – ferritic-perlitic and ferritic-martensitic steels (pressure vessels of water-water reactors), bainite steels (wrappers and claddings of fuel elements (FE) for fast reactors, pressure vessel internals of water-water reactors, first wall of fusion reactors); ferritic-martensitic steels (wrappers of FU for fast reactors, first wall of fusion reactors); ferritic ODS steels – low-activated steels for fusion reactors and reactors of next generation, zirconium alloys-materials for claddings and channels of thermal reactors (materials of control systems (CR)) – materials absorbing neutrons B, Cd, Hf absorb thermal neutrons, B, Ta, Eu absorb fast neutrons.

The importance of structural materials consists not only in the guarantee of stability of the core geometry for overall operational time and, first of all, stability of fuel assemblies and of fuel elements, but also in the retention of fission products, in the maintenance of serviceability of control systems and in the guarantee of minimal consequences of possible accidents, that is, in the solution of the key problems of reactor plants safety.

Reaching of high burn-up of fuel is limited by radiation resistance of materials for wrappers and ducts of fuel assemblies and the term of operation of reactors on thermal neutrons is limited by the service life of pressure vessel and pressure vessel internal materials.

Unfortunately, structural materials have more potential restrictions for reaching of high levels of radiation damage and impede the reaching of high burn-up of nuclear fuel [2].

Development of structural materials of operating and of developed nuclear plants is extremely complicated science-technical problem. Under the influence of fast particles and radiation complex structure-phase transformations occur in crystalline bodies that cause considerable variation and, unfortunately, degradation of their initial physical-mechanical characteristics [3]. Radiation resistance is determined by the microstructural composition and by structure state of irradiated material. Expediency of the use of the materials in nuclear power plants of definite type depends on special features of NPP, on used coolant, on energy spectrum of neutrons and so on.

The aim of this work is the study and understanding of the properties of materials used in nuclear power and the prospects for improvement in the growing nuclear industry, which is designed to provide humanity soon enough cheap, environmentally friendly and safe energy.

MATERIALS OF REACTORS ON THERMAL NEUTRONS

Now thermal-neutron reactors, pressurized water reactors or boiling reactors serve as the basis of the world nuclear power (WWER- 440. 1000. PWR, BWR). WWER-type reactors are manufactured by Russian plants, PWR,BWR- in foreign countries. The main components of thermal reactors that are subjected to the intensive radiation exposure are the pressure vessels, fuel elements claddings, pressure vessels internals.

The structural materials employed in current power plants both in the pressure vessel and in the core materials, are conventional materials, low allow steels in the case of the pressure vessel (clad internally with stainless steel) and austenitic stainless steels and nickel-base alloys in the case of internal structures.

PRESSURE VESSEL MATERIALS

Materials of pressure vessels must guarantee the safe operation during the whole service life. Typically ferritic-perlitic (Russia) and ferritic-bainitic steels (USA, France, Japan) are used for the fabrication of pressure vessels.

WWER-440 - 15Cr2MoA (C-0.11-0.21; Si-0.17-0.37; Mn-0.3-0.6; S-0.012-0.018; P-0.009-0.0038; Cr-2.5-3.0; Cu-0.09-0.17; Ni-0.19-0.27; Mo-0.6-0.8; V-0.25-0.35);

WWER-1000 – 15Cr2NiMoPA, 15Cr2NiMoPAA (C-0.13-0.18; Si-1; Mn-1; S<0.035; P<0.01; Cr-1.8-2.3; Ni-1.0-1.5; Mo-0.5-0.7; V-1.1-0.12);

PWR, BWR – A533-B (C<0.25; Si-0,15-0.30; Mn-0.15-1.50; S-0,4); P-0.035; Ni-0.40-0.70; Mo-0.45-0.60.

Given in Table 1 data of the operational conditions of thermal neutron reactor show that rather low fluences and rather low operational temperatures are the characteristic properties of pressure vessel material operation for the reactor of such type.

Table 1.

Reactors on thermal neutrons: WWER, PWR, BWR (power 440-1200 Mw)

Mean density of thermal neutron flux in core	$2.7\text{-}4.4.10^{-13}$ n/cm^2 sec
Mean density of fast neutrons in core	$1.9\text{-}4.0.10^{14}$
The rate of dose setting-up	10^{-7}dpa/s
Temperature of coolant (pressure vessel)	On inlet 285-290^{0}C On outlet 320-325^{0}C
Density of fast neutron flux on pressure vessel	1.10^{17}n/cm^{2}sec
Fluence of fast neutrons (E_n>0.1 MeV) on pressure vessel during 40 years of operation	$\Phi t=5.10^{19}-1.10^{20}$n/cm^2
Rate of damaging rate (steel)	10^{-10}dpa/sec
Dose of radiation damage of pressure during 40 years	0.1 dpa

The initial microstructure of these materials is one of the parameters that will influence their behavior under irradiation. Ferritic, tempered martensitic or bainitic microstructures are usually found in RPV steels containing different types of precipitates with size ranging from 10 nm to micrometer.

Exposure to high energy neutron coming from the fission of fuel, together with the overall nuclear reactor core

environment (e.g. gamma radiation, neutrons, radiolysis of water), affects significantly the physical and mechanical properties of these materials, resulting in ageing degradation effects during the life of the NPP that could result in early failure of these structural components if not detected or mitigated. Such events or necessary replacements are potentially expensive, impacting not only safety, but also economic viability of nuclear power plants [4].

Typically the wall of the RPV is exposed to high energy (e.g.>0.1 MeV) neutron irradiation, which results in localized embrittlement of the steel and welds in the area of the reactor core (i.e. the RPV core beltline region).

Obviously that such radiation-induced degradation of mechanical properties of pressure vessel steels during operation is the result of microstructure changes of nanostructure scale (nm). Evolution of microstructure under neutron irradiation at temperature of operation of pressure vessel (270- 300^{o}C) depends not only on the migration of point defects formed by irradiation, on their interaction and clustering but also on complex interaction with impurities.

Three main mechanisms responsible for the change of microstructure of pressure vessel steels under irradiation are now considered [4]:

1) Direct damage in the matrix due to the formation of radiation-induced clusters and dislocation loops. . It was detected that matrix damaging evolves with irradiation dose, the rate of dose set up and with irradiation temperature; this damage gives the resulting hardening proportional to the square root of accumulated dose [5].

2) Radiation-accelerated formation during matrix damage of matrix-coherent nano-precipitates and this also causes matrix hardening and embrittlement. Elements of solid solution of pressure vessel steels have the trend to radiation-accelerated clustering and formation of precipitates with nanosize (2-3 nm). These precipitates mainly enriched by copper and called copper-rich precipitates.

It must be noted that chemical composition of these precipitates remains uncertain, different elements are present in these precipitates (Fe, Mn, Ni and possibly Si and P). Even insignificant variation in steel composition and in neutron spectrum causes the significant differences in morphology and concentration of precipitates [6]. In steels of reactor WWER-1000 precipitates are radiation-stimulated and in steels of reactor WWER-440 they are radiation-induced [6].

3) Radiation induced segregation (RIS) on grain boundaries and interphase boundaries of embrittling elements such as phosphorus, sulphur, arsenic, also in combination with matrix damage or attracted into the Cu-rich precipitates

Now the question about relationship of contributions into the radiation embrittlement of different mechanisms demands the further investigation under higher irradiation doses.

Investigation of Ni role in the processes of embrittlement is of special interest because due to the technological causes in pressure vessels of nuclear reactor operating in Ukraine the content of nickel exceeds 1.5 % weight. The deleterious effect of nickel on temper brittleness of steel Cr-Ni-Mo-V was known a long time ago and the existing experimental data on nickel contribution to the radiation embrittlement of reactor steels are limited

Thus, most of these mechanisms are classified as “hardening” ones (matrix damage, copper-rich precipitates, partially also segregations when they are inside grains), but P segregation on grain boundaries is classified as “non-hardening” (non-hardening embrittlement, since not detectable with conventional hardness tests). The last type of embrittlement can manifest itself as intergranular (grain boundary) fracture, rather than the usual transgranular cleavage fracture. Thus, their effect on radiation hardening and embrittlement can be quite different (Fig.1).

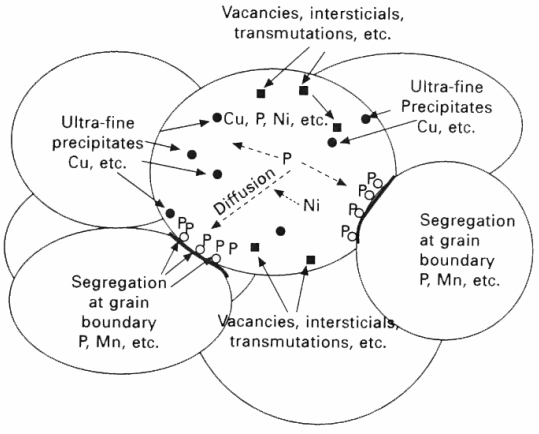


Fig. 1. Schematic embrittlement processes for RPV materials

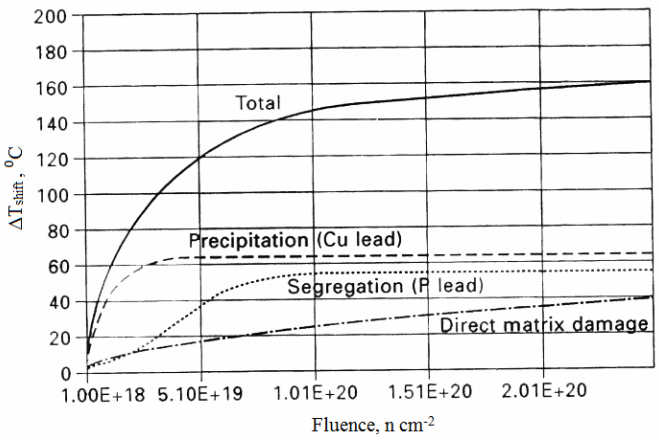


Fig. 2. Schematic diagram showing the effect of three damage mechanisms on irradiation embrittlement of RPV steel

Sum radiation embritterment curve (change of the temperature of brittle-ductile transition) is presented on Fig.2.

In high –nickel (Ni) RPV steels (with Ni content more than approx.1.2 mass %-it is typically for few Ukrainian and Russian units) another damage mechanism can be observed as previously predicted based on thermodynamic considerations and modeling. This “late blooming effect” can cause an additional increase in yield stress and higher transition temperature shifts at larger neutron fluences, where a saturation trend usually takes place (Fig.3).

Key issues are the combined effects of irradiation temperature, content of Ni, Mn and Cu and neutron flux/fluence

$6 \cdot 10^{23} m^{-2}$ which are larger than end-of-life fluences for 40 years of PWR operation.

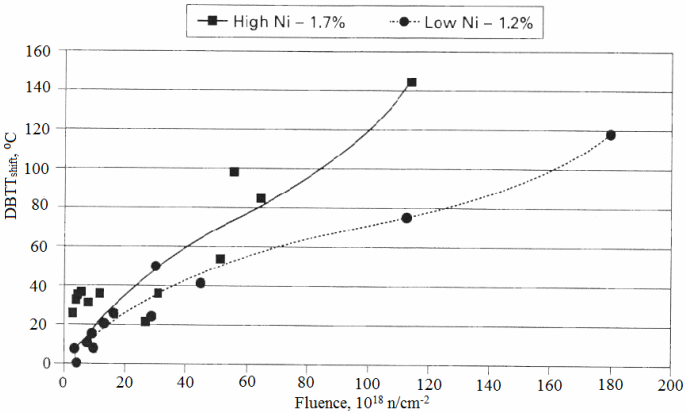


Fig. 3. Late blooming effect in high-nickel WWER-1000 weld metals

An analysis and generalization of great number of the admixtures given about influence on a radiation embrittlement allowed to pull out a requirement about limitation of maintenance of phosphorus and copper accordingly to 0.006 and 0.06% accordingly, and also reduction of total maintenance of antimony, of tin and arsenic(<0.015%).It is assumed that additional alloying by a nickel in an amount 0.6-0.8 % and adjustment of maintenance of chrome(<3%) will provide stability of descriptions became and will allow will get a possible resource no less than 60 with a possible extension 80-100 to [7].

ZIRCONIUM- BASE ALLOYS

Zirconium alloys are of special importance for nuclear power as material of fuel cladding for water-cooled reactors due to unique low cross section of neutron capture (0.18-0.19 barn) and high radiation and corrosion resistance. These elements are subjected to the considerably higher radiation load in comparison with materials of pressure vessels. The main problems revealed under zirconium alloys operation are radiation growth and related phenomenon of radiation creep caused by the anisotropic nature of α-zirconium.

Zirconium alloys (domestic: E110. E125, E635 and foreign Zry-2, Zry-4, M5, ZIRLO) (Table 2) used now in reactors WWER, RBMK, PWR, DWR differ considerably by radiation growth, radiation creep, corrosion resistance, high-temperature strength, hydrogenation and other characteristics that guarantee reliability of articles.

Despite the high number of studied round the world zirconium alloys, including that containing niobium, it is recognized that only five alloys are well studied and prepared for operation in reactors PWR and WWER , namely American Zircaloy-4 and Zirlo, Russian E110 and E635 and French M5 (Table 2 [8]).

The characteristic feature of zirconium alloys of Russian production that are used in nuclear reactors of Ukraine is the presence of niobium. Niobium is the main alloying element for binary and for multi components alloys. Base zirconium alloys of foreign production (Zircaloy-2 and Zircaloy-4 are alloyed by tin, iron, chromium and nickel. Different chemical composition of alloys strongly influence on their radiation and corrosion behaviour.

Alloy E110 is based on the system Zr-Nb where niobium is completely soluble in high-temperature phase of zirconium and is poorly soluble in low-temperature phase (to 1% [8]). Increase of this alloys strength is related with the presence of heterogeneous structure consisted of α-solid solution with inclusions of dispersed particles of β_{Nb}.

This alloy is used in recrystallized state, its ductility reaches 40% but is highly dependent on oxygen content.

Table 2.

Chemical composition of zirconium alloys used in modern reactor

Alloys	Chemical composition, **%**								
	Nb	**Sn**	**Fe**	**Cr**	**Ni**	**C**	**O**	**N**	**S**
E110	0.9-1.1	-	-	-	-	$\leq 2 \cdot 10^{-2}$	$\leq 10^{-1}$	$\leq 6 \cdot 10^{-3}$	-
E110M	0.9-1.1	-	0.1	-	-	$\leq 2 \cdot 10^{-2}$	0.12		
E125	2.5	-	-	-	-	$\leq 2 \cdot 10^{-2}$	$\leq 10^{-1}$	$\leq 6 \cdot 10^{-3}$	
Zircaloy -2	-	1.2-1.7	0.07-0.2	0.05-0.1	0.03-0.08	$\leq 2.7 \cdot 10^{-2}$	-	$\leq 8 \cdot 10^{-3}$	-
Zircaloy -4	-	1.2-1.7	0.18-0.24	0.07-0.13	-	$\leq 2.7 \cdot 10^{-2}$	-	$\leq 8 \cdot 10^{-3}$	-
E635	0.9-1.1	1.0-1.5	0.3-0.5	-	-	$\leq 2 \cdot 10^{-2}$	$\leq 10^{-2}$	$\leq 6 \cdot 10^{-3}$	-
Zirlo	0.9-1.1	0.9-1.1	0.09-0.11	-	-	$\leq 2.7 \cdot 10^{-2}$	-	-	-
M5	0.8-1.2	-	0.015-0.06	-	-	0.0025-0.012	0.09-0.18	-	≤0.0035

Typically irradiation behaviour of Zr-base alloys is determined by behaviour of structural elements- mainly dislocation in Zr-1%Nb alloy, precipitates in Zr-2.5Nb alloy, dislocation components and aged solid solution-in alloy E635. In conditions of reactor irradiation under the doses higher than 15dpa formation of dislocation loops of the type <c>[0001] is observed in the microstructure of alloy E110. This correlates with the start of the stage of accelerated radiation growth.

It is shown that alloying of Zr-1%Nb with oxygen to concentration 0.19% leads to the suppression of dislocation loops <c> production and, consequently, to the shift of the start of accelerated radiation growth to higher irradiation doses (Fig.4) [9].

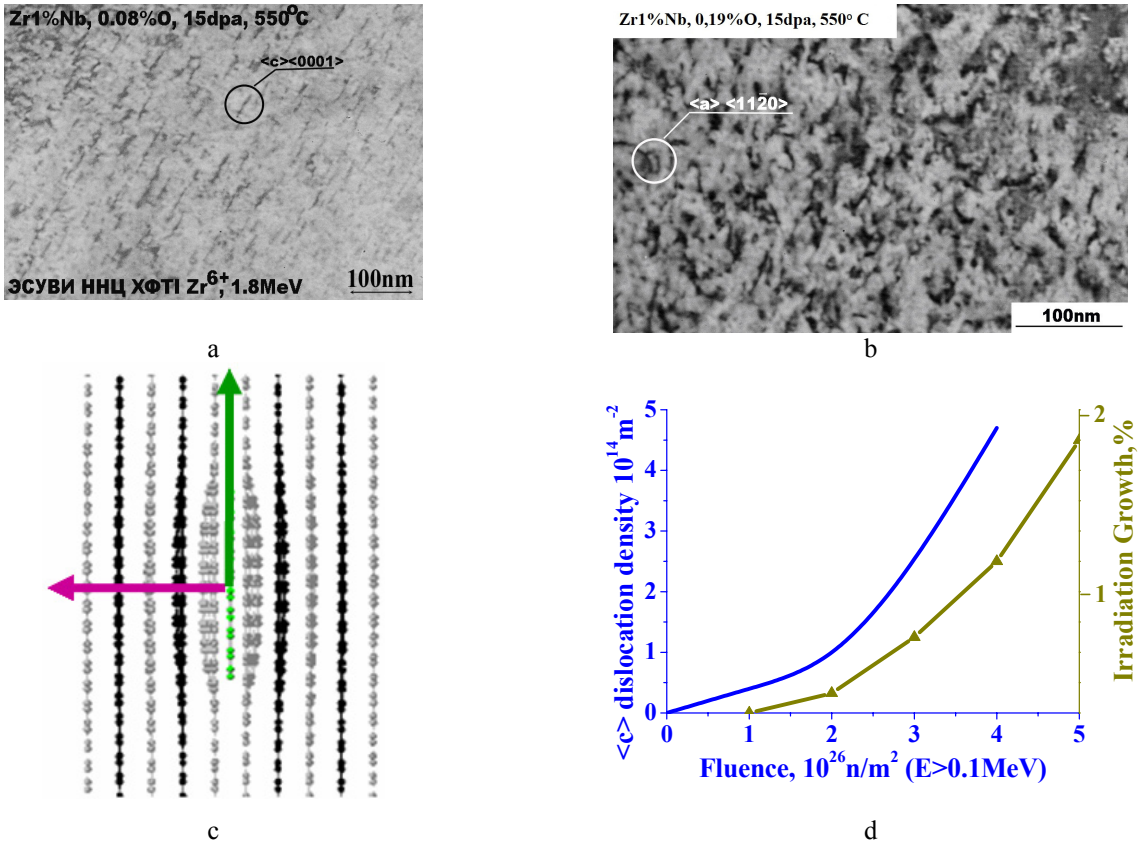


Fig.4. Oxygen influence on <c> components dislocation nucleation in Zr-1%Nb alloy.
a, b-microstructure of alloys; c- scheme of radiation growth in Zr; d- the dislocation density versus fluence.

Alloy E110M (Zr, 1% Nb, 0.1% Fe, 0.12% O) is produced on the base of alloy E110 by alloying with increased content of iron and oxygen (0.1 Fe%, 0.12 O %). This modified alloy demonstrates higher resistance to creep and lower radiation growth (Fig.5).

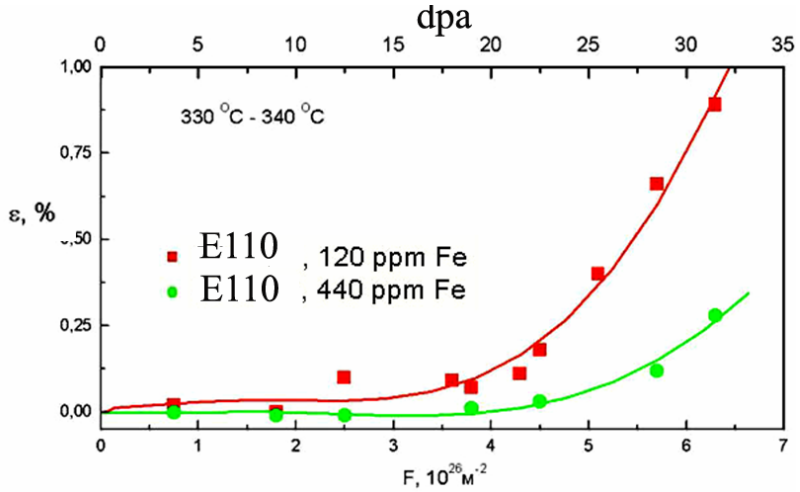
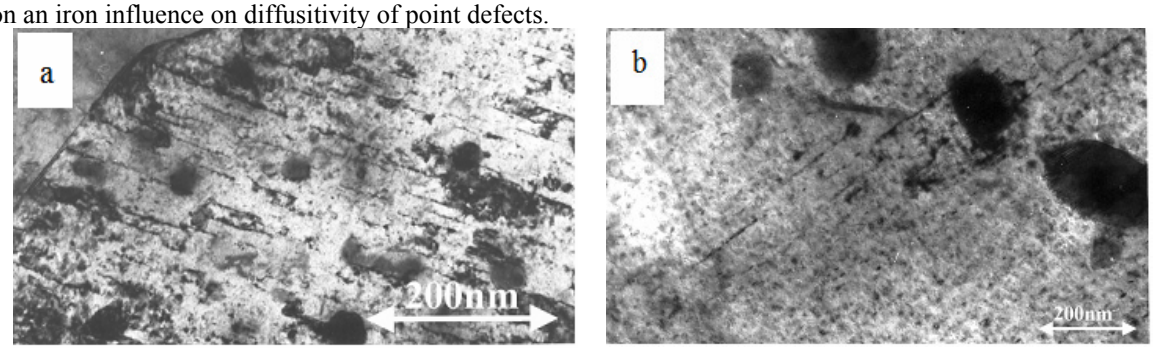


Fig. 5. Radiation growth versus chemical composition E110 alloy

Alloy E125 is specially developed for channel tubes, casings and elements of fuel assembly hangers for reactors RBMK, also for Candu-type reactor. The main requirement for material of channel tubes is the minimal rate of diameter creep (not more 1-1.5·10^{-5} %/hour). The high creep resistance and resistance to radiation growth of this alloy is attained due to the presence in its microstructure of high density of precipitates of β-Nb (6·$10^{20}$$m^{-3}$)

From the point of view of microstructure, the resistance to the radiation growth may be explained by the special features of dislocation structure evolution under irradiation (Fig.6, 7, 8). In alloy E635 with very high resistance to the radiation growth the high concentration of radiation-induced dislocation loops of <c> type responsible for the processes of radiation growth may be formed only under very high irradiation doses (>50 dpa) that are practically unreachable in commercial reactors. This singularity of alloy E635 evolution may be explained by the role of α-solid solution enriched

by iron an iron influence on diffusitivity of point defects.



a b

Fig. 6. c-component dislocation microstructure of alloys
a-E-110, b-E-635

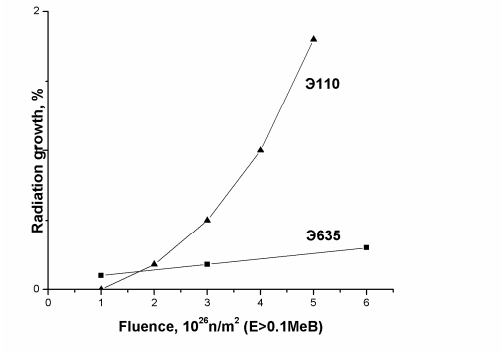


Fig. 7. Plots of the dependence of radiation growth on fluence of neutrons (E<0.1 MeV)

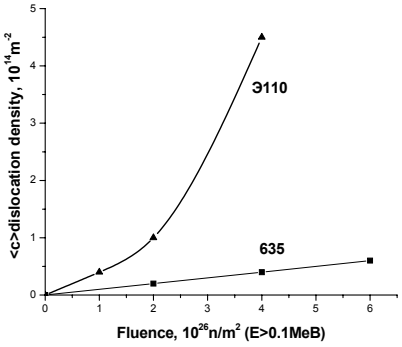


Fig. 8. Density of dislocation loops of c-type on fluence of neutrons (E<0.1 MeV)

MATERIALS OF PRESSURE VESSEL INTERNAL (PVI)

A new important challenge for radiation material science is now the substantiation of radiation resistance of materials of pressure vessel internal (PVI) for reactors PWR and WWER. These structures play an important role as they support the reactor core, they channel the water flow inside the vessel and they support and guide the instrumentation necessary for controlling and monitoring the reactor PVI were designed as not replaceable element of construction with the operation delay equal to the service life of the reactor pressure vessels [10]. Currently, the first commercial WWER units are approaching their design lifetime of 30 years. Consideration is now being given to life extension for another 10 to 30 years. Life extension requires that an assessment be made of the potential behavior of PVI materials under long-term irradiation.

Characteristic property of PVI elements and, first of all of the baffle, produced for Russian reactors of steel Cr08Ni18Ti10 and for reactors of type PWR and BWR, where baffle is manufactured from steel AISI 321, is that during operation they accumulate quite high fluence of neutrons and have the temperature level caused by the absorption of γ-quanta and of neutrons; the considerable volume changes of the material of PVI may occur at such temperature level due to the vacancy swelling under irradiation (Fig.9). This problem is potentially more dangerous for reactors WWER-100 the baffle of which has more complicated shape and is thicker than in reactors PWR. This causes the local increase of temperature up to 460^{o}C and leads to the void formation even without temperature shift. Early the possibility of such radiation swelling in this temperature range was rejected. Recently it became known that this phenomenon may proceed in light-water thermal reactors.

In American, French, Japanese and Russian works voids were detected in PVI of reactors of PWR type (Fig.10) [11, 12].

In the 1990s and 2000s, it was realized that the dpa rate is important, if not more important, than the irradiation temperature in determining the duration of the incubation or transient regime of swelling of austenitic stainless steels [14-16]. Based on experimental data from EBR-II over a wide range of dpa rates a bilinear swelling equation was developed for annealed AISI 304 stainless steel that explicitly incorporated the dpa rate, as well as the total dpa and temperature as variables that determine the development of swelling [16]. The effect of dpa rate on swelling was very pronounced, with the transient regime of swelling reduced very strongly as the dpa rate increased. Despite the fact that a great number of experimental results on radiation effects in 18Cr10NiTi steels is currently available obtained in different reactor and accelerator conditions as well as for different constructional materials, there are still no rated or conventional dependencies of swelling versus the dose, temperature and displacement rate. Approximating function describing 18Cr10NiTi steel swelling over a wide range of dose rates was obtained in [17]. The empirical dependence

of 18Cr10NiTi steel swelling against the dose, irradiation temperature and dose rate reads:

$$S = (0.25 - 0.022 \ln k) \cdot \varphi(D - 103 + 0.1T - 2.6 \ln k) \cdot \exp\left\{ - \frac{(T - 690 - 15.5 \ln k)^2}{2 \cdot (12.3 - 1.9 \ln k)^2} \right\}, \quad (1)$$

where S is swelling in %, D is the damaging dose in dpa; T is the irradiation temperature in °C; k is the dose rate in dpa/s; $\varphi(x) = x \cdot \theta(x)$ and $\theta(x)$ are Heaviside unit step functions; $\theta(x) = 1, \quad x > 0$ or $0, \quad x \le 0$.

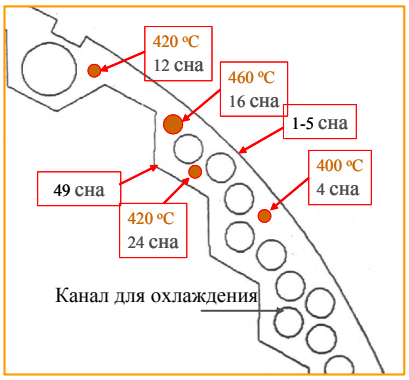


Fig. 9. Temperature-dose field in section with maximum of neutron flux on height [13].

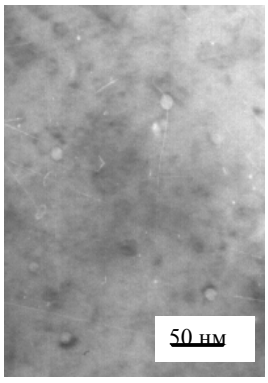


Fig. 10.Voids observed in pressure vessel internal of reactor WWER-1000 (steel 06Cr18Ni10Ti) RNPS –3 [13].

Fig. 11 presents dose-temperature maps of 18Cr10NiTi steel swelling calculated with function (1) with different dose rates typical both for irradiation on an accelerator (k = 10^{-3} dpa/sec) and for fast neutron (k = 10^{-6} dpa/sec) and thermal neutron (k = 10^{-8} dpa/sec) reactors.

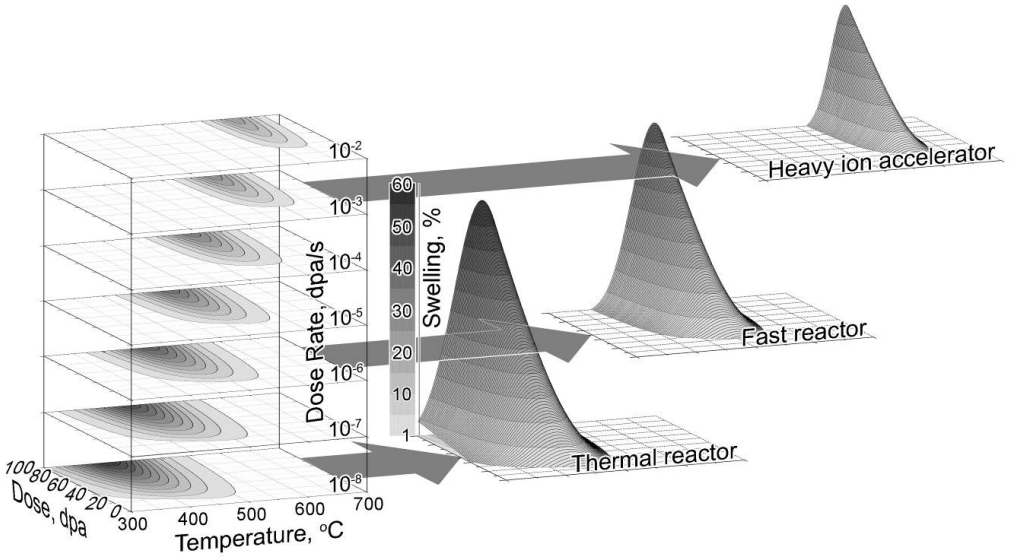


Fig.11. Temperature-dose maps of 18Cr10NiTi steel swelling for different dose rates calculated with modeling function equations (1)

The present results demonstrate that with due attention for dose rate scaling the basic physical processes involved in the swelling phenomenon occur under both heavy-ion and fast reactor irradiation conditions in a very general manner.

Employing simulation by heavy-ion irradiation it has been demonstrated that with a decrease in dose rate toward levels characteristic of WWERs the temperature regime of swelling for 18Cr10NiTi steel will get broader and show a shift of the swelling peak toward lower temperatures. Increased swelling at lower dpa rates develops primarily from a decrease in the incubation period of swelling and an apparent increase in the post-transient swelling rate. Increases in irradiation temperature were also found to decrease the post-transient swelling rate. These results agree with the results of other neutron irradiation studies on this steel and other austenitic steels.

On the basis of the developed empirical equation relatively large levels of swelling are anticipated to occur in the WWER baffle ring, especially at dose levels to be reached following plant life extension. Such information is crucial in making decisions concerning extended operation of WWERs, with or without replacement of the internals.

The main task for the solution of the problem of low-temperature swelling is the study of the operational conditions (rate dose, temperature, doses, environment, synergetic effect of gaseous impurities, stresses, material

composition, its initial condition and others).

In nuclear power installations besides creation of radiation defects at co-operating of neutrons with the atoms of materials of PVI of reactors it takes place to formation of foreign atoms from the nuclear reactions of transmutation. The special value of nuclear reactions of transmutation consists in the generation of gas transmutation- helium and hydrogen. In the intercase devices of thermal reactors of type of VVER work of helium and hydrogen for 30 of exploitation of reactor exceeds 1000 and 2000 appm accordingly [18,19]. Such high concentrations of gases can change character of the structural-phase converting into materials. In this connection research of speed of work of gases is a necessity as an additional parameter. Such researches are now conducted in National Science Center "Kharkov Institute of Physics and technology".

MATERIALS FOR REACTORS OF NEXT GENERATION

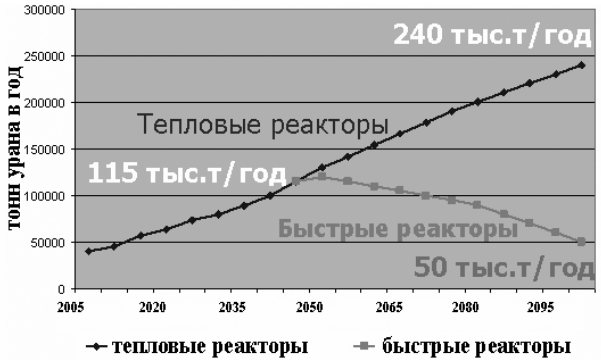


Fig.12. Forecast of the world needs in uranium up to 2100 year [21]

Generation III light water reactors (LWRs) are anticipated to be built in large numbers to replace exist in nuclear power plants or to augment the nuclear production capacity. Beyond the commercialization of best available light water reactor technologies , it is essential to start now the development of break through technologies that will be needed to prepare the longer term future for nuclear power. Fast neutron reactors (sodium , gas or lead cooled) with a closed fuel cycle which afford making an efficient use of uranium resource (more than 80% instead of 1% at most by light water reactors which essentially consume 235U) and minimizing long-lived radioactive waste, thus making nuclear energy more sustainable[20].

Development of large-scale nuclear power is not possible without the use of fast-neutron reactors guaranteeing the nuclear fuel breeding and using in nuclear power cycle of all produced nature uranium and consequently – of thorium (Fig.12).

High temperatures and irradiation doses in reactors fast neutrons (Table 3) lead to the situation that the problem of structural material production for claddings of fuel elements became the key one; such material must have the complex of mechanical and technological properties, compatibility with coolant and fuel material and also stability of properties under irradiation.

Table 3.

Parameters of fast-neutron reactors

Density of neutron flux	3.10^{15}-10^{16}n/cm^{2}sec
Rate of He generation	20-30 appm/year
Rate of dose setting	10-50 dpa/year (Totally 150-200 dpa)
Temperature	400-600^{o}C

These challenging requirements imply that in most cases, the use of conventional nuclear materials is excluded, even after optimization and a new range of materials has to be developed and qualified for nuclear use. Stainless steels of different classes with different alloying and after different thermo-mechanical treatments are more reliable materials as clads and wrappers of such type reactors.

AUSTENITIC STAINLESS STEELS

The most investigated and have technological attractive for the core of fast reactors, are austenitic stainless steels. Austenitic steel shows excellent corrosion resistance, overall mechanical property, but poor irradiation resistance.

These steels were developed intensively in different countries (Table 4).

Radiation swelling up to now is the major problem for using this type of structural materials [22].

Phenomena of swelling in multi component ASS is the result of complex structure-phase transformations during irradiation therefore the achievement of necessary level of resistance of austenitic steels to swelling may be obtained only on the base of understanding of all phenomena involved in the processes of radiation swelling.

In authors opinion the achievement of minimum level of swelling is related with the increase of stability of all structural components (dislocation structure, solid solution, systems of secondary phases precipitates) under irradiation.

Radiation resistance of ASS may be improved at the expense of introduction of insignificant quantities of alloying elements and subsequent thermal-mechanical treatment [23]. Component and impurity composition of steels influencing on energy of stacking fault and energy characteristics of point defects may modify the evolution of dislocation structure during irradiation.

It must be noted that the local variation of composition induced by radiation induced segregation (RIS), leads to the decay of solid solution and forms the precipitates of two types:

► precipitates suppressing the swelling at the expense of accelerated recombination of point defects on interface particle-matrix. These are carbides of type MC (principally TiC, NbC, VC), phosphides Fe_2P or Ni_3Ti (Fig. 13 a, b);

►precipitates produced in the result of solid solution decay (especially due to the segregation of Ni and Si) are the sign of radiation resistance loss on last stages of evolution of structure - M_6C and G-phase (Fig.13 c).

Table 4.

Chemical composition of austenitic steels used in core of nuclear reactors

Steel	Ni	Cr	Mo	C	Ti	Nb	Si	V	P	S	Mn	Others
AISI 316 USA	10.00-14.00	16.0 18.0	2.0-3.0	≤0.08	-	-	≤1,0	-	-	-	≤2,0	B 0.0002
D9 USA	14.0-16.0	14.0	1.4-2.3	-	0.2-0.35	-	0.8-1.0	-	-	-	1.8-2.3	-
PNC316 Japan	13.8	16.5	2.5	-	0.098	0.07	0.93	-	0.031	-	1.78	B 0.0044
15/15Ti, France	14.5-15.0	14.5-15.0	1.3-1.5	-	0.45-0.5	-	0.5	-	0.007	-	1.4-1.6	B 0.0065
FV-548,Great Britain	16.0-17.0	11.5-12.0	1.1-1.2	1.4-1.5	0.9-1.0	-	0.3-0.4	-	-	-		
09Cr16Ni15Mo3B(EI-847), Russia	14.0-16.0	15.0-17.0	2.5-3.0	≤0.09	-	0.8-0.9	≤0.8	-	-	-	≤0.8	-
15Cr15Ni2Mo2GTP (ChS-68) Russia	14,0-15.5	15.5-17.0	1.9-2.5	0.06-0.08	0.2-0.5	-	0.3-0.6	0.1-0.3	0.014	0.004	1.1-2.0	B≤0.005
EK-99 Ukraine	15.0-16.0	15.0-16.0	2.0-2.5	-	0.2-0.4	-	0.2-0.4	-	0.010	-	0.9-1.3	B≤0.005

*base-iron

Key processes leading to instability of fine MC or Fe_2P particles appears to be segregation mechanisms on precipitates surface. After irradiation at a higher dose, precipitates which have a coherent interface or interfaces with low degree of incoherence are observed in the steels. The higher stability of coherent precipitates can be connected with absence of defect sites on coherent interface and minimization of segregation [20]. The change in phase composition with the dose increasing is explained by the infiltration of Ni and Si into MX phases through the incoherence stage of evolution and MX→G-phase transition, where (in G-phase) interstitial elements are dissolved.

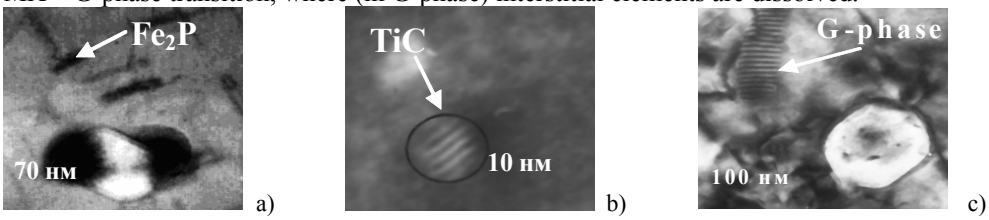


Fig.13. Precipitates of second phases in irradiated ASS
a) phosphydes Fe_2P; b) carbides TiC; c) G-phase $(Ti, V, Nb, Mn)_6(Ni, Co)_{16}Si_7$).

Deceleration of formation G-phase and η-carbides and containing such elements P, Ni and Si, influence on the initiation of voids and its growth.

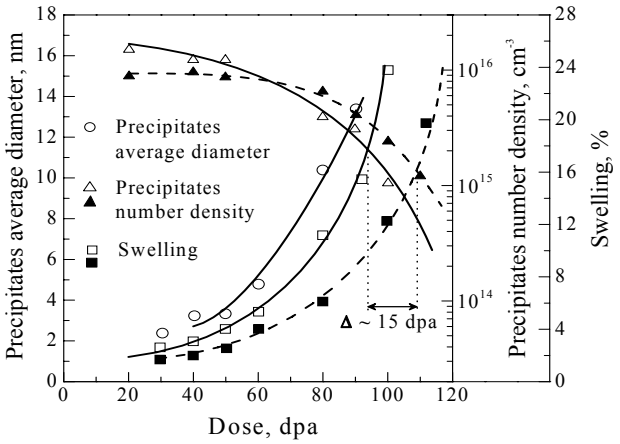


Fig.14. Typical relationship between MC precipitates evolution and swelling in 16Cr15Ni3MoNb (Δ, □) and 16Cr15Ni3MoNbB (▲, ■) steels (Cr^{3+}, E=3 MeV, T_{irr}=650^{0}C)

The principal effect of cold working in these steels is a shift the MC precipitation curve to lower doses and to displace the G-phase curve to higher doses. Cold work provides a higher density of nucleation sites for MC precipitates, beside it, the segregation solute will be distributed between much higher density sinks than in the solution annealed case.

The onset of the regime of swelling at a high rate appeared to be associated with the dissolution of fine titanium - rich MC type precipitates with dose increasing. It's significant that the moment of changing in precipitate form coincides with the beginning of steady state swelling (Fig.14).

Evolution of defected structure is the result of "competition" between the evolution of phases preventing the swelling, and phases produced in the result of decay of solid solution. This "competition" may be extended by the selection of optimal composition and by the thermal-mechanical treatment (Fig.15). Unfortunately, the role of precipitates as the main mechanism suppressing the swelling depends on the matrix surrounding and may vary during irradiation. The alloying elements included into precipitates change the nature of precipitates and modified precipitates interact with

point defects in different way under irradiation. Interaction of matrix and precipitates throughout the flows of point defects makes the processes of evolution of microstructure complex and creates some contradictions for understanding of the influence of alloying elements or the role of precipitates.

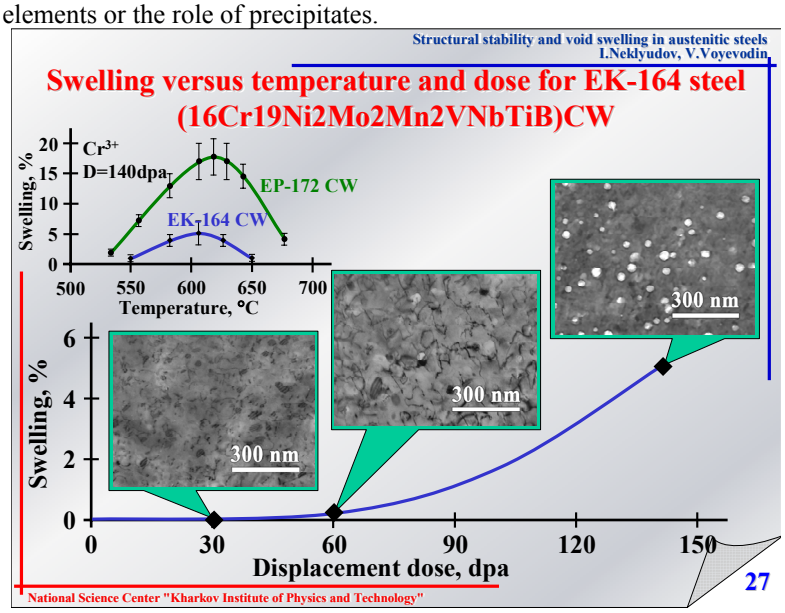


Fig.15. Swelling versus temperature and dose

The obtained results show:

- The maintenance of desirable swelling is directly coupled with maintaining a more stable microstructure during neutron exposure. Alloying influence together with treatment consists in:
- Formation of more stable dislocation structure (mainly existence of slow mobile Frank loops number density) up to higher doses. It can be achieved due to cold work or segregation processes on dislocation components, which restrict dislocation mobility;
- Save small precipitates of carbides and phosphides (prolong their life), which serve as dominant swelling suppressor in these steels, from dissolution - shift dose interval of formation for G-phases and η-carbides to region of higher doses;
- Retarding of G-phase and η-carbides formation will keep in solid solution sufficient quantities of such elements as Ni, Si and P, which mainly influence on void nucleation and growth;
- Typically for all analyzed steels stability of fine precipitates is necessary condition for preventing of high swelling.

FERRITIC-MARTENSITIC STEELS

Ferritic-martensitic steels are now the more attractive materials-candidates for claddings and wrappers of nuclear reactors and for the first wall of fusion reactors due to their low induced activity, low void swelling and creep, high resistance to high-temperature and helium embrittlement.

There are different international programs of development of reactors of 4 generation and of fusion reactors. These programs are based on the use of ferritic-martensitic steels that will operate in the wide range of temperatures under damaging doses of 200 dpa and higher and also of high levels of gases production (of helium and hydrogen) [24-26].

American company “TerraPower” develops a new concept of fast reactor named Traveling Wave reactor (TWR). This reactor concept uses the principle “produce and burn up”; this concept was proposed by Russian scientist Feinberg in 1958. Such reactor may produce more energy than thermal reactor. Depleted uranium or natural uranium may be used as fuel material for this reactor.

The designed burn-up in such reactor will be 20 and possibly 30%. (Let us note that Russian nuclear power poses the task of reaching the fuel burn-up of 20% in fast reactors).

Under such level of burn-up the damaging doses will be 400…500 dpa. In view of this it is necessary to select the structural materials for claddings and wrappers of fuel assemblies and investigations of materials-candidates under super-high irradiation doses are needed.

It is supposed to use ferritic-martensitic steels for claddings in reactor TWR; it is known that these steels have the lower swelling under high doses of irradiation.

The investigation of swelling of industrial ferritic-martensitic steels EP-450 (of Russian production) under irradiation by chromium ions up to the doses of 300 dpa is presented on Fig. 16. Irradiation by heavy ions is used for investigation of radiation resistance of this material. This simulation method is used in KIPT for a long time and gives many useful results during the study of mechanisms of radiation damage and selection of prospective reactor materials [26]. And now this is the only method round the world for reaching the super-high irradiation doses.

Mixing the alloy additives promote the formation of precipitates in ferritic martensitic steels. It has some properties, which important for developing stable micro structure.

F/M STEELS PRECIPITATES BEHAVIOUR

The Cr behaviour in irradiated ferritic steels affects mainly the evolution of the second phase precipitates. It was showed [27] that during irradiation 9% and 12% Cr steels to have formation of a few kinds of second-phase precipitates:

- M_6X and $M_{23}C_6$ precipitates are distributed mainly at grain boundaries and did not change their composition during irradiation.
- α′-phase precipitates are predominantly Cr (up to 85–90%), are ≤10 nm in size, and are uniformly distributed through both ferrite and tempered martensite. Most of the precipitates are coherent. Irradiation of lower Cr-content steels (9% to 10% Cr) can also reduce the amount of Cr sufficiently to cause the formation of the ′α-phase.
- M_2X precipitates exist in 13% as well in 9% Cr steels. They can have a needle-shaped form (in EP-450 steel) and are finely dispersed (in 9Cr-1Mo-NbVB steel).
- New phase - the formation of Si-enrichment precipitates with stoichiometric compositions $(Cr,Fe)_9Nb_3Si_8$, as well as the enrichment of Cr_2N and M_6X precipitates with silicon and vanadium, can serve as proof that segregation processes occur in irradiated ferritic steels.
- Typical for Laves phases $Fe_2(Mo,Nb)$ in 10Cr6MoNbV steel it was founded the phase transformation to $\chi(Fe_{36}Cr_{12}Mo_{10})$ phase according with suggested model of phase transformations.

Table 5.

Chemical composition of some 9-12% chromium steels [28]

Steel mark/ country	C	Si	Mn	Cr	Ni	Mo	V	W	Nb	B	Other elem
EM12 Belgium/France	0.08-0.12	0.30-0.50	0.90-1.20	9.0-10.0		1.9-2.1	0.25-0.35	0.35-0.45			
F82H Japan	0.10	0.20	0.50	8.0			0.20	2.0		0.003	Ta-0.04 N-less 0.01
JLF-1 Japan	0.1	0.05		8.0			0.2	1.95			Ti-0.002 Ta-0.09 N-0.023
EUROFER, Europe	0.10.-0.12	0.05	0.4-0.6	8.0-9.0			0.20-0.30	1.0-1.2		0.004-0.006	Ta-0.06-0.10; n-0.02-0.04
FV448, England	0.10	0.46	0.86	10.7	0.65	0.60	0.14		0.26		N-0.05
EP-450. Russia	0.10-0.15	0.60	0.60	11.0-13.5	0.05-0.30	1.2-1.4	0.10-0.30		0.30-0.60	0.004	
EP-823, Russia	0.10-0.18	1.15-1.3	0.5-0.8	11.3	0.5-0.85	0.6-0.82	0.32	0.5-0.8	0.26-0.4	0.006	Ti 0.004

The main attention is paid to the analysis of swelling in ferritic-martensitic steels. The Fig. 15 illustrated dose dependence of swelling for the most investigated ferritic martensitic steel EP-450 (13Cr2MoNbVB). As it is seen from this Figure the dose dependence of swelling of duplex steel EP-450 have took the traditional form characteristic for all metals and alloys, namely, the presence of incubation period, transient stages with increasing rate of swelling and steady state stages of swelling The high increase of swelling rate in steel EP-450 is related with the high increase of void size (Fig. 16). The mean size of voids under the dose ≥200 dpa makes more than 50 nm and some voids reach the size more than 100 nm and contribute substantially to swelling.

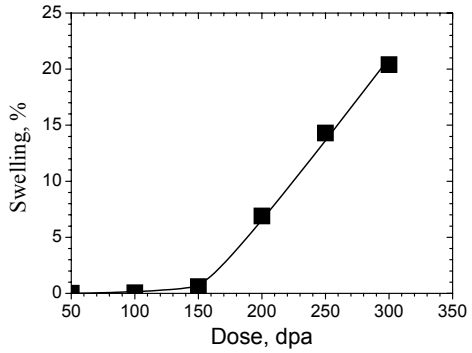


Fig.16. Dose dependence of swelling of steels EP-450 (T=480°C)

During the steady state stage the rate of swelling of steel EP-450 makes 0.14%/dpa. Due to the comparatively high rate the swelling of ferritic steel under the dose 300 dpa reaches~20%. Such swelling of ferritic steel is unexpected because ferritic steels were considered as material with low swelling [26].

DISPERSION-HARDENED STEELS

Many studies are directed toward the development of innovative metallic materials for applications in the nuclear industry [29, 30], fulfilling the design requirements for fission or fusion nuclear reactors. Among these are oxide dispersion strengthened (ODS) alloy materials [31] obtained by powder metallurgy [32]

which are of interest as structural materials due to their creep rupture strength at high temperature [33] and their resistance to severe neutron exposure. This high temperature creep strength [34] comes from the presence within the matrix of nanometric size oxide populations, blocking the motion of dislocations and thus making it possible to consider nominal operating temperatures over 1000 C for some ODS materials (Fig.17).

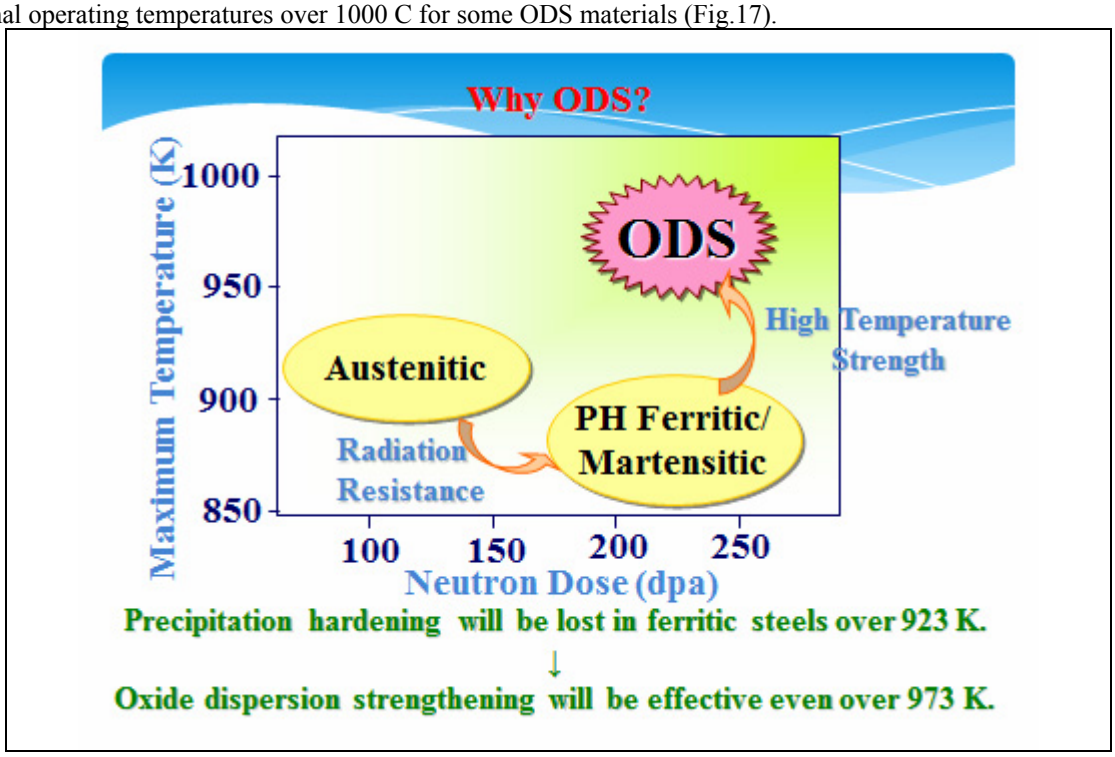


Fig. 17. The preference of dispersion hardened steels

Dispersion hardened ferritic steels(which contain 9-12Cr%) are now ones of the more prospective materials for FA clad of fast reactors and first wall of fusion reactors (FR) and also as structural material of reactors of next generation (See Fig.18).

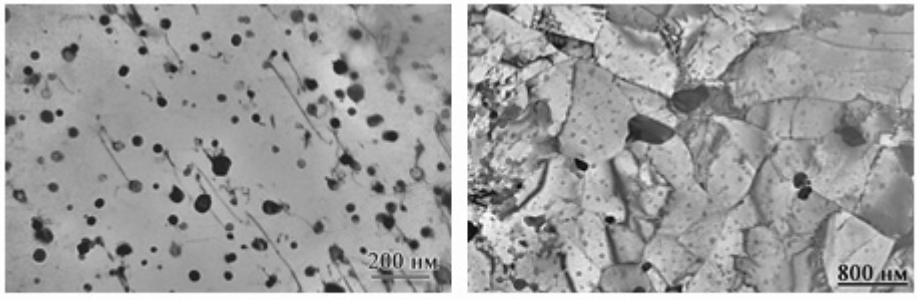


Fig. 18. Initial structure of dispersion hardened ferritic steels

The required increase of high-temperature strength is attained by the proper dispersion hardening of fine particles of titanium (TiO_2) and/or yttrium (Y_2O_3). The unique combination of fine grains, of high density of dislocations and nanoclusters containing atoms of solution Y-O and Y-O-Ti supposes the production of materials with unique properties [35-36].

The more important factor influencing on the properties of dispersion hardened steels is the provision of the deformation dissolution in steel matrix of sufficiently “coarse” oxides of yttrium with dimension 40-100 nm and their subsequent precipitation as effectively hardening nanooxides.

The necessity of the investigation of material properties under such severe operational conditions is caused by the last observations that make doubtful the serviceability of ferritic-martensitic steels for their use at high temperatures and high rates of gases generation [24]. Therefore it is necessary to analyze the evolution of microstructure and modification of composition for better understanding not only the nature of low swelling but also the cause of the embrittlement.

The features of these ODS-steel will be nanosize particles introduction of that to the initial matrix gives all material the improvement of his properties. It is such excretions as: Y_2O_3, TiO, $Y_4Al_2O_9$, $YAlO_3$, $Y_3Al_5O_{12}$, $Y_2Si_2O_7$, Al_2O_3, $Y_2Ti_2O_7$, FeY, Y_2TiO_5, $Y_2Ti_2O_7$, that have different composition, different methods of receipt, but have one goal

- increase of descriptions of different types of ODS-steel, that can become construction materials of the future before long. Although irradiation data are scarce, the bcc crystalline structure should present an excellent resistance to swelling.

The necessity of the investigation of material properties under such severe operational conditions is caused by the last observations that make doubtful the serviceability of ferritic-martensitic steels for their use at high temperatures and high rates of gases generation. Therefore it is necessary to analyze the evolution of microstructure and modification of composition for better understanding not only the nature of low swelling but also the cause of the embrittlement. The road map of development of materials for fast breeder reactors is shown on picture (Fig.19).

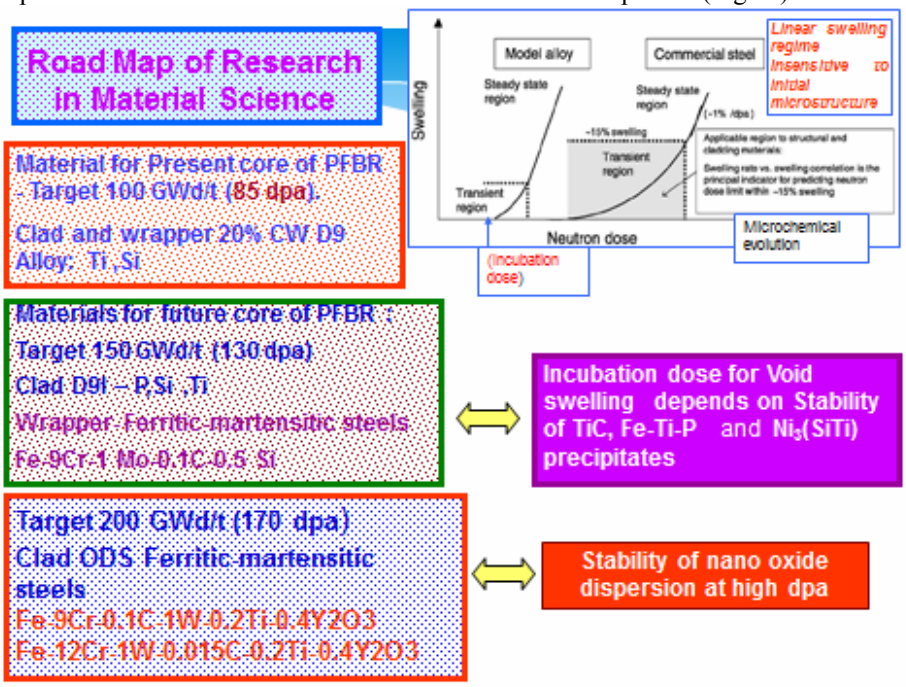


Fig. 19. The road map of development of materials for fast breeder reactors

The main in-service issues, in the low temperature range, remain the effect of the a/a' unmixing on the mechanical properties and, in the high operating temperature domain, the required stability of the oxide dispersion to maintain the improved creep resistance of this type of material and the absence of heavy intermetallic phase precipitation that could degrade the toughness the cladding. Preliminary results under mixed and fast neutron spectrum show that a/a' demixing should allow this type of materials to keep reasonable ductility and fracture toughness. The under irradiation stability of the oxide dispersion is an open issue to be settled. The required increase of high-temperature strength is attained by the proper dispersion hardening of fine particles of titanium (TiO_2) and/or yttrium (Y_2O_3). The unique combination of fine grains, of high density of dislocations and nanoclusters containing atoms of solution Y-O and Y-O-Ti supposes the production of materials with unique properties.

The more important factor influencing on the properties of dispersion hardened steels is the provision of the deformation dissolution in steel matrix of sufficiently “coarse” oxides of yttrium with dimension 40-100 nm and their subsequent precipitation as effectively hardening monoxides.

CONCLUSION

In spite of considerable efforts of researchers in all countries developing the nuclear power the economically necessary levels of operation of existing nuclear reactors are not reached so far.

It is determined in considerable degree by the insufficient radiation resistance of the main structural materials of existing nuclear facilities – of zirconium base alloys and different classes of stainless steels.

Challenges of the 21 Century for radiation material science are the guaranteeing of the problems of security and economy of nuclear power plants.

The main of them are:

1. Substantiation of overhaul period prolongation for operating thermal reactors, that is, study of the influence of the dose, of rate dose, of processes of segregation, special features of material (composition, thermal treatment, structure) on microstructure evolution in structural materials during operational period of reactor.
2. Development of radiation-resistant materials for reactors of new generations. Study of the influence on the material physical – mechanical properties of the dose rate, of stresses, of segregation processes (fast reactors); influence of the dose, of gas concentration (He, H), of gaseous and solid transmutants (fusion reactors, electronuclear systems (“spallation”).

The presented aims may be realized only on the base of modern understanding of the role of microstructural processes responsible for the evolution of structural state under irradiation and for degradation of initial physical-mechanical properties.

REFERENCES

1. Rosumkov O. Ukrainian center of economic and political studies //National security and defense.-2006.-№6.-P.3.
2. Garner F.A. Irradiation Performance of Cladding and Structural Steels in the Liquid Metal Reactors, in Material Science and Technology // Nuclear Materials.-1994.-10A.-P.12-14.
3. Voyevodin V.N., Neklyudov I.M. Evolution of the structure phase state and radiation resistance of structural materials.-Kiev:Naukova Dumka,2006.-354 s.
4. Brumovsky M. Irradiation hardening and materials emrittlement in light water reactor (LWR) environments // Nuclear Research Institute.-2010.-Vyp.3.-P.357-373.
5. Eyre B.L., Maher D.M., Perrin R.C. Embrittlement in steels // Metal Phys.-1999.-№77.-P.371.
6. Kuleshova E.A., Gurovich B.A., Shtrombakh Ya.I. Comparision of microstructural features of radiation embrittlement of VVER-440 and VVER-1000 reactor pressure vessel steels // JNM.-2002.-Vyp 300.-P.127-140.
7. Морозов А.М., Филимонов Г.Н., Цуканов В.В. Основные принципы легирования сталей для корпусов атомных реакторов типа ВВЭР // Вопросы материаловедения.-2006.-№1(45).-P.103-111.
8. Solonin M.I., Reshetnikov F.G., Nikulina A.V. New Construction Materials for Active Zone in Nuclear Power Plants // Nuclear Materials.-2004.-Vol.25.-P.12-14.
9. Borodin O.V., Bryk V.V., Vasilenko R.L., Voyevodin V.N. Petelguzov I.A. Rybalchenko N.D. Influence of oxygen content on evolution of the structure of alloy Zr1%Nb under ion irradiation // Problem of atomic science and technology.-2008.-№2.-P. 53-61.
10. Neustroyev V.S., Golovanov V.N., Shamardin D.K., Ostrovskiy Z.Ye., Pecherin A.M. Radiation effects in X18H10T steel irradiated in different reactors under conditions close to operation conditions of WWER PVI // Proceedings of VI Russian conference on reactor materials science.-2000.-Vol.3.-Part 1.-P.3-23.
11. Miller M.K. Understanding and mitigating ageing in nuclear power plants // Materials and operational aspects of plant life management (PLiM).-2010.-Vol.3.-P.914.
12. Neustroev V.S., Dvoretsky V.G., Ostrovsky Z.E., Shamardin V.K., Shimansky G.A. Studies into the Microstructure and Mechanical Properties of 18Cr10NiTi Steel after Irradiation in the WWER-1000 Core // Problems of Atomic Science and Technology.-2003.-№3(83).-P.73-78.
13. Garner F.A. Void swelling of austenitic internal components of PWRs and VVERs, and its possible impact on plant life extension // 5th International Conference on Nuclear and Radiation Physics.-2005.- issued in CD format.
14. Garner F.A., Porollo S.I., Konobeev Yu.V., Maksimkin O.P. Void swelling of austenitic steels irradiated with neutrons at low temperatures and very low dpa rates // 12th International Conference on Environmental Degradation of Materials in Nuclear Power Systems.-2005.-P.439–448.
15. Garner F.A. Void swelling and irradiation creep in light water reactor environments // Chapter 10 of Understanding and mitigating ageing in nuclear power plants.-2010.-Vol.6.-P.175-179.
16. Garner F.A., Makenas B.J. Recent experimental results on neutron-induced void swelling of AISI 304 stainless steel concerning its interactive dependence on temperature and displacement rate // Fontevraud-6 Symposium on Contribution of Materials Investigations to Improve the Safety and Performance of LWRs.-18–22 September 2006,Fontevraud, France.-P.625-636.
17. Kalchenko A.S., Bryk V.V., Lazarev N.P., Neklyudov I.M., Voyevodin V.N. Prediction of swelling of 18Cr10NiTi austenitic steel over a wide range of displacement rates // JNM.-2010.-Vol.399.-Issue 1.-P.114–121.
18. Garner F.A., Simonen E.P., Oliver B.M. Retention of hydrogen fcc metals irradiated at temperatures leading to high densities of bubbles or void // JNM.-2006.–Vol.356.–P.122–135.
19. Edwards D. J. Nano-cavities observed in a 316SS PWR flux thimble tube irradiated to 33 and 70 dpa //JNM.–2009.–Vol.384.–P.249–255.
20. Neklyudov I.M., Borodin O.V., Bryk V.V., Voyevodin V.N. Problem of Radiation Resistance of Structural Materials of Nuclear Power // Progress in High Energy Physics and Nuclear Safety.-2007.-Vol.126.-P.259-277.
21. Golovinski S.A., Boitsov A.V. Intl. Conf "Progress in atomic energy based on fast neutron with a closed fuel cycle. Strategy and perspectives of the international collaboration".-Moskow, Nov.2005.-available on CD.
22. Garner F.A. Irradiation Performance of Cladding and Structural Steels in the Liquid Metal Reactors, in Material Science and Technology // Nuclear Materials.-1994.-Vol.10A.-P.12-14.
23. Voyevodin V.N., Neklyudov I.M. Evolution of the structure-phase state and radiation stability of the construction materials.-Kiev: Naukova Dumka, 2006.-387 p.
24. Klueh R.L., Harries D.R. High-Chromium Ferritic and Martensitic Steels for Nuclear Applications // JNM.-2001.-Vol.56.-P.71-74.
25. Carlan Y., Averty X., Brachet J-C., Bertin J-L. Post-Irradiation Tensile Behavior and Residual Activity of Several Ferritic/Martensitic and Austenitic Steels Irradiated in Osiris Reactor at 325 C up to 9 dpa // Journal of ASTM Intern.-2005.-P.67.
26. Borodin O.V., Bryk V.V., Voyevodin V.N., Kalchenko A.S., Kupriyanova Yu.E., Melnichenko V.V., Neklyudov I.M., Permyakov A.V. Radiation swelling of ferritic-martensitic steels EP-450 and HT-9 under irradiation by metallic ions to super-higher doses // Problem of atomic science and technology.-2008.-Vol.45.-P.256-258.
27. Borodin O.V., Bryk V.V., Neklyudov I.M., Shamardin V.K., Voyevodin V.N. Investigation of microstructure of ferritic-martensitic steels containing 9 and 13 % Cr irradiated with fast neutrons // Journal of Nuclear Materials.-1994.-Vol.207.-P.295-302.
28. Lanskaya K.A. High-chromic heat-proof steels.-M: Metallurgia, 1976.-216 p.
29. Klueh R.L., Gelles D.S., Jitsukawa S., Kimura A., Odette G.R., Schaaf B., Van der. Victoria M. Development of innovative

metallic materials for applications in the nuclear industry // JNM.-2002.-Vol.455.-P.307–311.
30. Jitsukawa S., Kimura A., Kohyama A., Klueh R.L., Tavassoli A.A., Schaaf B., van der. Odette G.R., Rensman J.W. Materials for fission and fusion reactors // JNM.-2004.-Vol.39.-P.329–333.
31. Klueh R.L., Shingledecker J.P., Swindeman R.W., Hoelzer D.T. Oxide dispersion strengthened (ODS) alloy materials // JNM.-2005.-Vol.341.-P.103.
32. de Castro V., Leguey T., Monge M.A., Munoz A., Pareja R., Amador D.R., Torralba J.M., Victoria M. Powder metallurgy for steel production // JNM.-2003.- Vol.228.-P.322.
33. Ukai S., Harada M., Okada H., Inoue M., Nomura S., Shikakura S., Nishida T., Fujiwara M., Asabe K. Structural materials due to their creep rupture strength at high temperature // JNM.-1993.-Vol.74.-P.204.
34. Lindau R., Moslang A., Schirra M., Schlossmacher P., Klimenkov M. Nano-dispersion particles in ODS // JNM-2002.-Vol.769.-P.307–311.
35. Klimenkov M., Lindau R., Moslang A. TEM characterization of structure and composition of nanosized ODS particles in reduced activation ferritic-martensitic steels // JNM.-2004.-Vol.347.-P.329-333.
36. Miller M.K., Hoelzer D.T., Kenik E.A., Russel K.F. Nanometer scale precipitation in ferritic MA/ODS alloy MA957 // JNM.-2004. - Vol.329.-P.338-341.



Azarenkov Nikolay Alekseevich - Academician of National Academy of Sciences of Ukraine, D.Sc., Professor, Honoured worker of science Ukraine, Head of department of nuclear materials, Prorector from scientifically-educationally work of the Kharkiv national university named V.N. Karazin.
Scientific interests: physics of the systems of lacking amenities, nonlinear physics of plasma, cooperation of plasma with substances, radiation materials. An author and coauthor are the over 400 publications.



Neklyudov Ivan Matveevich - Academician-secretary department of nuclear physics and power engineering national academy of sciences of Ukraine, Director general national research center "Kharkov Institute of Physics and Technology", NAS of Ukraine.
Scientific interests: materials, physics of durability and plasticity, radiation firmness of metals and alloys. Publications: coauthor 15 monographs, more than 600 publications and 47 patents and inventions.



Voyevodin Viktor Nikolaevich – Corresponding Member of the Academy of Sciences, D.Sci. of Physics and Mathematics, Professor. Director of the Institute of Solid State Physics, Materials Science and Technology KIPT NASU.
Scientific interests: physics of the radiation phenomena and radiation materials. Author more than 400 publications.

UDC 537.8; 532.6; 533.9

ON NEW REPRESENTATIONS OF WELL-KNOWN PHYSICAL PHENOMENA

V.M. Kuklin
V.N. Karazin Kharkiv National University
Svobody Sq. 4, 61022, Kharkiv. Ukraine
E-mail: kuklinvm1@rambler.ru
Received 18 June 2012, revised 3 August 2012, accepted 9 August 2012

New theoretical description of well-known physical phenomena are announced. 1. The description of wave interaction in plasma in terms of spontaneous and stimulated processes is discussed. Such a description is not only attractive from the methodological point of view, but also offers new possibilities for the understanding of physical processes related to the interaction of radiation with matter. Moreover, there exists an intimate relationship between spontaneous and stimulated processes that can simplify the calculation of nonlinear terms for systems with multi-wave interactions. 2. It is shown by the example of two-level system that generation of coherent radiation is realized in excess of the threshold, determined by the equality of the squared population inversion to the half of the total number of all possible states. 3. The spectrum of waves emitted by oscillator, trapped in an external potential well is analyzed. It is assumed that the eigenfrequency of the oscillator is much greater than the frequency of oscillations in the potential well. The effect of the recoil on the absorption and emission of the oscillator is discussed. Since the energy of the slow oscillations in well is equal to the recoil energy, the intensity of the absorption and emission lines at the eigenfrequency exceeds the intensity of other spectral lines. 4. The formation of gravity surface waves with abnormally high amplitude, that occurs only in initial stage of nonlinear regime of modulation instability in the ocean, is considered. 5. The intensive long-wave Langmuir oscillation in plasma has been generated by a high-current charged-particle beam and a maser radiation is unstable. It being known the field energy density often exceeds the thermal energy density of plasma. In this case the modulation instability of intensive oscillation results one plasma density cavity over a wavelength of the intensive oscillation. It is shown, that kinetic limitation mechanism of cavity deepening is the local capture of ions. It should be noted, the potential of cavity is quite low for capture of great part of electrons with considerable kinetic energy.
KEY WORDS: spontaneous and stimulated processes, multi-wave interactions, threshold of coherent radiation, emission by oscillator, trapped in an potential well, modulation instability.

О НОВЫХ ОПИСАНИЯХ ХОРОШО ИЗВЕСТНЫХ ФИЗИЧЕСКИХ ЯВЛЕНИЙ

В.М. Куклин
Харьковский национальный университет имени В.Н. Каразина
пл. Свободы 4, 61022, Харьков, Украина

Анонсированы новые описания известных физических явлений. 1. Обсуждается описание волновых взаимодействий в плазме в терминах спонтанных и индуцированных процессов. Такое описание привлекательно не только с методологической точки зрения, но и открывает новые возможности для понимания физических процессов, относящихся к взаимодействию излучения с веществом. Кроме того, существует глубокая связь между спонтанными и индуцированными процессами, которая позволяет упростить вычисления нелинейных слагаемых в выражениях для многоволновых взаимодействий. 2. На примере двухуровневой системы показано, что возникновение когерентного излучения возможно при превышении порога, определяемого равенством квадрата инверсии населенностей половине полного числа состояний системы. 3. Изучен спектр волн, генерируемых осциллятором, захваченным во внешнюю потенциальную яму. Собственная частота осциллятора при этом много больше частоты его колебаний в потенциальной яме. Учитывается эффект отдачи осциллятора при излучении и поглощении. В том случае, если энергия отдачи равна энергии медленных колебаний осциллятора в потенциальной яме, интенсивность линий излучения и поглощения на его собственной частоте превышает интенсивности других спектральных линий. 4. Показано, что формирование гравитационных поверхностных волн аномально большой амплитуды, происходит только на начальной стадии нелинейного режима модуляционной неустойчивости океанского волнения. 5.Генерируемые пучками заряженных частиц или мазерным излучением интенсивные длинноволновые ленмюровские колебания плазмы оказываются модуляционно неустойчивы. Причем часто плотность энергии поля достигает и порой превосходит плотность тепловой энергии плазмы. В этом случае результатом модуляционной неустойчивости является возникновение каверны плотности плазмы на масштабах длины интенсивной волны. Показано, что кинетическим механизмом стабилизации дальнейшего углубления каверны плотности является локальный захват ионов. Отмечено, что потенциал каверны оказывается недостаточным для захвата большей части электронов, обладающих значительной кинетической энергией.
КЛЮЧЕВЫЕ СЛОВА: спонтанные и индуцированные процессы, многоволновые взаимодействия, порог когерентной генерации, излучение осциллятора, захваченного в потенциальную яму; модуляционная неустойчивость.

ПРО НОВІ ОПИСИ ДОБРЕ ВІДОМИХ ФІЗИЧНИХ ЯВИЩ

В.М. Куклін
Харківський національний університет імені В.Н. Каразіна
м. Свободи 4, 61022 Харків, Україна

Анонсовано нові описи відомих фізичних явищ. 1. Обговорюється опис хвилевих взаємодій в плазмі у термінах спонтанних та вимушених процесів. Такий опис привертає увагу не тільки з методологічної точки зору, а також відкриває нові можливості для розуміння фізичних процесів, що відносяться до взаємодії випромінювання з речовиною. Крім того

© Kuklin V.M., 2012

існує значний зв'язок між спонтанними та вимушеними процесами, що дозволяє спростити обчислення нелінійних доданків в виразах для багатохвильових процесів. 2. На прикладі дворівневої системи показано, що виникнення когерентного випромінювання можливо при перевищенні порогу, що визначається рівністю квадрата інверсії половині повного числа станів системи. 3. Проаналізовано спектр хвиль, що генерує осцилятор, який захвачено в зовнішню потенційну яму. Власна частота осцилятора набагато більша частоти його коливань в потенційної ямі. Враховано ефект віддачі осцилятора при випромінюванні та поглинанні. В тому випадку, коли енергія віддачі дорівнює енергії повільних коливань осцилятора в потенційної ямі, інтенсивність ліній випромінювання та поглинання на його власної частоті значно перевищує інтенсивність інших ліній спектру. 4. Показано, що формування гравітаційних поверхневих хвиль аномально великої амплітуди в океані можна побачити тільки на начальної стадії нелінійного режиму модуляційної нестійкості хвиль в океані. 5. Інтенсивні довгохвилеві ленгмюрівські коливання, що генеруються пучками заряджених часток та мазерним випромінюванням, виявляються модуляційне нестійкими. Досить часто густина енергії поля значно перевищує густину теплої енергії плазми. В цьому випадку результатом модуляційної нестійкості є виникнення однієї каверни густини плазми на масштабі довжини інтенсивної хвилі. Показано, що кінетичним механізмом обмеження процесу поглиблення каверни є локальний захват іонів. Відмічається, що потенціал каверни замалий для захвату значної частини електронів, які мають значну кінетичну енергію.
КЛЮЧОВІ СЛОВА: спонтанні та вимушені процеси, багатохвильові взаємодії, поріг когерентного випромінювання, випромінювання осцилятора, що рухається в зовнішньої потенційної ямі, модуляційна нестійкість.

1. INTRODUCTION

That paper announces new theoretical description of following well-known physical phenomena and new results of its analyses. At first we apply this concept for a description of some processes in plasma in terms of spontaneous and stimulated emission. By spontaneous emission, one means the process by which an emission source such as a charge or current emits an electromagnetic wave and this emission does not depend on the external electromagnetic field at the same frequency. By stimulated emission (or absorption), we mean the process, caused by the interaction between an emission source (absorption channel) and an external electromagnetic field at the corresponding frequency. It is not difficult to generalize the method suggested by Einstein [1] and derive [2,3] the equation for the radiation energy density $W_k = \hbar\omega \cdot N_k$:

$$dW_k / dt = S_2 + \frac{\partial S_2}{\partial(\hbar\omega)} W_k , \qquad (1)$$

here N_k - number of emitted quanta, S_n the change in energy density on level *n* caused by spontaneous processes. The term $(S_2 - S_1)N_k = W_k \cdot \partial S_2 / \partial(\hbar\omega)$ corresponds to stimulated processes. Interaction between waves and currents has an allocated character and depends on the integral phase relations, which causes some difficulties in the interpretation of these processes as radiative. But one can formulate a simple criterion for the existence of spontaneous radiation. If the work done by the field on the current, which generates this field, has a non-zero real part, then spontaneous radiation takes place. This criterion becomes very important when the current and the related field occupy the whole interaction space, e.g. the current is not localized and the field in the far-field zone cannot be analyzed. In the 2 part one can see that oscillations, generated by nonlinear currents at combined frequencies, demonstrate all the characteristics of spontaneous and stimulated emission.

The major problem is the interpretation of an induced radiation in quantum description as coherent radiation. In contrast to the classical description here is impossible to say something about field phases of atoms and molecules radiating. But though Charles Townes considered that "…energy is radiated from molecular systems has the same field distribution and the same frequency as external emission, and consequently permanent (probably zero-order) phase difference" [4]. Stimulative problem for thinking are degree of coherence in maser; inversion level, which is the necessary value for coherent radiation and the role of noncoherent radiation in depletion of inversion. The other unsolved problem is the physical role of noise emission into the process dynamics of generation for traditional and plasma electronics devices. That problems [5] are proposed for discussion in the 3 part.

The scattering of high-energy photons by free electrons results in a decrease in energy of photons due to the recoil effect (the Compton effect). This fact together with the phenomenon of the photoelectric effect confirmed the basic principles of quantum theory of radiation [6-8]. The processes underlying the interaction of radiation and matter are characterized by an impressive variety and form the basis for many physical research directions [9]. One of the problems, that arises when considering the processes of absorption and emission by a substance, is the problem of interaction with the external radiation field of the oscillating particle trapped in the potential well formed by the spatial structure of the medium. This problem requires the use of the quantum model for describing the behavior of the excited oscillator in a potential well, take into account the effect of the recoil. The purpose of the 4 part is discussion [10] of the quantum-mechanical model of the interaction between a charged particle-oscillator trapped in the potential well and an external electric field.

The modulation instability of regular spatial patterns form the spectra of perturbations, which growth rates have local maxima both in the bands of small and large scales [11-12]. The modulation instability occurs, for example, in systems described by the Lighthill equation (or NSE) [11]. It also underlies the instability of Langmuir waves in plasma described by Zakharov equations [13] or Silin equations [14]. In recent years, the attention of researchers was attracted to the phenomenon of large-amplitude short-lived waves observed in various nonlinear dispersive wave media. These

waves were named as freaks or rogue waves. Of particular interest are the experimental observations of extreme ocean waves. A complete review on the various phenomena yielding to rogue waves in ocean can be found in the book [15]. Later, it has been found experimentally that freak waves can be generated in optical systems [16-17] and in space plasma [18]. Zakharov and co-authors (see detailed review [19] and book [20]) have formulated the theory of the nonlinear stage of modulation instability based on excites the spectrum satisfying the conditions of space-time synchronism of the form $2\omega_0 = \omega(k) + \omega(-k)$ and interaction by pairs of waves symmetric with respect to the pump $\omega(k) + \omega(-k) = \omega(k') + \omega(-k')$. This model, as shown in the 5 part, allows to analyze some specific futures of the instability, in particular, the symmetry breaking of the excited spectrum during the progress of the modulation instability in a medium with strong dispersion and the formation of gravity waves with abnormally high amplitude [21].

The intensive long-wave Langmuir oscillation in plasma has been generated by a high-current charged-particle beam and a maser radiation is unstable. It being known the field energy density often exceeds the thermal energy density of plasma [14]. In this case the modulation instability of intensive oscillation results one plasma density cavity over a wavelength of the intensive oscillation [13,14]. In the 6 part one may see the potential well bottom is capable of ions capture, but the potential of cavity is quite low for a capture of great part of electrons. The energy of captured ion considerably exceeds initial energy of electron. But capture region is too small and the total energy of ions is substantially smaller the initial total energy of system. That local capture of ions is the kinetic (but non hydrodynamic) limitation mechanism of cavity deepening.

2. WAVE INTERACTIONS IN PLASMA IN TERMS OF SPONTANEOUS AND STIMULATED PROCESSES

Let us consider the interaction of three ion-acoustic waves in non-isothermal plasma. Let two ion-acoustic waves with frequencies ω_2 and ω_3 propagate in a nonlinear medium and excite a nonlinear current, $\tilde{j}_{23}$, capable of radiating proper waves of the medium at a frequency ω_1 under conditions of spatial–temporal synchronism $\omega_1 \approx \omega_2 + \omega_3$ and $\vec{k}_1 = \vec{k}_2 + \vec{k}_3$. The radiation of quanta ω_1 by the nonlinear current $\tilde{j}_{23}$ can be considered as a spontaneous process if one takes into account the action of waves of frequencies ω_2, ω_3 on $\tilde{j}_{23}$. The Fourier transform of the current at combination frequency $\omega_2 + \omega_3$ can be represented as follows:

$$j_{23}(\omega, k) = (k_2 + k_3)\frac{n_0 e^3 \{E_2 E_3\}_\omega}{m_i^2 \omega_1 \omega_2 \omega_3}\delta(k_1 - k_2 - k_3), \tag{2}$$

where for E_2, E_3 and $\{E_2 E_3\}_\omega$ we use the expressions

$$\{E_2 E_3\}_\omega = \{E_2 E_3\}_0 \frac{1}{\Delta_{\Omega 23}\sqrt{\pi}} \exp\left\{-(\omega - \omega_2 - \omega_3)^2 / \Delta^2_{\Omega 23}\right\}, \tag{3}$$

By applying the Borel theorem at small detunings $-(\omega_1 - \omega_2 - \omega_3) = \Delta_{-1,2,3} = \Delta$, ($\Delta_{\Omega 23}$ - is dispersion spreading) the rate of emission at the frequency ω_1 due to the interaction of the field with the nonlinear current at combination frequency $\omega_2 + \omega_3$ is determined by the following expression:

$$-(E_{23}^{(2)*} j_{23}^{(2)} + E_{23}^{(2)} j_{23}^{(2)*})/2 = \alpha\left(\frac{e}{m_i v_s}\right)^2 W_2 W_3 \frac{8}{3}\frac{\omega_1}{\omega_2 \omega_3} \tag{4}$$

where $j_{23}^{(2)}$ is the nonlinear current, which is generated by two ion-acoustic waves with frequencies ω_2 and ω_3, and $E_{23}^{(2)}$ is the field at a frequency ω_1 which is generated by that current in turn. Note that the sign of the rhs of (4) is positive and does not depend on phases of interacting waves, which correspond to the emission process. This sign-definiteness is characteristic of spontaneous processes. In addition, the generation at the frequency ω_1 is provided by an external source in relation to the wave at the frequency ω_1 (here by the waves at frequencies ω_2 and ω_3) that also common to spontaneous processes. We have used the following notation: $W_1 = \frac{1}{8\pi}\omega_1 \frac{\partial \varepsilon}{\partial \omega_1} |E_1|^2 = 2\frac{\Omega_i^2}{8\pi\omega_1^2}|E_1|^2$ - is the intensity of oscillations at the frequency ω_1 and $\Delta_{-1,2,3} = (-\omega_1 + \omega_2 + \omega_3) = 3\omega_1\omega_2\omega_3 / 2\Omega_i^2$ is a frequency detuning via dispersion,

$$\alpha = \pi \cdot \frac{3\omega_1\omega_2\omega_3}{2\Omega_i^2}\frac{1}{\Delta_{\Omega 23}\sqrt{\pi}} \exp\left[-(\omega_1 - \omega_2 - \omega_3)^2 / \Delta^2_{\Omega 23}\right] \tag{5}$$

A similar equations can be written for the number of quanta $N_i = W_i / \hbar\omega_i$:

$$\frac{\partial N_1}{\partial t} = \alpha \frac{8\hbar}{3}\left(\frac{e}{m_i v_s}\right)^2 N_2 N_3 - \mathrm{Re}\frac{2\Omega_i^2 eE_2 E_3 E_1^*}{\pi m_i \hbar v_s \omega_2 \omega_3 \omega_1} + \\ + \frac{8\hbar}{3}\left(\frac{e}{m_i v_s}\right)^2 \left[\alpha' N_1 N_1 + \alpha N_1 (N_2 + N_3)\right]. \tag{6}$$

and for the slow phase of oscillations at frequency ω_1:

$$N_1 \frac{\partial \phi_1}{\partial t} = \frac{8\hbar}{6}\left(\frac{e}{m_i v_s}\right)^2 N_2 N_3 - \mathrm{Im}\frac{\Omega_i^2 eE_2 E_3 E_1^*}{\pi m_i \hbar v_s \omega_2 \omega_3 \omega_1} - \\ - \frac{8\hbar}{6}\left(\frac{e}{m_i v_s}\right)^2 \left[N_1 N_1 - N_1 (N_2 + N_3)\right]. \tag{7}$$

The first term in the rhs of (6) and (7) describes the spontaneous effects, the second term governs the interaction of all three waves and the third term is responsible for stimulated self-action ($\propto N_1^2$) and cross-modulation effects, which can be obtained by direct calculation. Equation (6) can be rewritten without considering the self-action term $\propto N_1^2$ as follows (compare with (1)):

$$dW_1 / dt = S + \left\{ j_{23} E_1^* + j_{23}^* E_1 \right\} + \frac{\partial S}{\partial(\hbar\omega)} W_1 \tag{8}$$

where $S = \alpha \frac{8}{3}\left(\frac{e}{m_i v_s}\right)^2 \omega_1 \frac{W_2}{\omega_2}\frac{W_3}{\omega_3}$.

Unexpectedly, ex facte, the equation for the slow phase (7) can be rewritten by the same sort. The term $\propto N_1^2$ is responsible for stimulated self-action can be obtained by such procedure [22]. Note that the first terms in (6) and (7) are of the same order as the last terms of these equations. This gives reason to believe sometimes that the physical mechanisms for which they are responsible are of the same type, which is not true. Note that spontaneous emission of nonlinear currents gives rise to terms of fourth order on the field and has no appreciable effect on the dynamics of wave processes, where the third-order terms play a dominating role. Moreover, if one knows the term of emission at the frequency ω_1 due to the interaction of the field with the nonlinear current at combination frequency $\omega_2 + \omega_3$, one will find all other terms of fourth order on the field. Such fourth order terms can be decisive in determining the steady-state emission spectra of plasma systems.

3. ON THRESHOLD OF COHERENT GENERATION

According to conception, formulated by A. Einstein, the description of two level system in presence of radiation with transition frequency $\varepsilon_2 - \varepsilon_1 = \hbar\omega_{12}$ the following:

$$\partial n_2 / \partial t = -\left(u_{21} + w_{21} \cdot N_k\right) \cdot n_2 + w_{12} \cdot N_k \cdot n_1, \\ \partial n_1 / \partial t = -w_{12} \cdot N_k \cdot n_1 + \left(u_{21} + w_{21} \cdot N_k\right) \cdot n_2, \tag{9}$$

where general number of particles of system is invariable $n_1 + n_2 = Const, u_{21} \cdot n_2$ - the rate of change of quantum number on second excited level at the expense of spontaneous emission. The expressions $w_{21} \cdot N_k \cdot n_2$ and $w_{12} \cdot N_k \cdot n_1$ determine the rate of change of quantum number at the expense of induced emission and absorption, respectively. Here N_k - quantum number on transition frequency. The equation, which describes the behavior of N_k is

$$\frac{\partial N_k}{\partial t} = \left(u_{21} + w_{21} \cdot N_k\right) \cdot n_2 - \left(w_{12} \cdot N_k\right) \cdot n_1 \cdot \tag{10}$$

It will be recalled that the oscillator radiates with the same frequency and phase as the outer emission. Note, the outer radiation and induced emission of oscillator are appeared coherent [6,23,24] (also see [25-29]). The more intensive coherent component of outer radiation, the more energy in unit time the oscillator loses. The spontaneous emission does not depend on the outer emission and is noncoherent. Assume on qualitative level the terms in right side of equation (9), (10), which are proportional to N_k, to be responsible for coherent processes [5]. It is reasonable to submit $\mu = n_2 - n_1$, $N_k = N_k^{(incoh)} + N_k^{(coh)}$ and represent the equations (9)-(10) in a form

$$2\partial n_2 / \partial \tau = \partial \mu / \partial \tau = -2n_2 - 2\mu \cdot N_k^{(coh)}; \qquad \partial N_k^{(incoh)} / \partial \tau = n_2; \qquad \partial N_k^{(coh)} / \partial \tau = \mu \cdot N_k^{(coh)}, \tag{11}$$

where $u_{21} = w_{21} = w_{12}$, $\tau = u_{21} \cdot t$. From the solution (11) one can see the threshold of coherent generation [5]

$$\mu = \mu_{TH2} = \sqrt{2N}, \tag{12}$$

where $N = n_1 + n_2$ - general number of states. Let illustrate the dynamics of generation process by the instrumentality

of numerical solution of equations (12) in handy shape

$$\partial \mathrm{N}_{inc}/\partial T = N_0/2; \qquad \partial \mathrm{N}_c/\partial T = \mathrm{M}\cdot \mathrm{N}_c; \qquad \partial \mathrm{M}/\partial T = -N_0 - 2M\cdot \mathrm{N}_c \tag{13}$$

where $\mathrm{N}_{inc} = N_k^{(incoh)}/\mu_0$, $\mathrm{N}_c = N_k^{(coh)}/\mu_0$, $\mathrm{M} = \mu/\mu_0$, $T = w_{21}\cdot\mu_0\cdot t = \mu_0\cdot\tau$, the single free parameter is $N_0 = N/\mu_0^2$, initial conditions: $\mathrm{M}(T=0)=1$, $\mathrm{N}_{inc}(T=0) = 0{,}001$, $\mathrm{N}_c(T=0) = 0{,}001$. The results of the calculations are represented on Fig.1. The value of normalized quantities N_{inc} (solid curve 1), M (solid curve 2), N_c (solid curve 3), and the stationary solution of Eqs. (9)-(10) N_k/μ_0 (upper dotted line) and $\mathrm{M} = \mu/\mu_0$ (lower dotted line) are demonstrated in the line of Y-direction.

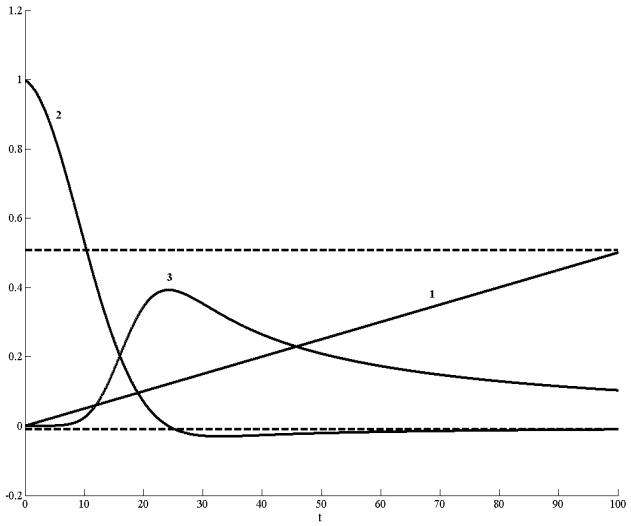


Fig.1. The dynamic behavior of normalized noncoherent quanta number N_{inc} (1), relational inversion M (2) and normalized coherent quanta number N_c (3); $N_0 = N/\mu_0^2 = 0.01$. The dashed lines - the stationary solution of Eqs. (9)-(10): N_k/μ_0 (upper dotted line) and $\mathrm{M} = \mu/\mu_0$ (lower dotted line).

In case of sufficiently large initial inversion $\mu_0 = 10\sqrt{N}$, exponentially fast ($T \propto 20$) current value of inversion tent to zero, coherent quanta number $N_k^{(coh)}$ reaches $\mu_0/2$, it is typical of super-radiation. Noncoherent component is smallish under such conditions. After that in what follows normalized coherent quanta number N_c decreases, but noncoherent quanta number N_{inc} on the contrary is increasing (Fig.1). In case of small initial inversion $\mu_0 = \sqrt{N/30}$, growing noncoherent component rapidly depletes current value of inversion and coherent field is depressed by stimulated absorption. The growth (even not exponential) of coherent component N_c below threshold (12) is impossible.

4. ON THE EMISSION AND ABSORPTION SPECTRA OF OSCILLATOR, TRAPPED IN THE POTENTIAL WELL

The important problems that arises when considering the processes of absorption and emission by a substance is the problem of interaction with the external radiation field of the oscillating particle trapped in the potential well. Suppose that a charge Q is at rest near the bottom of the outer potential well. We also assume that the recoil energy is not enough to ensure that the particle has left the potential well in which it is located. Upon emitting the high-frequency quantum $E_\nu = \hbar(\omega_0 + \Omega)$, the charged particle obtains the recoil momentum $M_Q V_Q$, becomes the excited oscillator with the proper frequency ω_0, which executes a slow periodic motion in the well. The particle motion can be represented as $x = b\sin\Omega t$. The conservation laws at this take the form:

$$\hbar(\omega_0 + \Omega)/c = M_Q V_Q, \qquad \hbar\Omega = M_Q V_Q^2/2. \tag{14}$$

Note that the energy of oscillations in the potential well is equal to $\hbar\Omega$. That is why the energy of the absorbed photon must exceed the energy of the oscillator excitation $\hbar\omega_0$ namely on this value. The frequency of oscillations in the potential well can be found from Eqs. (14)

$$\Omega \approx \hbar\omega^2{}_0 / 2M_Q c^2. \tag{15}$$

Here we assume the condition $\hbar\omega_0 << 2M_Q c^2$ is fulfilled. On the other hand, Eq. (15) implies the circle frequency of oscillations in the potential well is equal $\Omega = V_Q/b$. Since the energy of the quantum $\hbar\Omega$ is equal to the recoil energy, it follows [30]

$$\omega_0 b/c = kb \approx 2. \tag{16}$$

Note that the potential well should be significantly wider than b and the wavelength $\lambda = 2\pi/k = \pi b$ and deeper than the recoil energy (15). The highest intensity of the absorption and emission lines is observed on the eigenfrequency of the oscillator just when the recoil energy is equal to energy of the quantum of low-frequency oscillations in the potential well [10]. The Hamiltonian's correction of interaction between the oscillator and the field can be written in the form ($Q = e, M_Q = m$)

$$\mathrm{H}' = -e\cdot v_x A_x / c \tag{17}$$

The interaction energy (17) is proportional to the product of the velocity of the oscillator on the field at the point where it is located. Note, $v_x = v_{x0}\cdot cos\omega_0 t$ - velocity of the oscillator , $A_x = \sqrt{2}\cdot q_0 Cos((\omega \pm \Omega)t)\cdot Cos\{kb\sin\Omega t + \delta\}$ - component

of the vector potential. Minus sign corresponds to absorption, when the energy of the absorbed quantum must exceed the value of the excitation energy on the value of the recoil energy (14). Plus sign corresponds to emission when the energy of the emitted quantum must be less than the value of the excitation energy on the value of the recoil energy. The interaction energy under condition is nonzero at $\omega = \omega_0 + (m \mp 1)\Omega$:

$$\mathrm{H}' = -\frac{e \cdot v_{x0}}{c} q_0 \sqrt{2} \cdot \sum_m J_m(kb) \cdot \cos\delta. \tag{18}$$

Authors of [10] consider the cases of absorption ($m = -1$) and emission ($m = +1$) on the proper frequency (eigenfrequency) of the oscillator ω_0 and when the oscillator is not at rest on the bottom of the potential well. That is the frequencies of the absorbed and emitted field are the same and equal to ω_0 . The probability of transition with the emission (upper sign) and with absorption (lower sign) on the proper frequency of the motionless oscillator ω_0

$$P_{if} = \frac{8\pi e^2}{hc^3} \omega_0^2 (|x_{ab}|^2 + |y_{ab}|^2) \cdot J_1^2(kb) \cdot Cos^2\delta \cdot \begin{Bmatrix} n+1 \\ n \end{Bmatrix}. \tag{19}$$

Note that under condition (16), the intensity of the absorption and emission lines at the frequency ω_0 in $J^2_1(kb) / J^2_0(kb)$ times exceeds the intensity of spectral lines $\omega = \omega_0 \pm \Omega$.

5. MODULATION INSTABILITY OF GRAVITY WAVES IN OCEAN WITH DAMPING AND FORCING

Consider the modulation instability of externally driven wave in a medium with sufficiently strong dispersion and weak dissipation, which can be observed in plasma wave-guides, as well as on the water surface and other physical situations. We use below the following dispersion relation that characteristic, as an example, of gravity waves on deep water [31]:

$$\omega = \sqrt{gk} \left\{ 1 + A^2 k^2 / 2 + ... \right\}, \tag{20}$$

where g is some dimensional coefficient (for the gravity waves on deep water it is the acceleration of gravity).

Experimental data for ocean waves give us the following characteristics [32]: the maximal steepness of stable waves = $H / \lambda = 0.13 - 0.14$, where $H \propto 2A$ and λ are the vertical distance between the wave crest and the deepest trough preceding or following the crest and wave-length correspondingly. It follows from here that $Ak < 1$. Denote frequency ω_0, the average wave amplitude as $|A_0|$, the average wave height as $\bar{H} = 2|A_0|$. The gravity waves with $H = (2 \div 3) \cdot 2|A_0|$ are considered as extremely high. It follows from here that $(4 \div 6)|A_0|k_0 / 2\pi \propto 0.13$ and it is easy to see that the width of spatial spectrum of the instability in this case is not so small. The simplified representation [19-21], which describes only in initial stage of nonlinear regime of modulation instability, one takes into consideration to the following diagrams $2\omega_0 = \omega(k) + \omega(-k)$ and interaction by pairs of waves symmetric with respect to the pump $\omega(k) + \omega(-k) = \omega(k') + \omega(-k')$. Introducing real amplitudes and phases $A_K = |u_K| \exp(i\varphi_K)$, we have obtained the system of equations, which describes the modulation instability in a medium with strong dispersion [21]:

$$\frac{\partial u_K}{\partial \tau} = -\delta u_K + (1+K)^{2.5} \left[u_{-K} u_0^2 \sin\Phi_K + u_{-K} \sum_{\mathrm{K} \neq K,0} u_{\mathrm{K}} u_{-\mathrm{K}} \sin(\Phi_{\mathrm{K}} - \Phi_K) \right], \tag{21}$$

where $\Phi_K = 2\varphi_0 - \varphi_K - \varphi_{-K}$ is the total phase (or the phase of the instability channel). A distinction needs to be drawn between modes with wave numbers K and K and phases Φ_K and $\Phi_{\mathrm{K}} = \varphi_K + \varphi_{-K} - \varphi_{\mathrm{K}} - \varphi_{-\mathrm{K}}$.

$$\frac{\partial \varphi_K}{\partial \tau} = -\frac{2}{\alpha}\left(\sqrt{(1+K)} - 1\right) - (1+K)^{2.5} \left[2u_0^2 + u_K^2 + 2 \sum_{K' \neq K,0} u_{K'}^2 + \frac{u_{-K}}{u_K} u_0^2 \cos\Phi_K + \frac{u_{-K}}{u_K} \sum_{\mathrm{K} \neq K,0} u_{\mathrm{K}} u_{-\mathrm{K}} \cos(\Phi_{\mathrm{K}} - \Phi_K) \right], \tag{22}$$

where the mode frequencies are $\omega(K) - \omega_0 = \omega[k_0(1+K)] - \omega(k_0) = \sqrt{gk_0(1+K)} - \sqrt{gk_0}$. We use the following notations $\omega_0 t / 2 = \tau / \alpha$, $\alpha = k_0^2 |A_0|^2$, $K = (k - k_0) / k_0$, $A_K / A_0(\tau = 0) = a_K = u_K \exp\{i\varphi_K\}$, and also $\Delta_K = 2\left(\sqrt{(1+K)} - 1] + \sqrt{(1-K)} - 1\right) / \alpha$, $\mathrm{P}_K = 2(1+K)^{2.5} + 2(1-K)^{2.5} - 2$.

In order to analyze the wave height distribution (e.g. the distribution of vertical distances between the wave crest and the deepest trough preceding or following the crest), we take a third of highest waves. Then we find the average height of all waves U_{CP}, average height of a highest third U_{SWH} and the maximum wave height U_{MAX} in consideration domain ($\zeta \subset L = 2\pi / (\Delta K / k_0) = \pi N / K_m = \pi N / \sqrt{2\alpha}$, where $\Delta K = 2K_{\max} / N$, $\zeta = k_0 x$, x - spatial value). Calculations were performed for 600 modes in the spectrum. The ratio of dissipation level δ to the maximum growth rate was chosen as 0.1 (e.g. $\delta = 0.1$). In order to provide the unit amplitude of the fundamental wave at the initial stage of the instability we have also chosen the value of the external drive force as $G = \delta = 0.1$. The results of that calculations are represented on Fig.2.

Note that the criterion which defines the extremely high waves with amplitude U_{AG} is $U_{AG} > 2U_{SWH}$ or something

like this, should be used with caution because this criterion as usual is applied to statistics obtained on sufficiently large observation periods, but the highest amplitudes are observed at the initial stage of the instability.

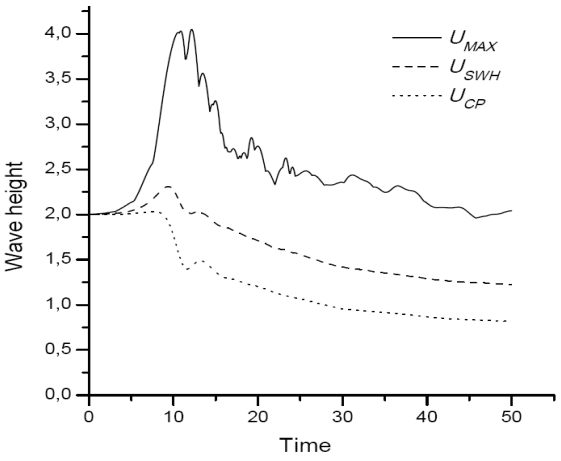


Fig. 2. Time evolution of wave height parameters: U_{CP} – the average height of all waves in the observation domain, U_{SWH} – the average height of a highest third, U_{MAX} – the maximum wave height [22].

The considered model shows that the appearance of waves with abnormally large amplitudes is characteristic of the initial stage of the modulation instability. The average and maximum wave heights noticeably decrease with the development of the instability. However, even in the later case ($\tau \propto 30$) abnormally high waves can be detected according to the criterion $U_{AG} > 2U_{SWH}$, although their amplitude is already one and a half - two times less than in the most interesting case ($\tau \propto 10$). There are few waves fits at the modulation length in the initial stage of the process and one of which may be abnormally large in some realizations (that result [21] comes to agreement with observed data [15,33]). At the stage of developed instability, the number of waves for the modulation length increases to three or four times. The probability of abnormally high wave events in our numerical simulations is qualitatively consistent with the known observations of ocean waves. It should be noted that the total energy of wave motion is approximately conserved with reasonable accuracy in the domain under consideration (both in time and space) and the condition that the amplitudes of individual side-band modes remain much smaller of the fundamental wave amplitude is satisfied during the entire simulation time [21]. The latter allows us to assume such a description of the modulation instability sufficiently correct.

6. THE LIMITATION MECHANISM OF THE DENSITY CAVITY DEEPING ON MODULATION INSTABILITY OF INTENSIVE OSCILLATION IN PLASMA

Let us consider the behavior of electrons ($\alpha = e$) and ions ($\alpha = i$) of cold plasma in the electric field of intensive Langmuir oscillation $E = E_0 \cdot Sin(\omega_0 t - k_0 x + \varphi)$ with the frequency ω_0 near Langmuir frequency $\omega_{pe} = \sqrt{4\pi e^2 n_0 / m_e}$ where e – charge, m_α - mass of a particles, E_0 , φ - slowly varying amplitude and phase of the field. The generalized 1D Silin's equations, which are describing the modulation instability [34] (see also [35]) of intensive oscillations with excitation of wave spectra (the wavelength of which is $2\pi / nk_0$, where $n \le 100$) are

$$\partial N_n / \partial \tau - i\Delta N_n - iM_n \cdot J_1(na)/2n = 0.5i\sum_m M_m \cdot [N_{n-m} \cdot J_0(ma) - N^*_{n-m} \cdot J_2(ma) \cdot \exp(2i\phi)], \quad (23)$$

$$\partial[a \cdot \exp(i\varphi)] / \partial \tau = 2i\sum_s M_s \cdot [J_0(sa) N_s + J_2(sa) \cdot N^*_s \cdot \exp(2i\varphi)], \quad (24)$$

$$\frac{d^2\xi}{d\tau^2} = \frac{\delta}{2\pi}\sum_n \{2J_1(na) \cdot \mathrm{Re}[N_n \exp\{-i\varphi\}] + n \cdot \sum_m J_0(na_n) N^*_m N_{n-m} - J_2(na)\,\mathrm{Re}(N^*_m N^*_{n-m} \exp\{-i\varphi\})\} \cdot \sin(2\pi n\xi), \quad (25)$$

where $\delta \cdot t = \tau$; $\delta = (m_e / m_i)^{1/3}$; $a_n = a \cdot n = n \cdot ek_0 E_0 / m_e \omega_0^2$; $N_n = u_n / enn_0$ - relative disturbance of electron and $M_n = \delta^{-1} \cdot \int_{-0.5}^{0.5} d\xi_0 \cdot \cos(2\pi n\xi)$ - ion densities, $J_m(x)$ - Bessel function, $\Delta_n = \Delta_0 + \beta n^2 = -\delta^{-1}(1 - \omega_{pe}^2 / \omega^2) + 3k_0^2 T_e / 4\delta m_e \omega^2$ - detuning; T_e - electron temperature in units of energy. Let us assume the condition $E_0^2 / 4\pi n_0 T_e = W / n_0 T_e >> 1$ is satisfied. The result of the solution of equations (23)-(25) is represented in [34] on conditions that $a(\tau = 0) = k_0 eE_0(\tau = 0) / m_e \omega_0^2 = v_0 / c = 0.06$; $n \le 100$, $\delta = 0.1$, which answer the requirements the high-current electron-beam excitation.

The energy of intensive long-wave ($\lambda_0 = 2\pi / k_0 = 2\pi c / \omega_{pe}$) oscillation in plasma reaches several tens of percent of total beam energy. The maximum value of modulation instability increment $\sim \delta \cdot \omega_0 \cdot J_1(na)$ is achieved when $an \sim 2$. It follows from this that the number of spectra modes $n \ge 30$. The electric field amplitude of mode is $E_n \sim N_n \omega_0^2 m_e / k_0 e$. The numerical experiment [34] shows $N_n \sim 10^{-2}$. The electrons on a scale of intensive oscillation length ($\lambda_0 = 2\pi / k_0 = 2\pi c / \omega_{pe}$) practically are not captured by the plasma density cavity. Therefore the spectra growth transmits on the modes with numbers $n_{\max} \sim 60$. HF energy flux becomes formed just because increment maximum moves in short-wave region $n \sim 2 / a$ on account of intensive long-wave oscillations amplitude is decreasing.

The half of initial energy approximately is transferred in the short-wave HF spectra energy. The ratio of ion

oscillation frequency at the bottom of potential well of plasma density cavity to linear increment of modulation instability is

$$\sqrt{ek_0\sum_s sE_s / m_i\omega_0^2\delta^2} = 10^{-1} n_{\max}\delta^{1/2} / 2 \sim 1\cdot \qquad (26)$$

There is the fulfillment of conditions of ions capture. This fact explains the choice of ion kinetic description (25). The ions capture occurs on a small scale $\pi / n_{\max}k_0$, and the ion oscillation frequency at the bottom of cavity on the order of linear increment of modulation instability. Therefore at the bottom of cavity ion velocity is $\sim \pi\delta\omega_0 / n_{\max}k_0 \sim 0.05\cdot c\delta$ and its energy considerably exceeds initial energy of electron. The major portion of ions on periphery of the cavity and a great distance away from it is moving in opposite direction, "fill up" the cavity, at the same time disintegrate previous interaction between the Langmuir spectrum and the ion oscillations. However, summarized energy of ions is remained substantially least of the initial total energy of system [34-37].

CONCLUSION

The purpose of that paper is to announce new theoretical description of following well-known physical phenomena.

The nonlinear current (2), which generated by the fields with frequencies ω_2, ω_3, radiates the wave with frequency ω_1 and this emission does not depend on the external electromagnetic field at the same frequency. That features is typical ones for emitter of spontaneous radiation. If such emitter characteristics are known, it is not difficult to determine all components of the induced radiation with frequency ω_1, which is proportional to the intensity of the spectrum line. Such procedures are applied to the phase expression.

If the induced radiation is believed an coherent radiation, and spontaneous radiation is random process, very low threshold and pulse shaping of coherent (maser) radiation can be find out. The pulse has sharp rise-up portion and very lengthy descending part.

The high-frequency oscillator in the external potential well is capable of linear spectrum emission. Let emission and absorption of HF quantum accompany the recoil effect. When the recoil energy is equal to energy of the quantum of low-frequency oscillations in the potential well, the highest intensity of the absorption and emission lines is observed on the eigenfrequency of the HF oscillator. That assertion is consequence of the quantum description, which is discussed in [10] and in that paper.

The theory of the nonlinear stage of modulation instability based on excites the spectrum satisfying the conditions of space-time synchronism of the form $2\omega_0 = \omega(k) + \omega(-k)$ and interaction by pairs of waves symmetric with respect to the pump $\omega(k) + \omega(-k) = \omega(k') + \omega(-k')$ is reviewed. That description is applied to analysis of sea waves instability and detects gravity surface waves with abnormally high amplitude, that occurs only in initial stage of nonlinear regime of that process. The high coincidence of theoretical results and observed data is succeed.

The plasma density cavity is formed as a result of the modulation instability of intensive long-wave Langmuir oscillations. The instability scales down of density cavity. There is no hydrodynamic mechanisms to stabilize the dimension of density cavity, except the dispersion and the damping of short-wave Langmuir spectrum. But often cavity dimension in hydrodynamic description comes not nearer to that critical scale [34-36, 38]. However there is the kinetic limitation mechanism of cavity deepening. The potential well bottom of cavity is capable of ions capture and the cavity will be not become deeper. The condition of ions capture (26) is determined the minimum dimension of cavity.

REFERENCES

1. Einstein A. Quantentheorie der Strahlung // Mitteilungen d. Phys. Ges. Zurich. – 1916. - Nr. 18; Phys. Zs. – 1917. - Nr.18. - P.121.
2. Kirichok A.V., Kuklin V.M., Zagorodny A.G. A Theory of Some Nonlinear Processes in Plasma in Terms of the Spontaneous and Induced Radiation //Modern Problem of Theoretical and Mathematical Physics: Proc.Bogolubov Kyiv Conference, Kyiv, Ukrane, 15-18 Sept. 2009.
3. Kirichok A.V., Kuklin V.M. Theory of Some Nonlinear Processes in Plasma in Terms of Spontaneous and Stimulated Radiation //Phys. Scripta . – 2010. - Vol.82, №6. – P.065506
4. Charles H. Townes Production of Coherent Radiation by Atoms and Molecules // IEEE Spectrum. – 1965. - Vol. 2 (2).-P. 30.
5. Kuklin V.M., Zagorodny A.G. To realization condition of maser radiation // XIV Khariton topical scientific readings "High‐Power Pulsed Electrophysics", VNIIEF, Sarov, Russia, March 12-16, 2012.
6. Born M. Atomic Physics.- London: Blackie, 1935.
7. Heitler W. The Quantum Theory of Radiation. - Clarendon Press, 1953.
8. Berestetskii V. B, Lifshitz E. M., Pitaevskii L. P. Quantum electrodynamics. - Oxford: Pergamon Press, 1982. - 652 p.
9. Wertheim. G. K. Mossbauer effect. Principles and applications. - Academic Press, 1964.
10. Kirichok A.V., Kuklin V.M. .Zagorodny A.G. On the emission and absorption spectra of oscillator trapped in the potential well (in print).
11. Lighthill M.J. Contribution to the Theory of Waves in Nonlinear Dispersive System // J. Inst. Math. Appl.- 1965. – Vol.1. – P.269-306.
12. Zakharov V.E. The Instability of Waves in Nonlinear Dispersive Media // Sov. Phys. JETP. -1967. –Vol. 24. – P.740.

13. Zakharov V.E. Collapse of Langmuir Waves // Sov. Phys. JETP. -1972. –Vol. 35(5). –P.908-914.
14. Silin V.P. Parametric Influences of high-energy Radiation on Plasma.- Moscow: Nauka, 1973.
15. Kharif C., Pelinovsky E., Slunyaev A. Rogue Waves in the Ocean. - Springer-Verlag, Berlin, Heidelberg, 2009.
16. Solli D.R., Ropers C., Koonath A., Jalali B. Optical Rogue Waves // Nature. – 2007. – Vol.450. – P.1054.
17. Yeom D.-I., Eggleton B.J. Photonics: Rogue Waves Surface in Light //Nature. -2007. –Vol. 450.- P.953.
18. Burlaga L.F., Ness N.F., Acuna M.H., Linear Magnetic Holes in a Unipolar Region of the Heliosheath observed by Voyager 1, // J. Geophys. Res. -2007. –Vol. 112. – P.A07106.
19. Zakharov V.E., L'vov V.S., Starobinets S.S. Spin-Wave Turbulence beyond the Parametric Excitation Threshold //Sov. Phys. Usp. – 1975. –Vol.17(6). – P.896-919.
20. L'vov V.S. Nonlinear Spin Waves. - Moscow: Nauka, 1987.
21. Belkin E.V., Kirichok A.V., Kuklin V.M. On Interference in Multimode Operations of Modulation Instability //VANT.- 2008.- № 4 (6).- P. 222-227.
22. Kuklin V.M. On the emission processes in nonequilibrium media // The Journal of Kharkiv National University, physical series: Nuclei, Particles, Fields. – 2010. - № 933. - Iss.4 (48). - P.4-27.
23. Dicke R. H. Coherence in Spontaneous Radiation Processes // Physical Review. - 1954. - Vol.93. - № 1. - P.99-110.
24. Tsytovich V.N. Theory of Turbulent Plasma. – Moscow: Atomizdat, 1971.
25. Zheleznyakov V.V., Kocharovskii V.V., Kocharovskii V.V. Polarization waves and super-radiance in active media // Sov. Phys. Usp. – 1989. – №32. – P.835–870.
26. Andreev A.V. Optical superradiance: new ideas and new experiments // Sov. Phys. Usp. – 1990. - №33 (12). – P.997–1020.
27. Men'shikov L.I. Superradiance and related phenomena // Phys. Usp. – 1999. - №42.- P.107.
28. Fomin P.I., Fomina A.P. Dicke Superradiance on Landau Levels // Problems of Atomic Science and Technology. – 2001. - №6. - P.45-48.
29. Zagorodny A.G., Fomin P.I., Fomina A.P. Electron Superradiance in magnetic field and nonrelativistic girotron // Dop. NAN Ukraine. – 2004. - №4. - P.75-80.
30. Kuklina O.V., Kuklin V.M. On the relative role of phonon spectrum and the collisional relaxation in processes of generation and scatterin // The Journal of Kharkiv National University, physical series: Nuclei, Particles, Fields. – 2009. - №846. - Iss.2(50). - P.20-28.
31. Karpman V.I. Nonlinear waves in dispersive media. - M.: Nauka, 1973.
32. Schwartz L.W., Fenton J.D., Strongly nonlinear Waves // Ann. Rev. Fluid. Mech. -1982. –Vol. 14. – P.39-60.
33. Kharif C., Pelinovsky E. Physical Mechanisms of the Rogue Wave Phenomenon // Eur. J. Mech. B-Fluid. – 2003. – Vol.22 (6). – P.603-633.
34. Chernousenko V.V., Kuklin.V.M., Panchenko I.P. The structure in nonequilibrium media. In book: The integrability and kinetic equations for solitons / AN USSR, ITPh. K. Nauk. Dumka, 1990. - 472p.
35. Kuklin.V.M. The role of absorption and dissipation in spatial nonlinear structure formation in nonequilibriun media // Ukr. Phys. J., – 2004. - Vol.1, №1. - P.49-81.
36. Andreev N.E., Silin V.P., Stenchikov G.L. On saturation of plasma parametrical instability in strong electric field // Sov. Plasma Physics. – 1977. - Vol.3, №5. - P.1088-1096.
37. Batanov G.M., et al. The large amplitude Langmuir waves and particle acceleration in plasma microwave discharge // Sov. Plasma Physics. – 1986. - Vol.12, №5. – P.552-565.
38. Kuznetsov E.A. On averaged description of Langmuir waves in plasma // Sov. Plasma Physics. – 1976. - Vol.2, №2. - P. 327-333.



Kuklin Volodymyr Michailovich - Ph.D.; D.Sc.; Professor of Department of Reactor Material Science; Head of Department of Artificial Intelligence and Software, School (Faculty) of Computer Science, Karazin's Kharkiv National University.

UDC 539.12

POLYADIC SYSTEMS, REPRESENTATIONS AND QUANTUM GROUPS

S.A. Duplij*
Center for Mathematics, Science and Education Rutgers University,
118 Frelinghuysen Rd., Piscataway, NJ 08854-8019
E-mail: duplij@math.rutgers.edu, http://homepages.spa.umn.edu/˜duplij
Received 20 May 2012

A review of polyadic systems and their representations is given. The classification of general polyadic systems is done. The multiplace generalization of homomorphisms, preserving associativity, is presented. The multiplace representations and multiactions are defined, concrete examples of matrix representations for some ternary groups are given. The ternary algebras and Hopf algebras are defined, their properties are studied. At the end some ternary generalizations of quantum groups and the Yang-Baxter equation are presented.
KEY WORDS: n-ary group, Post theorem, commutativity, homomorphism, group action, Yang-Baxter equation

ПОЛИАДИЧЕСКИЕ СИСТЕМЫ, ПРЕДСТАВЛЕНИЯ И КВАНТОВЫЕ ГРУППЫ

С.А. Дуплий
Центр математики, науки и образования, университет Ратгерса, Пискатавэй, 08854-8019, США

Приведен обзор полиадических систем и их представлений, дана классификация общих полиадических систем. Построены многоместные обобщения гомоморфизмов, сохраняющие ассоциативность. Определены мультидействия и мультиместные представления. Приведены конкретные примеры матричных представлений для некоторых тернарных групп. Определены тернарные алгебры и Хопф алгебры, изучены их свойства. В заключение, предствлены некоторые тернарные обобщения квантовых групп и уравнения Янга-Бакстера.
КЛЮЧЕВЫЕ СЛОВА: n-арная группа, теорема Поста, коммутативность, гомоморфизм, групповое действие, уравнение Янга-Бакстера

ПОЛІАДИЧНІ СИСТЕМИ, ПРЕДСТАВЛЕННЯ І КВАНТОВІ ГРУПИ

С.А. Дуплій
Центр математики, науки та освіти, університет Ратгерсу, Піскатавей, 08854-8019, США

Зроблено огляд поліадичних систем та їх представлень, дана класифікація загальних поліадичних систем. Побудовані багатомісні узагальнення гомоморфізмів, що зберігають асоціативність. Визначені мультидії і мультимісні представлення. Наведені конкретні приклади матричних представлень для деяких тернарних груп. Визначені тернарна алгебра і алгебри Хопфа, вивчені їх властивості. На закінчення, предствлені деякі тернарні узагальнення квантових груп та рівняння Янга-Бакстера.
КЛЮЧОВІ СЛОВА: n-арна група, теорема Поста, комутативність, гомоморфізм, групова дія, рівняння Янга-Бакстера

One of the most promising steps in generalizing physical theories is consideration of higher arity algebras [1], in other words ternary and n-ary algebras, in which the binary composition law is substituted by ternary or n-ary one [2].

Firstly ternary algebraic operations (with the arity $n = 3$) were introduced already in the XIX-th century by A. Cayley in 1845 and later by J. J. Silvester in 1883. The notion of an n-ary group was introduced in 1928 by [3] (inspired by E. Nöther) which is a natural generalization of the notion of a group. Even before in 1924, a particular case, that is, ternary group of idempotents, was used in [4] to study infinite abelian groups. The important Post's coset theorem explained the connection between n-ary groups and their covering binary groups [5]. The next step in study of n-ary groups was the Gluskin-Hosszú theorem [6, 7]. Another definition of n-ary group can be given as a universal algebra with additional laws [8] or identities containing special elements [9].

The representation theory of (binary) groups [10, 11] plays an important role in their physical applications [12]. It is initially based on a matrix realization of group elements and abstract group action as a usual matrix multiplication [13, 14]. The cubic and n-ary generalizations of matrices and determinants were made is [15, 16], and their physical application appeared in [17,18]. In general, particular questions of n-ary group representations were considered in and matrix representations were derived by the author [19], and some general theorems

*On leave of absence from V.N. Karazin Kharkov National University, Svoboda Sq. 4, Kharkov 61022, Ukraine.

© Duplij S.A., 2012

connecting representations of binary and n-ary groups were presented in [20]. Here to generalize the above constructions of n-ary group representations to more complicated and nontrivial cases.

In physics the most applicable structures are nonassociative Grassmann, Clifford and Lie algebras [21–23], and so their higher arity generalizations play the key role in further applications. Indeed, the ternary analog of Clifford algebra was considered in [24], the ternary analog of Grassmann algebra [25] was exploited to construct various ternary extensions of supersymmetry [26].

The construction of realistic physical models is based on the Lie algebras, such that the fields take their values in the concrete binary Lie algebra [23]. In the higher arity considerations the standard Lie bracket is replaced by a linear n-ary bracket, and the algebraic structure of the corresponding model is defined by the additional characteristic identity for this generalized bracket, the Jacobi identity [2]. There are two possibilities to construct the generalized Jacobi identity: 1) The Lie bracket is a derivation by itself; 2) A double Lie bracket vanishes, when antisymmetrized with respect of its entries. The first case leads to so called Filippov algebras [27] (or n-Lie algebra) and second case corresponds to generalized Lie algebras [28] (or higher order Lie algebras).

The infinite-dimensional version of n-Lie algebras are the Nambu algebras [29, 30], and their n-bracket is given by the Jacobian determinant of n functions, the Nambu bracket, which in fact satisfies the Filippov identity [27]. Recently, the ternary Filippov algebras were successfully applied to a three-dimensional superconformal gauge theory describing effective worldvolume theory of coincident $M2$-branes of M-theory [31–33]. The infinite-dimensional Nambu bracket realization [34] gave possibility to describe a condensate of nearly coincident $M2$-branes [35].

From another side, Hopf algebras [36–38] play a fundamental role in the quantum group theory [39, 40]. Previously, it was introduced their Von Neumann generalization in [41–43], also their actions on quantum plane were classified in [44], and the ternary Hopf algebras were defined and studied in [45, 46].

The goal of this paper is to give a comprehensive review of polyadic systems and their representations. First, we classify general polyadic systems and introduce n-ary semigroups and groups. Then we consider their homomorphisms and the multiplace generalizations, paying attention on their associativity. We define multiplace representations and multiactions, give examples of matrix representations for some ternary groups. We define and investigate ternary algebras and Hopf algebras, study their properties and give some examples. At the end we consider some ternary generalizations of quantum groups and the Yang-Baxter equation.

PRELIMINARIES

Let G be a non-empty set (underlying set, universe, carrier), its elements we denote by lower-case Latin letters $g_i \in G$. The n-`tuple` (or `polyad`) $g_1, \ldots, g_n$ of elements from G is denoted by $(g_1, \ldots, g_n)$. The Cartesian product[1] $\overbrace{G \times \ldots \times G}^{n} = G^{\times n}$ consists of all n-tuples $(g_1, \ldots, g_n)$, such that $g_i \in G$, $i = 1, \ldots, n$. For all equal elements $g \in G$, we denote n-tuple (polyad) by power (g^n). If the number of elements in the n-tuple is clear from the context or is not important, we denote it in one bold letter $(\boldsymbol{g})$, in other case we use power in brackets $\left(\boldsymbol{g}^{(n)}\right)$. Introduce two important constructions on sets.

The i-`projection` of the Cartesian product $G^{\times n}$ on its i-th "axis" is the map $\mathsf{Pr}_i^{(n)} : G^{\times n} \to G$ such that $(g_1, \ldots g_i, \ldots, g_n) \longmapsto g_i$.

The i-`diagonal` $\mathsf{Diag}_n : G \to G^{\times n}$ sends one element to the equal element n-tuple $g \longmapsto (g^n)$.

The one-point set $\{\bullet\}$ can be treated as a unit for the Cartesian product, since there are bijections between G and with $G \times \{\bullet\}^{\times n}$, where G can be on any place. On the Cartesian product $G^{\times n}$ one can define a polyadic (n-ary, n-adic, if it is necessary to specify n, its arity or rank) operation $\mu_n : G^{\times n} \to G$. For operations we use small Greek letters and place arguments in square brackets $\mu_n[\boldsymbol{g}]$. The operations with $n = 1, 2, 3$ are called `unary, binary and ternary`. The case $n = 0$ is special and corresponds to fixing a distinguished element of G, a "constant" $c \in G$, and it is called a `0-ary operation` $\mu_0^{(c)}$, which maps the one-point set $\{\bullet\}$ to G, such that $\mu_0^{(c)} : \{\bullet\} \to G$, and formally has the value $\mu_0^{(c)}[\{\bullet\}] = c \in G$. The 0-ary operation "kills" arity, which can be seen from the following [47]: the composition of n-ary and m-ary operations $\mu_n \circ \mu_m$ gives $(n + m - 1)$-ary operation by

$$\mu_{n+m-1}[\boldsymbol{g}, \boldsymbol{h}] = \mu_n[\boldsymbol{g}, \mu_m[\boldsymbol{h}]]. \tag{1}$$

Then, if to compose μ_n with the 0-ary operation $\mu_0^{(c)}$, we obtain

$$\mu_{n-1}^{(c)}[\boldsymbol{g}] = \mu_n[\boldsymbol{g}, c], \tag{2}$$

because $\boldsymbol{g}$ is a polyad of length $(n-1)$. So, it is needed to make a clear distinction between the 0-ary operation $\mu_0^{(c)}$ and its value c in G, which will be seen and important below.

[1] We place the sign of the Cartesian product ($\times$) into the power, because the same abbreviation will be used below also for other types of products.

A `polyadic system` G is a set G which is closed under polyadic operations.

We will write $\mathrm{G} = \langle \text{set} \,|\text{operations}\,\rangle$ or $\mathrm{G} = \langle \text{set} \,|\text{operations}\,|\text{relations}\,\rangle$, where "relations" are some additional properties of operations (e.g., associativity conditions for semigroups or cancellation property). In such definition it is not needed to list the images of 0-ary operations (e.g. unit, zero in groups), as it is done in various other definitions. Here, we mostly consider concrete polyadic systems with one "chief" (fundamental) n-ary operation μ_n, which is called `polyadic multiplication` (or n-`ary multiplication`).

A n-`ary system` $\mathrm{G}_n = \langle G \mid \mu_n \rangle$ is a set G closed under one n-ary operation μ_n (without any other additional structure).

Note that a set with one closed binary operation without any other relations was called a groupoid by Hausmann and Ore [48] (see, also [49]). However, nowadays the term "groupoid" is widely used in the category theory and homotopy theory for a different construction with binary multiplication, the so-called Brandt groupoid [50] (see, also, [51]). Alternatively, and much later on, Bourbaki [52] introduced the term "magma" for binary systems. Then, the above terms were extended to the case of one fundamental n-ary operation as well. Nevertheless, we use some neutral notations "polyadic system" and "n-ary system" (when arity n is fixed/known/important), which adequately indicates all their main properties.

Let us consider the `changing arity problem`:

For a given n-ary system $\langle G \mid \mu_n \rangle$ to construct another polyadic system $\langle G \mid \mu'_{n'} \rangle$ over the same set G, which multiplication has different arity n'.

The formulas (1) and (2) give us the simplest examples, how to change arity of a polyadic system. In general, there are 3 ways:

1. *Iterating*. Using composition of the operation μ_n with itself, one can increase arity from n to n'_{iter} (as in (1)) without changing signature of the system. We denote the number of iterating multiplications by ℓ_μ, and use the bold Greek letters $\boldsymbol{\mu}_n^{\ell_\mu}$ to for the resulting composition of n-ary multiplications, such that

$$\mu'_{n'} = \boldsymbol{\mu}_n^{\ell_\mu} \stackrel{def}{=} \overbrace{\mu_n \circ \left(\mu_n \circ \ldots \left(\mu_n \times \mathrm{id}^{\times(n-1)}\right) \ldots \times \mathrm{id}^{\times(n-1)}\right)}^{\ell_\mu}, \tag{3}$$

where

$$n' = n_{iter} = \ell_\mu\,(n-1) + 1, \tag{4}$$

which gives the length of a polyad $(\boldsymbol{g})$ in the notation $\boldsymbol{\mu}_n^{\ell_\mu}[\boldsymbol{g}]$. Without assuming associativity there many variants of placing μ_n's among id's in r.h.s. of (3). The operation $\boldsymbol{\mu}_n^{\ell_\mu}$ is named a `long product` [3] or `derived` [53].

2. *Reducing*. Using n_c distinguished elements or constants (or n_c additional 0-ary operations $\mu_0^{(c_i)}$, $i = 1, \ldots n_c$), one can decrease arity from n to n'_{red} (as in (2)), such that[2]

$$\mu'_{n'} = \mu_{n'}^{(c_1 \ldots c_{n_c})} \stackrel{def}{=} \mu_n \circ \left(\overbrace{\mu_0^{(c_1)} \times \ldots \times \mu_0^{(c_{n_c})}}^{n_c} \times \mathrm{id}^{\times(n-n_c)} \right), \tag{5}$$

where

$$n' = n_{red} = n - n_c, \tag{6}$$

and the 0-ary operations $\mu_0^{(c_i)}$ can be on any places.

3. *Mixing*. Changing (increasing or decreasing) arity by combining the iterating and reducing (maybe with additional operations of different arity). If we do not use additional operations the final arity can be presented in general form using (4) and (6). It will depend on the order of iterating and reducing, so we have two subcases:

   (a) *Iterating→Reducing*. We have

$$n' = n_{iter \to red} = \ell_\mu\,(n-1) - n_c + 1. \tag{7}$$

   The maximal number of constants (when $n'_{iter \to red} = 2$) is equal to

$$n_c^{\max} = \ell_\mu\,(n-1) - 1 \tag{8}$$

   and can be any by increasing the number of multiplications ℓ_μ.

[2] In [54] $\mu_n^{(c_1 \ldots c_{n_c})}$ is named a retract (which is already busy and widely used in the category theory for another construction).

(b) *Reducing→Iterating*. We obtain

$$n' = n_{red\to iter} = \ell_\mu (n - 1 - n_c) + 1. \tag{9}$$

Now the maximal number of constants is

$$n_c^{\max} = n - 2 \tag{10}$$

and is achieved, only when $\ell_\mu = 1$.

To give examples to the third (mixed) case we put $n = 4$, $\ell_\mu = 3$, $n_c = 2$ for both subcases of opposite ordering:

1. *Iterating→Reducing*. We can put

$$\mu_8^{(c_1,c_2)\prime}\left[\boldsymbol{g}^{(8)}\right] = \mu_4\left[g_1, g_2, g_3, \mu_4\left[g_4, g_5, g_6, \mu_4\left[g_7, g_8, c_1, c_2\right]\right]\right]. \tag{11}$$

2. *Reducing→Iterating*. We can have

$$\mu_4^{(c_1,c_2)\prime}\left[\boldsymbol{g}^{(4)}\right] = \mu_4\left[g_1, c_1, c_2, \mu_4\left[g_2, c_1, c_2, \mu_4\left[g_3, c_1, c_2, g_4\right]\right]\right]. \tag{12}$$

It is important to find conditions, when the iterating and reducing compensate each other, i.e. they do not change arity. Indeed, let the number of the iterating multiplications ℓ_μ is fixed, then we can find such number of reducing constants $n_c^{(0)}$, that the final arity will coincide with the initial arity n. The result will depend on the order of operations. There are two cases:

1. *Iterating→Reducing*. For the number of reducing constants $n_c^{(0)}$ we obtain from (4) and (6)

$$n_c^{(0)} = (n - 1)(\ell_\mu - 1), \tag{13}$$

such that there is no restriction on ℓ_μ.

2. *Reducing→Iterating*. For $n_c^{(0)}$ we get

$$n_c^{(0)} = \frac{(n - 1)(\ell_\mu - 1)}{\ell_\mu}, \tag{14}$$

and now $\ell_\mu \le n - 1$. The requirement that $n_c^{(0)}$ should be integer gives two further possibilities

$$n_c^{(0)} = \begin{cases} \dfrac{n-1}{2}, & \ell_\mu = 2, \\ n - 2, & \ell_\mu = n - 1. \end{cases} \tag{15}$$

The above relations can be useful in the study of various n-ary multiplication structures and their presentation in special form needed in concrete problems.

SPECIAL ELEMENTS AND PROPERTIES OF POLYADIC SYSTEMS

Let us remind definitions of some standard algebraic systems and their special elements, which will be considered in this paper, using our notation.

A `zero` of a polyadic system is a distinguished element z (and the corresponding 0-ary operation $\mu_0^{(z)}$) such that for any $(n-1)$-tuple (polyad) $\boldsymbol{g} \in G^{\times(n-1)}$ we have

$$\mu_n[\boldsymbol{g}, z] = z, \tag{16}$$

where z can be on any place in the l.h.s. of (16).

There is only one zero (if not to fix its place) which can be possible in a polyadic system. As in the binary case, an analog of positive power of an element [5] should coincide with the number of multiplications ℓ_μ in the iterating (3).

A (positive) `polyadic power` of an element is

$$g^{\langle \ell_\mu \rangle} = \boldsymbol{\mu}_n^{\ell_\mu}\left[g^{\ell_\mu(n-1)+1}\right]. \tag{17}$$

An element of a polyadic system g is called ℓ_μ-`nilpotent` (or simply `nilpotent` for $\ell_\mu = 1$), if there exist such ℓ_μ that

$$g^{\langle \ell_\mu \rangle} = z. \tag{18}$$

A polyadic system with zero z is called ℓ_μ-`nilpotent`, if there exist such ℓ_μ that for any $(\ell_\mu (n-1)+1)$-tuple (polyad) $\boldsymbol{g}$ we have

$$\boldsymbol{\mu}_n^{\ell_\mu}[\boldsymbol{g}] = z. \tag{19}$$

Therefore, the `index of nilpotency` (number of elements whose product is zero) of ℓ_μ-nilpotent n-ary system is $(\ell_\mu (n-1)+1)$, while its polyadic power isℓ_μ .

A `polyadic (`n`-ary) identity` (or neutral element) of a polyadic system is a distinguished element e (and the corresponding 0-ary operation $\mu_0^{(e)}$) such that for any element $g \in G$ we have

$$\mu_n\left[g, e^{n-1}\right] = g, \tag{20}$$

where g can be on any place in the l.h.s. of (20).

In binary groups the identity is the only neutral element, while in polyadic systems, there exist `neutral polyads` $\boldsymbol{n}$ consisting of elements of G satisfying

$$\mu_n[g, \boldsymbol{n}] = g, \tag{21}$$

where g can be also on any place. The neutral polyads are determined not uniquely. It follows from (20) that the sequence of polyadic identities e^{n-1} is a neutral polyad.

An element of a polyadic system g is called ℓ_μ-`idempotent` (or simply `idempotent` for $\ell_\mu = 1$), if there exist such ℓ_μ that

$$g^{\langle \ell_\mu \rangle} = g. \tag{22}$$

Both zero and identity are ℓ_μ-idempotents with arbitrary ℓ_μ. We define the `(total) associativity` as invariance of the composition of two n-ary multiplications

$$\boldsymbol{\mu}_n^2[\boldsymbol{g}, \boldsymbol{h}, \boldsymbol{u}] = \mu_n[\boldsymbol{g}, \mu_n[\boldsymbol{h}], \boldsymbol{u}] = inv \tag{23}$$

under placement of the internal multiplication in r.h.s. with the fixed order of elements in the whole polyad of $(2n-1)$ elements $\boldsymbol{t}^{(2n-1)} = (\boldsymbol{g}, \boldsymbol{h}, \boldsymbol{u})$. Informally, "internal brackets/multiplication can be moved on any place", which gives n relations

$$\mu_n \circ \left(\mu_n \times \mathrm{id}^{\times(n-1)}\right) = \ldots = \mu_n \circ \left(\mathrm{id}^{\times(n-1)} \times \mu_n\right). \tag{24}$$

There are many other particular kinds of associativity which were introduced in [55] and studied in [56,57]. Here we will confine ourselves the most general total associativity (23). In this case, the iterating does not depend of the placement of internal multiplications in the r.h.s of (3).

A `polyadic semigroup` (`n-ary semigroup`) is a n-ary system which operation is associative, or $\mathrm{G}_n^{semigrp} = \langle G \mid \mu_n \mid \text{associativity} \rangle$.

In a polyadic system with zero (16) one can have the `trivial associativity`, when all n terms is (23) are equal to zero, i.e.

$$\boldsymbol{\mu}_n^2[\boldsymbol{g}] = z \tag{25}$$

for any $(2n-1)$-tuple $\boldsymbol{g}$. Therefore, we state that

Any 2-nilpotent n-ary system (having index of nilpotency $(2n-1)$) is a polyadic semigroup.

In the case of changing arity one should use in (25) not the changed final arity n', but the "real" arity which is n for the reducing case and $\ell_\mu (n-1)+1$ for all other cases. Let us give the examples.

In the mixed (interating-reducing) case with $n=2$, $\ell_\mu = 3$, $n_c = 1$, we have a ternary system $\langle G \mid \mu_3 \rangle$ iterated from a binary system $\left\langle G \mid \mu_2, \mu_0^{(c)} \right\rangle$ with one distinguished element c (or an additional 0-ary operation)[3]

$$\mu_3^{(c)}[g, h, u] = (g \cdot (h \cdot (u \cdot c))), \tag{26}$$

where for binary multiplication we denote $g \cdot h = \mu_2[g, h]$. Thus, if the ternary system $\left\langle G \mid \mu_3^{(c)} \right\rangle$ is nilpotent of index 7 (see 9), then it is a ternary semigroup (because $\mu_3^{(c)}$ is trivially associative) independently of associativity of μ_2 (see, e.g. [19]).

It is very important to find the `associativity preserving` conditions (constructions), when associative initial operation μ_n leads to associative final operation $\mu'_{n'}$ during the change of arity.

[3]This construction is named the b-derived groupoid in [54].

The associativity preserving reducing can be given by construction of the binary associative operation using $(n-2)$*-tuple* $\boldsymbol{c}$ *consisting of* $n_c = n-2$ *different constants*

$$\mu_2^{(\boldsymbol{c})}[g,h] = \mu_n[g,\boldsymbol{c},h]. \tag{27}$$

The associativity preserving mixing constructions with different arities and places were considered in [54, 57, 58].

An associative polyadic system with identity (20) is called a `polyadic monoid`.

The structure of any polyadic monoid is fixed [59]: it can be obtained by iterating of a binary operation [60] (for polyadic groups this was shown in [3]).

In polyadic systems, there are several analogs of binary commutativity. The most straightforward one comes from commutation of the multiplication with permutations.

A polyadic system is σ-`commutative`, if $\mu_n = \mu_n \circ \sigma$, or

$$\mu_n[\boldsymbol{g}] = \mu_n[\sigma \circ \boldsymbol{g}], \tag{28}$$

where $\sigma \circ \boldsymbol{g} = \left(g_{\sigma(1)}, \ldots, g_{\sigma(n)}\right)$ is a permutated polyad and σ is a fixed element of S_n, a permutation group of n elements. If (28) holds for all $\sigma \in S_n$, then a polyadic system is `commutative`.

A special type of the σ-commutativity

$$\mu_n[g,\boldsymbol{t},h] = \mu_n[h,\boldsymbol{t},g], \tag{29}$$

where $\boldsymbol{t}$ is any fixed $(n-2)$-polyad, is called `semicommutativity`. So for a n-ary semicommutative system we have

$$\mu_n\left[g,h^{n-1}\right] = \mu_n\left[h^{n-1},g\right]. \tag{30}$$

If a n-ary semigroup $\mathrm{G}^{semigrp}$ is iterated from a commutative binary semigroup with identity, then $\mathrm{G}^{semigrp}$ is semicommutative.

Let G *be the set of natural numbers* $\mathbb{N}$*, and the 5-ary multiplication is defined by*

$$\mu_5[\boldsymbol{g}] = g_1 - g_2 + g_3 - g_4 + g_5, \tag{31}$$

then $\mathrm{G}_5^{\mathbb{N}} = \langle \mathbb{N}, \mu_5 \rangle$ *is a semicommutative 5-ary monoid having the identity* $e_g = \mu_5\left[g^5\right] = g$ *for each* $g \in \mathbb{N}$*. Therefore,* $\mathrm{G}_5^{\mathbb{N}}$ *is the idempotent monoid.*

Another possibility is to generalize the binary `mediality` in semigroups

$$(g_{11} \cdot g_{12}) \cdot (g_{21} \cdot g_{22}) = (g_{11} \cdot g_{21}) \cdot (g_{12} \cdot g_{22}), \tag{32}$$

which, obviously, follows from the binary commutativity. But for n-ary systems they are different. It is seen that the mediality should contain $(n+1)$ multiplications, it is a relation between $n \times n$ elements, and therefore can be presented in a matrix from. The latter can be achieved by placing arguments of the external multiplication as a column.

A polyadic system is `medial` (or `entropic`), if [56, 61]

$$\mu_n\begin{bmatrix} \mu_n[g_{11},\ldots,g_{1n}] \\ \vdots \\ \mu_n[g_{n1},\ldots,g_{nn}] \end{bmatrix} = \mu_n\begin{bmatrix} \mu_n[g_{11},\ldots,g_{n1}] \\ \vdots \\ \mu_n[g_{1n},\ldots,g_{nn}] \end{bmatrix}. \tag{33}$$

For polyadic semigroups we use the notation (3) and can present the mediality as follows

$$\boldsymbol{\mu}_n^n[\boldsymbol{G}] = \boldsymbol{\mu}_n^n\left[\boldsymbol{G}^T\right], \tag{34}$$

where $\boldsymbol{G} = \|g_{ij}\|$ is the $n \times n$ matrix of elements and $\boldsymbol{G}^T$ is its transpose. The semicommutative polyadic semigroups are medial, as in the binary case, but, in general (except $n=3$) not vise versa [62]. A more general concept is σ-permutability [63], such that the mediality is its particular case with $\sigma = (1,n)$.

A polyadic system is `cancellative`, if

$$\mu_n[g,\boldsymbol{t}] = \mu_n[h,\boldsymbol{t}] \Longrightarrow g = h, \tag{35}$$

where g,h can be on any place. This means that the mapping μ_n is one-to-one in each variable. If g,h are on the same i-th place on both sides, the polyadic system is called i-`cancellative`.

The `left` and `right` cancellativity are 1-cancellativity and n-cancellativity respectively. A right and left cancellative n-ary semigroup is `cancellative` (with respect to the same subset).

A polyadic system is called (uniquely) i-`solvable`, if for all polyads $\boldsymbol{t}$, $\boldsymbol{u}$ and element h, one can (uniquely) resolve the equation (with respect to h) for the fundamental operation

$$\mu_n\left[\boldsymbol{u},h,\boldsymbol{t}\right]=g \tag{36}$$

where h can be on any i-th place.

A polyadic system which is uniquely i-solvable for *all* places i is called a n-`ary` (or `polyadic`) `quasigroup`.

It follows, that, if (36) uniquely i-solvable for all places, than

$$\boldsymbol{\mu}_n^{\ell_\mu}\left[\boldsymbol{u},h,\boldsymbol{t}\right]=g \tag{37}$$

can be (uniquely) resolved with respect to h being on any place.

An associative polyadic quasigroup is called a n-`ary` (or `polyadic`) `group`.

The above definition is the most general one, but it is overdetermined. Much work on polyadic groups was done [64] to minimize the set of axioms (solvability not in all places [5, 65], decreasing or increasing number of unknowns in determining equations [66]) or made it in terms of additionally defined objects (various analogs of identity and sequences [67]), as well as using not the total associativity, but various partial ones [57, 68, 69].

In a polyadic group the only solution of (36) is called a `querelement` of g and denoted by $\bar{g}$ [3], such that

$$\mu_n\left[\boldsymbol{h},\bar{g}\right]=g, \tag{38}$$

where $\bar{g}$ can be on any place. So, any idempotent g coincides with its querelement $\bar{g}=g$. It follows from (38) and (21), that the polyad

$$\boldsymbol{n}_g=\left(g^{n-2}\bar{g}\right) \tag{39}$$

is neutral for any element of a polyadic group, where $\bar{g}$ can be on any place. If this i-th place is important, then we write $\boldsymbol{n}_{g;i}$. The number of relations in (38) can be reduced from n (number of possible places) to only 2 (when g is on the first and last places [3, 70], or other 2 places). In a polyadic group the `Dörnte relations`

$$\mu_n\left[g,\boldsymbol{n}_{h;i}\right]=\mu_n\left[\boldsymbol{n}_{h;j},g\right]=g \tag{40}$$

hold valid for any allowable i,j. In the case of a binary group the relations (40) become $g\cdot h\cdot h^{-1}=h\cdot h^{-1}\cdot g=g$.

The relation (38) can be treated as a definitions of the unary `queroperation`

$$\bar{\mu}_1\left[g\right]=\bar{g}. \tag{41}$$

A `polyadic group` is a universal algebra

$$\mathrm{G}_n^{grp}=\left\langle G\mid\mu_n,\bar{\mu}_1\mid\text{associativity, Dörnte relations}\right\rangle, \tag{42}$$

where μ_n is n-ary associative operation and $\bar{\mu}_1$ is the queroperation.

A straightforward generalization of the queroperation concept and corresponding definitions can be made by substituting in the above formulas (38)–(41) the n-ary multiplication μ_n by the iterating multiplication $\boldsymbol{\mu}_n^{\ell_\mu}$ (3) (cf. [71] for $\ell_\mu=2$).

Let us define the `querpower` k of g recursively

$$\bar{g}^{\langle\langle k\rangle\rangle}=\overline{\left(\bar{g}^{\langle\langle k-1\rangle\rangle}\right)}, \tag{43}$$

where $\bar{g}^{\langle\langle 0\rangle\rangle}=g$, $\bar{g}^{\langle\langle 1\rangle\rangle}=\bar{g}$, or as the k composition $\bar{\mu}_1^{\circ k}=\overbrace{\bar{\mu}_1\circ\bar{\mu}_1\circ\ldots\circ\bar{\mu}_1}^{k}$ of the queroperation (41).

For instance [66], $\bar{\mu}_1^{\circ 2}=\boldsymbol{\mu}_n^{n-3}$, such that for any ternary group $\bar{\mu}_1^{\circ 2}=\mathrm{id}$, i.e. one has $\overline{\bar{g}}=g$. Using the queroperation in polyadic groups we can define the `negative polyadic power` of an element g by the following recursive relation

$$\mu_n\left[g^{\langle\ell_\mu-1\rangle},g^{n-2},g^{\langle-\ell_\mu\rangle}\right]=g, \tag{44}$$

or (after use of (17)) as a solution of the equation

$$\boldsymbol{\mu}_n^{\ell_\mu}\left[g^{\ell_\mu(n-1)},g^{\langle-\ell_\mu\rangle}\right]=g. \tag{45}$$

It is known that the querpower and the polyadic power are mutually connected [72]. Here, we reformulate this connection using the so called Heine numbers [73] or q-deformed numbers [74]

$$\left[\left[k\right]\right]_q=\frac{q^k-1}{q-1}, \tag{46}$$

which have the "nondeformed" limit $q \to 1$ as $[k]_q \to k$. Then

$$\bar{g}^{\langle\langle k\rangle\rangle} = g^{\left\langle -[[k]]_{2-n}\right\rangle}, \tag{47}$$

which can be treated as follows: the querpower coincides with the negative polyadic `deformed` power with the "deformation" parameter q which is equal to the "deviation" $(2-n)$ from the binary group.

HOMOMORPHISMS OF POLYADIC SYSTEMS

Let $\mathrm{G}_n = \langle G; \mu_n\rangle$ and $\mathrm{G}'_{n'} = \langle G'; \mu'_{n'}\rangle$ be two polyadic systems of any kind (quasigroup, semigroup, group, etc.). If they have the multiplications of the same arity $n = n'$, then one can define the mappings from G_n to G'_n. Usually such polyadic systems are `similar`, and we call mappings between them `the equiary mappings`.

Let us take $n+1$ mappings $\varphi_i^{GG'} : G \to G'$, $i = 1, \ldots, n+1$. An ordered system of mappings $\left\{\varphi_i^{GG'}\right\}$ is called a `homotopy` from G_n to G'_n, if

$$\varphi_{n+1}^{GG'}\left(\mu_n\left[g_1, \ldots, g_n\right]\right) = \mu'_n\left[\varphi_1^{GG'}\left(g_1\right), \ldots, \varphi_n^{GG'}\left(g_n\right)\right], \qquad g_i \in G. \tag{48}$$

In general, one should add to this definition the "mapping" of the multiplications

$$\mu_n \overset{\psi_{nn'}^{(\mu\mu')}}{\mapsto} \mu'_{n'}. \tag{49}$$

In such a way, the homotopy can be defined as the extended system of mappings $\left\{\varphi_i^{GG'}; \psi_{nn}^{(\mu\mu')}\right\}$.

The existence of the additional "mapping" $\psi_{nn}^{(\mu\mu')}$ acting on the second component of $\langle G; \mu_n\rangle$ is tacitly implied. We will write/mention the "mappings" $\psi_{nn'}^{(\mu\mu')}$ manifestly, e.g.,

$$\mathrm{G}_n \overset{\left\{\varphi_i^{GG'}; \psi_{nn}^{(\mu\mu')}\right\}}{\rightrightarrows} \mathrm{G}'_{n'}, \tag{50}$$

as needed only. If all the components $\varphi_i^{GG'}$ of a homotopy are bijections, it is called an `isotopy`. In case of polyadic quasigroups [56] all mappings $\varphi_i^{GG'}$ are usually taken as permutations of the same set $G = G'$. If the multiplications are also coincide $\mu_n = \mu'_n$, then $\left\{\varphi_i^{GG}; \mathrm{id}\right\}$ is called an `autotopy` of the polyadic system G_n. Various properties of the homotopy in universal algebras were studied, e.g. in [75, 76].

A `homomorphism` from G_n to G'_n is given, if there exists a mapping $\varphi^{GG'} : G \to G'$ satisfying

$$\varphi^{GG'}\left(\mu_n\left[g_1, \ldots, g_n\right]\right) = \mu'_n\left[\varphi^{GG'}\left(g_1\right), \ldots, \varphi^{GG'}\left(g_n\right)\right], \qquad g_i \in G. \tag{51}$$

Usually the homomorphism is denoted by the same one letter $\varphi^{GG'}$, while it would be more consistently to use for its notation the extended `pair` of mappings $\left\{\varphi^{GG'}; \psi_{nn}^{(\mu\mu')}\right\}$. We will use both notations on a par.

We, first, mention some small subset of known generalizations of the homomorphism (for bibliography till 1982 see, e.g., [77]) and then introduce a concrete construction for an analogous mapping which can change arity of the multiplication (fundamental operation) without introducing additional (term) operations. A general approach to mappings between free algebraic systems was initiated in [78], where the so-called basic mapping formulas for generators were introduced, and its generalization to many-sorted algebras was given in [79]. In [80] it was shown that the construction of all homomorphisms between similar polyadic systems can be reduced to some homomorphisms between corresponding mono-unary algebras [81]. The notion of the n-ary homomorphism as a sequence of n consequent homomorphisms φ_i, $i = 1, \ldots, n$, of n similar polyadic systems

$$\overbrace{\mathrm{G}_n \overset{\varphi_1}{\to} \mathrm{G}'_n \overset{\varphi_2}{\to} \ldots \overset{\varphi_{n-1}}{\to} \mathrm{G}''_n \overset{\varphi_n}{\to} \mathrm{G}'''_n}^{n} \tag{52}$$

(generalizing the Post n-adic substitutions [5]) was introduced in [82], and studied in [83, 84].

The above constructions do not change arity of polyadic systems, because they are based on the corresponding diagram which is a definition of an `equiary` mapping. To change arity one has to:

1) add another equiary diagram with `additional` operations using `the same` formula (51), both do not change arity;

2) use `one` modified (and not equiary) diagram and the underlying formula (51) by themselves, which will allow us to change arity `without` introducing additional operations.

The first way leads the concept of the `weak homomorphism` which was introduced in [85–87] for non-indexed algebras and in [88] for indexed algebras, then developed in [89] for Boolean and Post algebras, in [90] for coalgebras and F-algebras [91] (see also [92]). To define the weak homomorphism in our notation we should incorporate into the polyadic systems $\langle G;\mu_n\rangle$ and $\langle G';\mu'_{n'}\rangle$ the following additional term operations of opposite arity $\nu_{n'} : G^{\times n'} \to G$ and $\nu'_n : G'^{\times n} \to G'$ and consider `two` equiary mappings between $\langle G;\mu_n,\nu_{n'}\rangle$ and $\langle G';\mu'_{n'},\nu'_n\rangle$.

A `weak homomorphism` from $\langle G;\mu_n,\nu_{n'}\rangle$ to $\langle G',\mu'_{n'},\nu'_n\rangle$ is given, if there exists a mapping $\varphi^{GG'} : G \to G'$ satisfying `two` relations simultaneously

$$\varphi^{GG'}\left(\mu_n\left[g_1,\dots,g_n\right]\right) = \nu'_n\left[\varphi^{GG'}\left(g_1\right),\dots,\varphi^{GG'}\left(g_n\right)\right], \tag{53}$$

$$\varphi^{GG'}\left(\nu_{n'}\left[g_1,\dots,g_{n'}\right]\right) = \mu'_{n'}\left[\varphi^{GG'}\left(g_1\right),\dots,\varphi^{GG'}\left(g_{n'}\right)\right]. \tag{54}$$

If only one of the relations (53) or (54) takes place, such a mapping is called a `semi-weak homomorphism` [93]. If $\varphi^{GG'}$ is bijective, then it defines a `weak isomorphism`. Any weak epimorphism can be decomposed into a homomorphism and a weak isomorphism [94], therefore the study of weak homomorphisms reduces to weak isomorphisms (see also [95–97]).

MULTIPLACE MAPPINGS OF POLYADIC SYSTEMS

Let us turn to the second way of changing arity of the multiplication and use only one relation which we modify in some natural manner. First, recall that in any set G there always exists the additional distinguished mapping, viz. the identity id_G. We use the multiplication μ_n with its combination of id_G. We define an (ℓ_{id}-`intact`) `id-product` for the polyadic system $\langle G;\mu_n\rangle$ as

$$\mu_n^{(\ell_{\mathrm{id}})} = \mu_n \times \left(\mathrm{id}_G\right)^{\times \ell_{\mathrm{id}}}, \tag{55}$$

$$\mu_n^{(\ell_{\mathrm{id}})} : G^{\times(n+\ell_{\mathrm{id}})} \to G^{\times(1+\ell_{\mathrm{id}})}. \tag{56}$$

To indicate the exact i-th place of μ_n in r.h.s. of (55), we write $\mu_n^{(\ell_{\mathrm{id}})}(i)$, as needed. Here we use the id-product to generalize the homomorphism and consider mappings between polyadic systems of different arity. It follows from (56) that, if the image of the id-product is G alone, than $\ell_{\mathrm{id}} = 0$. Let us introduce a `multiplace mapping` $\Phi_k^{\binom{n,n'}{}}$ acting as follows

$$\Phi_k^{\binom{n,n'}{}} : G^{\times k} \to G'. \tag{57}$$

We are allowed to take only one upper $\Phi_k^{\binom{n,n'}{}}$, because of one G' in the upper right corner. Since we already know that the lower right corner is exactly $G'^{\times n'}$ (as a pre-image of one multiplication $\mu'_{n'}$), the lower horizontal arrow should be a product of n' multiplace mappings $\Phi_k^{\binom{n,n'}{}}$. So we can write a definition of a multiplace analog of the homomorphism which changes arity of the multiplication using one relation.

A k-`place heteromorphism` from G_n to $\mathrm{G}'_{n'}$ is given, if there exists a k-place mapping $\Phi_k^{\binom{n,n'}{}}$ (57) such that the corresponding defining equation (a modification of (51)) depends of the place i of μ_n in (55). For $i = 1$ it can read as

$$\Phi_k^{\binom{n,n'}{}}\begin{pmatrix}\mu_n\left[g_1,\dots,g_n\right]\\ g_{n+1}\\ \vdots\\ g_{n+\ell_{\mathrm{id}}}\end{pmatrix} = \mu'_{n'}\left[\Phi_k^{\binom{n,n'}{}}\begin{pmatrix}g_1\\ \vdots\\ g_k\end{pmatrix},\dots,\Phi_k^{\binom{n,n'}{}}\begin{pmatrix}g_{k(n'-1)}\\ \vdots\\ g_{kn'}\end{pmatrix}\right]. \tag{58}$$

This notion is motivated by [98, 99], where mappings between objects from different categories were considered and called chimera morphisms. See, also, [100].

In the particular case $n = 3$, $n' = 2$, $k = 2$, $\ell_{\mathrm{id}} = 1$ we have

$$\Phi_2^{(3,2)}\begin{pmatrix}\mu_3\left[g_1,g_2,g_3\right]\\ g_4\end{pmatrix} = \mu'_2\left[\Phi_2^{(3,2)}\begin{pmatrix}g_1\\ g_2\end{pmatrix},\Phi_2^{(3,2)}\begin{pmatrix}g_3\\ g_4\end{pmatrix}\right]. \tag{59}$$

This formula was used in the construction of the bi-element representations of ternary groups [19]. Consider the example.

Let $G = M_2^{adiag}(\mathbb{K})$, a set of antidiagonal 2×2 matrices over the field $\mathbb{K}$ and $G' = \mathbb{K}$, where $\mathbb{K} = \mathbb{R}, \mathbb{C}, \mathbb{Q}, \mathbb{H}$. The ternary multiplication μ_3 is a product of 3 matrices. Obviously, μ_3 is nonderived. For the elements $g_i = \begin{pmatrix} 0 & a_i \\ b_i & 0 \end{pmatrix}$, $i = 1, 2$, we construct a 2-place mapping $G \times G \to G'$ as

$$\Phi_2^{(3,2)} \begin{pmatrix} g_1 \\ g_2 \end{pmatrix} = a_1 a_2 b_1 b_2, \tag{60}$$

which satisfies (59). We can introduce a standard 1-place mapping by $\varphi(g_i) = a_i b_i$. It is important to note, that $\varphi(g_i)$ satisfies (51) for a commutative field $\mathbb{K}$ only $(= \mathbb{R}, \mathbb{C})$ becoming a homomorphism, and in this case we can have the relation between the heteromorhism $\Phi_2^{(3,2)}$ and the standard homomorphism

$$\Phi_2^{(3,2)} \begin{pmatrix} g_1 \\ g_2 \end{pmatrix} = \varphi(g_1) \cdot \varphi(g_2), \tag{61}$$

where the product $(\cdot)$ in l.h.s. is taken in $\mathbb{K}$, such that (51) and (59) coincide. For noncommutative field $\mathbb{K}$ $(= \mathbb{Q}$ or $\mathbb{H})$ we can define the heteromorphism (60) only.

A heteromorphism is called `derived`, if it can be expressed through ordinary (1-place) homomorphism. So, in the above example the heteromorphism is derived (by formula (61)) for a commutative field $\mathbb{K}$ and nonderived for a noncommutative one.

For arbitrary n a slightly modified construction (59) with still binary final arity, defined by $n' = 2$, $k = n-1$, $\ell_{\mathrm{id}} = n-2$,

$$\Phi_{n-1}^{(n,2)} \begin{pmatrix} \mu_n[g_1, \ldots, g_{n-1}, h_1] \\ h_2 \\ \vdots \\ h_{n-1} \end{pmatrix} = \mu_2' \left[\Phi_{n-1}^{(n,2)} \begin{pmatrix} g_1 \\ \vdots \\ g_{n-1} \end{pmatrix}, \Phi_{n-1}^{(n,2)} \begin{pmatrix} h_1 \\ \vdots \\ h_{n-1} \end{pmatrix} \right]. \tag{62}$$

was used in [53] to study representations of n-ary groups. However, no new results compared with [19] (other than changing 3 to n in some formulas) were obtained. This reflects the fact that a major role play the final arity n' and number of n-ary multiplications in l.h.s. of (59) and (62). In the above cases, the latter number was one, but can make it arbitrary below n.

A heteromorphism is called a ℓ_μ-`ple heteromorphism`, if it contains ℓ_μ multiplications in the argument of $\Phi_k^{(n,n')}$ in its defining relation. According this definition the mapping defined by (58) is the 1_μ-ple heteromorphism. So by analogy with (55)–(56) we define a ℓ_μ-`ple` ℓ_{id}-`intact id-product` for the polyadic system $\langle G; \mu_n \rangle$ as

$$\mu_n^{(\ell_\mu, \ell_{\mathrm{id}})} = (\mu_n)^{\times \ell_\mu} \times (\mathrm{id}_G)^{\times \ell_{\mathrm{id}}}, \tag{63}$$

$$\mu_n^{(\ell_\mu, \ell_{\mathrm{id}})} : G^{\times (n\ell_\mu + \ell_{\mathrm{id}})} \to G^{\times (\ell_\mu + \ell_{\mathrm{id}})}. \tag{64}$$

A ℓ_μ-`ple` k-`place heteromorphism` from G_n to $\mathrm{G}'_{n'}$ is given, if there exists a k-place mapping $\Phi_k^{(n,n')}$ (57). The corresponding `main heteromorphism equation` is

$$\Phi_k^{(n,n')} \begin{pmatrix} \left.\begin{matrix} \mu_n[g_1, \ldots, g_n], \\ \vdots \\ \mu_n[g_{n(\ell_\mu - 1)}, \ldots, g_{n\ell_\mu}] \end{matrix}\right\} \ell_\mu \\ \left.\begin{matrix} g_{n\ell_\mu + 1}, \\ \vdots \\ g_{n\ell_\mu + \ell_{\mathrm{id}}} \end{matrix}\right\} \ell_{\mathrm{id}} \end{pmatrix} = \mu_{n'}' \left[\Phi_k^{(n,n')} \begin{pmatrix} g_1 \\ \vdots \\ g_k \end{pmatrix}, \ldots, \Phi_k^{(n,n')} \begin{pmatrix} g_{k(n'-1)} \\ \vdots \\ g_{kn'} \end{pmatrix} \right]. \tag{65}$$

Obviously, we can consider various permutations of the multiplications in both sides, as further additional demands (associativity, commutativity, etc.), which will be considered below. The system of equation connecting initial and final arities is

$$kn' = n\ell_\mu + \ell_{\mathrm{id}}, \tag{66}$$

$$k = \ell_\mu + \ell_{\mathrm{id}}. \tag{67}$$

Excluding ℓ_μ or ℓ_{id}, we obtain two `arity changing formulas`, respectively

$$n' = n - \frac{n-1}{k} \ell_{\mathrm{id}}, \tag{68}$$

$$n' = \frac{n-1}{k} \ell_\mu + 1, \tag{69}$$

where $\frac{n-1}{k}\ell_{\mathrm{id}} \geq 1$ and $\frac{n-1}{k}\ell_{\mu} \geq 1$ are integer. The following inequalities hold valid

$$1 \leq \ell_{\mu} \leq k, \tag{70}$$

$$0 \leq \ell_{\mathrm{id}} \leq k-1, \tag{71}$$

$$\ell_{\mu} \leq k \leq (n-1)\,\ell_{\mu}, \tag{72}$$

$$2 \leq n' \leq n, \tag{73}$$

which are important for further classification of heteromorphisms. The main statement follows from (73):

The heteromorphism $\Phi_k^{(n,n')}$ defined by the relation (65) decreases arity of the multiplication.

Another important observation is the fact that only the id-product (63) with $\ell_{\mathrm{id}} \neq 0$ leads to change of the arity. In the extreme case, when k approaches its minimum, $k = k_{\min} = \ell_{\mu}$, the final arity approaches its maximum $n'_{\max} = n$, and the id-rpoduct becomes a product of ℓ_{μ} initial multiplications μ_n without id's, since now $\ell_{\mathrm{id}} = 0$ in (65). Therefore, we call a heteromorphism defined by (65) with $\ell_{\mathrm{id}} = 0$ `a` $k\,(=\ell_{\mu})$`-place homomorphism`. The ordinary homomorphism (48) corresponds to $k = \ell_{\mu} = 1$, and so it is really the 1-place homomorphism. An opposite extreme case, when the final arity approaches its minimum $n'_{\min} = 2$ (the final operation is binary), corresponds to the maximal value of k, that is $k = k_{\max} = (n-1)\,\ell_{\mu}$. The number of id's now is $\ell_{\mathrm{id}} = (n-2)\,\ell_{\mu} \geq 0$, which vanishes, when the initial operation is binary as well. This is the case of the ordinary homomorphism (48) for both binary operations $n' = n = 2$ and $k = \ell_{\mu} = 1$. We conclude that:

Any polyadic system can be mapped into a binary system by means of the special k-place ℓ_{μ}-ple heteromorphism $\Phi_k^{(n,n')}$, where $k = (n-1)\,\ell_{\mu}$ (we call it a `binarizing heteromorphism`) which is defined by (65) with $\ell_{\mathrm{id}} = (n-2)\,\ell_{\mu}$.

In the relation with the Gluskin-Hosszú theorem [7] (any n-ary group can be constructed by the special binary group and its homomorphism) our statement can be treated as an opposite one: *any n-ary system (not only a group) can be mapped into a binary system, but now using another construction, that is, the binarizing heteromorphism.*

The case of 1-ple binarizing heteromorphism ($\ell_{\mu} = 1$) corresponds to the formula (62). Further requirements (associativity, commutativity, etc.) will give additional relations between multiplications and $\Phi_k^{(n,n')}$, and fix the exact structure of (65). Thus, we arrive to the following

Classification of ℓ_{μ}-ple heteromorphisms:

1. $n' = n'_{\max} = n \Longrightarrow \Phi_k^{(n,n)}$ *is the ℓ_{μ}-place or* ***`multiplace homomorphism`****, i.e.,*

$$k = k_{\min} = \ell_{\mu}. \tag{74}$$

2. $2 < n' < n \Longrightarrow \Phi_k^{(n,n')}$ *is the* ***`intermediate heteromorphism`*** *with*

$$k = \frac{n-1}{n'-1}\ell_{\mu}. \tag{75}$$

In this case the number of intact elements is proportional to the number of multiplications

$$\ell_{\mathrm{id}} = \frac{n-n'}{n'-1}\ell_{\mu}. \tag{76}$$

3. $n' = n'_{\min} = 2 \Longrightarrow \Phi_k^{(n,2)}$ *is the $(n-1)\,\ell_{\mu}$-place (multiplace)* ***`binarizing heteromorphism`****, i.e.,*

$$k = k_{\max} = (n-1)\,\ell_{\mu}. \tag{77}$$

In the extreme (first and third) cases there are no restrictions on the initial arity n, while in the intermediate case n is "quantized" due to the fact that fractions in (68) and (69) should be integer. Thus, we have established a general structure and classification of heteromorphisms defined by (65). The next important issue is preservation of special properties (associativity, commutativity, etc.), while passing from μ_n to $\mu'_{n'}$, which will further restrict the concrete shape of the main relation (65) for each choice of the `heteromorphism parameters`: arities n, n', places k, number of intacts ℓ_{id} and multiplications ℓ_{μ}.

ASSOCIATIVITY AND HETEROMORPHISMS

The most important property of the heteromorphism, which is needed for its next applications in the representation theory, is associativity of the final operation $\mu'_{n'}$, when the initial operation μ_n is associative. In other words, here we consider the concrete form of semigroup heteromorphisms. In general, this is a complicated task, because it is not clear from (65), which permutation in l.h.s. should be taken to get an associative product in its r.h.s. for each set of the heteromorphism parameters. Straightforward checking of the associativity of the final operation $\mu'_{n'}$ for each permutation in l.h.s. of (65) is almost impossible, especially for higher n. To solve this difficulty we introduce the concept of the associative polyadic quiver and special rules to construct the associative final operation $\mu'_{n'}$.

A `polyadic quiver of product` is the set of elements from G_n (presented as several copies of some matrix of the elements glued together) and arrows, such that the elements along arrows form n-ary product μ_n. For instance, for the multiplication $\mu_4\left[g_1,h_2,g_2,u_1\right]$ the 4-adic quiver is denoted by $\{g_1 \to h_2 \to g_2 \to u_1\}$. Here the elements from G_n are arbitrary and have no connection with heteromorphisms.

Next we define `polyadic quivers` which are related to the main heteromorphism equation (65) in the following way: 1) the matrix of elements is the transposed matrix from r.h.s. of (65), such that different letters correspond to their place in $\Phi_k^{\left(n,n'\right)}$ and the low index of an element is related to its position in the $\mu'_{n'}$ product; 2) the number of polyadic quivers is ℓ_μ, which corresponds to ℓ_μ multiplications in the l.h.s. of (65); 3) the heteromorphism parameters (n, n', k, ℓ_{id} and ℓ_μ) are not arbitrary, but satisfy the arity changing formulas (68)-(69). In this way, a polyadic quiver makes clear visualization of the main heteromorphism equation (65); 4) The intact elements will be placed after semicolon.

For example, the polyadic quiver $\{g_1 \to h_2 \to g_2 \to u_1; h_1, u_2\}$ corresponds to the heteromorphism with $n=4$, $n'=2$, $k=3$, $\ell_{\mathrm{id}}=2$ and $\ell_\mu=1$ is

$$\Phi_3^{(4,2)}\begin{pmatrix}\mu_4\left[g_1,h_2,g_2,u_1\right]\\ h_1\\ u_2\end{pmatrix}=\mu'_2\left[\Phi_3^{(4,2)}\begin{pmatrix}g_1\\ h_1\\ u_1\end{pmatrix},\Phi_3^{(4,2)}\begin{pmatrix}g_2\\ h_2\\ u_2\end{pmatrix}\right]. \tag{78}$$

As it is seen from (78), the product μ'_2 is not associative, if μ_4 is associative. So, not all polyadic quivers preserve associativity.

An `associative polyadic quiver` is a polyadic quiver which ensures the final associativity of $\mu'_{n'}$ in the main heteromorphism equation (65), when the initial multiplication μ_n is associative.

So, one of the associative polyadic quivers which corresponds to the same heteromorphism parameters as the non-associative quiver (78) is $\{g_1 \to h_2 \to u_1 \to g_2; h_1, u_2\}$ which corresponds to

$$\Phi_3^{(4,2)}\begin{pmatrix}\mu_4\left[g_1,h_2,u_1,g_2\right]\\ h_1\\ u_2\end{pmatrix}=\mu'_2\left[\Phi_3^{(4,2)}\begin{pmatrix}g_1\\ h_1\\ u_1\end{pmatrix},\Phi_3^{(4,2)}\begin{pmatrix}g_2\\ h_2\\ u_2\end{pmatrix}\right]. \tag{79}$$

We propose the classification of associative polyadic quivers and the rules of construction of the corresponding heteromorphism equations, and use for the heteromorphism parameters the classification of ℓ_μ-ple heteromorphisms (75). In other words, we describe the consistent procedure of building the semigroup heteromorphisms.

Let us consider the first class of heteromorphisms (without intact elements $\ell_{\mathrm{id}}=0$ or `intactless`), that is ℓ_μ-place (multiplace) homomorphisms. In the simplest case, associativity can be reached, when all elements in a product are taken from the same row. The number of places k is not fixed by the arity relation (68) and can be arbitrary, while the arrows can have various directions. There are 2^k such combinations which preserve associativity. If the arrows have the same direction, this kind of mapping is also called homomorphism. As an example, for $n=n'=3$, $k=2$, $\ell_\mu=2$ we have

$$\Phi_2^{(3,3)}\begin{pmatrix}\mu_3\left[g_1,g_2,g_3\right]\\ \mu_3\left[h_1,h_2,h_3\right]\end{pmatrix}=\mu'_3\left[\Phi_2^{(3,3)}\begin{pmatrix}g_1\\ h_1\end{pmatrix},\Phi_2^{(3,3)}\begin{pmatrix}g_2\\ h_2\end{pmatrix},\Phi_2^{(3,3)}\begin{pmatrix}g_3\\ h_3\end{pmatrix}\right]. \tag{80}$$

Note that the analogous quiver with opposite arrow directions is

$$\Phi_2^{(3,3)}\begin{pmatrix}\mu_3\left[g_1,g_2,g_3\right]\\ \mu_3\left[h_3,h_2,h_1\right]\end{pmatrix}=\mu'_3\left[\Phi_2^{(3,3)}\begin{pmatrix}g_1\\ h_1\end{pmatrix},\Phi_2^{(3,3)}\begin{pmatrix}g_2\\ h_2\end{pmatrix},\Phi_2^{(3,3)}\begin{pmatrix}g_3\\ h_3\end{pmatrix}\right]. \tag{81}$$

The latter mapping was used in constructing the middle representations of ternary groups [19].

The important class of intactless heteromorphisms (with $\ell_{\mathrm{id}}=0$) preserving associativity can be constructed using analogy with the Post substitutions [5], and therefore we call it the `Post-like associative quiver`.

The number of places k is now fixed by $k=n-1$, while $n'=n$ and $\ell_\mu=k=n-1$. An example of the Post-like associative quiver with the same heteromorphisms parameters as in (80)-(81) is

$$\Phi_2^{(3,3)}\left(\begin{array}{c}\mu_3\left[g_1,h_2,g_3\right]\\ \mu_3\left[h_1,g_2,h_3\right]\end{array}\right)=\mu_3'\left[\Phi_2^{(3,3)}\left(\begin{array}{c}g_1\\ h_1\end{array}\right),\Phi_2^{(3,3)}\left(\begin{array}{c}g_2\\ h_2\end{array}\right),\Phi_2^{(3,3)}\left(\begin{array}{c}g_3\\ h_3\end{array}\right)\right]. \tag{82}$$

This construction appeared in the study of ternary semigroups of morphisms [101–103]. Its n-ary generalization was used in consideration of polyadic operations on Cartesian powers [104], polyadic analogs of the Cayley and Birkhoff theorems [84, 105] and special representations of n-groups [106, 107] (where the n-group with the multiplication μ_2' was called the `diagonal n-group`). Consider the example.

Let Λ be the Grassmann algebra consisting of even and odd parts $\Lambda=\Lambda_{\bar{0}}\oplus\Lambda_{\bar{1}}$ (see e.g., [108]). The odd part can be considered as a ternary semigroup $\mathrm{G}_3^{(\bar{1})}=\langle\Lambda_{\bar{1}},\mu_3\rangle$, its multiplication $\mu_3:\Lambda_{\bar{1}}\times\Lambda_{\bar{1}}\times\Lambda_{\bar{1}}\to\Lambda_{\bar{1}}$ is defined by $\mu_3\left[\alpha,\beta,\gamma\right]=\alpha\cdot\beta\cdot\gamma$, where $(\cdot)$ is multiplication in Λ and $\alpha,\beta,\gamma\in\Lambda_{\bar{1}}$, so $\mathrm{G}_3^{(\bar{1})}$ is nonderived and contains no unity. The even part can be treated as a ternary group $\mathrm{G}_3^{(\bar{0})}=\langle\Lambda_{\bar{0}},\mu_3'\rangle$ with the multiplication $\mu_3':\Lambda_{\bar{0}}\times\Lambda_{\bar{0}}\times\Lambda_{\bar{0}}\to\Lambda_{\bar{0}}$, defined by $\mu_3\left[a,b,c\right]=a\cdot b\cdot c$, where $a,b,c\in\Lambda_{\bar{0}}$, thus $\mathrm{G}_3^{(\bar{0})}$ is derived and contains unity. We introduce the heteromorphism $\mathrm{G}_3^{(\bar{1})}\to\mathrm{G}_3^{(\bar{0})}$ as a mapping (2-place homomorphism) $\Phi_2^{(3,3)}:\Lambda_{\bar{1}}\times\Lambda_{\bar{1}}\to\Lambda_{\bar{0}}$ by the formula

$$\Phi_2^{(3,3)}\left(\begin{array}{c}\alpha\\ \beta\end{array}\right)=\alpha\cdot\beta, \tag{83}$$

where $\alpha,\beta\in\Lambda_{\bar{1}}$. It is seen that $\Phi_2^{(3,3)}$ defined by (83) satisfies the Post-like heteromorphism equation (82), but not the "vertical" one (80), due to anticommutativity of odd elements from $\Lambda_{\bar{1}}$. In other words, $\mathrm{G}_3^{(\bar{0})}$ can be treated as a nontrivial example of the "diagonal" semigroup of $\mathrm{G}_3^{(\bar{1})}$ (according to the notation of [106, 107]).

Note that for $k\geq 3$ there exists additional (to the above) associative quivers having the same heteromorphisms parameters. For instance, when $n'=n=4$ and $k=3$ we have the Post-like associative quiver

$$\Phi_3^{(4,4)}\left(\begin{array}{c}\mu_4\left[g_1,h_2,u_3,g_4\right]\\ \mu_4\left[h_1,u_2,g_3,h_4\right]\\ \mu_4\left[u_1,g_2,h_3,u_4\right]\end{array}\right)=\mu_4'\left[\Phi_3^{(4,4)}\left(\begin{array}{c}g_1\\ h_1\\ u_1\end{array}\right),\Phi_3^{(4,4)}\left(\begin{array}{c}g_2\\ h_2\\ u_2\end{array}\right),\Phi_3^{(4,4)}\left(\begin{array}{c}g_1\\ h_1\\ u_1\end{array}\right),\Phi_3^{(4,4)}\left(\begin{array}{c}g_2\\ h_2\\ u_2\end{array}\right)\right]. \tag{84}$$

Also, we have one intermediate non-Post associative quiver

$$\Phi_3^{(4,4)}\left(\begin{array}{c}\mu_4\left[g_1,u_2,h_3,g_4\right]\\ \mu_4\left[h_1,g_2,u_3,h_4\right]\\ \mu_4\left[u_1,h_2,g_3,u_4\right]\end{array}\right)=\mu_4'\left[\Phi_3^{(4,4)}\left(\begin{array}{c}g_1\\ h_1\\ u_1\end{array}\right),\Phi_3^{(4,4)}\left(\begin{array}{c}g_2\\ h_2\\ u_2\end{array}\right),\Phi_3^{(4,4)}\left(\begin{array}{c}g_1\\ h_1\\ u_1\end{array}\right),\Phi_3^{(4,4)}\left(\begin{array}{c}g_2\\ h_2\\ u_2\end{array}\right)\right]. \tag{85}$$

The next type of heteromorphisms (intermediate) is described by the equations (66)-(76), it contains intact elements ($\ell_{\mathrm{id}}\geq 1$) and changes (decreases) arity $n'<n$. For each fixed k the arities are not arbitrary. There are many other possibilities (using permutations and different variants of quivers) to obtain an associative final product $\mu_{n'}'$ corresponding the same heteromorphism parameters. The above examples are sufficient to understand the rules of their construction for each concrete case.

MULTIPLACE REPRESENTATIONS OF POLYADIC SYSTEMS

The representation theory (see e.g. [109]) deals with mappings from abstract algebraic systems into linear systems, such that, e.g. linear operators in vector spaces, or into general (semi)groups of transformations of some set. In our notation, this means that in the mapping of polyadic systems (50) the final multiplication $\mu_{n'}'$ is a linear map. This leads to some restriction on the final polyadic structure $\mathrm{G}_{n'}'$, which are considered below.

Let V be a vector space over a field $\mathbb{K}$ (usually algebraically closed) and $\mathrm{End}\,V$ be a set of linear endomorphisms of V, which is in fact a binary group. In the standard way, a linear representation of a binary semigroup $\mathrm{G}_2=\langle G;\mu_2\rangle$ is a (1-place) map $\Pi_1:\mathrm{G}_2\to\mathrm{End}\,V$, such that Π_1 is a homomorphism

$$\Pi_1\left(\mu_2\left[g,h\right]\right)=\Pi_1\left(g\right)*\Pi_1\left(h\right), \tag{86}$$

where $g,h\in G$ and $(*)$ is the binary multiplication in $\mathrm{End}\,V$ (usually, it is a (semi)group with multiplication as composition of operators or product of matrices, if a basis is chosen). If G_2 is a binary group with the unity e, then we have the additional condition

$$\Pi_1\left(e\right)=\mathrm{id}_V. \tag{87}$$

We generalize these known formulas to corresponding polyadic systems along with the introduced above heteromorphism concept. Our general idea is to use the heteromorphism equation (65) instead of the standard

homomorphism equation (86), such that the arity of representation will be different from the arity of the initial polyadic system $n' \neq n$.

Consider the structure of the final n'-ary multiplication $\mu'_{n'}$ in (65), taking into account that the final polyadic system $\mathrm{G}'_{n'}$ should be constructed from $\mathrm{End}\, V$. The most natural and physically applicable way is to consider the binary $\mathrm{End}\, V$ and to put $\mathrm{G}'_{n'} = \mathrm{der}_{n'}(\mathrm{End}\, V)$, as it was proposed for the ternary case in [19]. In this way $\mathrm{G}'_{n'}$ becomes a derived n'-ary (semi)group of endomorphisms of V with the multiplication $\mu'_{n'} : (\mathrm{End}\, V)^{\times n'} \to \mathrm{End}\, V$, where

$$\mu'_{n'}[v_1, \ldots, v_{n'}] = v_1 * \ldots * v_{n'}, \quad v_i \in \mathrm{End}\, V. \tag{88}$$

Because the multiplication $\mu'_{n'}$ (88) is derived and therefore, associative by definition, we consider the associative initial polyadic systems (semigroups and groups) and the associativity preserving mappings, that are the special heteromorphisms constructed in the previous section.

Let $\mathrm{G}_n = \langle G; \mu_n \rangle$ be an associative n-ary polyadic system. By analogy with (57), we introduce the following k-place mapping

$$\Pi_k^{(n,n')} : G^{\times k} \to \mathrm{End}\, V. \tag{89}$$

`A multiplace representation` of an associative polyadic system G_n in a vector space V is given, if there exists a k-place mapping (89) which satisfies the (associativity preserving) heteromorphism equation (65), that is

$$\Pi_k^{(n,n')} \begin{pmatrix} \left.\begin{matrix} \mu_n[g_1, \ldots, g_n], \\ \vdots \\ \mu_n\left[g_{n(\ell_\mu - 1)}, \ldots, g_{n\ell_\mu}\right] \end{matrix}\right\} \ell_\mu \\ \left.\begin{matrix} g_{n\ell_\mu + 1}, \\ \vdots \\ g_{n\ell_\mu + \ell_{\mathrm{id}}} \end{matrix}\right\} \ell_{\mathrm{id}} \end{pmatrix} = \overbrace{\Pi_k^{(n,n')} \begin{pmatrix} g_1 \\ \vdots \\ g_k \end{pmatrix} * \ldots * \Pi_k^{(n,n')} \begin{pmatrix} g_{k(n'-1)} \\ \vdots \\ g_{kn'} \end{pmatrix}}^{n'}, \tag{90}$$

where $\mu_n^{(\ell_\mu, \ell_{\mathrm{id}})}$ is given by (63), ℓ_μ and ℓ_{id} are numbers of multiplications and intact elements in the l.h.s. of (90), respectively.

The exact permutation in the l.h.s. of (90) is given by the associative quiver presented in the previous section. The representation parameters (n, n', k, ℓ_μ `and` ℓ_{id}) in (90) are the same as the heteromorphism parameters, and they satisfy the same arity changing formulas (68) and (69). Therefore, a general classification of multiplace representations can be done by analogy with one of the heteromorphisms (74)–(77) as follows:

1. The `hom-like multiplace representation` which is a multiplace homomorphism with $n' = n'_{\max} = n$, without intact elements $l_{\mathrm{id}} = l_{\mathrm{id}}^{(\min)} = 0$, and minimal number of places
$$k = k_{\min} = \ell_\mu. \tag{91}$$

2. The `intact element multiplace representation` which is the intermediate heteromorphism with $2 < n' < n$ and the number of intact elements
$$l_{\mathrm{id}} = \frac{n - n'}{n' - 1} \ell_\mu. \tag{92}$$

3. The `binary multiplace representation` which is a binarizing heteromorphism (77) with $n' = n'_{\min} = 2$, maximal number of intact elements $l_{\mathrm{id}}^{(\max)} = (n-2)\,\ell_\mu$ and maximal number of places
$$k = k_{\max} = (n-1)\,\ell_\mu. \tag{93}$$

The multiplace representations for n-ary semigroups have no additional defining relations, as compared with (90). In case of n-ary groups, we need an analog of the "normalizing" relation (87). If the n-ary group has the unity e, then one can put

$$\Pi_k^{(n,n')} \left(\left.\begin{matrix} e \\ \vdots \\ e \end{matrix}\right\} k \right) = \mathrm{id}_V\,. \tag{94}$$

If there is no unity at all, one can "normalize" the multiplace representation, using analogy with (87) in the form

$$\Pi_1\left(h^{-1} * h\right) = \mathrm{id}_V, \tag{95}$$

as follows

$$\Pi_k^{(n,n')}\begin{pmatrix} \left.\begin{matrix}\bar{h}\\ \vdots \\ \bar{h}\end{matrix}\right\}\ell_\mu \\ \left.\begin{matrix}h\\ \vdots \\ h\end{matrix}\right\}\ell_{\mathrm{id}}\end{pmatrix} = \mathrm{id}_V, \tag{96}$$

for all $h \in \mathrm{G}_n$, where $\bar{h}$ is the querelement of h. The latter ones can be placed on any places in l.h.s. of (96) due to the Dörnte identities. Also, the multiplications in l.h.s. of (90) can change their place due to the same reason.

A general form of multiplace representations can be found by applying the Dörnte identities to each n-ary product in l.h.s. of (90). Than, using (96) we schematically have

$$\Pi_k^{(n,n')}\begin{pmatrix} g_1 \\ \vdots \\ g_k \end{pmatrix} = \Pi_k^{(n,n')}\begin{pmatrix} t_1 \\ \vdots \\ t_{\ell_\mu} \\ \left.\begin{matrix}g\\ \vdots \\ g\end{matrix}\right\}\ell_{\mathrm{id}} \end{pmatrix}, \tag{97}$$

where g is an arbitrary fixed element of the n-ary group and

$$t_a = \mu_n\left[g_{a1}, \dots, g_{an-1}, \bar{g}\right], \quad a = 1, \dots, \ell_\mu. \tag{98}$$

This is the special shape of some multiplace representations, while the concrete formula should be obtained in each case separately. Nevertheless, some conclusions can be done from (97). First, the equivalent classes on which $\Pi_k^{(n,n')}$ is constant are determined by fixing $\ell_\mu + 1$ elements, i.e. by the surface $t_a = const$, $g = const$. Second, some k-place representations of n-ary group can be reduced to ℓ_μ-place representations of its retract. In the case $\ell_\mu = 1$, multiplace representations of n-ary group derived from a binary group correspond to ordinary representations of the latter (see [19, 53]).

The above formulas describe various properties of multiplace representations, but they give no idea, how to build representations for concrete polyadic systems. The most common method of representation construction is using the concept of group action on a set. Below we extend this concept to the multiplace case, as it was done above for homomorphisms and representations.

MULTIACTIONS AND G-SPACES

Let $\mathrm{G}_n = \langle G; \mu_n \rangle$ be a polyadic system and X be a set. A (left) 1-place action of G_n on X is the external binary operation $\boldsymbol{\rho}_1^{(n)} : G \times \mathsf{X} \to \mathsf{X}$ such that it is consistent with the multiplication μ_n, i.e. composition of the binary operations $\boldsymbol{\rho}_1 \{g|\mathsf{x}\}$ gives the n-ary product, that is,

$$\boldsymbol{\rho}_1^{(n)}\left\{\mu_n\left[g_1, \dots g_n\right]|\mathsf{x}\right\} = \boldsymbol{\rho}_1^{(n)}\left\{g_1|\boldsymbol{\rho}_1^{(n)}\left\{g_2|\dots|\boldsymbol{\rho}_1^{(n)}\left\{g_n|\mathsf{x}\right\}\right\}\dots\right\}, \quad g_1, \dots, g_n \in G,\ \mathsf{x} \in \mathsf{X}. \tag{99}$$

If the polyadic system is n-ary group, then in addition to (99) it is implied the there exist such $e_x \in G$ (which may or may not coincide with the unity of G_n) that $\boldsymbol{\rho}_1^{(n)}\{e_x|\mathsf{x}\} = \mathsf{x}$ for all $\mathsf{x} \in \mathsf{X}$, and the mapping $\mathsf{x} \mapsto \boldsymbol{\rho}_1^{(n)}\{e_x|\mathsf{x}\}$ is a bijection of X. The right 1-place action of G_n on X is defined in the symmetric way, and therefore we will consider below only one of them. Obviously, that we cannot compose $\boldsymbol{\rho}_1^{(n)}$ and $\boldsymbol{\rho}_1^{(n')}$ with $n \neq n'$. Usually X is called a G-set or G-space depending of its properties (see, e.g., [110]).

The application of the 1-place action defined by (99) to the representation theory of n-ary groups gave mostly repetitions of the ordinary (binary) group representation results (except mentioning trivial b-derived ternary groups) [20]. Also, it is obviously seen that the construction (99) with the binary external operation $\boldsymbol{\rho}_1$ cannot be applied for studying the most important regular representations of polyadic systems, when the X coincides with G_n itself and the action arises from translations.

Here we introduce the multiplace concept of action for polyadic systems which is consistent with heteromorphisms and multiplace representations. Then we show, how it naturally appears when $\mathsf{X} = \mathrm{G}_n$ and apply it to construct examples of representations including the regular ones.

For a polyadic system $\mathrm{G}_n = \langle G; \mu_n \rangle$ and a set X we introduce an external polyadic operation

$$\boldsymbol{\rho}_k : G^{\times k} \times \mathsf{X} \to \mathsf{X}, \tag{100}$$

which is called a (left) k-`place action` or `multiaction`. To generalize the 1-action composition (99), we use the analogy with multiplication laws of the heteromorphisms (65) and the multiplace representations (90) and propose (schematically)

$$\boldsymbol{\rho}_k^{(n)}\left\{\begin{array}{c}\left.\begin{array}{c}\mu_n\left[g_1,\ldots,g_n\right],\\ \vdots\\ \mu_n\left[g_{n(\ell_\mu-1)},\ldots,g_{n\ell_\mu}\right]\end{array}\right\}\ell_\mu\\ \left.\begin{array}{c}g_{n\ell_\mu+1},\\ \vdots\\ g_{n\ell_\mu+\ell_{\mathrm{id}}}\end{array}\right\}\ell_{\mathrm{id}}\end{array}\right|\mathsf{x}\right\}=\boldsymbol{\rho}_k^{(n)}\overbrace{\left\{\begin{array}{c|c|c}g_1 & \ldots & \rho_k^{(n)}\left\{\begin{array}{c}g_{k(n'-1)}\\ \vdots\\ g_{kn'}\end{array}\right|\mathsf{x}\right\}\ldots\\ \vdots & & \\ g_k & & \end{array}\right\}}^{n'}. \tag{101}$$

The connection between all parameters here is the same as in the arity changing formulas (68)–(69). Composition of mappings is associative, therefore in concrete cases we can use the associative quiver technique, as it is described in the previous sections. If G_n is n-ary group, then we should add to (101) the "normalizing" relations analogous with (94) or (96). So, if there is a unity $e\in\mathrm{G}_n$, then

$$\boldsymbol{\rho}_k^{(n)}\left\{\begin{array}{c|c}e & \\ \vdots & \mathsf{x}\\ e & \end{array}\right\}=\mathsf{x},\qquad\text{for all }\ \mathsf{x}\in\mathsf{X}. \tag{102}$$

In terms of the querelement the normalization has the form

$$\boldsymbol{\rho}_k^{(n)}\left\{\begin{array}{c}\left.\begin{array}{c}\bar{h}\\ \vdots\\ \bar{h}\end{array}\right\}\ell_\mu\\ \left.\begin{array}{c}h\\ \vdots\\ h\end{array}\right\}\ell_{\mathrm{id}}\end{array}\right|\mathsf{x}\right\}=\mathsf{x},\qquad\text{for all }\ \mathsf{x}\in\mathsf{X}\ \text{ and for all }\ h\in\mathrm{G}_n. \tag{103}$$

The multiaction $\rho_k^{(n)}$ is `transitive`, if any two points x and y in X can be "connected" by $\rho_k^{(n)}$, i.e. there exist $g_1,\ldots,g_k\in G_n$ such that

$$\rho_k^{(n)}\left\{\begin{array}{c|c}g_1 & \\ \vdots & \mathsf{x}\\ g_k & \end{array}\right\}=\mathsf{y}. \tag{104}$$

If $g_1,\ldots,g_k$ are unique, then $\rho_k^{(n)}$ is `sharply transitive`. The subset of X, in which any points are connected by (104) with fixed $g_1,\ldots,g_k$ can be called the `multiorbit` of X. If there is only one multiorbit, then we call X the `heterogenous` G-space (by analogy with the homogeneous one). By analogy with the (ordinary) 1-place actions, we define a G-equivariant map Ψ between two G-sets X and Y by (in our notation)

$$\Psi\left(\rho_k^{(n)}\left\{\begin{array}{c|c}g_1 & \\ \vdots & \mathsf{x}\\ g_k & \end{array}\right\}\right)=\boldsymbol{\rho}_k^{(n)}\left\{\begin{array}{c|c}g_1 & \\ \vdots & \Psi\left(\mathsf{x}\right)\\ g_k & \end{array}\right\}\in\mathsf{Y}, \tag{105}$$

which makes G-space into a category (for details, see, e.g., [110]). In the particular case, when X is a vector space over $\mathbb{K}$, the multiaction (100) can be called a `multi-`G-module which satisfies (102) and the additional (linearity) conditions

$$\rho_k^{(n)}\left\{\begin{array}{c|c}g_1 & \\ \vdots & a\mathsf{x}+b\mathsf{y}\\ g_k & \end{array}\right\}=a\boldsymbol{\rho}_k^{(n)}\left\{\begin{array}{c|c}g_1 & \\ \vdots & \mathsf{x}\\ g_k & \end{array}\right\}+b\boldsymbol{\rho}_k^{(n)}\left\{\begin{array}{c|c}g_1 & \\ \vdots & \mathsf{y}\\ g_k & \end{array}\right\}, \tag{106}$$

where $a,b\in\mathbb{K}$. Then, comparing (90) and (101) we can define a multiplace representation as a multi-G-module by the following formula

$$\Pi_k^{(n,n')}\left(\begin{array}{c}g_1\\ \vdots\\ g_k\end{array}\right)\left(\mathsf{x}\right)=\boldsymbol{\rho}_k^{(n)}\left\{\begin{array}{c|c}g_1 & \\ \vdots & \mathsf{x}\\ g_k & \end{array}\right\}. \tag{107}$$

In a similar way, one can generalize to the polyadic systems many other notions of the group action theory [109].

REGULAR MULTIACTIONS

The most important role in the study of polyadic systems plays the case, when $\mathsf{X}=\mathrm{G}_n$, and the multiaction coincides with the n-ary analog of translations [111], so called i-translations [56]. In the binary case ordinary translations lead to the regular representations [109], therefore we call such action a `regular multiaction` $\boldsymbol{\rho}_k^{reg(n)}$. In this connection, the analog of the Cayley theorem for n-ary groups was obtained in [105, 112]. Now we show in examples, how the regular multiactions can arise from i-translations.

Let G_3 be a ternary semigroup, $k=2$, and $\mathsf{X}=\mathrm{G}_3$, then 2-place (left) action can be defined as

$$\boldsymbol{\rho}_2^{reg(3)}\left\{\begin{array}{c|c} g & \\ h & u\end{array}\right\}\stackrel{def}{=}\mu_3\left[g,h,u\right]. \tag{108}$$

This gives the following composition law for two regular multiactions

$$\boldsymbol{\rho}_2^{reg(3)}\left\{\begin{array}{c|c} g_1 & \\ h_1 & \boldsymbol{\rho}_2^{reg(3)}\left\{\begin{array}{c|c} g_2 & \\ h_2 & u\end{array}\right\}\end{array}\right\}=\mu_3\left[g_1,h_1,\mu_3\left[g_2,h_2,u\right]\right]$$

$$=\mu_3\left[\mu_3\left[g_1,h_1,g_2\right],h_2,u\right]=\boldsymbol{\rho}_2^{reg(3)}\left\{\begin{array}{c|c} \mu_3\left[g_1,h_1,g_2\right] & \\ h_2 & u\end{array}\right\}. \tag{109}$$

Thus, using the regular 2-action (108) we, in fact, derived the associative quiver corresponding to (59).

The formula (108) can be simultaneously treated as 2-translation [56]. In this way, the following `left regular multiaction`

$$\boldsymbol{\rho}_k^{reg(n)}\left\{\begin{array}{c|c} g_1 & \\ \vdots & h\\ g_k & \end{array}\right\}\stackrel{def}{=}\mu_n\left[g_1,\ldots,g_k,h\right], \tag{110}$$

corresponds to (62), where in r.h.s. there is the i-translation with $i=n$. The `right regular multiaction` corresponds to the i-translation with $i=1$. The binary composition of the left regular multiactions corresponds to (62). In general, the value of i fixes the minimal final arity n'_{reg} which differs for even and odd values of the initial arity n.

It follows from (110) that for regular multiactions the number of places is fixed

$$k_{reg}=n-1, \tag{111}$$

and the arity changing formulas (68)–(69) become

$$n'_{reg}=n-\ell_{\mathrm{id}} \tag{112}$$

$$n'_{reg}=\ell_\mu+1. \tag{113}$$

From (112)–(113) we conclude that for any n a regular multiaction having one multiplication $\ell_\mu=1$ is binarizing and has $n-2$ intact elements. For $n=3$ see (109). Also, it follows from (112) that for regular multiactions the number of intact elements gives exactly the difference between initial and final arities.

If the initial arity is odd, then there exist a special `middle regular multiaction` generated by the i-translation with $i=(n+1)/2$. For $n=3$ the corresponding associative quiver is (81) and such 2-actions were used in [19] to construct middle representations of ternary groups, which did not change arity ($n'=n$). Here we give a more complicated example of middle regular multiaction, which can contain intact elements and therefore can change arity.

Let us consider 5-ary semigroup and the following middle 4-action

$$\boldsymbol{\rho}_4^{reg(5)}\left\{\begin{array}{c|c} g & \\ h & \\ u & s\\ v & \end{array}\right\}=\mu_5\left[\begin{array}{c} \overset{i=3}{\overset{\downarrow}{s}}\\ g,h,\ \ ,u,v\end{array}\right]. \tag{114}$$

Using (113) we observe that there are two possibilities for the number of multiplications $\ell_\mu=2,4$. The last case $\ell_\mu=4$ is similar to the vertical associative quiver (81), but with more complicated l.h.s., that is

$$\boldsymbol{\rho}_4^{reg(5)}\left\{\begin{array}{c|c} \mu_5\left[g_1,h_1,g_2,h_2,g_3\right] & \\ \mu_5\left[h_3,g_4,h_4,g_5,h_5\right] & \\ \mu_5\left[u_5,v_5,u_4,v_4,u_3\right] & s\\ \mu_5\left[v_3,u_2,v_2,u_1,v_1\right] & \end{array}\right\}=$$

$$\boldsymbol{\rho}_4^{reg(5)}\left\{\begin{array}{c|c} g_1 & \\ h_1 & \\ u_1 & \boldsymbol{\rho}_4^{reg(5)}\left\{\begin{array}{c|c} g_2 & \\ h_2 & \\ u_2 & \boldsymbol{\rho}_4^{reg(5)}\left\{\begin{array}{c|c} g_3 & \\ h_3 & \\ u_3 & \boldsymbol{\rho}_4^{reg(5)}\left\{\begin{array}{c|c} g_4 & \\ h_4 & \\ u_4 & \boldsymbol{\rho}_4^{reg(5)}\left\{\begin{array}{c|c} g_5 & \\ h_5 & \\ u_5 & s\end{array}\right\}\end{array}\right\}\end{array}\right\}\end{array}\right\}\end{array}\right\}. \tag{115}$$

Now we have an additional case with two intact elements ℓ_{id} and two multiplications $\ell_\mu = 2$ as

$$\boldsymbol{\rho}_4^{reg(5)}\left\{\begin{array}{c}\mu_5\left[g_1,h_1,g_2,h_2,g_3\right]\\ h_3\\ \mu_5\left[h_3,v_3,u_2,v_2,u_1\right]\\ v_1\end{array}\middle|\, s\right\} = \boldsymbol{\rho}_4^{reg(5)}\left\{\begin{array}{c}g_1\\ h_1\\ u_1\\ v_1\end{array}\middle|\, \boldsymbol{\rho}_4^{reg(5)}\left\{\begin{array}{c}g_2\\ h_2\\ u_2\\ v_2\end{array}\middle|\, \boldsymbol{\rho}_4^{reg(5)}\left\{\begin{array}{c}g_3\\ h_3\\ u_3\\ v_3\end{array}\middle|\, s\right\}\right\}\right\}, \tag{116}$$

with changing arity from $n = 5$ to $n'_{reg} = 3$. In addition to (116) we have 3 more possible regular multiactions due to associativity of μ_5, when the multiplication brackets in the sequences of 6 elements in the first two rows and the second two ones can be shifted independently.

For $n > 3$, in addition to left, right and middle multiactions, there exist intermediate cases. First observe that the i-translations with $i = 2$ and $i = n-1$ immediately fix the final arity $n'_{reg} = n$. Therefore, the composition of multiactions will be similar to (115), but with some permutations in l.h.s.

Now we consider some multiplace analogs of regular representations of binary groups [109]. The straightforward generalization is considering the introduced regular multiactions (110) in the r.h.s. of (107). Let G_n be a finite polyadic associative system and $\mathbb{K}\mathrm{G}_n$ be a vector space spanned by G_n (some properties of n-ary group rings were considered in [113, 114]). This means that any element of $\mathbb{K}\mathrm{G}_n$ can be uniquely presented in the form $w = \sum_l a_l \cdot h_l$, $a_l \in \mathbb{K}$, $h_l \in G$. Then, using (110) and (107) we define the *i*-`regular` *k*-`place representation` by

$$\Pi_k^{reg(i)}\begin{pmatrix} g_1\\ \vdots\\ g_k\end{pmatrix}(w) = \sum_l a_l \cdot \mu_{k+1}\left[g_1\dots g_{i-1}h_l g_{i+1}\dots g_k\right]. \tag{117}$$

Comparing (110) and (117) one can conclude that all general properties of multiplace regular representations are similar to those of the regular multiactions. If $i = 1$ or $i = k$, the multiplace representation is called `right` or `left regular representation` correspondingly. If k is even, the representation with $i = k/2 + 1$ is called a `middle regular representation`. The case $k = 2$ was considered in [19] for ternary groups.

MULTIPLACE REPRESENTATIONS OF TERNARY GROUPS

Let us consider the case $n = 3$, $k = 2$ in more details paying attention on its special peculiarities, which corresponds to the 2-place (bi-element) representations of ternary groups [19]. Let V be a vector space over $\mathbb{K}$ and $\mathrm{End}\,V$ be a set of linear endomorphisms of V. From now on we denote the ternary multiplication by the square bracket only, as follows $\mu_3\left[g_1,g_2,g_3\right] \equiv [g_1g_2g_3]$, and use the "horizontal" notation $\Pi\begin{pmatrix} g_1\\ g_2\end{pmatrix} \equiv \Pi\left(g_1,g_2\right)$.

A `left representation` of a ternary group $G,[\,]$ in V is a map $\Pi^L : G\times G \to \mathrm{End}\,V$ such that

$$\Pi^L\left(g_1,g_2\right)\circ\Pi^L\left(g_3,g_4\right) = \Pi^L\left(\left[g_1g_2g_3\right],g_4\right), \tag{118}$$

$$\Pi^L\left(g,\overline{g}\right) = \mathrm{id}_V, \tag{119}$$

where $g,g_1,g_2,g_3,g_4 \in G$.

Replacing in (119) g by $\overline{g}$ we obtain $\Pi^L\left(\overline{g},g\right) = id_V$, which means that in fact (119) has the form $\Pi^L\left(\overline{g},g\right) = \Pi^L\left(g,\overline{g}\right) = \mathrm{id}_V$, $\forall g \in G$. Note that the axioms considered in the above definition are the natural ones satisfied by left multiplications $g \mapsto [abg]$. For all $g_1,g_2,g_3,g_4 \in G$ we have

$$\Pi^L\left(\left[g_1g_2g_3\right],g_4\right) = \Pi^L\left(g_1,\left[g_2g_3g_4\right]\right).$$

For all $g,h,u \in G$ we have

$$\Pi^L\left(g,h\right) = \Pi^L\left(\left[gu\overline{u}\right],h\right) = \Pi^L\left(g,u\right)\circ\Pi^L\left(\overline{u},h\right) \tag{120}$$

and

$$\Pi^L\left(g,u\right)\circ\Pi^L\left(\overline{u},\overline{g}\right) = \Pi^L\left(\overline{u},\overline{g}\right)\circ\Pi^L\left(g,u\right) = \mathrm{id}_V, \tag{121}$$

and therefore every $\Pi^L\left(g,u\right)$ is invertible and $\left(\Pi^L\left(g,u\right)\right)^{-1} = \Pi^L\left(\overline{u},\overline{g}\right)$. This means that any left representation gives a representation of a ternary group by a binary group [19]. If the ternary group is medial, then

$$\Pi^L\left(g_1,g_2\right)\circ\Pi^L\left(g_3,g_4\right) = \Pi^L\left(g_3,g_4\right)\circ\Pi^L\left(g_1,g_2\right),$$

i.e. obtained group is commutative. If the ternary group $\langle G,[\,]\rangle$ is commutative, then also $\Pi^L\left(g,h\right) = \Pi^L\left(h,g\right)$, because

$$\Pi^L\left(g,h\right) = \Pi^L\left(g,h\right)\circ\Pi^L\left(g,\overline{g}\right) = \Pi^L\left(\left[g\,h\,g\right],\overline{g}\right) = \Pi^L\left(\left[h\,g\,g\right],\overline{g}\right) = \Pi^L\left(h,g\right)\circ\Pi^L\left(g,\overline{g}\right) = \Pi^L\left(h,g\right).$$

In the case of the commutative and idempotent ternary group any its left representation is idempotent and $\left(\Pi^L(g,h)\right)^{-1} = \Pi^L(g,h)$, so that commutative and idempotent ternary groups are represented by Boolean groups.

Let $\langle G,[\,]\rangle = \mathrm{der}\,(G,\odot)$ be a ternary group derived from a binary group $\langle G,\odot\rangle$, then there is one-to-one correspondence between representations of $(G,\odot)$ and left representations of $(G,[\,])$.

Indeed, because $(G,[\,]) = \mathrm{der}\,(G,\odot)$, then $g\odot h = [geh]$ and $\overline{e} = e$, where e is unity of the binary group $(G,\odot)$. If $\pi \in \mathrm{Rep}\,(G,\odot)$, then (as it is not difficult to see) $\Pi^L(g,h) = \pi(g)\circ\pi(h)$ is a left representation of $\langle G,[\,]\rangle$. Conversely, if Π^L is a left representation of $\langle G,[\,]\rangle$ then $\pi(g) = \Pi^L(g,e)$ is a representation of $(G,\odot)$. Moreover, in this case $\Pi^L(g,h) = \pi(g)\circ\pi(h)$, because we have

$$\Pi^L(g,h) = \Pi^L(g,[ehe]) = \Pi^L([geh],e) = \Pi^L(g,e)\circ\Pi^L(h,e) = \pi(g)\circ\pi(h).$$

Let $(G,[\,])$ be a ternary group and $(G\times G,*)$ be a semigroup used to the construction of left representations. According to Post [5] one says that two pairs (a,b), (c,d) of elements of G are equivalent, if there exists an element $g\in G$ such that $[abg] = [cdg]$. Using a covering group we can see that if this equation holds for some $g\in G$, then it holds also for all $g\in G$. This means that

$$\Pi^L(a,b) = \Pi^L(c,d) \Longleftrightarrow (a,b)\sim(c,d),$$

i.e.

$$\Pi^L(a,b) = \Pi^L(c,d) \Longleftrightarrow [abg] = [cdg]$$

for some $g\in G$. Indeed, if $[abg] = [cdg]$ holds for some $g\in G$, then

$$\begin{aligned}\Pi^L(a,b) &= \Pi^L(a,b)\circ\Pi^L(g,\overline{g}) = \Pi^L([abg],\overline{g})\\ &= \Pi^L([cdg],\overline{g}) = \Pi^L(c,d)\circ\Pi^L(g,\overline{g}) = \Pi^L(c,d).\end{aligned}$$

By analogy we can define

A `right representation` of a ternary group $(G,[\,])$ in V is a map $\Pi^R : G\times G\to \mathrm{End}\,V$ such that

$$\Pi^R(g_3,g_4)\circ\Pi^R(g_1,g_2) = \Pi^R(g_1,[g_2g_3g_4]), \tag{122}$$

$$\Pi^R(g,\overline{g}) = \mathrm{id}_V, \tag{123}$$

where $g,g_1,g_2,g_3,g_4\in G$.

From (122)-(123) it follows that

$$\Pi^R(g,h) = \Pi^R(g,[u\,\overline{u}\,h]) = \Pi^R(\overline{u},h)\circ\Pi^R(g,u). \tag{124}$$

It is easy to check that $\Pi^R(g,h) = \Pi^L\left(\overline{h},\overline{g}\right) = \left(\Pi^L(g,h)\right)^{-1}$. So it is enough to consider only left representations (as in binary case). Consider the following example of group algebra ternary generalization [19].

Let G be a ternary group and $\mathbb{K}G$ be a vector space spanned by G, which means that any element of $\mathbb{K}G$ can be uniquely presented in the form $t = \sum_{i=1}^n k_ih_i$, $k_i\in\mathbb{K}$, $h_i\in G$, $n\in\mathbb{N}$ (we do not assume that G has finite rank). Then left and right regular representations are defined by

$$\Pi^L_{reg}(g_1,g_2)\,t = \sum_{i=1}^n k_i\,[g_1g_2h_i], \tag{125}$$

$$\Pi^R_{reg}(g_1,g_2)\,t = \sum_{i=1}^n k_i\,[h_ig_1g_2]. \tag{126}$$

Let us construct the middle representations as follows.

A `middle representation` of a ternary group $\langle G,[\,]\rangle$ in V is a map $\Pi^M : G\times G\to\mathrm{End}\,V$ such that

$$\Pi^M(g_3,h_3)\circ\Pi^M(g_2,h_2)\circ\Pi^M(g_1,h_1) = \Pi^M([g_3g_2g_1],[h_1h_2h_3]), \tag{127}$$

$$\Pi^M(g,h)\circ\Pi^M\left(\overline{g},\overline{h}\right) = \Pi^M\left(\overline{g},\overline{h}\right)\circ\Pi^M(g,h) = \mathrm{id}_V \tag{128}$$

It is seen that a middle representation is a ternary group homomorphism $\Pi^M : G\times G^{op}\to \mathrm{der}\,\mathrm{End}\,V$. Note that instead of (128) one can use $\Pi^M\left(g,\overline{h}\right)\circ\Pi^M(\overline{g},h) = id_V$ after changing g to $\overline{g}$ and taking into account that $g = \overline{\overline{g}}$. In the case idempotents elements g and h we have $\Pi^M(g,h)\circ\Pi^M(g,h) = id_V$, which means that the matrices Π^M are Boolean. Thus all middle representation matrices of idempotent ternary groups are Boolean. The composition $\Pi^M(g_1,h_1)\circ\Pi^M(g_2,h_2)$ is not a middle representation, but the following proposition holds.

Let Π^M is a middle representation of a ternary group $\langle G,[\,]\rangle$, then, if $\Pi^L_u(g,h)=\Pi^M(g,u)\circ\Pi^M(h,\overline{u})$ is a left representation of $\langle G,[\,]\rangle$, then $\Pi^L_u(g,h)\circ\Pi^L_{u'}(g',h')=\Pi^L_{u'}([ghu'],h')$, and, if $\Pi^R_u(g,h)=\Pi^M(u,h)\circ\Pi^M(\overline{u},g)$ is a right representation of $\langle G,[\,]\rangle$, then $\Pi^R_u(g,h)\circ\Pi^R_{u'}(g',h')=\Pi^R_u(g,[hg'h'])$. In particular, Π^L_u (Π^R_u) is a family of left (right) representations.

If a middle representation Π^M of a ternary group $\langle G,[\,]\rangle$ satisfies $\Pi^M(g,\overline{g})=\mathrm{id}_V$ for all $g\in G$, then it is a left and right representation and $\Pi^M(g,h)=\Pi^M(h,g)$ for all $g,h\in G$. Note that in general $\Pi^M_{reg}(g,\overline{g})\neq\mathrm{id}$. For regular representations we have the following commutation relations

$$\Pi^L_{reg}(g_1,h_1)\circ\Pi^R_{reg}(g_2,h_2)=\Pi^R_{reg}(g_2,h_2)\circ\Pi^L_{reg}(g_1,h_1).$$

Let $\langle G,[\,]\rangle$ be a ternary group and let $\langle G\times G,[\,]'\rangle$ be a ternary group used to the construction of the middle representation. In $\langle G,[\,]\rangle$, and in the consequence in $\langle G\times G,[\,]'\rangle$, we define the relation

$$(a,b)\sim(c,d)\Longleftrightarrow[aub]=[cud]$$

for all $u\in G$. It is not difficult to see that this relation is a congruence in a ternary group $\langle G\times G,[\,]'\rangle$. For regular representations $\Pi^M_{reg}(a,b)=\Pi^M_{reg}(c,d)$ if $(a,b)\sim(c,d)$. We have the following relation

$$a\approx a'\Longleftrightarrow a=[\overline{g}a'g]\ \text{ for some }\ g\in G$$

or equivalently

$$a\approx a'\Longleftrightarrow a'=[ga\overline{g}]\ \text{ for some }\ g\in G.$$

It is not difficult to see that it is an equivalence relation on $\langle G,[\,]\rangle$, moreover, if $\langle G,[\,]\rangle$ is medial, then this relation is a congruence.

Let $\langle G\times G,[\,]'\rangle$ be a ternary group used for a construction of middle representations, then

$$\begin{aligned}(a,b)\approx(a',b)\Longleftrightarrow a'=[ga\overline{g}]\ \text{ and}\\ b'=[hb\overline{b}]\ \text{ for some }\ (g,h)\in G\times G\end{aligned}$$

is an equivalence relation on $\langle G\times G,[\,]'\rangle$. Moreover, if $(G,[\,])$ is medial, then this relation is a congruence. Unfortunately, it is a weak relation. In a ternary group $\mathbb{Z}_3$, where $[ghu]=(g-h+u)\,(\mathrm{mod}\,3)$ we have only one class, i.e. all elements are equivalent. In $\mathbb{Z}_4$ with the operation $[ghu]=(g+h+u+1)\,(\mathrm{mod}\,4)$ we have $a\approx a'\Longleftrightarrow a=a'$. But for this relation holds the following statement. If $(a,b)\approx(a',b')$, then

$$\mathrm{tr}\,\Pi^M(a,b)=\mathrm{tr}\,\Pi^M(a',b').$$

We have $\mathrm{tr}(AB)=\mathrm{tr}(BA)$ for all $A,B\in\mathrm{End}V$, and

$$\begin{aligned}\mathrm{tr}\,\Pi^M(a,b)&=\mathrm{tr}\,\Pi^M([ga'\overline{g}],[hb'\overline{h}])=\mathrm{tr}\left(\Pi^M(g,\overline{h})\circ\Pi^M(a',b')\circ\Pi^M(\overline{g},h)\right)\\&=\mathrm{tr}\left(\Pi^M(g,\overline{h})\circ\Pi^M(\overline{g},h)\circ\Pi^M(a',b')\right)=\mathrm{tr}\left(id_V\circ\Pi^M(a'b')\right)=\mathrm{tr}\,\Pi^M(a',b')\end{aligned}$$

In our derived case the connection with the standard group representations is given by the following. Let $(G,\odot)$ be a binary group, and the ternary derived group as $\langle G,[\,]\rangle=\mathrm{der}\,(G,\odot)$. There is one-to-one correspondence between a pair of commuting binary groups representations and a middle ternary derived group representation. Indeed, let $\pi,\rho\in Rep\,(G,\odot)$, $\pi(g)\circ\rho(h)=\rho(h)\circ\pi(g)$ and $\Pi^L\in Rep\,(G,[\,])$. We take

$$\Pi^M(g,h)=\pi(g)\circ\rho\left(h^{-1}\right),\quad\pi(g)=\Pi^M(g,e),\quad\rho(g)=\Pi^M(e,\overline{g}).$$

Then using (127) we prove the needed representation laws.

Let $\langle G,[\,]\rangle$ be a fixed ternary group, $\langle G\times G,[\,]'\rangle$ a corresponding ternary group used in the construction of middle representations, $((G\times G)^*,\circledast)$ a covering group of $\langle G\times G,[\,]'\rangle$, $(G\times G,\diamond)=\mathrm{ret}_{(a,b)}(G\times G,\langle\,\rangle)$. If $\Pi^M(a,b)$ is a middle representation of $\langle G,[\,]\rangle$, then π defined by

$$\pi(g,h,0)=\Pi^M(g,h),\quad\pi(g,h,1)=\Pi^M(g,h)\circ\Pi^M(a,b)$$

is a representation of the covering group [5]. Moreover

$$\rho(g,h)=\Pi^M(g,h)\circ\Pi^M(a,b)=\pi(g,h,1)$$

is a representation of the above retract induced by (a,b). Indeed, $(\overline{a},\overline{b})$ is the identity of this retract and $\rho(\overline{a},\overline{b})=\Pi^M(\overline{a},\overline{b})\circ\Pi^M(a,b)=\mathrm{id}_V$. Similarly

$$\begin{aligned}\rho\left((g,h)\diamond(u,u)\right)&=\rho\left(\langle(g,h),(a,b),(u,u)\rangle\right)=\rho\left([gau],[ubh]\right)=\Pi^M\left([gau],[ubh]\right)\circ\Pi^M(a,b)\\&=\Pi^M(g,h)\circ\Pi^M(a,b)\circ\Pi^M(u,u)\circ\Pi^M(a,b)=\rho(g,h)\circ\rho(u,u)\end{aligned}$$

But $\tau(g)=(g,\overline{g})$ is an embedding of $(G,[\,])$ into $\langle G\times G,[\,]'\rangle$. Hence μ defined by $\mu(g,0)=\Pi^M(g,\overline{g})$ and $\mu(g,1)=\Pi^M(g,\overline{g})\circ\Pi^M(a,\overline{a})$ is a representation of a covering group G^* for $(G,[\,])$ (see the Post theorem [5] for $a=c$). On the other hand, $\beta(g)=\Pi^M(g,\overline{g})\circ\Pi^M(a,\overline{a})$ is a representation of a binary retract $(G,\cdot)=\mathrm{ret}_a(G,[\,])$. That β can induce some middle representation of $(G,[\,])$ (by Gluskin-Hosszú theorem [7]).

Note that in a ternary group of the quaternions $\langle\mathbb{K},[\,]\rangle$ (with norm 1), where $[ghu]=ghu(-1)=-ghu$ and gh is a multiplication of quaternions (-1 is a central element) we have $\overline{1}=-1$, $\overline{-1}=1$ and $\overline{g}=g$ for others. In $\langle\mathbb{K}\times\mathbb{K},[\,]'\rangle$ we have $(a,b)\sim(-a,-b)$ and $(a,-b)\sim(-a,b)$, which gives 32 two-elements equivalence classes. The embedding $\tau(g)=(g,\overline{g})$ suggest that $\Pi^M(i,i)=\pi(i)\neq\pi(-i)=\Pi^M(-i,-i)$. Generally $\Pi^M(a,b)\neq\Pi^M(-a,-b)$ and $\Pi^M(a,-b)\neq\Pi^M(-a,b)$.

The relation $(a,b)\sim(c,d)\Longleftrightarrow[abg]=[cdg]$ for all $g\in G$ is a congruence on $(G\times G,*)$. Note that this relation can be defined as "for some g". Indeed, using a covering group we can see that if $[abg]=[cdg]$ holds for some g then holds also for all g. Thus $\pi^L(a,b)=\Pi^L(c,d)\Longleftrightarrow(a,b)\sim(c,d)$. Indeed

$$\begin{aligned}\Pi^L(a,b)&=\Pi^L(a,b)\circ\Pi^L(g,\overline{g})=\Pi^L([a\ b\ g],\overline{g})\\&=\Pi^L([c\ d\ g],\overline{g})=\Pi^L(c,d)\circ\Pi^L(g,\overline{g})=\Pi^L(c,d).\end{aligned}$$

We conclude, that every left representation of a commutative group $\langle G,[\,]\rangle$ is a middle representation. Indeed,

$$\Pi^L(g,h)\circ\Pi^L(\overline{g},\overline{h})=\Pi^L([g\ h\ \overline{g}],\overline{h})=\Pi^L([g\ \overline{g}\ h],\overline{h})=\Pi^L(h,\overline{h})=\mathrm{id}_V$$

and

$$\begin{aligned}\Pi^L(g_1,g_2)\circ\Pi^L(g_3,g_4)\circ\Pi^L(g_5,g_6)&=\Pi^L([[g_1g_2g_3]g_4g_5],g_6)=\Pi^L([[g_1g_3g_2]g_4g_5],g_6)=\Pi^L([g_1g_3[g_2g_4g_5]],g_6)\\&=\Pi^L([g_1g_3[g_5g_4g_2]],g_6)=\Pi^L([g_1g_3g_5],[g_4g_2g_6])=\Pi^L([g_1g_3g_5],[g_6g_4g_2]).\end{aligned}$$

Note that the converse holds only for the special kind of middle representations such that $\Pi^M(g,\overline{g})=\mathrm{id}_V$. Therefore,

There is one-one-correspondence between left representations of $\langle G,[\,]\rangle$ *and binary representations of the retract* $\mathrm{ret}_a(G,[\,])$.

Indeed, let $\Pi^L(g,a)$ is given, then define $\rho(g)=\Pi^L(g,a)$ is such representation of the retract which can be directly shown. Conversely, assume that $\rho(g)$ is a representation of the retract $\mathrm{ret}_a(G,[\,])$. Define $\Pi^L(g,h)=\rho(g)\circ\rho(\overline{h})^{-1}$, then $\Pi^L(g,h)\circ\Pi^L(u,u)=\rho(g)\circ\rho(\overline{h})^{-1}\circ\rho(u)\circ\rho(\overline{u})^{-1}=\rho(g\circledast(\overline{h})^{-1}\circ\circledast u)\circ\rho(\overline{u})^{-1}=\rho([[g\,a\,[\overline{a}\,h\,\overline{a}]]\,a\,u])\circ\rho(\overline{u})^{-1}=\rho([g\,h\,g])\circ\rho(\overline{u})^{-1}=\Pi^L([g\,h\,u],u)$,

MATRIX REPRESENTATIONS OF TERNARY GROUPS

Here we give several examples of matrix representations for concrete ternary groups. Let $G=\mathbb{Z}_3\ni\{0,1,2\}$ and the ternary multiplication is $[ghu]=g-h+u$. Then $[ghu]=[uhg]$ and $\overline{0}=0$, $\overline{1}=1$, $\overline{2}=2$, therefore $(G,[\,])$ is an idempotent medial ternary group. Thus $\Pi^L(g,h)=\Pi^R(h,g)$ and

$$\Pi^L(a,b)=\Pi^L(c,d)\Longleftrightarrow(a-b)=(c-d)\mathrm{mod}\,3. \tag{129}$$

The calculations give the left regular representation in the manifest matrix form

$$\Pi^L_{reg}(0,0)=\Pi^L_{reg}(2,2)=\Pi^L_{reg}(1,1)=\Pi^R_{reg}(0,0)=\Pi^R_{reg}(2,2)=\Pi^R_{reg}(1,1)=\begin{pmatrix}1&0&0\\0&1&0\\0&0&1\end{pmatrix}=[1]\oplus[1]\oplus[1], \tag{130}$$

$$\begin{aligned}\Pi^L_{reg}(2,0)=\Pi^L_{reg}(1,2)=\Pi^L_{reg}(0,1)=\Pi^R_{reg}(2,1)=\Pi^R_{reg}(1,0)=\Pi^R_{reg}(0,2)&=\begin{pmatrix}0&1&0\\0&0&1\\1&0&0\end{pmatrix}\\&=[1]\oplus\begin{pmatrix}-\frac{1}{2}&-\frac{\sqrt{3}}{2}\\\frac{\sqrt{3}}{2}&-\frac{1}{2}\end{pmatrix}=[1]\oplus\left[-\frac{1}{2}+\frac{1}{2}i\sqrt{3}\right]\oplus\left[-\frac{1}{2}-\frac{1}{2}i\sqrt{3}\right],\end{aligned} \tag{131}$$

$$\begin{aligned}\Pi^L_{reg}(2,1)=\Pi^L_{reg}(1,0)=\Pi^L_{reg}(0,2)=\Pi^R_{reg}(2,0)=\Pi^R_{reg}(1,2)=\Pi^R_{reg}(0,1)&=\begin{pmatrix}0&0&1\\1&0&0\\0&1&0\end{pmatrix}\\&=[1]\oplus\begin{pmatrix}-\frac{1}{2}&\frac{\sqrt{3}}{2}\\-\frac{\sqrt{3}}{2}&-\frac{1}{2}\end{pmatrix}=[1]\oplus\left[-\frac{1}{2}-\frac{1}{2}i\sqrt{3}\right]\oplus\left[-\frac{1}{2}+\frac{1}{2}i\sqrt{3}\right].\end{aligned} \tag{132}$$

Consider the middle representation construction. The middle regular representations is defined by

$$\Pi^M_{reg}\,(g_1,g_2)\,t=\sum_{i=1}^{n}k_i\,[g_1h_ig_2]\,.$$

For regular representations we have

$$\Pi^M_{reg}\,(g_1,h_1)\circ\Pi^R_{reg}\,(g_2,h_2)=\Pi^R_{reg}\,(h_2,h_1)\circ\Pi^M_{reg}\,(g_1,g_2)\,, \tag{133}$$

$$\Pi^M_{reg}\,(g_1,h_1)\circ\Pi^L_{reg}\,(g_2,h_2)=\Pi^L_{reg}\,(g_1,g_2)\circ\Pi^M_{reg}\,(h_2,h_1)\,. \tag{134}$$

For the middle regular representation matrices we obtain

$$\Pi^M_{reg}\,(0,0)=\Pi^M_{reg}\,(1,2)=\Pi^M_{reg}\,(2,1)=\begin{pmatrix}1&0&0\\0&0&1\\0&1&0\end{pmatrix},$$

$$\Pi^M_{reg}\,(0,1)=\Pi^M_{reg}\,(1,0)=\Pi^M_{reg}\,(2,2)=\begin{pmatrix}0&1&0\\1&0&0\\0&0&1\end{pmatrix},$$

$$\Pi^M_{reg}\,(0,2)=\Pi^M_{reg}\,(2,0)=\Pi^M_{reg}\,(1,1)=\begin{pmatrix}0&0&1\\0&1&0\\1&0&0\end{pmatrix}.$$

The above representation Π^M_{reg} of $\langle\mathbb{Z}_3,[\,]\rangle$ is equivalent to the orthogonal direct sum of two irreducible representations

$$\Pi^M_{reg}\,(0,0)=\Pi^M_{reg}\,(1,2)=\Pi^M_{reg}\,(2,1)=[1]\oplus\begin{bmatrix}-1&0\\0&1\end{bmatrix},$$

$$\Pi^M_{reg}\,(0,1)=\Pi^M_{reg}\,(1,0)=\Pi^M_{reg}\,(2,2)=[1]\oplus\begin{bmatrix}\frac{1}{2}&-\frac{\sqrt{3}}{2}\\-\frac{\sqrt{3}}{2}&-\frac{1}{2}\end{bmatrix},$$

$$\Pi^M_{reg}\,(0,2)=\Pi^M_{reg}\,(2,0)=\Pi^M_{reg}\,(1,1)=[1]\oplus\begin{bmatrix}\frac{1}{2}&\frac{\sqrt{3}}{2}\\\frac{\sqrt{3}}{2}&-\frac{1}{2}\end{bmatrix},$$

i.e. one-dimensional trivial [1] and two-dimensional irreducible. Note, that in this example $\Pi^M(g,\overline{g})=\Pi^M(g,g)\neq \mathrm{id}_V$, but $\Pi^M(g,h)\circ\Pi^M(g,h)=\mathrm{id}_V$, and so Π^M are of the second degree.

Consider a more complicated example of left representations. Let $G=\mathbb{Z}_4\ni\{0,1,2,3\}$ and the ternary multiplication is

$$[ghu]=(g+h+u+1)\bmod 4. \tag{135}$$

We have the multiplication table

$$[g,h,0]=\begin{pmatrix}1&2&3&0\\2&3&0&1\\3&0&1&2\\0&1&2&3\end{pmatrix}\qquad [g,h,1]=\begin{pmatrix}2&3&0&1\\3&0&1&2\\0&1&2&3\\1&2&3&0\end{pmatrix}$$

$$[g,h,2]=\begin{pmatrix}3&0&1&2\\0&1&2&3\\1&2&3&0\\2&3&0&1\end{pmatrix}\qquad [g,h,3]=\begin{pmatrix}0&1&2&3\\1&2&3&0\\2&3&0&1\\3&0&1&2\end{pmatrix}$$

Then the skew elements are $\overline{0}=3,\ \overline{1}=2,\ \overline{2}=1,\ \overline{3}=0$, therefore $(G,[\,])$ is an (non-idempotent) commutative ternary group. The left representation is defined by expansion $\Pi^L_{reg}\,(g_1,g_2)\,t=\sum_{i=1}^{n}k_i\,[g_1g_2h_i]$, which means that (see the general formula (117))

$$\Pi^L_{reg}\,(g,h)\,|u>=|\,[ghu]>\,.$$

Analogously, for right and middle representations

$$\Pi^R_{reg}\,(g,h)\,|u>=|\,[ugh]>,\quad \Pi^M_{reg}\,(g,h)\,|u>=|\,[guh]>\,.$$

Therefore $|\,[ghu] >= |\,[ugh] >= |\,[guh] >$ and

$$\Pi^L_{reg}(g,h) = \Pi^R_{reg}(g,h)\,|u >= \Pi^M_{reg}(g,h)\,|u >,$$

so $\Pi^L_{reg}(g,h) = \Pi^R_{reg}(g,h) = \Pi^M_{reg}(g,h)$. Thus it is sufficient to consider the left representation only.

In this case the equivalence is $\Pi^L(a,b) = \Pi^L(c,d) \Longleftrightarrow (a+b) = (c+d) \bmod 4$, and we obtain the following classes

$$\Pi^L_{reg}(0,0) = \Pi^L_{reg}(1,3) = \Pi^L_{reg}(2,2) = \Pi^L_{reg}(3,1) = \begin{pmatrix} 0 & 0 & 0 & 1 \\ 1 & 0 & 0 & 0 \\ 0 & 1 & 0 & 0 \\ 0 & 0 & 1 & 0 \end{pmatrix} = [1] \oplus [-1] \oplus [-i] \oplus [i]\,,$$

$$\Pi^L_{reg}(0,1) = \Pi^L_{reg}(1,0) = \Pi^L_{reg}(2,3) = \Pi^L_{reg}(3,2) = \begin{pmatrix} 0 & 0 & 1 & 0 \\ 0 & 0 & 0 & 1 \\ 1 & 0 & 0 & 0 \\ 0 & 1 & 0 & 0 \end{pmatrix} = [1] \oplus [-1] \oplus [-1] \oplus [-1]\,,$$

$$\Pi^L_{reg}(0,2) = \Pi^L_{reg}(1,1) = \Pi^L_{reg}(2,0) = \Pi^L_{reg}(3,3) = \begin{pmatrix} 0 & 1 & 0 & 0 \\ 0 & 0 & 1 & 0 \\ 0 & 0 & 0 & 1 \\ 1 & 0 & 0 & 0 \end{pmatrix} = [1] \oplus [-1] \oplus [i] \oplus [-i]\,,$$

$$\Pi^L_{reg}(0,3) = \Pi^L_{reg}(1,2) = \Pi^L_{reg}(2,1) = \Pi^L_{reg}(3,0) = \begin{pmatrix} 1 & 0 & 0 & 0 \\ 0 & 1 & 0 & 0 \\ 0 & 0 & 1 & 0 \\ 0 & 0 & 0 & 1 \end{pmatrix} = [1] \oplus [-1] \oplus [1] \oplus [1]\,.$$

It is seen that, due to the fact that the ternary operation (135) is commutative, there are only one-dimensional irreducible left representations.

Let us "algebralize" the above regular representations in the following way. From (118) we have for the left representation

$$\Pi^L_{reg}(i,j) \circ \Pi^L_{reg}(k,l) = \Pi^L_{reg}(i,[jkl])\,, \tag{136}$$

where $[jkl] = j-k+l$, $i,j,k,l \in \mathbb{Z}_3$. Denote $\gamma^L_i = \Pi^L_{reg}(0,i)$, $i \in \mathbb{Z}_3$, then we obtain the algebra with the relations

$$\gamma^L_i \gamma^L_j = \gamma^L_{i+j}. \tag{137}$$

Conversely, any matrix representation of $\gamma_i\gamma_j = \gamma_{i+j}$ leads to the left representation by $\Pi^L(i,j) = \gamma_{j-i}$. In the case of the middle regular representation we introduce $\gamma^M_{k+l} = \Pi^M_{reg}(k,l)$, $k,l \in \mathbb{Z}_3$, then we obtain

$$\gamma^M_i \gamma^M_j \gamma^M_k = \gamma^M_{[ijk]}, \quad i,j,k \in \mathbb{Z}_3. \tag{138}$$

In some sense (138) can be treated as a `ternary analog of the Clifford algebra`. As before, any matrix representation of (138) gives the middle representation $\Pi^M(k,l) = \gamma_{k+l}$.

TERNARY ALGEBRAS AND HOPF ALGEBRAS

Let us consider associative ternary algebras [2,115]. One can introduce autodistributivity property $[[xyz]\,ab] = [[xab]\,[yab]\,[zab]]$ (see [72]). If we take 2 ternary operations $\{\ ,\ ,\ \}$ and $[\ ,\ ,\ ]$, then distributivity is $\{[xyz]\,ab\} = [\{xab\}\,\{yab\}\,\{zab\}]$. If $(+)$ is a binary operation (addition), then `left linearity` is

$$[(x+z)\,,a,b] = [xab] + [zab]\,. \tag{139}$$

By analogy one can define central (middle) and right linearity. `Linearity` is defined, when left, middle and right linearity hold valid simultaneously.

An `associative ternary algebra` is a triple $\left(A, \mu_3, \eta^{(3)}\right)$, where A is a linear space over a field $\mathbb{K}$, μ_3 is a linear map $A \otimes A \otimes A \to A$ called `ternary multiplication` $\mu_3(a \otimes b \otimes c) = [abc]$ which is ternary associative $[[abc]\,de] = [a\,[bcd]\,e] = [ab\,[cde]]$ or

$$\mu_3 \circ (\mu_3 \otimes \mathrm{id} \otimes \mathrm{id}) = \mu_3 \circ (\mathrm{id} \otimes \mu_3 \otimes \mathrm{id}) = \mu_3 \circ (\mathrm{id} \otimes \mathrm{id} \otimes \mu_3)\,. \tag{140}$$

There are two types [45] of ternary unit maps $\eta^{(3)} : \mathbb{K} \to A$:

1) One `strong` unit map

$$\mu_3 \circ \left(\eta^{(3)} \otimes \eta^{(3)} \otimes \mathrm{id}\right) = \mu_3 \circ \left(\eta^{(3)} \otimes \mathrm{id} \otimes \eta^{(3)}\right) = \mu_3 \circ \left(\mathrm{id} \otimes \eta^{(3)} \otimes \eta^{(3)}\right) = \mathrm{id}; \tag{141}$$

2) Two `sequential` units $\eta_1^{(3)}$ and $\eta_2^{(3)}$ satisfying

$$\mu_3 \circ \left(\eta_1^{(3)} \otimes \eta_2^{(3)} \otimes \mathrm{id}\right) = \mu_3 \circ \left(\eta_1^{(3)} \otimes \mathrm{id} \otimes \eta_2^{(3)}\right) = \mu_3 \circ \left(\mathrm{id} \otimes \eta_1^{(3)} \otimes \eta_2^{(3)}\right) = \mathrm{id}; \tag{142}$$

In first case the ternary analog of the binary relation $\eta^{(2)}(x) = x1$, where $x \in \mathbb{K}$, $1 \in A$, is

$$\eta^{(3)}(x) = [x, 1, 1] = [1, 1, x] = [1, x, 1]. \tag{143}$$

Let (A, μ_A, η_A), (B, μ_B, η_B) and (C, μ_C, η_C) be ternary algebras, then the `ternary tensor product` space $A \otimes B \otimes C$ is naturally endowed with the structure of an algebra. The multiplication $\mu_{A\otimes B\otimes C}$ on $A \otimes B \otimes C$ reads

$$[(a_1 \otimes b_1 \otimes c_1)(a_2 \otimes b_2 \otimes c_2)(a_3 \otimes b_3 \otimes c_3)] = [a_1 a_2 a_3] \otimes [b_1 b_2 b_3] \otimes [c_1 c_2 c_3], \tag{144}$$

and so the set of ternary algebras is closed under taking ternary tensor products. A `ternary algebra map` (homomorphism) is a linear map between ternary algebras $f : A \to B$ which respects the ternary algebra structure

$$f([xyz]) = [f(x), f(y), f(z)], \tag{145}$$

$$f(1_A) = 1_B. \tag{146}$$

Let C be a linear space over a field $\mathbb{K}$.

A `ternary comultiplication` $\Delta^{(3)}$ is a linear map over a field $\mathbb{K}$ such that

$$\Delta_3 : C \to C \otimes C \otimes C. \tag{147}$$

In the standard Sweedler notations [37] $\Delta_3(a) = \sum_{i=1}^{n} a_i' \otimes a_i'' \otimes a_i''' = a_{(1)} \otimes a_{(2)} \otimes a_{(3)}$. Consider different possible types of ternary coassociativity [45, 46].

1. A `standard` ternary coassociativity

$$(\Delta_3 \otimes \mathrm{id} \otimes \mathrm{id}) \circ \Delta_3 = (\mathrm{id} \otimes \Delta_3 \otimes \mathrm{id}) \circ \Delta_3 = (\mathrm{id} \otimes \mathrm{id} \otimes \Delta_3) \circ \Delta_3, \tag{148}$$

2. A `nonstandard` ternary Σ-coassociativity (Gluskin-type positional operatives)

$$(\Delta_3 \otimes \mathrm{id} \otimes \mathrm{id}) \circ \Delta_3 = (\mathrm{id} \otimes (\sigma \circ \Delta_3) \otimes \mathrm{id}) \circ \Delta_3,$$

where $\sigma \circ \Delta_3(a) = \Delta_3(a) = a_{(\sigma(1))} \otimes a_{(\sigma(2))} \otimes a_{(\sigma(3))}$ and $\sigma \in \Sigma \subset S_3$.

3. A `permutational` ternary coassociativity

$$(\Delta_3 \otimes \mathrm{id} \otimes \mathrm{id}) \circ \Delta_3 = \pi \circ (\mathrm{id} \otimes \Delta_3 \otimes \mathrm{id}) \circ \Delta_3,$$

where $\pi \in \Pi \subset S_5$.

A `ternary comediality` is

$$(\Delta_3 \otimes \Delta_3 \otimes \Delta_3) \circ \Delta_3 = \sigma_{medial} \circ (\Delta_3 \otimes \Delta_3 \otimes \Delta_3) \circ \Delta_3,$$

where $\sigma_{medial} = \binom{123456789}{147258369} \in S_9$. A `ternary counit` is defined as a map $\varepsilon^{(3)} : C \to \mathbb{K}$. In general, $\varepsilon^{(3)} \neq \varepsilon^{(2)}$ satisfying one of the conditions below. If Δ_3 is derived, then maybe $\varepsilon^{(3)} = \varepsilon^{(2)}$, but another counits may exist. There are two types of ternary counits:

1. Standard (`strong`) ternary counit

$$(\varepsilon^{(3)} \otimes \varepsilon^{(3)} \otimes \mathrm{id}) \circ \Delta_3 = (\varepsilon^{(3)} \otimes \mathrm{id} \otimes \varepsilon^{(3)}) \circ \Delta_3 = (\mathrm{id} \otimes \varepsilon^{(3)} \otimes \varepsilon^{(3)}) \circ \Delta_3 = \mathrm{id}, \tag{149}$$

2. Two `sequential` (polyadic) counits $\varepsilon_1^{(3)}$ and $\varepsilon_2^{(3)}$

$$(\varepsilon_1^{(3)} \otimes \varepsilon_2^{(3)} \otimes \mathrm{id}) \circ \Delta = (\varepsilon_1^{(3)} \otimes \mathrm{id} \otimes \varepsilon_2^{(3)}) \circ \Delta = (\mathrm{id} \otimes \varepsilon_1^{(3)} \otimes \varepsilon_2^{(3)}) \circ \Delta = \mathrm{id}, \tag{150}$$

Below we will consider only the first standard type of associativity (148). The σ-`cocommutativity` is defined as $\sigma \circ \Delta_3 = \Delta_3$.

A `ternary coalgebra` is a triple $\left(C,\Delta_3,\varepsilon^{(3)}\right)$, where C is a linear space and Δ_3 is a ternary comultiplication (147) which is coassociative in one of the above senses and $\varepsilon^{(3)}$ is one of the above counits.

Let $\left(A,\mu^{(3)}\right)$ be a ternary algebra and (C,Δ_3) be a ternary coalgebra and $f,g,h\in \mathrm{Hom}_{\mathbb{K}}(C,A)$. `Ternary convolution product` is

$$[f,g,h]_*=\mu^{(3)}\circ(f\otimes g\otimes h)\circ\Delta_3 \tag{151}$$

or in the Sweedler notation $[f,g,h]_*(a)=\left[f\left(a_{(1)}\right)g\left(a_{(2)}\right)h\left(a_{(3)}\right)\right]$.

A ternary coalgebra is called `derived`, if there exists a binary (usual, see e.g. [37]) coalgebra $\Delta_2: C\to C\otimes C$ such that

$$\Delta_{3,\mathrm{der}}=(\mathrm{id}\otimes\Delta_2)\otimes\Delta_2. \tag{152}$$

A ternary bialgebra B is $\left(B,\mu^{(3)},\eta^{(3)},\Delta_3,\varepsilon^{(3)}\right)$ for which $\left(B,\mu^{(3)},\eta^{(3)}\right)$ is a ternary algebra and $\left(B,\Delta_3,\varepsilon^{(3)}\right)$ is a ternary coalgebra and they are compatible

$$\Delta_3\circ\mu^{(3)}=\mu^{(3)}\circ\Delta_3 \tag{153}$$

One can distinguish four kinds of ternary bialgebras with respect to a "being derived" property:

1. A Δ-`derived` ternary bialgebra
$$\Delta_3=\Delta_{3,\mathrm{der}}=(\mathrm{id}\otimes\Delta_2)\circ\Delta_2 \tag{154}$$
2. A μ-`derived` ternary bialgebra
$$\mu^{(3)}_{der}=\mu^{(3)}_{der}=\mu^{(2)}\circ\left(\mu^{(2)}\otimes\mathrm{id}\right) \tag{155}$$
3. A `derived` ternary bialgebra is simultaneously μ-derived and Δ-derived ternary bialgebra.
4. A `non-derived` ternary bialgebra which does not satisfy (154) and (155).

Possible types of ternary antipodes can be defined using analogy with binary coalgebras.
A `skew ternary antipod` is

$$\mu^{(3)}\circ(S^{(3)}_{skew}\otimes\mathrm{id}\otimes\mathrm{id})\circ\Delta_3=\mu^{(3)}\circ(\mathrm{id}\otimes S^{(3)}_{skew}\otimes\mathrm{id})\circ\Delta_3=\mu^{(3)}\circ(\mathrm{id}\otimes\mathrm{id}\otimes S^{(3)}_{skew})\circ\Delta_3=\mathrm{id}\,. \tag{156}$$

If only one equality from (156) is satisfied, the corresponding skew antipod is called `left`, `middle` or `right`.
`Strong ternary antipod` is

$$\left(\mu^{(2)}\otimes\mathrm{id}\right)\circ(\mathrm{id}\otimes S^{(3)}_{strong}\otimes\mathrm{id})\circ\Delta_3=1\otimes\mathrm{id},\left(\mathrm{id}\otimes\mu^{(2)}\right)\circ(\mathrm{id}\otimes\mathrm{id}\otimes S^{(3)}_{strong})\circ\Delta_3=\mathrm{id}\otimes 1,$$

where 1 is a unit of algebra.

If in a ternary coalgebra the relation

$$\Delta_3\circ S=\tau_{13}\circ(S\otimes S\otimes S)\circ\Delta_3 \tag{157}$$

hold valid, where $\tau_{13}=\binom{123}{321}$, then it is called `skew-involutive`.

A ternary Hopf algebra $\left(H,\mu^{(3)},\eta^{(3)},\Delta_3,\varepsilon^{(3)},S^{(3)}\right)$ is a ternary bialgebra with a ternary antipod $S^{(3)}$ of the corresponding above type .

Let us consider concrete constructions of ternary comultiplications, bialgebras and Hopf algebras. A `ternary group-like element` can be defined by $\Delta_3(g)=g\otimes g\otimes g$, and for 3 such elements we have

$$\Delta_3([g_1g_2g_3])=\Delta_3(g_1)\,\Delta_3(g_2)\,\Delta_3(g_3)\,. \tag{158}$$

But an analog of the binary primitive element (satisfying $\Delta^{(2)}(x)=x\otimes 1+1\otimes x$) cannot be chosen simply as $\Delta_3(x)=x\otimes e\otimes e+e\otimes x\otimes e+e\otimes e\otimes x$, since the algebra structure is not preserved. Nevertheless, if we introduce `two` idempotent units e_1,e_2 satisfying "semiorthogonality" $[e_1e_1e_2]=0$, $[e_2e_2e_1]=0$, then

$$\Delta_3(x)=x\otimes e_1\otimes e_2+e_2\otimes x\otimes e_1+e_1\otimes e_2\otimes x \tag{159}$$

and now $\Delta_3([x_1x_2x_3])=[\Delta_3(x_1)\,\Delta_3(x_2)\,\Delta_3(x_3)]$. Using (159) $\varepsilon(x)=0$, $\varepsilon(e_{1,2})=1$, and $S^{(3)}(x)=-x$, $S^{(3)}(e_{1,2})=e_{1,2}$, one can construct a ternary universal enveloping algebra in full analogy with the binary case (see e.g. [39]).

One of the most important examples of noncocommutative Hopf algebras is the well known Sweedler Hopf algebra [37] which in the binary case has two generators x and y satisfying

$$\mu^{(2)}(x,x) = 1, \tag{160}$$
$$\mu^{(2)}(y,y) = 0, \tag{161}$$
$$\sigma_{+}^{(2)}(xy) = -\sigma_{-}^{(2)}(xy). \tag{162}$$

It has the following comultiplication

$$\Delta_2(x) = x \otimes x, \tag{163}$$
$$\Delta_2(y) = y \otimes x + 1 \otimes y, \tag{164}$$

counit $\varepsilon^{(2)}(x) = 1$, $\varepsilon^{(2)}(y) = 0$, and antipod $S^{(2)}(x) = x$, $S^{(2)}(y) = -y$, which respect the algebra structure. In the derived case a `ternary Sweedler algebra` is generated also by two generators x and y obeying

$$\mu^{(3)}(x,e,x) = \mu^{(3)}(e,x,x) = \mu^{(3)}(x,x,e) = e, \tag{165}$$
$$\sigma_{+}^{(3)}([yey]) = 0, \tag{166}$$
$$\sigma_{+}^{(3)}([xey]) = -\sigma_{-}^{(3)}([xey]). \tag{167}$$

The derived Hopf algebra structure is given by

$$\Delta_3(x) = x \otimes x \otimes x, \tag{168}$$
$$\Delta_3(y) = y \otimes x \otimes x + e \otimes y \otimes x + e \otimes e \otimes y, \tag{169}$$
$$\varepsilon^{(3)}(x) = \varepsilon^{(2)}(x) = 1, \tag{170}$$
$$\varepsilon^{(3)}(y) = \varepsilon^{(2)}(y) = 0, \tag{171}$$
$$S^{(3)}(x) = S^{(2)}(x) = x, \tag{172}$$
$$S^{(3)}(y) = S^{(2)}(y) = -y, \tag{173}$$

and it can be checked that (168)-(170) are algebra maps, while (172) is antialgebra maps. To obtain a non-derived ternary Sweedler example we have the possibilities: 1) one "even" generator x, two "odd" generators $y_{1,2}$ and one ternary unit e; 2) two "even" generators $x_{1,2}$, one "odd" generator y and two ternary units $e_{1,2}$. In the first case the ternary algebra structure is (no summation, $i = 1, 2$)

$$[xxx] = e, \tag{174}$$
$$[y_i y_i y_i] = 0, \tag{175}$$
$$\sigma_{+}^{(3)}([y_i x y_i]) = \sigma_{+}^{(3)}([x y_i x]) = 0, \tag{176}$$
$$[xey_i] = -[xy_i e],$$
$$[exy_i] = -[y_i xe], \tag{177}$$
$$[ey_i x] = -[y_i ex], \tag{178}$$
$$\sigma_{+}^{(3)}([y_1 x y_2]) = -\sigma_{-}^{(3)}([y_1 x y_2]). \tag{179}$$

The corresponding ternary Hopf algebra structure is

$$\Delta_3(x) = x \otimes x \otimes x,\ \Delta_3(y_{1,2}) = y_{1,2} \otimes x \otimes x + e_{1,2} \otimes y_{2,1} \otimes x + e_{1,2} \otimes e_{2,1} \otimes y_{2,1},$$
$$\varepsilon^{(3)}(x) = 1,\ \ \varepsilon^{(3)}(y_i) = 0,\ \ S^{(3)}(x) = x,\quad S^{(3)}(y_i) = -y_i. \tag{180}$$

In the second case we have for algebra structure

$$[x_i x_j x_k] = \delta_{ij}\delta_{ik}\delta_{jk} e_i,\quad [yyy] = 0,\ \ \sigma_{+}^{(3)}([yx_i y]) = 0,\ \sigma_{+}^{(3)}([x_i y x_i]) = 0,$$
$$\sigma_{+}^{(3)}([y_1 x y_2]) = 0,\quad \sigma_{-}^{(3)}([y_1 x y_2]) = 0, \tag{181}$$

and the ternary Hopf algebra structure is

$$\Delta_3(x_i) = x_i \otimes x_i \otimes x_i,$$
$$\Delta_3(y) = y \otimes x_1 \otimes x_1 + e_1 \otimes y \otimes x_2 + e_1 \otimes e_2 \otimes y, \quad (182)$$
$$\varepsilon^{(3)}(x_i) = 1, \quad (183)$$
$$\varepsilon^{(3)}(y) = 0, \quad (184)$$
$$S^{(3)}(x_i) = x_i, \quad (185)$$
$$S^{(3)}(y) = -y. \quad (186)$$

TERNARY QUANTUM GROUPS

A ternary commutator can be obtained in different ways [116]. We will consider a simplest version called a Nambu bracket (see e.g. [2,30]). Let us introduce two maps $\omega_{\pm}^{(3)} : A \otimes A \otimes A \to A \otimes A \otimes A$ by

$$\omega_{+}^{(3)}(a \otimes b \otimes c) = a \otimes b \otimes c + b \otimes c \otimes a + c \otimes a \otimes b, \quad (187)$$
$$\omega_{-}^{(3)}(a \otimes b \otimes c) = b \otimes a \otimes c + c \otimes b \otimes a + a \otimes c \otimes b. \quad (188)$$

Thus, obviously $\mu^{(3)} \circ \omega_{\pm}^{(3)} = \sigma_{\pm}^{(3)} \circ \mu^{(3)}$, where $\sigma_{\pm}^{(3)} \in S_3$ denotes sum of terms having even and odd permutations respectively. In the binary case $\omega_{+}^{(2)} = \mathrm{id} \otimes \mathrm{id}$ and $\omega_{-}^{(2)} = \tau$ is the twist operator $\tau : a \otimes b \to b \otimes a$, while $\mu^{(2)} \circ \omega_{-}^{(2)}$ is permutation $\sigma_{-}^{(2)}(ab) = ba$. So the Nambu product is $\omega_{N}^{(3)} = \omega_{+}^{(3)} - \omega_{-}^{(3)}$, and the ternary commutator is $[,,]_N = \sigma_{N}^{(3)} = \sigma_{+}^{(3)} - \sigma_{-}^{(3)}$, or [30]

$$[a,b,c]_N = [abc] + [bca] + [cab] - [cba] - [acb] - [bac] \quad (189)$$

An `abelian ternary algebra` is defined by vanishing of Nambu bracket $[a,b,c]_N = 0$ or `ternary commutation` relation $\sigma_{+}^{(3)} = \sigma_{-}^{(3)}$. By analogy with the binary case a `deformed ternary algebra` can be defined by

$$\sigma_{+}^{(3)} = q\sigma_{-}^{(3)} \text{ or } [abc] + [bca] + [cab] = q([cba] + [acb] + [bac]), \quad (190)$$

where multiplication by q is treated as an external operation.

Let us consider a ternary analog of the Woronowicz example of a bialgebra construction, which in the binary case has two generators satisfying $xy = qyx$ (or $\sigma_{+}^{(2)}(xy) = q\sigma_{-}^{(2)}(xy)$), then the following coproducts

$$\Delta_2(x) = x \otimes x \quad (191)$$
$$\Delta_2(y) = y \otimes x + 1 \otimes y \quad (192)$$

are algebra maps. In the derived ternary case using (190) we have

$$\sigma_{+}^{(3)}([xey]) = q\sigma_{-}^{(3)}([xey]), \quad (193)$$

where e is the ternary unit and ternary coproducts are

$$\Delta_3(e) = e \otimes e \otimes e, \quad (194)$$
$$\Delta_3(x) = x \otimes x \otimes x, \quad (195)$$
$$\Delta_3(y) = y \otimes x \otimes x + e \otimes y \otimes x + e \otimes e \otimes y, \quad (196)$$

which are `ternary algebra maps`, i.e. they satisfy

$$\sigma_{+}^{(3)}([\Delta_3(x)\,\Delta_3(e)\,\Delta_3(y)]) = q\sigma_{-}^{(3)}([\Delta_3(x)\,\Delta_3(e)\,\Delta_3(y)]). \quad (197)$$

Let us consider the group $G = SL(n,\mathbb{K})$. Then the algebra generated by $a_j^i \in SL(n,\mathbb{K})$ can be endowed by the structure of ternary Hopf algebra (see e.g. [117] for binary case) by choosing the ternary coproduct, counit and antipod as (here summation is implied)

$$\Delta_3\left(a_j^i\right) = a_k^i \otimes a_l^k \otimes a_j^l, \quad \varepsilon\left(a_j^i\right) = \delta_j^i, \quad S^{(3)}\left(a_j^i\right) = \left(a^{-1}\right)_j^i. \quad (198)$$

This antipod is a skew one since from (156) it follows

$$\mu^{(3)} \circ (S^{(3)} \otimes \mathrm{id} \otimes \mathrm{id}) \circ \Delta_3\left(a_j^i\right) = S^{(3)}\left(a_k^i\right) a_l^k a_j^l = \left(a^{-1}\right)_k^i a_l^k a_j^l = \delta_l^i a_j^l = a_j^i. \quad (199)$$

This ternary Hopf algebra is derived since for $\Delta^{(2)} = a^i_j \otimes a^j_k$ we have

$$\Delta_3 = \left(\mathrm{id} \otimes \Delta^{(2)}\right) \otimes \Delta^{(2)}\left(a^i_j\right) = \left(\mathrm{id} \otimes \Delta^{(2)}\right)\left(a^i_k \otimes a^k_j\right) = a^i_k \otimes \Delta^{(2)}\left(a^k_j\right) = a^i_k \otimes a^k_l \otimes a^l_j. \tag{200}$$

In the most important case $n = 2$ we can obtain the manifest action of the ternary coproduct Δ_3 on components. Possible non-derived matrix representations of the ternary product can be done only by four-rank $n \times n \times n \times n$ twice covariant and twice contravariant tensors $\left\{a^{ij}_{kl}\right\}$. Among all products the non-derived ones are only the following $a^{oi}_{jk} b^{jl}_{oo} c^{ko}_{il}$ and $a^{ij}_{ok} b^{ol}_{io} c^{ko}_{il}$ (where o is any index). So using e.g. the first choice we can define the non-derived Hopf algebra structure by

$$\Delta_3\left(a^{ij}_{kl}\right) = a^{i\mu}_{v\rho} \otimes a^{v\sigma}_{kl} \otimes a^{\rho j}_{\mu\sigma}, \tag{201}$$

$$\varepsilon\left(a^{ij}_{kl}\right) = \frac{1}{2}\left(\delta^i_k \delta^j_l + \delta^i_l \delta^j_k\right), \tag{202}$$

and the skew antipod $s^{ij}_{kl} = S^{(3)}\left(a^{ij}_{kl}\right)$ which is a solution of the equation $s^{i\mu}_{v\rho} a^{v\sigma}_{kl} = \delta^i_\rho \delta^\mu_k \delta^\sigma_l$.

Next consider ternary dual pair $k(G)$ (push-forward) and $\mathcal{F}(G)$ (pull-back) which are related by $k^*(G) \cong \mathcal{F}(G)$ (see e.g. [118]). Here $k(G) = \mathrm{span}(G)$ is a ternary group algebra (G has a ternary product $[\,]_G$ or $\mu^{(3)}_G$) over a field k. If $u \in k(G)$ ($u = u^i x_i, x_i \in G$), then

$$[uvw]_k = u^i v^j w^l [x_i x_j x_l]_G \tag{203}$$

is associative, and so $(k(G), [\,]_k)$ becomes a ternary algebra. Define a ternary coproduct $\Delta_3 : k(G) \to k(G) \otimes k(G) \otimes k(G)$ by

$$\Delta_3(u) = u^i x_i \otimes x_i \otimes x_i \tag{204}$$

(derived and associative), then $\Delta_3([uvw]_k) = [\Delta_3(u)\,\Delta_3(v)\,\Delta_3(w)]_k$, and $k(G)$ is a ternary bialgebra. If we define a ternary antipod by $S^{(3)}_k = u^i \bar{x}_i$, where $\bar{x}_i$ is a skew element of x_i, then $k(G)$ becomes a ternary Hopf algebra.

In the dual case of functions $\mathcal{F}(G) : \{\varphi : G \to k\}$ a ternary product $[\,]_{\mathcal{F}}$ or $\mu^{(3)}_{\mathcal{F}}$ (derived and associative) acts on $\psi(x, y, z)$ as

$$\left(\mu^{(3)}_{\mathcal{F}} \psi\right)(x) = \psi(x, x, x), \tag{205}$$

and so $\mathcal{F}(G)$ is a ternary algebra. Let $\mathcal{F}(G) \otimes \mathcal{F}(G) \otimes \mathcal{F}(G) \cong \mathcal{F}(G \times G \times G)$, then we define a ternary coproduct $\Delta_3 : \mathcal{F}(G) \to \mathcal{F}(G) \otimes \mathcal{F}(G) \otimes \mathcal{F}(G)$ as

$$(\Delta_3 \varphi)(x, y, z) = \varphi([xyz]_{\mathcal{F}}), \tag{206}$$

which is derive and associative. Thus we can obtain $\Delta_3([\varphi_1 \varphi_2 \varphi_3]_{\mathcal{F}}) = [\Delta_3(\varphi_1)\,\Delta_3(\varphi_2)\,\Delta_3(\varphi_3)]_{\mathcal{F}}$, and therefore $\mathcal{F}(G)$ is a ternary bialgebra. If we define a ternary antipod by

$$S^{(3)}_{\mathcal{F}}(\varphi) = \varphi(\bar{x}), \tag{207}$$

where $\bar{x}$ is a skew element of x, then $\mathcal{F}(G)$ becomes a ternary Hopf algebra.

Let us introduce a ternary analog of R-matrix. For a ternary Hopf algebra H we consider a linear map $R^{(3)} : H \otimes H \otimes H \to H \otimes H \otimes H$.

A ternary Hopf algebra $\left(H, \mu^{(3)}, \eta^{(3)}, \Delta_3, \varepsilon^{(3)}, S^{(3)}\right)$ is called `quasifiveangular`[4] if it satisfies

$$(\Delta_3 \otimes \mathrm{id} \otimes \mathrm{id}) = R^{(3)}_{145} R^{(3)}_{245} R^{(3)}_{345}, \tag{208}$$

$$(\mathrm{id} \otimes \Delta_3 \otimes \mathrm{id}) = R^{(3)}_{125} R^{(3)}_{145} R^{(3)}_{135}, \tag{209}$$

$$(\mathrm{id} \otimes \mathrm{id} \otimes \Delta_3) = R^{(3)}_{125} R^{(3)}_{124} R^{(3)}_{123}, \tag{210}$$

where as usual index of R denotes action component positions.

Using the standard procedure (see e.g. [39,119,120]) we obtain set of abstract `ternary quantum Yang-Baxter equations`, one of which has the form

$$R^{(3)}_{243} R^{(3)}_{342} R^{(3)}_{125} R^{(3)}_{145} R^{(3)}_{135} = R^{(3)}_{123} R^{(3)}_{132} R^{(3)}_{145} R^{(3)}_{245} R^{(3)}_{345}, \tag{211}$$

[4]The reason of such notation is clear from (211).

and others can be obtained by corresponding permutations. The classical ternary Yang-Baxter equations for one parameter family of solutions $R(t)$ can be obtained by the expansion

$$R^{(3)}(t) = e \otimes e \otimes e + rt + \mathcal{O}\left(t^2\right), \tag{212}$$

where r is a ternary classical R-matrix, then e.g. for (211) we have

$$\begin{aligned} &r_{342}r_{125}r_{145}r_{135} + r_{243}r_{125}r_{145}r_{135} + r_{243}r_{342}r_{145}r_{135} + r_{243}r_{342}r_{125}r_{135} + r_{243}r_{342}r_{125}r_{145} \\ &= r_{132}r_{145}r_{245}r_{345} + r_{123}r_{145}r_{245}r_{345} + r_{123}r_{132}r_{245}r_{345} + r_{123}r_{132}r_{145}r_{345} + r_{123}r_{132}r_{145}r_{245}. \end{aligned}$$

For three ternary Hopf algebras $\left(H_{A,B,C}, \mu^{(3)}_{A,B,C}, \eta^{(3)}_{A,B,C}, \Delta^{(3)}_{A,B,C}, \varepsilon^{(3)}_{A,B,C}, S^{(3)}_{A,B,C}\right)$ we can introduce a non-degenerate ternary "pairing" (see e.g. [119] for binary case) $\langle\ ,\ ,\ \rangle^{(3)} : H_A \times H_B \times H_C \to \mathbb{K}$, trilinear over $\mathbb{K}$, satisfying

$$\begin{aligned} &\left\langle \eta^{(3)}_A(a), b, c \right\rangle^{(3)} = \left\langle a, \varepsilon^{(3)}_B(b), c \right\rangle^{(3)}, \ \left\langle a, \eta^{(3)}_B(b), c \right\rangle^{(3)} = \left\langle \varepsilon^{(3)}_A(a), b, c \right\rangle^{(3)}, \\ &\left\langle b, \eta^{(3)}_B(b), c \right\rangle^{(3)} = \left\langle a, b, \varepsilon^{(3)}_C(c) \right\rangle^{(3)}, \ \left\langle a, b, \eta^{(3)}_C(c) \right\rangle^{(3)} = \left\langle a, \varepsilon^{(3)}_B(b), c \right\rangle^{(3)}, \\ &\left\langle a, b, \eta^{(3)}_C(c) \right\rangle^{(3)} = \left\langle \varepsilon^{(3)}_A(a), b, c \right\rangle^{(3)}, \ \left\langle \eta^{(3)}_A(a), b, c \right\rangle^{(3)} = \left\langle a, b, \varepsilon^{(3)}_C(c) \right\rangle^{(3)}, \end{aligned}$$

$$\begin{aligned} &\left\langle \mu^{(3)}_A(a_1 \otimes a_2 \otimes a_3), b, c \right\rangle^{(3)} = \left\langle a_1 \otimes a_2 \otimes a_3, \Delta^{(3)}_B(b), c \right\rangle^{(3)}, \\ &\left\langle \Delta^{(3)}_A(a), b_1 \otimes b_2 \otimes b_3, c \right\rangle^{(3)} = \left\langle a, \mu^{(3)}_B(b_1 \otimes b_2 \otimes b_3), c \right\rangle^{(3)}, \\ &\left\langle a, \mu^{(3)}_B(b_1 \otimes b_2 \otimes b_3), c \right\rangle^{(3)} = \left\langle a, b_1 \otimes b_2 \otimes b_3, \Delta^{(3)}_C(c) \right\rangle^{(3)}, \\ &\left\langle a, \Delta^{(3)}_B(b), c_1 \otimes c_2 \otimes c_3 \right\rangle^{(3)} = \left\langle a, b, \mu^{(3)}_C(c_1 \otimes c_2 \otimes c_3) \right\rangle^{(3)}, \\ &\left\langle a, b, \mu^{(3)}_C(c_1 \otimes c_2 \otimes c_3) \right\rangle^{(3)} = \left\langle \Delta^{(3)}_A(a), b, c_1 \otimes c_2 \otimes c_3 \right\rangle^{(3)}, \\ &\left\langle a_1 \otimes a_2 \otimes a_3, b, \Delta^{(3)}_C(c) \right\rangle^{(3)} = \left\langle \mu^{(3)}_A(a_1 \otimes a_2 \otimes a_3), b, c \right\rangle^{(3)}, \end{aligned}$$

$$\left\langle S^{(3)}_A(a), b, c \right\rangle^{(3)} = \left\langle a, S^{(3)}_B(b), c \right\rangle^{(3)} = \left\langle a, b, S^{(3)}_C(c) \right\rangle^{(3)},$$

where $a, a_i \in H_A$, $b, b_i \in H_B$. The ternary "paring" between $H_A \otimes H_A \otimes H_A$ and $H_B \otimes H_B \otimes H_B$ is given by $\langle a_1 \otimes a_2 \otimes a_3, b_1 \otimes b_2 \otimes b_3 \rangle^{(3)} = \langle a_1, b_1 \rangle^{(3)} \langle a_2, b_2 \rangle^{(3)} \langle a_3, b_3 \rangle^{(3)}$. These constructions can naturally lead to ternary generalization of duality concept and quantum double which are the key ingredients in the theory of quantum groups [39, 120, 121].

CONCLUSIONS

In this paper we presented a review of polyadic systems and their representations, ternary algebras and Hopf algebras. We classified general polyadic systems and considered their homomorphisms and the multiplace generalizations, paying attention on their associativity. We defined multiplace representations and multiactions, gave examples of matrix representations for some ternary groups. We defined and investigated ternary algebras and Hopf algebras, and give some examples. Then we considered some ternary generalizations of quantum groups and the Yang-Baxter equation.

REFERENCES

1. Kerner R. Ternary algebraic structures and their applications in physics // Paris, 2000. - 15 p. (Preprint Univ. P. & M. Curie).
2. de Azcarraga J. A., Izquierdo J. M. n-ary algebras: a review with applications // J. Phys. - 2010. - Vol. A43. - P. 293001.
3. Dörnte W. Unterschungen über einen verallgemeinerten Gruppenbegriff // Math. Z. - 1929. - Vol. 29. - P. 1–19.
4. Prüfer H. Theorie der abelshen Gruppen I. Grundeigenschaften // Math. Z. - 1924. - Vol. 20. - P. 165–187.
5. Post E. L. Polyadic groups // Trans. Amer. Math. Soc. - 1940. - Vol. 48. - P. 208–350.
6. Hosszú L. M. On the explicit form of n-group operation // Publ. Math. Debrecen. - 1963. - Vol. 10. - P. 88–92.

7. Gluskin L. M. Position operatives // Math. Sbornik. - 1965. - Vol. 68(110). - № 3. - P. 444–472.
8. Dudek W. A., Głazek K., Gleichgewicht B. A note on the axioms of n-groups // Coll. Math. Soc. J. Bolyai. 29. Universal Algebra. - Esztergom (Hungary). , 1977. - P. 195–202.
9. Rusakov S. A definition of an n-ary group // Dokl. Akad. Nauk BSSR. - 1979. - Vol. 23. - P. 965–967.
10. Weyl H. Classical Groups, Their Invariants and Representations. - Princeton: Princeton Univ. Press, 1946.
11. Fulton W., Harris J. Representation Theory: a First Course. - N. Y.: Springer, 1991.
12. Cornwell J. F. Group Theory in Physics: An Introduction. - London: Academic Press, 1997. - 349 p.
13. Curtis C. W., Reiner I. Representation theory of finite groups and associative algebras. - Providence: AMS, 1962.
14. Collins M. J. Representations And Characters Of Finite Groups. - Cambridge: Cambridge University Press, 1990. - 242 p.
15. Kapranov M., Gelfand I. M., Zelevinskii A. Discriminants, Resultants and Multidimensional Determinants. - Berlin: Birkhäuser, 1994. - 234 p.
16. Sokolov N. P. Introduction to the Theory of Multidimensional Matrices. - Kiev: Naukova Dumka, 1972. - 175 p.
17. Kawamura Y. Cubic matrices, generalized spin algebra and uncertainty relation // Progr. Theor. Phys. - 2003. - Vol. 110. - P. 579–587.
18. Rausch de Traubenberg M. Cubic extentions of the poincare algebra // Phys. Atom. Nucl. - 2008. - Vol. 71. - P. 1102–1108.
19. Borowiec A., Dudek W., Duplij S. Bi-element representations of ternary groups // Comm. Algebra. - 2006. - Vol. 34. - № 5. - P. 1651–1670.
20. Dudek W. A., Shahryari M. Representation theory of polyadic groups // Algebr. Represent. Theory. - 2012. - Vol. 15. - № 1. - P. 29–51.
21. Lõhmus J., Paal E., Sorgsepp L. Nonassociative Algebras in Physics. - Palm Harbor: Hadronic Press, 1994. - 271 p.
22. Lounesto P., Ablamowicz R. Clifford Algebras: Applications To Mathematics, Physics, And Engineering. - Birkhäuser, 2004. - 626 p.
23. Georgi H. Lie algebras in particle physics. - New York: Perseus Books, 1999. - 320 p.
24. Abramov V. $\mathbb{Z}_3$-graded analogues of Clifford algebras and algebra of $\mathbb{Z}_3$-graded symmetries // Algebras Groups Geom. - 1995. - Vol. 12. - № 3. - P. 201–221.
25. Abramov V. Ternary generalizations of Grassmann algebra // Proc. Est. Acad. Sci., Phys. Math. - 1996. - Vol. 45. - № 2-3. - P. 152–160.
26. Abramov V., Kerner R., Le Roy B. Hypersymmetry: a $\mathbb{Z}_3$-graded generalization of supersymmetry // J. Math. Phys. - 1997. - Vol. 38. - P. 1650–1669.
27. Filippov V. T. n-Lie algebras // Sib. Math. J. - 1985. - Vol. 26. - P. 879–891.
28. Michor P. W., Vinogradov A. M. n-ary Lie and associative algebras // Rend. Sem. Mat. Univ. Pol. Torino. - 1996. - Vol. 54. - № 4. - P. 373–392.
29. Nambu Y. Generalized Hamiltonian dynamics // Phys. Rev. - 1973. - Vol. 7. - P. 2405–2412.
30. Takhtajan L. On foundation of the generalized Nambu mechanics // Commun. Math. Phys. - 1994. - Vol. 160. - P. 295–315.
31. Bagger J., Lambert N. Comments on multiple M2-branes // - 2008. - Vol. 2. - P. 105.
32. Bagger J., Lambert N. Gauge symmetry and supersymmetry of multiple M2-branes // Phys. Rev. - 2008. - Vol. D77. - P. 065008.
33. Gustavsson A. One-loop corrections to Bagger-Lambert theory // Nucl. Phys. - 2009. - Vol. B807. - P. 315–333.
34. Ho P.-M., Hou R.-C., Matsuo Y., Shiba S. M5-brane in three-form flux and multiple M2-branes // - 2008. - Vol. 08. - P. 014.
35. Low A. M. Worldvolume superalgebra of BLG theory with Nambu-Poisson structure // - 2010. - Vol. 04. - P. 089.
36. Abe E. Hopf Algebras. - Cambridge: Cambridge Univ. Press, 1980. - 221 p.
37. Sweedler M. E. Hopf Algebras. - New York: Benjamin, 1969. - 336 p.
38. Montgomery S. Hopf algebras and their actions on rings. - Providence: AMS, 1993. - 238 p.
39. Kassel C. Quantum Groups. - New York: Springer-Verlag, 1995. - 531 p.
40. Shnider S., Sternberg S. Quantum Groups. - Boston: International Press, 1993. - 371 p.
41. Duplij S., Li F. Regular solutions of quantum Yang-Baxter equation from weak Hopf algebras // Czech. J. Phys. - 2001. - Vol. 51. - № 12. - P. 1306–1311.
42. Duplij S., Sinel'shchikov S. Quantum enveloping algebras with von Neumann regular Cartan-like generators and the Pierce decomposition // Commun. Math. Phys. - 2009. - Vol. 287. - № 1. - P. 769–785.
43. Li F., Duplij S. Weak Hopf algebras and singular solutions of quantum Yang-Baxter equation // Commun. Math. Phys. - 2002. - Vol. 225. - № 1. - P. 191–217.
44. Duplij S., Sinel'shchikov S. Classification of $U_q\left(\mathrm{sL}_2\right)$-module algebra structures on the quantum plane // J. Math. Physics, Analysis, Geometry. - 2010. - Vol. 6. - № 6. - P. 21–46.

45. Duplij S. Ternary Hopf algebras // Symmetry in Nonlinear Mathematical Physics. - Kiev. Institute of Mathematics, 2001. - P. 25-34.
46. Borowiec A., Dudek W., Duplij S. Basic concepts of ternary Hopf algebras // Journal of Kharkov National University, ser. Nuclei, Particles and Fields. - 2001. - Vol. 529. - № 3(15). - P. 21–29.
47. Bergman G. M. An invitation to general algebra and universal constructions. - Berkeley: University of California, 1995. - 358 p.
48. Hausmann B. A., Ore Ø. Theory of quasigroups // Amer. J. Math. - 1937. - Vol. 59. - P. 983–1004.
49. Clifford A. H., Preston G. B. The Algebraic Theory of Semigroups. Vol. 1 - Providence: Amer. Math. Soc., 1961.
50. Brandt H. Über eine Verallgemeinerung des Gruppenbegriffes // Math. Annalen. - 1927. - Vol. 96. - P. 360–367.
51. Bruck R. H. A Survey on Binary Systems. - New York: Springer-Verlag, 1966.
52. Bourbaki N. Elements of Mathematics: Algebra 1. - Springer, 1998.
53. Dudek W. A. Remarks to głazek's results on n-ary groups // Discuss. Math., Gen. Algebra Appl. - 2007. - Vol. 27. - № 2. - P. 199–233.
54. Dudek W. A., Michalski J. On retract of polyadic groups // Demonstratio Math. - 1984. - Vol. 17. - P. 281–301.
55. Thurston H. A. Partly associative operations // J. London Math. Soc. - 1949. - Vol. 24. - P. 260–271.
56. Belousov V. D. n-ary Quasigroups. - Kishinev: Shtintsa, 1972. - 225 p.
57. Sokhatsky F. M. On the associativity of multiplace operations // Quasigroups Relat. Syst. - 1997. - Vol. 4. - P. 51–66.
58. Michalski J. Covering k-groups of n-groups // Archiv. Math. - 1981. - Vol. 17. - № 4. - P. 207–226.
59. Pop M. S., Pop A. On some relations on n-monoids // Carpathian J. Math. - 2004. - Vol. 20. - № 1. - P. 87–94.
60. Čupona G., Trpenovski B. Finitary associative operations with neutral elements // Bull. Soc. Math. Phys. Macedoine. - 1961. - Vol. 12. - P. 15–24.
61. Evans T. Abstract mean values // Duke Math J. - 1963. - Vol. 30. - P. 331–347.
62. Głazek K., Gleichgewicht B. Abelian n-groups // Colloq. Math. Soc. J. Bolyai. Universal Algebra (Esztergom, 1977). - Amsterdam. North-Holland, 1982. - P. 321–329.
63. Stojaković Z., Dudek W. A. On σ-permutable n-groups // Publ. Inst. Math., Nouv. Sér. - 1986. - Vol. 40(54). - P. 49–55.
64. Rusakov S. A. Some Applications of n-ary Group Theory. - Minsk: Belaruskaya navuka, 1998. - 180 p.
65. Celakoski N. On some axiom systems for n-groups // Mat. Bilt. - 1977. - Vol. 1. - P. 5–14.
66. Gal'mak A. M. n-ary groups, Part 1. - Gomel: Gomel University, 2003. - 195 p.
67. Ŭsan J. n-groups in the light of the neutral operations // Math. Moravica. - 2003. - Vol. Special vol.
68. Sokolov E. I. On the theorem of Gluskin-Hosszú on Dörnte groups // Mat. Issled. - 1976. - Vol. 39. - P. 187–189.
69. Yurevych O. V. Criteria for invertibility of elements in associates // Ukr. Math. J. - 2001. - Vol. 53. - № 11. - P. 1895–1905.
70. Timm J. Verbandstheoretische Behandlung n-stelliger Gruppen // Abh. Math. Semin. Univ. Hamb. - 1972. - Vol. 37. - P. 218–224.
71. Dudek W. A. Remarks on n-groups // Demonstratio Math. - 1980. - Vol. 13. - P. 165–181.
72. Dudek W. A. Autodistributive n-groups // Annales Sci. Math. Polonae, Commentationes Math. - 1993. - Vol. 23. - P. 1–11.
73. Heine E. Handbuch der Kugelfunktionan. - Berlin: Reimer, 1878.
74. Kac V., Cheung P. Quantum calculus. - New York: Springer, 2002. - 112 p.
75. Petrescu A. On the homotopy of universal algebras. I. // Rev. Roum. Math. Pures Appl. - 1977. - Vol. 22. - P. 541–551.
76. Halaš R. A note on homotopy in universal algebra // Acta Univ. Palacki. Olomuc., Fac. Rerum Nat., Math. - 1994. - Vol. 33. - № 114. - P. 39–42.
77. Głazek K., Gleichgewicht B. Bibliography of n-groups (polyadic groups) and some group like n-ary systems // Proceedings of the Symposium on n-ary structures. - Skopje. Macedonian Academy of Sciences and Arts, 1982. - P. 253–289.
78. Fujiwara T. On mappings between algebraic systems // Osaka Math. J. - 1959. - Vol. 11. - P. 153–172.
79. Vidal J. C., Tur J. S. A 2-categorial generalization of the concept of institution // Stud. Log. - 2010. - Vol. 95. - № 3. - P. 301–344.
80. Novotný M. Homomorphisms of algebras // Czech. Math. J. - 2002. - Vol. 52. - № 2. - P. 345–364.
81. Novotný M. Mono-unary algebras in the work of Czechoslovak mathematicians // Arch. Math., Brno. - 1990. - Vol. 26. - № 2-3. - P. 155–164.
82. Gal'mak A. M. Generalized morphisms of algebraic systems // Vopr. Algebry. - 1998. - Vol. 12. - P. 36–46.
83. Gal'mak A. M. Generalized morphisms of Abelian m-ary groups // Discuss. Math. - 2001. - Vol. 21. - № 1. - P. 47–55.
84. Gal'mak A. M. n-ary groups, Part 2. - Minsk: Belarus State University, 2007. - 324 p.
85. Goetz A. On weak isomorphisms and weak homomorphisms of abstract algebras // Colloq. Math. - 1966. - Vol. 14. - P. 163–167.
86. Marczewski E. Independence in abstract algebras. Results and problems // Colloq. Math. - 1966. - Vol. 14. - P. 169–188.
87. Głazek K., Michalski J. On weak homomorphisms of general non-indexed algebras // Bull. Acad. Pol. Sci., Sér. Sci. Math. Astron. Phys. - 1974. - Vol. 22. - P. 651–656.

88. Głazek K. Weak homomorphisms of general algebras and related topics // Math. Semin. Notes, Kobe Univ. - 1980. - Vol. 8. - P. 1–36.
89. Traczyk T. Weak isomorphisms of Boolean and Post algebras // Colloq. Math. - 1965. - Vol. 13. - P. 159–164.
90. Denecke K., Wismath S. L. Universal Algebra and Coalgebra. - Singapore: World Scientific, 2009.
91. Denecke K., Saengsura K. State-based systems and (F_1, F_2)-coalgebras // East-West J. Math.,. - 2008. - Vol. Spec. Vol. - P. 1–31.
92. Chung K. O., Smith J. D. H. Weak homomorphisms and graph coalgebras // Arab. J. Sci. Eng., Sect. C, Theme Issues. - 2008. - Vol. 33. - № 2. - P. 107–121.
93. Kolibiar M. Weak homomorphisms in some classes of algebras // Stud. Sci. Math. Hung. - 1984. - Vol. 19. - P. 413–420.
94. Głazek K., Michalski J. Weak homomorphisms of general algebras // Commentat. Math. - 1977. - Vol. 19 (1976). - P. 211–228.
95. Czákány B. On the equivalence of certain classes of algebraic systems // Acta Sci. Math. (Szeged). - 1962. - Vol. 23. - P. 46–57.
96. Mal'tcev A. I. Free topological algebras // Izv. Akad. Nauk SSSR. Ser. Mat. - 1957. - Vol. 21. - P. 171—-198.
97. Mal'tsev A. I. The structural characteristic of some classes of algebras // Dokl. Akad. Nauk SSSR. - 1958. - Vol. 120. - P. 29–32.
98. Ellerman D. A theory of adjoint functors – with some thoughts about their philosophical significance // What is category theory? - Monza (Milan). Polimetrica, 2006. - P. 127–183.
99. Ellerman D. Adjoints and emergence: applications of a new theory of adjoint functors // Axiomathes. - 2007. - Vol. 17. - № 1. - P. 19–39.
100. csi B. P. On Morita contexts in bicategories // Applied Categorical Structures. - 2011. - P. 1–18.
101. Chronowski A. A ternary semigroup of mappings // Demonstr. Math. - 1994. - Vol. 27. - № 3-4. - P. 781–791.
102. Chronowski A. On ternary semigroups of homomorphisms of ordered sets // Arch. Math. (Brno). - 1994. - Vol. 30. - № 2. - P. 85–95.
103. Chronowski A., Novotný M. Ternary semigroups of morphisms of objects in categories // Archivum Math. (Brno). - 1995. - Vol. 31. - P. 147–153.
104. Gal'mak A. M. Polyadic associative operations on Cartesian powers // Proc. of the Natl. Academy of Sciences of Belarus, Ser. Phys.-Math. Sci. - 2008. - Vol. 3. - P. 28–34.
105. Gal'mak A. M. Polyadic analogs of the Cayley and Birkhoff theorems // Russ. Math. - 2001. - Vol. 45. - № 2. - P. 10–15.
106. Gleichgewicht B., Wanke-Jakubowska M. B., Wanke-Jerie M. E. On representations of cyclic n-groups // Demonstr. Math. - 1983. - Vol. 16. - P. 357–365.
107. Wanke-Jakubowska M. B., Wanke-Jerie M. E. On representations of n-groups // Annales Sci. Math. Polonae, Commentationes Math. - 1984. - Vol. 24. - P. 335–341.
108. Berezin F. A. Introduction to Superanalysis. - Dordrecht: Reidel, 1987. - 421 p.
109. Kirillov A. A. Elements of the Theory of Representations. - Berlin: Springer-Verlag, 1976.
110. Husemöller D., Joachim M., Jurčo B., Schottenloher M. G-spaces, G-bundles, and G-vector bundles // Basic Bundle Theory and K-Cohomology Invariants. - Berlin-Heidelberg. Springer, 2008. - P. 149-161.
111. Mal'tcev A. I. On general theory of algebraic systems // Mat. Sb. - 1954. - Vol. 35. - № 1. - P. 3–20.
112. Gal'mak A. M. Translations of n-ary groups. // Dokl. Akad. Nauk BSSR. - 1986. - Vol. 30. - P. 677–680.
113. Zeković B., Artamonov V. A. A connection between some properties of n-group rings and group rings // Math. Montisnigri. - 1999. - Vol. 15. - P. 151–158.
114. Zeković B., Artamonov V. A. On two problems for n-group rings // Math. Montisnigri. - 2002. - Vol. 15. - P. 79–85.
115. Carlsson R. N-ary algebras // Nagoya Math. J. - 1980. - Vol. 78. - № 1. - P. 45–56.
116. Bremner M., Hentzel I. Identities for generalized lie and jordan products on totally associative triple systems // J. Algebra. - 2000. - Vol. 231. - № 1. - P. 387–405.
117. Madore J. Introduction to Noncommutative Geometry and its Applications. - Cambridge: Cambridge University Press, 1995.
118. Kogorodski L. I., Soibelman Y. S. Algebras of Functions on Quantum Groups. - Providence: AMS, 1998.
119. Chari V., Pressley A. A Guide to Quantum Groups. - Cambridge: Cambridge University Press, 1996.
120. Majid S. Foundations of Quantum Group Theory. - Cambridge: Cambridge University Press, 1995.
121. Drinfeld V. G. Quantum groups // Proceedings of the ICM, Berkeley. - Phode Island. AMS, 1987. - P. 798–820.



Steven Duplij (Stepan Anatolievich Douplii) is a theoretical physicist, a Lead Staff Researcher of the Theory Group, Nuclear Physics Laboratory at V.N. Karazin Kharkov National University, and Doctor of Physical and Mathematical Sciences. He has more than hundred scientific publications, several monographs. The main scientific directions are supersymmetry and supermanifolds, quantum groups and their actions, singular theories and constrained systems, nonlinear and conformal electrodynamics, multigravity and Pauli-Fierz models, ternary and polyadic structures, von Neumann regularity and semigroups, DNA theory and genetic code. Editor-compiler of "Concise Encylopedia of Supersymmetry"(Springer), he has received grants from the Fulbright and Humboldt Foundations.

UDC 535.33.

ON THEORY OF SPECTRUM OF HYDROGEN-LIKE ATOMS

Yu.M. Poluektov*, V.N. Savchenko**
National Science Center "Kharkov Institute of Physics and Technology"
1, Akademicheskaya St., 61108 Kharkov, Ukraine
*** V.N. Karazin Kharkov National University*
Svobody Sq. 4, 61022, Kharkiv. Ukraine
E-mail: yuripoluektov@kipt.kharkov.ua
Received 30 May 2012, accepted 4 September 2012

Simple model of hydrogen-like atoms is proposed. Model is based on consideration of electron core, which consists of electrons in complete shells, using Thomas-Fermi model. Outer-shell electron is described by wave function. The model has no fitting parameters. Calculations of Rydberg correction for high-excited states with zero angular momentum are done. Calculations of energy of single ionization of hydrogen-like atoms and comparison with experimental data are done. The developed model can be used for further research of interaction of Bose-Einstein condensate and electromagnetic field.
KEY WORDS: Rydberg correction, alkali metals, atomic spectrum, Thomas-Fermi theory, atomic Bose – Einstein condensate**.**

К ТЕОРИИ СПЕКТРА ВОДОРОДОПОДОБНЫХ АТОМОВ
Ю.М. Полуэктов*, В.Н. Савченко**
** ННЦ ХФТИ*
ул. Академическая,1, Харьков, 61108
*** ХНУ им. В.Н. Каразина*
пл. Свободы 4, Харьков, 61022
Предложена достаточно простая модель водородоподобных атомов, основанная на том, что остов, состоящий из электронов заполненных оболочек, описывается моделью Томаса-Ферми, а внешний валентный электрон - волновой функцией. В рамках предложенной модели без использования подгоночных параметров вычислены поправка Ридберга для высоковозбужденных состояний с нулевым моментом и энергия однократной ионизации, проведено сравнение с экспериментальными данными. Развитая модель водородоподобных атомов может быть использована для дальнейшего развития теории взаимодействия бозе-эйнштейновских конденсатов с электромагнитным полем.
КЛЮЧЕВЫЕ СЛОВА: поправка Ридберга, щелочные металлы, спектр атома, теория Томаса-Ферми, атомарный бозе-эйнштейновский конденсат.

ДО ТЕОРІЇ СПЕКТРА ВОДНЬОПОДІБНИХ АТОМІВ
Ю.М. Полуектов*, В.М. Савченко**
** ННЦ ХФТІ*
вул. Академічна, 1, Харків, 61108
*** ХНУ ім. В.Н. Каразіна*
пл. Свободи, 4, Харків, 61022
Запропонована достатньо проста модель водньоподібних атомів, заснована на тому, що остов, який складається з електронів, що знаходяться у заповнених оболонках, описується за допомогою моделі Томаса-Фермі, а зовнішній валентний електрон описується хвильової функцією. В межах даної моделі без використання підгоночних параметрів обчислені поправка Рідберга для високозбуджених станів з нульовим моментом, енергія одноразової іонізації водньоподібних атомів, та проведено порівняння з експериментальними даними. Запропонована модель водньоподібних атомів може бути використана для подальшого розвинення теорії взаємодії бозе-ейнштейнівських конденсатів з електромагнітним полем.
КЛЮЧОВІ СЛОВА: поправка Рідберга, лужні метали, спектр атома, теорія Томаса-Фермі, атомарний бозе-ейнштейновський конденсат.

Hydrogen atoms and ions, that contain one electron, like, for example, He^{+}, Li^{++}, in non-relativistic approximation are described precisely [1-5]. Strict analytic calculations for atoms and ions containing two electrons, such as H^{-}, He, Li^{+}, are impossible, however these objects are simple enough to use different approximate methods, that provide sufficient accuracy [1-5]. Hartree - Fock self-consistent method usually is used to compute more complex atoms [6], but such calculations appear to be rather bulky, especially for atoms containing many electrons. Thomas-Fermi statistical method is widely used to investigate structure of many-electron atoms [7, 8]. Significance of this approach is simplicity, though it gives less accurate results and does not reproduce periodical dependence of atomic sizes and ionization potentials from atomic number.

Hydrogen-like atoms have simple enough energy spectrum similar to that of hydrogen atom. Atoms of alkali metals Li, Na, K, Rb, Cs, Fr , and so called Rydberg atoms, that have one electron in high-excited state [9], are considered as hydrogen-like atoms. Atoms of alkali metals drew attention in recent years, because they are used to obtain and investigate Bose-Einstein condensates in magnetic traps [10-12]. Phenomena in such condensates are theoretically described by Gross - Pitaevskii equation [13]. However, more consistent description of interaction of

© Poluektov Yu.M. , Savchenko V.N., 2012

Bose-Einstein condensate with electromagnetic field should take into account inner structure of atoms in condensate. Generalization of Gross-Pitaevskii equation, that takes structure of hydrogen-like atoms into consideration, is proposed in [14]. Influence of inner structure of atom on Bose – Einstein condensation in ideal gas of hydrogen-like atoms is considered in works [15, 16]. Development of rather simple model, that allows description of inner structure of alkali atoms, is significantly important for further development of theory of interaction of Bose-Einstein condensate with electromagnetic field.

Investigation of Rydberg atoms is of interest for astrophysics and for usage of such atoms as detectors of long-wave radiation [9]. Research of so called "Rydberg matter", which is metastable crystal consisting of high-excited atoms with the same principal quantum number [17], is of significant interest. Such matter should have density 10^{16} – 10^{19} cm^{-3} and thus be condensed matter with gas density and unique properties.

The aim of the present work is to develop rather simple model of structure of hydrogen-like atoms, which would allow taking into account influence of finite size of electron core, which consists of electrons in filled shells, on energy levels of valence electron with sufficient accuracy. In the proposed model electrons in atomic core are described by Thomas-Fermi approach and valence electron – by single-particle wave function. Calculations of quantum defect, energy of low-lying levels and ionization energy are done. The model has no fitting parameters.

MODEL DEFINITION

Hamiltonian of valence electron in hydrogen-like atom can be set as

$$H = -\frac{\hbar^2}{2\mu}\Delta + U(r), \tag{1}$$

where $\mu = mM/(m+M)$ is reduced mass, m is electron mass, M is overall mass of atomic nucleus and electron core, $U(r)$ is potential energy of electron in the field, produced by nucleus with charge $Z|e|$ and electron core with total charge $-(Z-1)|e|$. Hamiltonian of hydrogen-like atom (1) can be stated as sum of Hamiltonian of hydrogen atom and additional potential related to finite size of electron core

$$H = H_0 + V(r), \tag{2}$$

where

$$H_0 = -\frac{\hbar^2}{2\mu}\Delta - \frac{e^2}{r} \tag{3}$$

is Hamiltonian of hydrogen atom, and

$$V(r) = U(r) + \frac{e^2}{r}. \tag{4}$$

Potential energy can be stated as

$$U(r) = -|e|\Phi(r), \tag{5}$$

where $\Phi(r)$ is potential, created by nucleus with charge $Z|e|$ and electron core with full charge $-(Z-1)|e|$, that satisfy Poisson equation

$$\Delta\Phi(r) = -4\pi Z|e|\delta(\mathbf{r}) + 4\pi|e|n(r). \tag{6}$$

In (6) $n(r)$ is particle number density, which satisfies normalization condition

$$4\pi\int_0^{r_0} dr r^2 n(r) = Z - 1. \tag{7}$$

Here r_0 is boundary radius, where particle number density comes zero. As it is known [7, 8], neutral atom has $r_0 = \infty$, and for positively charged ion, as in our case of nucleus and electron core, r_0 is finite quantity.

In order to obtain electron core potential Thomas-Fermi approach is used. In this approach equation for electron density distribution is derived from condition of equality zero of variation of energy, which consists of kinetic energy, own electron potential energy and energy in external field [7, 8]. Thus, one has the equation

$$-\frac{5}{3}c_0\frac{\hbar^2}{m}n^{2/3} - U(r) + \mu = 0, \tag{8}$$

where $c_0 = 3^{5/3}\pi^{4/3}/10 \approx 2,871$. Chemical potential μ introduced in equation (8) allows taking into consideration conservation of overall electron number $N = Z - 1 = 4\pi\int_0^{r_0} dr r^2 n(r)$. From condition of turning electronic density

$n(r_0)=0$ into zero one concludes connection of chemical potential with electron core radius

$$\mu = U(r_0) = -\frac{e^2}{r_0}. \tag{9}$$

It is sufficient to use following function in further considerations

$$\chi(r) = U(r_0) - U(r). \tag{10}$$

This function is divergent from zero in $0 < r \le r_0$ range, is nonnegative everywhere and satisfies boundary conditions:

$$\chi(r_0) = 0, \qquad \chi(r) \to \frac{Ze^2}{r} \quad at \quad r \to 0 \tag{11}$$

and equation

$$\chi(r) = \frac{5}{3} c_0 \frac{\hbar^2}{m} n^{2/3}. \tag{12}$$

In the sequel it is suitable to introduce dimensionless function $\psi(x)$

$$\chi(r) = \frac{Ze^2}{r}\psi(x), \tag{13}$$

which depends from dimensionless variable $x \equiv r/L$. Here L denotes characteristic length, proportional to Bohr radius $a_0 = \hbar^2/me^2$:

$$L = \frac{a_0}{2Z^{1/3}}\left(\frac{3\pi}{4}\right)^{2/3}. \tag{14}$$

Taking into account (6), (11), (12) and (14) one gets Thomas-Fermi equation

$$x^{1/2}\frac{d^2\psi(x)}{dx^2} = \psi^{3/2}(x) \tag{15}$$

with boundary conditions

$$\psi(0) = 1, \qquad \psi(x_0) = 0, \tag{16}$$

where $x_0 = r_0/L$. Radius r_0 can be obtained from condition of continuity of electric field in point r_0

$$-\left.\frac{d\Phi}{dr}\right|_{r=r_0} = \frac{|e|}{r_0^2}. \tag{17}$$

Exact solution of Schrödinger equation for hydrogen atom is known. Influence of finite size of electron core (4) is considered with the use of perturbation theory. In terms of function (10) perturbation (4) takes the following form

$$V(r) = \begin{cases} \dfrac{e^2}{r} - \dfrac{e^2}{r_0} - \chi(r), & \text{при} \quad r < r_0, \\ 0, & \text{при} \quad r > r_0. \end{cases} \tag{18}$$

Hydrogen functions are known $\Psi_{nlm} = R_{nl}(r)Y_{lm}(\Omega)$, where $\Omega \equiv (\vartheta, \phi)$ are angular variables, and radial functions are normalized by condition $\int_0^\infty dr r^2 R_{nl}^2(r) = 1$. Every level is degenerated $2n^2$ times. Perturbation partially splits the levels. Using perturbation theory for degenerated states [2], one finds energy levels

$$E_{nl} = E_n^{(0)} + E_{nl}^{(1)}, \tag{19}$$

where $E_n^{(0)} = -\left(\mu e^4/2\hbar^2 n^2\right)$ are hydrogen energy levels. Under act of perturbation every level with given n splits into n levels, that are $2(2l+1)$ times degenerated. Correction to energy of the ground state is

$$E_{nl}^{(1)} = \int_0^{r_0} dr r^2 R_{nl}^2(r)\left(\frac{e^2}{r} - \frac{e^2}{r_0} - \chi(r)\right). \tag{20}$$

Solution of equation (15) is needed in order to obtain this correction.

APPROXIMATE SOLUTION OF THOMAS-FERMI EQUATION

Approximate solution of equation(15), obtained by Sommerfeld [7, 8], for neutral atom

$$\psi_0(x) = (1+z)^{-\lambda_1/2}, \tag{21}$$

where $z = \left(x/144^{1/3}\right)^{\lambda_2}$. Here $\lambda_1 = 7,772$, $\lambda_2 = 0,772$, and $\lambda_1\lambda_2 = 6$. For positively charged ion solution of (15) has the form

$$\psi(x) = \psi_0(x)\left[1 - \left(\frac{1+z}{1+z_0}\right)^{\frac{\lambda_1}{\lambda_2}}\right], \tag{22}$$

where $z_0 = \left(x_0/144^{1/3}\right)^{\lambda_2}$. Taking (17) into account, boundary radius is found from relation

$$q = \frac{Z-N}{Z} = -x_0 \left.\frac{d\psi(x)}{dx}\right|_{x_0}, \tag{23}$$

where $N = Z - 1$ is number of electrons in core. Substitution (22) into (23) gives the equation for obtaining z_0

$$\lambda_1 \frac{z_0}{(1+z_0)^{\frac{\lambda_1}{2}+1}} = q\ . \tag{24}$$

In the primary formulation, which is stated above, Thomas-Fermi theory took into consideration energy of self electric field of electrons. However, only energy of interaction of charged particles should be taken into account in quantum-mechanical description (see discussion in [18, 19]). Approximate way to eliminate self-field energy in Thomas-Fermi approach was proposed by Fermi and Amaldi [7].

Results of numeric calculations of electron core radii for atoms of alkali metals are stated in Table 1. Symbol $*$ marks results obtained taking into account Fermi-Amaldi correction. We should state that, strictly speaking, for lithium atom, which consists a few electrons, given model is non-applicable. Specifically, it appears in the fact, that equation for electron core radius for lithium atom with Fermi-Amaldi correction doesn't have solutions. Note, that elimination of self-field energy leads to decrease of core radius.

Table 1

Radius r_0 of singly ionized positive ions

Atom	Li	Na	K	Rb	Cs	Fr
r_0/a_0	2.555	4.483	5.100	5.742	6.074	6.419
r_{0*}/a_0	-	3.025	3.546	4.102	4.396	4.705

CALCULATION OF RYDBERG CORRECTION

Energy of high-excited levels of hydrogen-like atoms can be described by equation

$$E_{nl} = -\frac{Ry}{(n-\delta_l)^2}, \tag{25}$$

where $Ry = \mu e^4/2\hbar^2$ is Rydberg constant, and δ_l is quantum defect or Rydberg correction, which usually has positive sign. Taking quantum defect into account leads to splitting of energy levels, which are degenerated by principal quantum number in hydrogen atom. Rydberg correction is connected with first order correction to energy (20) by the following equation

$$\delta_l = -\frac{n^3}{2Ry}E_{nl}^{(1)}. \tag{26}$$

Since the perturbation in our case is always negative the first order correction is also negative. Thus, Rydberg correction is positive. Under the condition $r << na_0$ solution for radial part of wave function is expressed in terms of Bessel function [1]

$$R = \sqrt{\frac{2}{ra_0^2n^3}}J_{2l+1}\left(\sqrt{\frac{8r}{a_0}}\right). \tag{27}$$

Obtaining matrix element of perturbation with function (27) and substituting it into (26), one finds equation for Rydberg correction

$$\delta_l = -\frac{1}{a_0^2 Ry}\int_0^{r_0} drrV(r)J_{2l+1}^2\left(\sqrt{\frac{8r}{a_0}}\right). \tag{28}$$

Results of computations with equation (28) and experimental values are stated in Table 2. Obtained values at $l = 0$

appeared to be understated in comparison with experimental values [5]. However, accuracy of calculations, as one should suppose, increases with atom number. Calculated values of Rydberg correction at $l = 1,2,3$ appear to be significantly understated [20], what is conditioned by neglecting electric polarization of electron core by valence electron in present model.

Table 2

Values of Rydberg correction at $l = 0$

Atom	Li	Na	K	Rb	Cs	Fr
δ_0	0.148	0.832	1.402	2.482	3.403	4.823
$\delta_{0\exp}$	0.41	1.37	2.23	3.20	4.13	-

IONIZATION ENERGY OF HYDROGEN-LIKE ATOMS

In order to obtain ionization energy let's consider solutions for energy levels with azimuthal quantum number $l = 0$. Let R_n be radial part of solution of Schrödinger equation for valence electron

$$HR_n = ER_n, \tag{29}$$

where H is stated by equation (1). Solution R_n can be expanded into series in hydrogen radial functions with $l = 0$:

$$R_n = \sum_{n'} C_{nn'} R^{(0)}_{n'0}, \tag{30}$$

where $R^{(0)}_{nl}$ are radial functions for hydrogen atom. From Schrödinger equation (29) and series (30) one concludes infinite set of equations for expansion coefficients (30)

$$\sum_{n'} C_{nn'} \left(\left(E^{(0)}_{n'} - E \right) \delta_{n'n} + \left\langle n \left| \hat{V} \right| n' \right\rangle \right) = 0 \quad , n = 1,2,3\ldots . \tag{31}$$

System of equations (31) has nontrivial solution if determinant equals zero. Calculations considered a few lowest levels. Number of levels taken into account is determined from condition, that adding one more level changes energy less than on 1%. Results of such calculations are stated in Table 3. The last line of the table states the energy levels neglecting size of electron core.

Table 3

Ionization energies of atoms of alkali metals

Atom	Li	Na	K	Rb	Cs	Fr
Number of levels taken into account	4	10	13	16	18	20
Calculated energy, eV	4.61	4.49	3.51	3.50	3.11	3.08
Experimental value, eV	5.32	5.14	4.34	4.18	3.89	-
Point-like core, eV	3.40	1.51	0.85	0.54	0.38	0.28

Taking into account finite size of electron core significantly improves agreement between theoretical calculations and experimental values, especially for massive atoms.

CONCLUSION

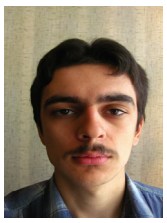
Simple enough model of hydrogen-like atoms, which are atoms of alkali metals and Rydberg atoms, is described in the present paper. In this model electron core, which consists of electrons in filled shells, is described by Thomas-Fermi approach, while outer-shell valence electron is described by wave function, which satisfies Schrödinger equation. Radii of electron cores, which are radii of singly ionized ions, are calculated. Rydberg corrections for high-excited states are calculated. Obtained values for s-states are in good agreement with experiment. Also, energies of single ionization of hydrogen-like atoms are calculated and compared with experimental data. It is shown, that taking into account finite size of electron core significantly improves agreement between theory and experiment. The theory allows further modification, related, in particular, with taking into considerations polarization of the core by valence electron. Core polarization should significantly influence on valence electron states with $l > 0$. Performed calculations lead to conclusion, that present model can be used, in particular, for describing many-particle systems of alkali metals, Bose-Einstein condensates and Rydberg matter.

REFERENCES

1. Bethe H., Salpeter E. Quantum Mechanics of One- and Two-electron Atoms. – M.: Fizmatgiz, 1960.
2. Landau L.D., Lifshits E.M. Kvantovaya Mekhanika. – M.: Nauka, 1989.
3. Condon E.U., Shortley G.H. Theory of Atomic Spectra. – M.: Inostrannaya Literatura, 1949.
4. Sobelman I.I. Vvedenie v Teoriyu Atomnykh Spektrov. – M.: Nauka, 1977.
5. Elyashevich M.A. Atomnaya i Molekulyarnaya Spektroskopiya. – M.: Fizmatgiz, 1962.
6. Hartree D. The Calculation of Atomic Structures. – M.: Inostrannaya Literatura, 1960.
7. Gombas P. The Statistical Theory of Atom and its Application. – M.: Inostrannaya Literatura, 1951.
8. Theory of Inhomogeneous Electron Gas. Edited by S. Lundqvist and N.H. March. – M.: Mir, 1987.
9. Smirnov B.M. Highly Exited Atomic States // Uspekhi Fiz. Nauk. - 1980. – Vol. 131. - P. 577. [Sov. Phys. Usp. – 1980. - Vol. 23. - P. 450.]
10. Anderson M.H., Ensher J.R., Matthews M.R., Wieman C.E., Cornell E.A. Observation of Bose-Einstein Condensation in a Dilute Atomic Vapor // Science. – 1995**. -** Vol. 269. - P. 198.
11. Davis K.B., Mewes M.-O., Andrews M.R., van Druten N.J., Durfee D.S., Kurn D.M., Ketterle W. Bose-Einstein Condensation in a Gas of Sodium Atoms // Phys. Rev. Lett. - 1995. - Vol. 75. - P. 3969.
12. Bradley C.C., Sackett C.A., Tollett J.J., Hulet R.G. Evidence of Bose-Einstein Condensation in an Atomic Gas with Attractive Interactions // Phys. Rev. Lett. – 1995. - Vol. 75. - P. 1687.
13. Pitaevskii L.P. Bose-Einstein Condensation in Magnetic Traps. Introduction to the Theory // Uspekhi Fiz. Nauk. - 1998**. -** Vol. 168. - P. 641. [Phys. Usp. – 1998**. -** Vol. 41. - P. 569.]
14. Poluektov Yu.M. Polarization Properties of Atomic Gas in a Coherent State // Fizika Nizkikh Temperatur. - 2011**. -** Vol. 37. - P. 1239.
15. Slyusarenko Yu.V., Sotnikov A.G. On the influence of the internal structure of the atom on Bose–Einstein condensation in an ideal gas of hydrogenlike atoms // Fizika Nizkikh Temperatur. – 2007. - Vol. 33. - P.41.
16. Slyusarenko Yu.V., Sotnikov A.G. Green-function method in the theory of ultraslow electromagnetic waves in an ideal gas with Bose-Einstein condensates // Phys. Rev. A. – 2008**.** - Vol. 78. – P.053622.
17. Holmlid L., Manykin E.A. Rydberg matter – a long-lived excited state of matter // Zhurnal Eksp. i Teor. Fiziki. – 1997. - Vol. 111. - P. 1601. [Journal of Exp. and Theor. Phys. – 1997. – Vol. 84. - P. 875.]
18. Vlasov A.D. The Schrödinger Atom // Uspekhi Fiz. Nauk. - 1993. **-** Vol. 163. - P. 97. [Phys. Usp. – 1993. - Vol. 36 (2).- P. 94.]
19. Pitaevskii L.P. On the Problem of the «Schrödinger Atom» // Uspekhi Fiz. Nauk. - 1993**. -** Vol. 163. - P. 119. [Phys. Usp. - 1993. - Vol. 36 (2). - P. 760.]
20. Kondratev V.N. Struktura Atomov i Molekul. – M.: Fizmatgiz, 1959.



Poluektov Yuri Matveevich - D.Sc. in physics and mathematics. Currently working as a Leading Researcher at Institute of theoretical physics at National Science Center "Kharkov Institute of Physics & Technology". His research interests are in the physics of many-particle systems, superconductivity, quantum fluids.



Savchenko Vladimir Nikolayevich - sixth year student in the department of Physics and Technology of V.N. Karazin Kharkov National University.

PACS: 52.55.Hc, 52.55.Rk, 52.55. Dj

ON PHYSICAL PARAMETERS OF THE DEMONSTRATION STELLARATOR-REACTOR OPERATING IN THE MODE OF SELF-SUPPORTED THERMONUCLEAR REACTION

V.A. Rudakov
Institute of Plasma Physics, NSC KIPT
Ukraine, 61108, Kharkiv, Akademichna st. 1
E-mail: rudakov@kipt.kharkov.ua
Received 2 July 2012, accepted 20 August 2012

With the use of a one-dimensional spatial-temporal numerical code under conditions of ambipolarity of neoclassical transport fluxes the regimes of the self-supported DT-fusion reaction in a reactor-stellarator are calculated. Cases of heating both ion and electron plasma components are considered. It is shown that powers of heating of plasma of scale 25 MW can be sufficient for excitation in reactor of the steady-state self-supported burning. Technical and physical parameters of such reactor correspond to characteristics of a demonstration reactor.
KEY WORDS: reactor-stellarator, ambipolar electric field, neoclassics, transport fluxes, plasma heating, power balance.

О ФИЗИЧЕСКИХ ПАРАМЕТРАХ ДЕМОНСТРАЦИОННОГО РЕАКТОРА-СТЕЛЛАРАТОРА, РАБОТАЮЩЕГО В РЕЖИМЕ САМОПОДДЕРЖИВАЮЩЕЙСЯ ТЕРМОЯДЕРНОЙ РЕАКЦИИ

В.А. Рудаков
Институт физики плазмы ННЦ ХФТИ,
Украина, 61108, Харьков, ул. Академическая, 1

С использованием одномерного пространственно-временного численного кода в условиях амбиполярности неоклассических транспортных потоков рассчитаны режимы поджига самоподдерживающейся реакции DT-синтеза в реакторе-стелларатоpе. Рассмотрены случаи нагрева как ионного, так и электронного компонентов плазмы. Показано, что мощности нагрева плазмы масштаба 25 МВт может быть достаточно для вывода реактора в режим устойчивого самоподдерживающегося горения. Технические и физические параметры такого реактора соответствуют характеристикам демонстрационного реактора.
КЛЮЧЕВЫЕ СЛОВА: реактор-стелларатор, амбиполярное электрическое поле, неоклассика, транспортные потоки, энергетический баланс.

ПРО ФІЗИЧНІ ПАРАМЕТРИ ДЕМОНСТРАЦІЙНОГО РЕАКТОРА-СТЕЛАРАТОРА, ЯКИЙ ДІЄ В РЕЖИМІ ТЕРМОЯДЕРНОЇ РЕАКЦІЇ ІЗ САМОПІДТРИМАННЯМ

В.А. Рудаков
Інститут фізики плазми ННЦ ХФТІ,
Україна, 61108, Харків, вул. Академічна, 1

Із використанням одновимірного просторово-часового чисельного коду в умовах амбіполярності неокласичних транспортних потоків розраховані режими підпалу реакції DT-синтезу, що самопідтримується в реакторі-стелараторі. Окремо розглянуті випадки нагрівання іонного і електронного компонентів плазми. Показано, що потужності нагрівання плазми масштабу 25 МВт може бути достатньо для виведення реактора в режим стійкого горіння, що сам підтримується. Технічні та фізичні параметри такого реактора відповідають характеристикам демонстраційного реактора.
КЛЮЧОВІ СЛОВА: реактор-стеларатор, амбіполярне електричне поле, неокласика, транспортні потоки, нагрівання плазми, енергетичний баланс.

Possibility of steady-state fusion reaction ignition and absence of global plasma disruptions, characteristic for tokamaks, can be considered as main properties of a stellarator determining its potentiality as a base for a fusion reactor. A stellarator possesses also some important features such as:

- Vacuum magnetic configuration providing the steady-state plasma confinement in the processes of burn phase and operating mode start-up and change;
- No pulsed thermal and power loads onto the first wall and equipment decreasing the device operating life;
- Lowering of design requirements to superconducting magnetic field systems and plasma heating systems;
- Possibility of divertor developing on the base of a natural magnetic field configuration.

Disadvantages of a classical stellarator include the complexity of a magnetic system including a toroidal field system and a helical field system. The problem was somewhat simplified by the torsatron idea, namely, to use unidirectional helical currents for creation of toroidal confining and helical magnetic fields, that was first suggested in [1] and subsequently developed in [2]. It turned out that it is possible to obtain longitudinal and helical magnetic fields using a solely system of unidirectional helical currents. A further research into simplification of the stellarator magnetic system resulted in different ideas on the modular system construction [3-6]. A modularity of the construction substantially simplifies the fabrication and maintenance of the system.

High plasma losses caused by the helical and toroidal magnetic field nonuniformity influence on the charged

© Rudakov V.A., 2012

particle drift motion, first predicted in [7], until recent times were one of the main obstacles in developing the fusion stellarator-reactor. Therefore, earlier fusion reactor studies led to large device sizes compared to similar projects on the base of a tokamak system. A prototype reactor developed in the USSR [8] had a major torus radius R=36 m and the minor plasma radius a=1.8 m. In the German project of a HSR reactor the major torus radius was equal to 22 m for the case of a five-field-period (M=5) and to 18 m in the M=4 variant [9,10]. The Japan projects of Force-Free Helical Reactors, (FFHR), based on the LHD experimental facility in different variants give a major radius R in the 10 – 20 m range [11].

In further investigations [12-14] the plasma losses under conditions characteristic for a fusion reactor were studied in more detail. An important peculiarity of these investigations was to learn about the role of an ambipolar electric field in the transport processes. The ambipolar electric field establishes the equality of ion and electron diffusion fluxes with conservation of plasma quasi-neutrality. It has been established that there are three electric field values permitting the equality of ion and electron diffusion fluxes [4], two of them being stable. It seems that the fusion modes permitting to realize a positive sign of radial electric field [14] (electron root) are more preferable.

The fusion plasma is characterized by the relatively low frequencies of Coulomb collisions at which the transport coefficients are strongly dependent on the amplitude of magnetic field ripples ε_h produced by helical harmonics. A high plasma loss level in the traditional stellarators because of a relatively high value of ε_h has stimulated the research of magnetic configurations providing confinement properties close to these of tokamaks. These properties can be reached by a special choice of a magnetic field harmonic composition when the effective helical field ripple is appreciably decreasing. Such configurations are referred to as quasi-symmetric ones. Therefore, in recent years the designing and building of new stellarator-type fusion facilities (e.g. NCSX, W7-X and CHS) is carried out with taking into account the idea of quasi-symmetry. When designing such magnetic systems high requirements are set up for accuracy in fabrication of magnetic field coils having a complicated spatial configuration that make their production difficult. Therefore the period of W7-X construction was prolonged in time and the NCSX facility creation was stopped. Besides, the magnetic systems with a LHD-type continuous helical winding and the modular version having similar properties allows one to obtain the field with sufficiently low values of helical ripples [6,15].

At forecasting the parameters of reactors and large-scale experimental facilities it is necessary to take into account the existing correspondence between the losses predicted by the neoclassical theory and losses observed in experiments using operating facilities. Paper [16] analyses the data of comparison between the experimental results and the neoclassical theory for three stellarators: LHD, W7-AS и TJ-II. The electric field values were calculated by the DKES code using the plasma density and plasma temperature distributions experimentally observed. In the case of ECR plasma heating the electron root is realized with a low plasma density ($n<3\cdot10^{19}\mathrm{m}^{-3}$) and the ion root – with $n>4\cdot10^{19}\mathrm{m}^{-3}$ [17]. For the central region of plasma column certain accordance between the neoclassical theory and experiment was obtained in the facilities LHD and TJ-II [18, 19].

Design works on stellarator-reactors are carried out practically in all the scientific centers where the plasma confinement in the stellarator systems is studied: Helias in Germany [10,20], series of FFHR reactors in Japan [11], ARIES–CS compact reactor project in the USA [21]. In this works one uses numerical codes considering the neoclassical transport (sometimes in combination with an anomalous one) and the ambipolar electrical field. The scalings obtained from analysis of experiments at fusion facilities are taken into account too. Although, there are many projects, it is difficult to find now these in which the steady-state fusion reaction can be realized as a result of a self-consistent solution from the coupled diffusion and heat conduction equations with given sources. In particular, the DKES code [22] is frequently used in which the spatial electric field distribution and other parameters are calculated from the given plasma density and temperature profiles. Only the transport TOTAL_P code realizes self-consistent solutions, which have been developed by T. Amano and K. Yamazaki, can be mentioned according to the available information [10]. One of the first results of this code application was density decreasing observed in the central plasma region under conditions of the reaction sustaining by fuel pellet injection.

In the previous author's paper [23] the one-dimensional space numerical code has been applied in which the system of heat conduction equations for ions and electrons, as well as, the diffusion equations with given initial and boundary conditions was used. The initial conditions were chosen so that the transition to the self-sustaining steady-state burn could occur without additional plasma heating sources. The LHD device was used as an analog for the structural model. The ambipolar electric field has been calculated from the condition of equality between the diffusion fluxes of electrons and ions. As a result, the system was self-consistently evolving to the steady state sustained by the fuel pellet injection model. It has been shown that using the fuel injection into the plasma column center it is possible to reach the self-sustaining steady-state burn in the comparatively compact reactor with major radius R=10 m, minor plasma radius a=2 m and magnetic field B=5 T. The results obtained were used to study in more detail the demonstration experiment feasibilities.

It is obvious that a necessary stage of R&D works on the problem of controlled nuclear fusion is the creation of the demonstration stellarator-reactor in order to demonstrate the self-sustaining fusion reaction of deuterium and tritium nuclei with expending costs as minimum as possible. The problem posed is not to realize an economically profitable project suitable for commercial use. Major R&D issues specific to the compact reactor include the following: the fact of demonstration of fusion burn modes and development of control methods for them. In solving this problem the

technical feasibilities for the project realization and its cost are very important. In particular, the engineering factors such as sizes, magnetic field values and plasma heating source powers, as well as, structural materials and design requirements should be within the limits of realizability. Then the reactor cost is proportional to its volume. In other words, the smaller is the reactor volume the lower is its cost.

The purpose of the presented work was to reach the self-sustained burn in the reactor having sizes as small as possible with conservation of acceptable magnetic field values using low plasma heating source powers as far as possible. In the work the author uses a set of equations described in [23] with thermal neoclassical transport coefficients. There the heat conduction equation includes additionally a term taking into account the energy exchange between ion and electron plasma components due to the radial electric field action. The nonzero plasma heating sources are used too.

SYSTEM OF EQUATIONS AND NUMERICAL MODEL

The system of equations being solved includes two heat conduction equations (for electrons and ions) and the diffusion equation describing the spatial-time behavior of plasma in the stellarator-reactor. A one-dimensional space dependence of plasma parameters on the average minor plasma radius is assumed. The system of equations differs from that of [23] as the heat conduction equations for electrons (1) and ions (2) contain an additional term taking into account the particle energy change as a result of their radial motion in the electric field.

$$\frac{3}{2}\mathrm{N}\frac{\partial T_e}{\partial t} = -\frac{1}{r}\frac{\partial}{\partial r} r\Pi_e + \frac{K_f N^2 \langle\sigma v\rangle}{4} E_\alpha + Q_{he} - Q_{ei} - Q_b - Q_c + Q_{\mathrm{E}}, \quad (1)$$

$$\frac{3}{2}N\frac{\partial T_i}{\partial t} = -\frac{1}{r}\frac{\partial}{\partial r} r\Pi_i + Q_{ei} + Q_{hi} - Q_{\mathrm{E}}, \quad (2)$$

$$\frac{\partial N}{\partial t} = -\frac{1}{r}\frac{\partial}{\partial r} rS_j + S_\delta. \quad (3)$$

The third equation in the system is the diffusion equation. The first term in the right-hand side of electron heat conduction equation (1) determines the temperature change provoked by the heat flux corresponding to the transport mode 1/ν in the neoclassical theory [13]. The second term in the right side describes the heating of electrons produced during the fusion by α– particles with the energy E_α=3.52 MeV. An equal deuterium and tritium content in the reactor plasma is assumed. The coefficient K_f determines the energy fraction given to electrons. It is considered that 95% of energy and α–particles goes for plasma heating, therefore in the calculations we have taken K_f=0.95. The next terms in the right-hand side of equation (1) are: Q_{he} - heating from external sources; Q_{ei} - heat exchange with ions as a result of Coulomb collisions; Q_b - bremsstrahlung; Q_c - cyclotron radiation; Q_{E} - particle energy change in the electric field due to their radial motion. When these reactor parameters are used the cyclotron radiation can transport a significant part of energy and, at the same time, it is well reflected from the chamber wall, therefore in the calculations its reflection coefficient is taken equal to 0.95. As a result, the main part of cyclotron radiation remains in the plasma and only 5% of power is absorbed by the reactor walls.

For numerical simulation we used different models of plasma heating by external sources: only the electron heating, only the ion heating or simultaneous heating of two components. It has been supposed that the specific heating power is proportional to the plasma density: $Q_{hj} = k_{hj} N$, where the subscript j denotes electrons or ions depending on the equation. The total heating power was determined by the integral through the plasma volume: $P_{hj} = \oint_V Q_{hj} d\mathrm{v}$.

The ambipolar electric field effect on the plasma particle energy is taken into account by the quantity $Q_{\mathrm{E}} = -S_j E_r$ under conditions when the diffusion fluxes of electrons and ions are equal: $S_e = S_i$.

In [23] and in this paper the heat fluxes and diffusion particle fluxes determined in [13] were used. The plasma electrons were assumed to be in the regime when the diffusion coefficient had the inverse dependence on the collision frequency and the ion diffusion follows the dependence $\sqrt{\nu}$. The right-hand side of density equation (3) contains the diffusion term and the term with the source S_δ with which the plasma density has been maintained at an approximately constant level. Diffusion losses have been compensated by the model of fuel pellet injection. As is shown in earlier studies [23] from the point of view of plasma confinement the fuel injection into the central plasma column region is optimum.

The system of equations (1 - 3) was supplemented with boundary and initial conditions. It has been assumed that the spatial derivatives of density, temperature and potential in the plasma column center are equal to zero.

$$T'_{j,x=0} = 0, N'_{x=0} = 0 \ , \ \Phi'_{x=0} = 0, \ T_{,x=1} = \delta_T, N_{x=1} = \delta_n \quad (4)$$

and the initial conditions satisfy the expressions:

$$T_{j,t=0} = T_{j,0}(1-x^n)+\delta_T, N_{j,t=0} = N_0(1-x^n)+\delta_n, \quad (5)$$

where the subscript j denotes a particle sort, x is the current plasma radius normalized to unity. In most calculations the exponent n at x in the initial conditions was taken equal to 2. The constants δ_n and δ_T determine the values of plasma density and temperature at the plasma column boundary. In these calculations they were taken equal to zero.

The electric field has been determined from the equation of equality between the ion and electron fluxes, $S_e = S_i$, at each step of space grid in the numerical code. Note, that in the general case there are three roots of the equation under consideration [14]. The calculations show that in different sections of the plasma radius there are the solutions with one and three roots simultaneously that complicates the choice of a solution which can be realized in the reactor. In [23] and in this paper it has been assumed that in all cases the electric field corresponds to the left (ion) root giving its negative values. Such a choice is not optimum from the point of view of reactor confinement properties. The more suitable might be the regime in which the electric field positive values are realized [14] (electron root), however, such solutions exist not always unlike the left (ion) root. It is logical to suppose that the reactor transition into the regime with a positive sign of ambipolar electric field will not lead to termination of the self-sustaining reaction and its power can be regulated by changing the corresponding parameters, for example, by the plasma density choice.

CALCULATION RESULTS

The present work similarly to [23] uses as a base the reactor concept providing the confining magnetic field B_0 equal to 5 T with a minor plasma radius a=2 m. The value of helical magnetic field ripple amplitude at the plasma edge ε_h has been taken 0.06. In the LHD stellarator the effective ripple at the plasma edge is 0.05 if the magnetic axis is shifted on the radius R = 3.53 m [15]. In [23] the self-sustaining burn regime has been set by the self-consistent evolution of plasma parameter profiles from the given initial conditions. The steady-state burning was successfully obtained in the reactor with R – 10 m by the fuel injection into the center of plasma column.

Here also the fuel pellet injection was simulated by the expression $\delta n = n_p(1 - r/\Delta)$ that corresponds to their "throwing" into the center of plasma having the evaporation region half-width Δ. The value Δ has been taken equal to the half plasma radius a. The fuel pellet mass contained 1% of the particle number in the reactor volume. The next fuel pellet is injected into the plasma when its density is less by 0.99 than the given value. In this case the energy losses on heating the injected particles are taken into account, and the energy losses on the pellet evaporation and atom ionization are neglected as they are comparatively small.

Unlike [23] here the fusion reaction ignition has been performed by the plasma heating starting from the relatively low temperatures. Following the results of [23] firstly the calculations have been carried out for parameters of the reactor with a major plasma radius R = 10 m. A total power of plasma heating used was varying from 20 to 80 MW. External heating sources were shut down after reaching the given fusion reaction power, then the steady-state burn was set with self-consistent spatial distributions of density, temperature and electric potential. In the case with a given average value of the plasma density independently on the initial distributions of rest parameters, the reactor reaches the ignition regime characterized by the same shape of spatial distribution of parameters and the same total fusion power.

In the process of heating and evolutionary alteration of parameters the shape of their distributions undergoes appreciable changes. Fig.1 shows the initial density and temperatures distributions with mean values $\langle N_0 \rangle = 7 \cdot 10^{19}$ m^{-3} and $\langle T_{e0} \rangle$ = 1keV, $\langle T_{i0} \rangle$ =1.5 keV, as well as, the ambipolar electric field distribution found from the equality of electron and ion diffusion fluxes, the initial conditions being given. The high gradient and the value of the ambipolar electric field are observed at the plasma boundary. A maximum negative electric field value is 60 kV/m at relatively low electron and ion temperature values.

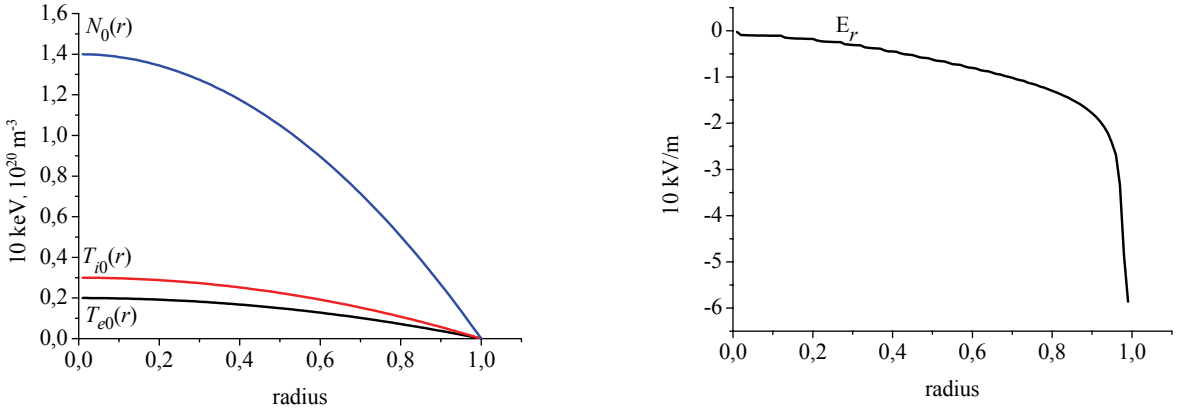
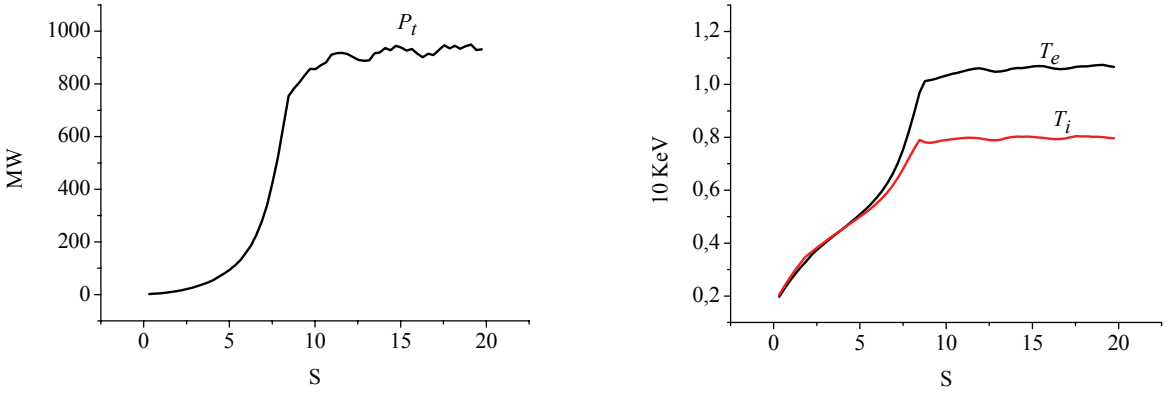


Fig.1 Initial distributions of plasma parameters
a – density, temperatures of ions and electrons, *b* – ambipolar electric field. R=10 m, a=2, B_0=5 T.

The Fig. 2 shows the behavior in time of the reactor fusion power and average values of electron and ion temperatures in the process of heating with subsequent transition to the self-sustaining burn regime. In the case under consideration the ion heating has been carried out (P_h = 40 MW). After reaching the thermal fusion power of 800 MW the heating source was shut down and the system evolved to the steady-state regime with a power of about 900 MW. It should be noted that this regime may be named as steady only conditionally because it is easy to see a slight variation with time in the temperature of both components and in the total reactor power too. Are these variations a consequence of in-reactor processes or the cause is related with the numerical code instability? It is yet not clear. Only one argument argues for internal processes: similar solutions are repeated independently on the initial conditions and heating power. By conserving the same average value of the plasma density the solutions give the same thermal power value in the steady-state burn regime.

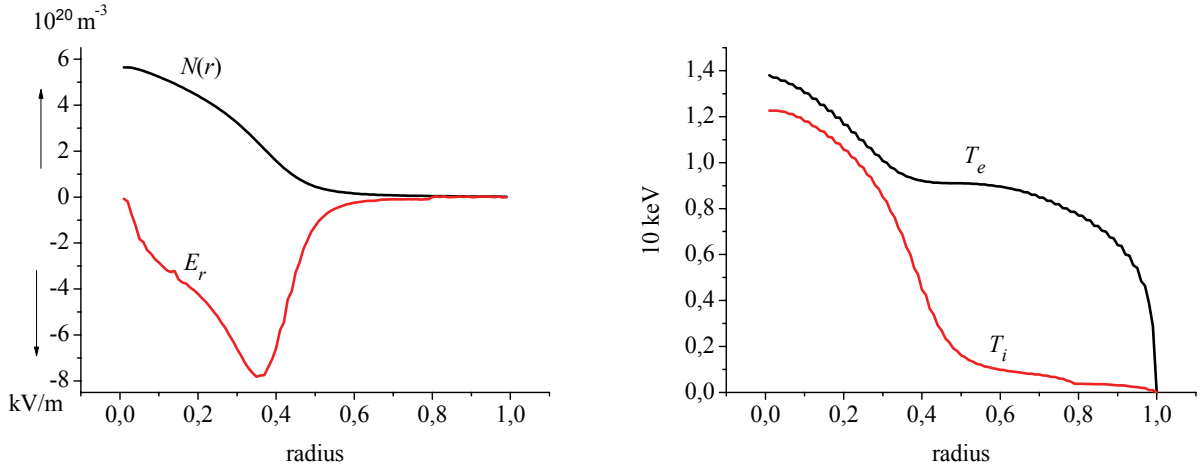
Note also that unlike the results of [23] the reactor thermal power is significantly lower (in that case with R=10 m and $\langle N\rangle$=6.4·10^{19} m^{-3} the steady-state burn was started at P_t= 1500 MW) that is a consequence of the lower ion temperature. The difference between the ion and electron temperature values is also appreciably larger then in the case published earlier. The causes of the difference will be explained below.



a *b*

Fig. 2. Ignition process and reactor transition into the steady-state burn regime
a – reactor thermal power in time, *b* – variation of electron and ion temperatures. R=10 m, a=2 , B_0=5 T, $\langle N\rangle$=7·10^{19} m^{-3}, ion heating P_h = 40 MW up to P_t =800 MW

Fig.3 illustrates the spatial distribution of the density, electric field, ion and electron temperatures of the plasma for the case of the steady-state burn. In the internal half of plasma column the plasma density considerably increases to N=6 10^{20} m^{-3} in the center. In the external radius section the plasma density decreases almost by two orders of magnitude as compared with the center of plasma. The electrical field behavior is the same as described in [23] – decreasing from zero in the center of plasma to 80 kV/m in the region of radius middle with a subsequent sharp rise to the close-to- zero values at the plasma boundary. The phenomenon of a deep minimum of radial electric field is revealed in experiments and is confirmed by calculations in installation W7-AS [16].



a *b*

Fig.3. Spatial distribution of parameters in the steady-state burn regime
a – densities of plasma and electric field, *b* – ion and electron temperatures. R=10 m, a=2 m, B_0=5 T, $\langle N\rangle$=7·10^{19} m^{-3}, ion heating P_h = 40 MW up to P_t =800 MW, t = 19.75 s.

The profiles of ion and electron temperatures are very different from these obtained in [23]. In the external half of

plasma radius the ion temperature behaves similarly to the plasma density profile decreasing with a sharp gradient in the middle radius section. In the external half of plasma the electron temperature has a convex profile with a much larger value than that of ions. The difference in the spatial temperature distributions is caused by the electron-ions interaction with the radial electric field: ions, overcoming the positive potential, give up their energy to the field, and electrons, moving radially, on the contrary, take away the energy from the field. As a result, the average ion temperature is appreciably lower than the average electron temperature that leads to the thermal reactor power lowering.

The calculations confirmed that the self-sustaining reaction can be reached not only for the case with a major radius R = 10 m, but also in the reactor with R = 8 m by conserving the confining magnetic field values and minor plasma radius: B_0=5 T, a=2 m. The Fig.4 represents the fusion power variation in time in the process of ion component heating with P_h = 40 MW for three values of the average plasma density: <N>=0.7..; 0.75… and $0.8\cdot10^{20}$ m^{-3}. The figure also shows the temperature behavior in time for the case <N>=$0.75\cdot10^{20}$ m^{-3}. In all the cases the heating source has been shut down after reaching the fusion power of 800 MW. In the case of the plasma density <N> = $0.8\cdot10^{20}$ m^{-3} the fusion power increase continues up to the level of 900 MW. When <N> = $0.75\cdot10^{20}$ m^{-3}, the reactor power decreases and reaches the steady-state level of about 780 MW. An appreciable power decreasing is observed when the plasma density decreases to <N> = $0.7\cdot10^{20}$ m^{-3}. In this case the thermal reactor power reaches the level of 600 MW.

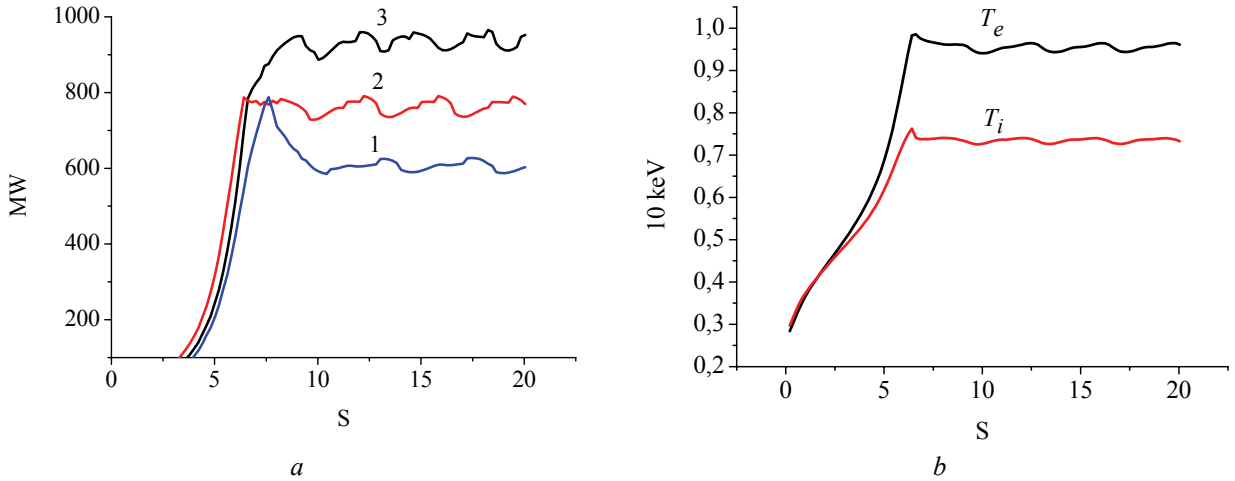


Fig. 4. Ignition process and reactor transition into the steady-state burn regime
a – thermal reactor power in time:1 - <N> = $7\cdot10^{19}$, 2 - <N> = $7{,}5\cdot10^{19}$, 3 - <N> = $8\cdot10^{19}$ m^{-3}; *b* – variation of electron and ion temperatures <N> = $7.5\cdot10^{19}$ m^{-3}, R=8 m, a=2 m, B_0=5 T, P_{hi} = 40 MW up to P_t =800 MW.

In the case of R = 8 m the spatial distributions of plasma density, electric field, temperatures, electrons and ions are similar to the distributions given in Fig.3 for the reactor with the major radius R = 10 m. The Fig. 5 illustrates the behavior in time of the bremsstrahlung and cyclotron radiation powers in the process of plasma heating and reactor transition into the steady-state burn regime. The figure shows also the change in time of the electric potential difference between the center and the edge of the plasma for the average density <N> = $7.5\cdot10^{19}$ m^{-3} and the plasma heating power P_h = 40 MW. After the reactor transition into the steady-state burn regime (t > 5 s) the potential, as well as, the rest plasma parameters are not changing.

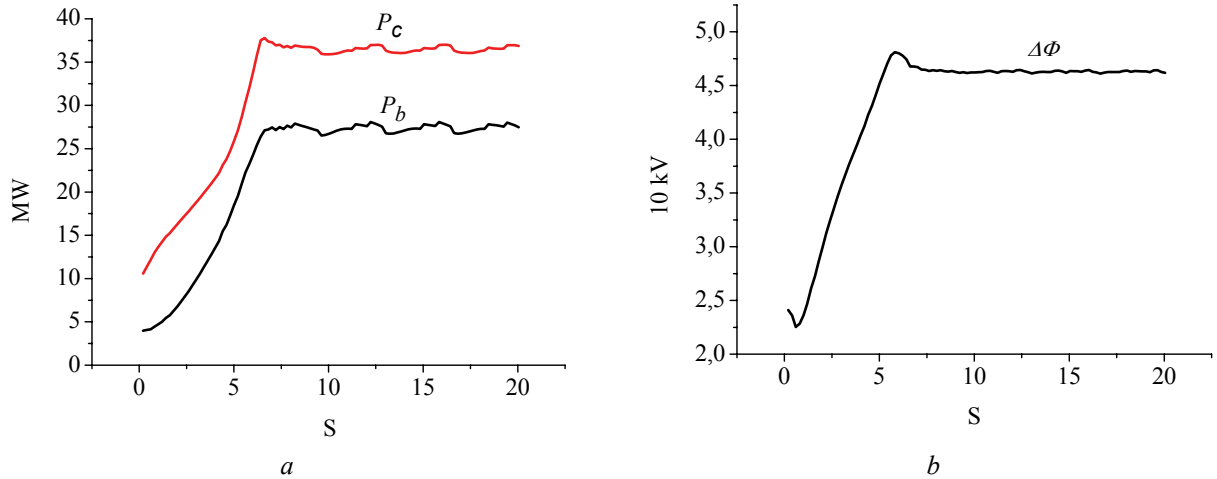


Fig. 5. Ignition process and reactor transition into the steady-state burn regime:
a – cyclotron radiation power - P_c and bremsstrahlung power – P_b in time ; *b* – behavior of the electric potential difference - $\Delta\Phi$ between the center and edge of the plasma. <N> = $7.5\cdot10^{19}$ m^{-3}. R=8 m, a=2 m , B_0=5 T, P_{hi} = 40 MW up to P_t =800 MW.

In the reactor with a power of 800 MW no more than 160 MW is released due to the α– particle energy absorption in the plasma. As a result of bremsstrahlung and cyclotron radiations the power losses are 65 MW that makes more than one third of all the power lost by the plasma. But, in the problem the impurity losses are not taken into account and, in particular, one should consider the loss increase provoked by the bremsstrahlung due to the presence in the plasma of some fraction of α– particles. Besides, in the problem it is assumed that only 5% of cyclotron irradiation is taken up by the first reactor wall, and the rest 95% are absorbed in the plasma. An appreciable decrease in the coefficient of cyclotron radiation can complicate the problem of obtaining steady-state burn regimes.

The energy loss increasing along the bremsstrahlung channel due to the α– particle presence in the plasma will be evaluated using the following considerations. Denote the α– particle lifetime in the plasma by the symbol τ_α. A number of α– particles produced in the process of fusion in time τ_α is easily determined using the division of the total reactor power by the energy of one fusion event with the multiplication by the α– particle confinement time

$$N_\alpha = P_t \tau_\alpha / E_f , \quad (6)$$

where E_f is the energy released as a result of one fusion event. And the relative α– particle fraction is the result of number N_α division by the total number of plasma ions. Such an evaluation for the reactor with R = 8 m, average density $\langle N \rangle = 7.5 \cdot 10^{19}$ m^{-3} and thermal power P_t=800 MW gives for the α– particle fraction

$$\eta_\alpha = N_\alpha \tau_\alpha / \langle N \rangle V = 6.2 \cdot 10^{-3} \tau_\alpha ,$$

where V is the plasma volume. It may be assumed that the order of α– particle diffusion is comparable with the main diffusion order. If the particle lifetime is approximately 3 s, a possible fraction of α– particles will be about 2% and their influence on the bremsstrahlung loss value will be, probably, insignificant.

The Fig. 6 presents the spatial distribution of the specific fusion power P_f and the quantity β determining the ratio of gas-kinetic and magnetic pressures. Also, in the figure shown is the time dependence of the pellet number that allows one to determine the particle loss rate and. consequently, to determine their confinement time. Note the high level of the quantity β in the plasma center (about 25%) despite a relatively low level of its average value. The dependences under consideration are the result of relatively sharp plasma density and temperature profiles. The same spatial distributions of β and specific fusion power were observed in [23] too.

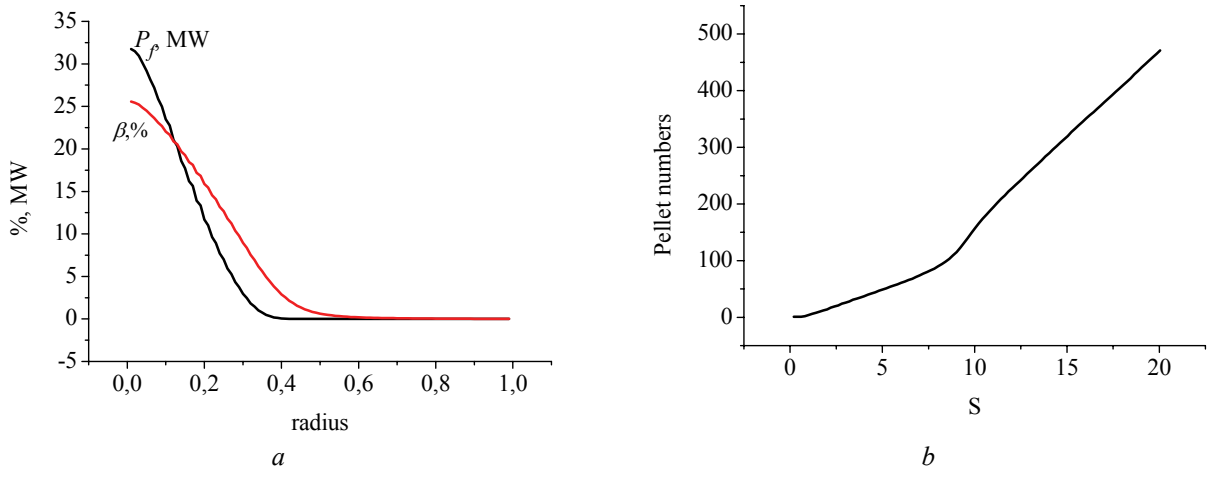
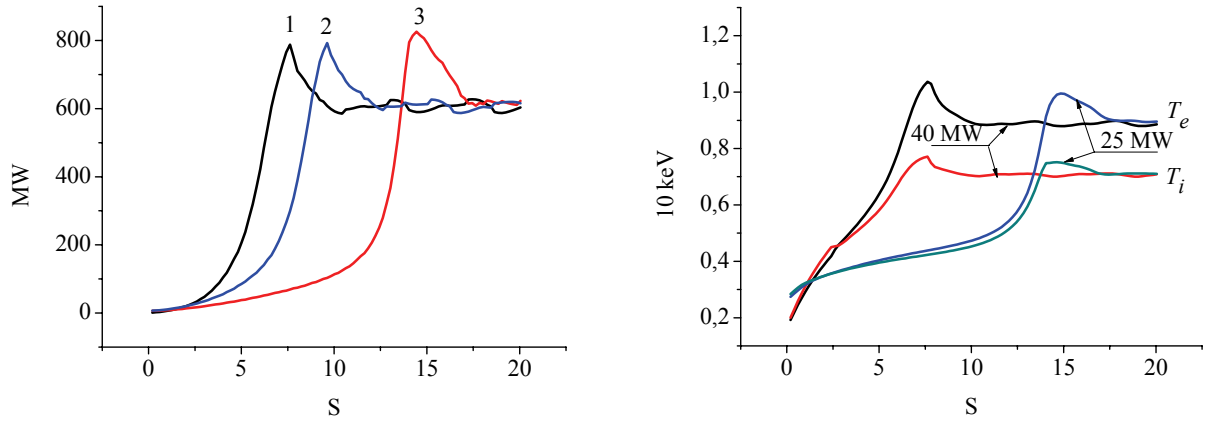


Fig. 6. Spatial distributions of specific fusion power and β values, and the time dependence of the pellet number
a – specific fusion power - P_f and quantity β in percents; *b* – increase of the pellet number in time. $\langle N \rangle = 7.5 \cdot 10^{19}$ m^{-3}. R=8 m, a=2 m, B_0=5 T, P_{hi} = 40 MW up to P_t =800 MW

The Fig. 2-6 illustrate the ignition and steady-state burn regimes in the stellarator-reactor for the heating power P_h = 40 MW. The calculations for other heating powers have shown that the self-sustaining fusion reaction can be reached with lower fusion powers. The Fig. 7 shows the fusion power behavior in the process of plasma heating using three power values from three heating sources - 40, 30 and 25 MW, as well as, the ion and electron temperature variations in time by injecting 40 and 25 MW into the plasma.

The use of a 40 MW heating power allows one to reach a 800 MW thermal fusion power in 7.5 s after the heating startup, and then the reactor turns into the steady-state regime of the self-sustaining reaction. In the case of 25 MW heating power the reactor reaches the 800 MW power level approximately in 14 s after the heating startup. When lower powers have been used, the reactor transition into the self-sustaining burn regime was not achieved. Note that independently on the P_h value, having other parameters conserved, the reactor goes to the fusion power level with like distributions of spatial density, electric field and plasma component temperatures.



a *b*

Fig. 7. Time dependences of the total thermal reactor power and of the plasma temperature calculated for different values of plasma heating power - P_h; *a* – thermal power behavior: 1- P_{hi} = 40 MW, 2 - 30 MW, 3 – 25 MW; *b* – time dependence of the temperature for two values of P_{hi} – 40 and 25 MW. Ion heating up to 800 MW with subsequent shut down of the heating source. $\langle N\rangle = 7\cdot10^{19}$ m^{-3}, R=8 m, a=2 m, B_0=5 T.

DISCUSSION AND CONCLUSION

The table presents the result of reactor parameter calculations for two values of the major torus radius R = 10 m and R = 8 m, and the parameters of the demonstration reactor of the DEMO-C tokamak are given too [24]. The minor plasma radius, magnetic field and amplitude of helical magnetic field distortion in all the stellarator-reactor variants were unchangeable. The average plasma density for the case R = 10 m was taken equal to $7\cdot10^{19}$ m^{-3}, and for R = 8 m the density was changing from $7\cdot10^{19}$ to $8\cdot10^{19}$ m^3. All the rest parameters are the consequence of the self-consistent solution of the system of equations (1-3) with a given initial and boundary conditions determined by expressions (4, 5).

Table

Reactor parameters

	RSt-1	DSt-2	DSt-3	DSt-4	DEMO-C [24]
Confining magnetic field –B, T	5	5	5	5	7.7
Major torus radius – R, m	10	8	8	8	7.8
Minor plasma radius – a, m	2	2	2	2	1.5
Mean density – $\langle N\rangle$,10^{20}/m^3	0.7	0.7	0.75	0.8	1.55
Electron temperature – T_e, keV	10.7	8.8	9.5	10.1	21
Ion temperature – T_i, keV	8	7.1	7.3	7.6	23
Helical ripple at the plasma boundary–ε_{hmax}	0.06	0.06	0.06	0.06	0
Total thermal power – P_t, MW	920	600	780	900	2400
Load onto the wall – Q_w, MW/m^2	1.15	0.94	1.22	1.4	2.5/3.4
Plasma pressure – $\langle\beta\rangle$, %	2.1	1.7	2.2	2.26	4.6
Energy confinement time – τ_E, s	1.33	1.4	1.24	1.16	2.1
Particle confinement time – τ_n, s	3.1	3.3	2.8	2.44	[1)]

Note a distinct difference in the reactor temperature and power from the results of [23] for the variant of a reactor with a major radius R = 10 m. Consideration of the radial electric field has led to the appearance of a significant difference in the ion and electron temperatures in the external plasma region. The average ion temperature was approximately by 2 keV lower as compared to the electron temperature. As a result, the reactor power was decreased. Nevertheless, the regime of self-sustaining burn was conserved.

In the tokamak reactor the major radius is sufficiently close to the torus radius dimension of the stellarator-reactor in the variant with R=8 m. The minor plasma radius in the tokamak is distinctly less (a=1.5 m against 2 m in the stellarator), however, its decrease is compensated by the significant increase of the magnetic field induction from 5 T to 7.7 T. The paper [24] does not contain information how have been obtained the plasma-physical parameters of the demonstration tokamak reactor. Note that the plasma temperature and density values in the tokamak reactor are several times higher than the corresponding values in the stellarator-reactor. As a result, the average value of β in the tokamak reactor is more than twice higher than in the stellarator-reactor despite the higher value of the confining magnetic field.

[1] The time of particle confinement is unknown.

Taking into account that the plasma temperature and density distributions have a maximum in the center of plasma, the local values of β here can reach several tens of percents and, consequently, there is a problem of a steady-state operation in such regimes. The local values of β for the case of the stellarator-reactor are shown in Fig.6 where β_{max}=25%. So, the problem of β values is common for both reactor types.

The present work shows a possibility for the reactor to reach a self-sustaining burn regime using a comparatively low (25 MW) power of the heating sources. Note, that in the DEMO-C project it is planned to use the plasma heating sources with a power up to 110 MW [24]. And at the same time the reactor in any case will not operate in the regime of self-sustaining reaction. Also here is shown the opportunity to control the reactor power by varying the plasma density. When the average plasma density is changing from $7\cdot10^{19}$ m^3 to $8\cdot10^{20}$ m^{-3} the reactor power increases by a factor of 1.5. At the same time, the fusion reaction ignition in the stellarator-reactor occurs with a much lower value of the confining magnetic field and, consequently, under conditions being less stressed in the view of engineering problems. And so, the demonstration stellarator-reactor seems more preferred than the tokamak reactor.

REFERENCES

1. Aleksin V.F. K raschetu magnitnogo polya stellaratora // ZhTF. – 1961.- T.3. - №11.- S. 1284 – 1288.
2. Gourdon C., Marty D., Maschke E.K., Touche J. // Nucl. Fusion. – 1971. – Vol.11. – P.161-166.
3. Wobig W. and Rehker S., Proc. 7-th Symp. on Fusion Technology . Grenoble, France. – 1972, October 24-27. – P. 333-343.
4. Miller R.L. et al. The Modular Stellarator-reactor: A Fusion Power Plant // Los Alamos National Laboratory report. La-9737-MS (July, 1983).
5. Kantan V.V., Emel'yanov G.S., Semenov A.A. i dr. Analiz i konstruktorskie prorabotki osnovnykh sistem TYaES s reaktorom-torsatronom // Voprosy atomnoy nauki i tekhniki. Ser. Termoyadernyy sintez. -1984. - Vyp. 2(15). - S. 25-35.
6. Rubtsov K. S., Rudakov V.A. New modular helical system properties close to a continuous helical trap / 23rd European Physical Society Conference on Controlled Fusion and Plasma Physics, Kiev, 24-28 June 1996. Contributed Papers. - Part II. - P. 543.
7. Galeev A.A., Sagdeev R.Z., Furth H.P., Rosenbluth M.N. // Phys. Rev. Lett.-1969.- Vol.22. – P. 511.
8. Anisimov V.V., Artyugina I.M., Kantan V.V. i dr. Vybor parametrov i tekhniko-ekonomicheskie otsenki TYaES na osnove chistogo reaktora-torsatrona // Voprosy atomnoy nauki i tekhniki, Ser. Termoyadernyy sintez.- 1984.- Vyp. 2(15). – S. 16-25.
9. Beidler C.D., Harmeyer E.et al. // Nucl. Fusion. -2001.- Vol. 41.- P. 12.
10. Amano T., Beidler, C. D. et al. Helias Reactor Studies // J. Plasma Fusion Res. SERIES.-2000.-Vol. 3. – P. 135-139.
11. Beidler C.D., Harmeyer E., Hernegger F. et al. Stellarator Fusion Reactors - an Overview // J. Plasma Fusion Res. SERIES .- 2002. – Vol. 5. – P.149-155.
12. Galeev A.A., Sagdeev R.Z. // Rev. Plasma Phys. -1979. -Vol. 7. – P. 257.
13. Kovrizhnykh L.M., The Energy Confinement Time in Stellarators // Nucl. Fusion. – 1984. – Vol. 24. – P. 435.
14. Mynick H.E., Hitchon W.N.G. Effect of the ambipolar potential on stellarator confinement // Nucl. Fusion. – 1983. - Vol.23. – P.1053.
15. Murakami S., Wakasa A., Maasberg H.et al. Neoclassical transport optimization of LHD // Nucl. Fusion. – 2002. -Vol 42. - L19-L22.
16. Turkin Y., Beider C.D., Maasberg H. et al. Neoclassical transport simulations for stellarators // Physics of Plasmas. – 2011. – Vol. 18. – P.022505.
17. J. Baldzuhn, et. al., Measurements and calculation of the radial electric field in the stellarator W7-AS // Plasma Phys. Control. Fusion. – 1998. – P.40 967.
18. Olaya J.G. Study of electron heat transport in LHD and TJ-II // PhD thesis presented for degree of doctor, Universitat Politechnica de Catalunya, 188 p.
19. Wakasa A., Murakami S., Oikawa S. Study of Neoclassical Transport in LHD Plasmas by Applying the DCOM/NNW Neoclassical Transport Database // Plasma and Fusion Research. - 2008. – Vol. 3. - P.1030.
20. Wobig H., Andreeva T., Beidler C.D. et. al. Development of Wendelstein Line towards a Helias Reactor // 36-th EPS Conference on Plasma Phys., Sofia, June 29 – Jully 3. – 2009. – ECA. – Vol. 33E. – P.4.192.
21. Najmabadi F., Rafray A.R., Long-Poe Ku, Lyon J. ARIES team Optimization of compact stellarator configuration as fusion devices // Physics of Plasmas. –2006. – Vol. 13. – P.056123.
22. Hirshman S.P., Shaing K.C., Van Rij W.I., Beasley C.O., Crume E.C. Plasma transport coefficients for nonsymmetric toroidal confinement systems // Phys Fluids. –1986. – Vol. 29. –P. 2951.
23. Rudakov V.A. O parametrakh reaktora stellaratora v usloviyakh ambipolyarnosti neoklassicheskikh transportnykh potokov // The Journal of Kharkiv National University, physical series "Nuclei, Particles, Fields". – 2012. – Vyp.2/54/.- S.15-23.
24. Kolbasov V.N., Borisov A.A., Vasil'ev N.N. i dr. Kontseptsiya demonstratsionnogo termoyadernogo energeticheskogo reaktora DEMO-S // Voprosy atomnoy nauki i tekhniki, Ser. Termoyadernyy sintez. - 2007.-Vyp.4. - S.3-13.



Rudakov Vasiliy, Ph.D., of physics-mathematical sciences, senior research worker of Institute of Plasma Physics National Scientific Center Kharkov Institute of Physics and Technology (NSC KIPT).
Scientific interests: thermonuclear fusion – reactor-stellarator problems, plasma confinement, magnetic field calcullations.

UDC 539.1.074:519.876.5; PACS 29.40.Wk, 85.30De, 07.85.-m

DETERMINATION OF SENSITIVITY OF SEMICONDUCTOR DETECTORS OF GAMMA-RADIATION

A.A. Zakharchenko
National Science Center "Kharkov Institute of Physics and Technology"
1, Akademicheskaya St., 61108 Kharkov, Ukraine
e-mail: az@kipt.kharkov.ua
Received 07 June 2012, accepted 09 August 2012

Properties of response functions of room temperature gamma-radiation detectors based on wide band-gap semiconductors are researched using Monte-Carlo method. It is shown that approximate formulas which connect detector sensitivity with absorbed energy of monochromatic radiation in the energy range between 0.06 and 3 MeV can be obtained for some kinds of semiconductors. We determined gamma-quantum energy regions and detector thicknesses where obtained approximate formulas are correct. Regions of maximum error of approximate formulas are also determined.
KEY WORDS: semiconductor detector, gamma-radiation, Monte-Carlo method, response function, sensitivity.

ОПРЕДЕЛЕНИЕ ЧУВСТВИТЕЛЬНОСТИ ПОЛУПРОВОДНИКОВЫХ ДЕТЕКТОРОВ ГАММА-ИЗЛУЧЕНИЯ

А.А. Захарченко
Национальный научный центр «Харьковский физико-технический институт»
61108, г. Харьков, ул. Академическая, 1

Методом Монте-Карло исследованы свойства функций отклика комнатно-температурных детекторов гамма-излучения на основе широкозонных полупроводников. Показано, что для ряда полупроводников можно получить приближенные формулы, связывающие чувствительность детекторов с энергией поглощаемого монохроматического излучения в диапазоне 0,06…3 МэВ. Исследованы области энергий гамма-квантов и толщин детекторов, где справедливы полученные зависимости. Также определены области максимальной погрешности приближенных формул.
КЛЮЧЕВЫЕ СЛОВА: полупроводниковый детектор, гамма-излучение, метод Монте-Карло, функция отклика, чувствительность.

ВИЗНАЧЕННЯ ЧУТЛИВОСТІ НАПІВПРОВІДНИКОВИХ ДЕТЕКТОРІВ ГАММА-ВИПРОМІНЮВАННЯ

О.О. Захарченко
Національний науковий центр «Харківський фізико-технічний інститут»
вул. Академічна 1, м. Харків 61108, Україна

Методом Монте-Карло досліджені властивості функцій відгуку кімнатно-температурних детекторів гамма-випромінювання на основі широкозонних напівпровідників. Показано, що для ряду напівпровідників можна отримати наближені формули, що пов'язують чутливість детекторів в діапазоні 0,06…3 МеВ з енергією монохроматичного випромінювання, що поглинається. Визначені області енергій гамма-квантів і товщини детекторів, де справедливі отримані залежності. Також визначені області максимальної похибки наближених формул.
КЛЮЧОВІ СЛОВА: напівпровідниковий детектор, гамма-випромінювання, метод Монте-Карло, функція відгуку, чутливість.

The measurement of energy dependence of gamma-radiation detector sensitivity is one of the laborious problems at investigation of room-temperature semiconductor detectors (SCD) which work in the pulse counting mode or pulse amplitude analysis mode. More than 10 certified gamma-radiation sources are required for measurement of SCD sensitivity in the energy range between 0.03 and 3 MeV. Most of these sources are produced from short-lived radioactive isotopes that have half-live about 1…2 years [1]. The lack of uniformity of electrophysical characteristics of room-temperature SCD [2] is a reason of considerable spread of absolute value of sensitivity δ and reason of necessity of detailed measurements of energy dependence $\delta(E_\gamma)$ for each detector. Through instability of SCD contact characteristics [3] it is necessary to repeat these measurements of $\delta(E_\gamma)$ periodically in order to have an opportunity to agree data obtained at different time periods.

Moreover isotopic gamma-radiation sources are not monochromatic. Efficiency of low energy (less than 60 keV) gamma-quantum registration with SCD is no less than 80%. At the same time the efficiency of relatively high energy (more than 500 keV) gamma-quantum registration of SCD does not exceed 5–7% (detector thickness is about 3 mm). When these both energy lines are present in the spectrum of the same source the Compton scattering region of high energy gamma-quanta is distorted by pulses from fully absorbed low energy quanta.

The Monte-Carlo simulation of SCD response can be used to overcome these difficulties but to obtain coincident results it is necessary to know control parameters of detector model with adjusted precision that is not always possible [2].

In this work we present results of numerical experiments to study the gamma-radiation semiconductor detector response functions $\delta(E_\gamma)$ for HgI_2, TlBr and CdZnTe semiconductor compound. Approximation formulas for calculation

© Zakharchenko A.A., 2012

of energy dependence $\delta(E_\gamma)$ of SCD sensitivity are obtained based on the analysis of properties of detector response functions. These formulas can be efficient for detector sensitivity calculation in the whole range of gamma-quantum energy between 0.06 MeV and 3 MeV using experimental measurements at the few energies. Maximum disagreement between approximation formula data and detailed Monte-Carlo calculation are evaluated.

The main objective of this work is to obtain the minimal set of approximate formulas which would allow to quickly calculating the sensitivity of wide band-gap semiconductor detectors nearly in the whole energy range of gamma-quanta emitted by radioactive isotopes.

FACTORS AFFECTING MEASUREMENTS OF ENERGY DEPENDENCE OF SCD SENSITIVITY

The sensitivity δ of semiconductor detector which used to detect single gamma-quanta (discrete sensitivity) is defined as ratio of pulse number N to unit of radiation dose [4]. Energy dependence of cross-sections of gamma-quantum interaction with detector material is a basic factor which defines the behavior of sensitivity $\delta(E_\gamma)$ with change of gamma-quantum energy. The total attenuation coefficient of gamma-quantum flow (μ) in the semiconductors is changed on four orders of magnitude in the energy range between 10 keV and 1 MeV (Fig. 1). The final form of $\delta(E_\gamma)$ (Fig. 2) depends on charge collection efficiency (*CCE*) of nonequilibrium carriers that are created at full or partial absorption of gamma-quantum energy inside detector material.

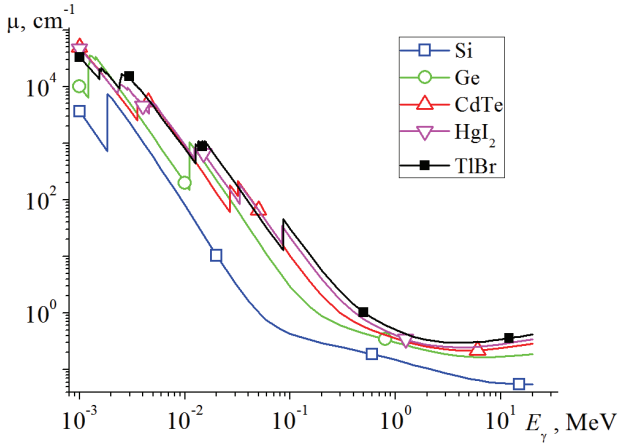


Fig. 1. The linear attenuation coefficient of gamma-quantum flow in the some semiconductors [5].

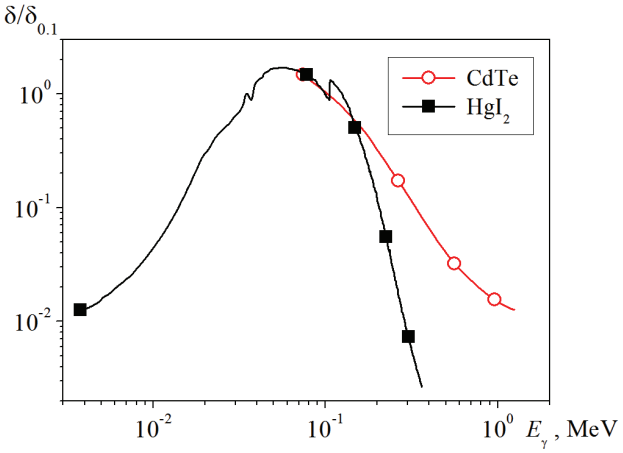


Fig. 2. The dependence of sensitivity vs gamma-quantum energy for CdTe [6] and HgI_2 [7] detectors.

Fig. 2 shows examples of experimentally measured dependencies of $\delta(E_\gamma)$. For convenience both curves are normalized to detector sensitivity $\delta_{0.1}$ which is measured at the energy $E_\gamma = 0.1$ MeV. CdTe detector with thickness of 2.8 mm is investigated in the Ref. [6] so $\delta_{CdTe}(E_\gamma)$ is measured in the energy range between 0.06 and 1.2 MeV. The energy dependence of CdTe detector sensitivity $\delta_{CdTe}(E_\gamma)$ is built according to measurement results with 9 gamma-radiation sources. Thickness of HgI_2 detector was about 0.5 mm and the measured energy dependence $\delta_{HgI_2}(E_\gamma)$ is restricted within range between 0.005 and 0.3 MeV [7]. Thickness of HgI_2 detector is a reason of low efficiency of gamma-quantum registration in the energy range more than 0.2 MeV and observable sharp loss of detector sensitivity (Fig. 2).

CCE is defined by great number of factors: coordinates of gamma-quantum interaction inside detector, mobility and lifetime of charge carriers (electrons and holes) and internal electric field intensity inside the detector [8, 9]. When detector with planar contacts and uniform distribution of internal electric field registers interaction between single gamma-quantum and detector material that *CCE* function has the rather simple form [8]:

$$CCE(x,d,\mu_e,\tau_e,\mu_h,\tau_h,U)=\frac{Q_{ind}}{Q_{tot}}=\frac{\mu_e\tau_e U}{d^2}\left(1-e^{\frac{-(d-x)d}{\mu_e\tau_e U}}\right)+\frac{\mu_h\tau_h U}{d^2}\left(1-e^{\frac{-xd}{\mu_h\tau_h U}}\right), \quad (1)$$

where Q_{ind} – charge that is induced on the detector contacts; Q_{tot} – average charge that is produced at absorption of the energy E in the detector; d – detector thickness; x – depth of gamma-quantum interaction with detector matter ($0 < x < d$); $\mu_{e,h}$ ($\tau_{e,h}$) – average mobility (mean lifetime) of electrons and holes; U – SCD bias.

Considerable variations of mobility ($\mu_{e,h}$) and mean lifetime ($\tau_{e,h}$) of nonequilibrium charge carriers are characteristic feature of all semiconductor materials which can be used for producing room-temperature gamma-radiation detectors [2]. The reasons of nonuniformity of electrophysical detector characteristics were not finally determined. For example, tellurium precipitate formation in the single crystal growing process can be defined as one of the factors that have influence on the characteristics CdZnTe detectors [10]. The sizes of these tellurium precipitates are changed in the range from about 1–2 μm to several hundred microns [11]. A great number of vacancies are formed near the bounds of Te precipitate. They form complexes of defects with Te atoms and trap holes at energetic levels located near top of the valence band [12]. These complexes of traps can be reason of the dark current increasing. As the traps

are non-uniformly distributed in the crystal [10, 11] that variations of dark currents and, correspondingly, variations of intrinsic noises are unpredictable from one detector to another.

The Refs. [10, 11] also showed that considerable variety of defects (point, lengthy, volumetric) is typical for as-grown CdZnTe ingots. In the aggregate these defects can essentially decrease charge carrier mobility and life time in the detector and at the same time they also can increase dark currents. The negative consequence of these effects is reduction of limiting work detector bias. The results of Ref. [13] show that if at selected SCD bias the intensity of internal electric field is less than 150 V/mm that planar CdZnTe detectors have inactive areas with null charge collection efficiency *CCE*. If the internal electric field intensity is less than 100 V/mm that *CCE* in the CdZnTe detectors can be decreased down to 4–5 times relatively maximum for specific detector.

One more factor which influences on the gamma-radiation SCD sensitivity is an polarization effect. In the general case the term «polarization» is used for identification of uncontrolled time changes of nuclear radiation detector characteristics after bias set up [14]. These changes can appear at the time distances from about a few minutes to a few weeks. Good known demonstrations of such changes are time variations of the energy resolution and gamma-quantum registration efficiency. The change of the registration efficiency directly influences on SCD sensitivity.

In the next part Monte-Carlo simulation of SCD response is used for illustration of influence of some above-listed processes on detector sensitivity.

SIMULATION OF RESPONSE FUNCTION OF ROOM-TEMPERATURE SCD

The model of calculation of response functions of room-temperature SCD was originally developed and tested for CdTe and CdZnTe detectors equipped planar contacts [15, 16]. Subsequently, this model has been applied for analysis of characteristics of other wide band-gap semiconductor materials [17, 18]. The universal EGSnrc code for the Monte-Carlo simulation of the passage of photons, electrons and positrons through matter [19] was used for computation. Besides interaction of gamma-quanta and charged particles with detector matter the model Ref. [15] allow to take into account the influence of noises and losses of nonequilibrium charge on the output signal amplitude.

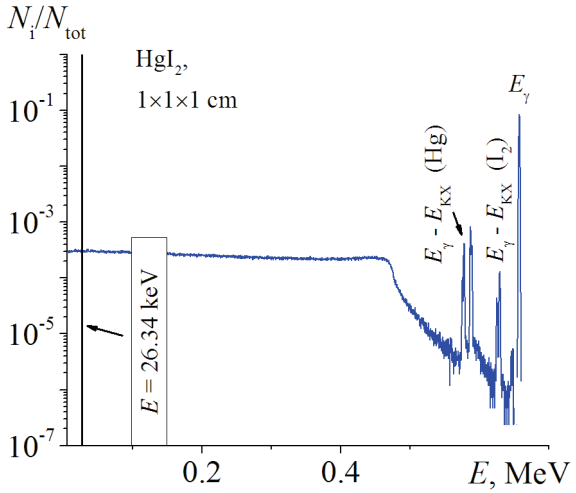


Fig. 3. The response function of HgI_2 detector on gamma-quanta with energy 662 keV without taking into consideration the charge collection and noises.

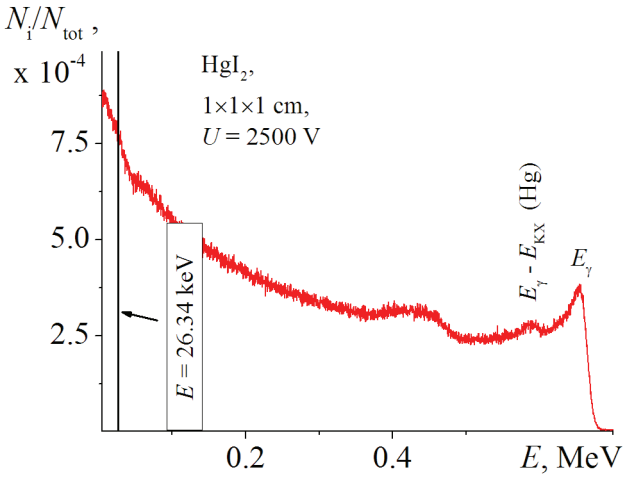


Fig. 4. The response of HgI_2 detector at the output of the measuring channel corresponded to Ref. [20].

Fig. 3 and 4 show calculated response function of HgI_2 detector equipped planar contacts on gamma-quanta with energy E_γ = 662 keV (^{137}Cs source) and its transform in the measuring channel. Plot ordinate is defined as the ratio of pulse counts N_i in i channel of the simulated analog-digital converter (ADC) to total pulse counts $N_{tot} = \sum_i N_i$.

Detector parameters correspond to data of Ref. [20]: sizes of 1×1×1 cm^3, charge transport characteristics – $(\mu\tau)_e = 5\times10^{-3}$ cm^2/V, $(\mu\tau)_h = 3\times10^{-5}$ cm^2/V, SCD bias U = 2.5 kV. Fig. 3 demonstrates processes of gamma-quantum energy absorption and nonequilibrium charge production in the detector. The investigated detector has sufficiently high probability of the complete absorption (photoeffect) of gamma-quanta with energy E_γ = 662 keV. Simulation shows that about fifty percent of the interacted quanta are fully absorbed. The efficiency of gamma-quanta registration for energy E_γ = 662 keV is about 42% and so absolute probability of scattering in the photopeak is about 21%. It means that less than 25% of input gamma-quantum flow is fully absorbed in HgI_2 at the length 1 cm. Escape peaks corresponded to characteristic gamma-quanta of the mercury and iodine which have left the detector volume are clearly visible on the Compton valley background (0.45 < E < 0.65 MeV). The ratio of photopeak amplitude E_γ to the average pulse amplitude in the Compton continuum region (0 < E < 0.45 MeV) exceeds two orders of magnitude. Small peak spreading is connected with fast electron energy losses due to the generation of lattice vibrations (losses up to 5%).

Fig. 4 shows changes of response function of HgI_2 detector (Fig. 3) at the output of the measuring channel. A main part of pulse amplitudes is shifted to the Compton continuum region. The escape peaks are almost completely spreaded.

The ratio of the photopeak amplitude E_γ to the average amplitude in the Compton continuum region (i.e. where $0 < E < 0.45$ MeV) is less than 1.3. In whole the response function (Fig. 4) has satisfactory agreement with calculation in Ref. [20].

The total number of pulses N_{tot} is the same in both cases (Fig. 3 and Fig. 4). However it is necessary to notice that in the real measurements the initial part of region of small amplitudes is not taken into account by reason of its overlapping with noise region. If the discrimination threshold is specified as 26.34 keV (it is one of the gamma-lines of ^{241}Am source) that calculated sensitivity value δ_3 is about 1249.4 (Fig. 3) and δ_4 is about 1163.9 pulse/μR (Fig. 4), respectively. In other words experimentally measured value of sensitivity does not exceed 93% from theoretically possible value (ratio δ_4/δ_3 is about 0.93). It is an acceptable result.

Unfortunately, mentioned value of difference is not final. Results of simulation (Fig. 4) are satisfactorily conformed to calculations that presented in the Ref. [20] but the shape of the showed there experimental ^{137}Cs spectrum differs from the shape of calculated spectrum. The most important distinctions are the photopeak lack and higher value of experimental ratio N_i/N_{tot} at the initial energy range in comparison with simulation. The variation of the model parameters showed that we can achieve such spectral distribution if the intensity of internal electric field inside the detector is much less than expected value that is U/d = 2500 V/cm for planar detectors. It can be a consequence of the distortion of the internal electric fields near numerous growth defects of semiconductors as in Ref. [13, 21]. This case can be reproduced within the used model at lower bias U (Fig. 5). From Fig. 5 it follows that the photopeak is absent as it occurs for the real spectrum of ^{137}Cs source that was presented in Ref. [20]. The pulse number in the initial channels exceeds the average value of pulse number in the Compton continuum up to one order of magnitude.

Fig. 6 shows change $CCE(x)$ corresponding to reduction of the internal electric field intensity inside the detector. At the same time the detector thickness-averaged collection efficiency CCE is decreased from 57.6% to 42.9%. It leads to complete degradation of the 662 keV photopeak (Fig. 5).

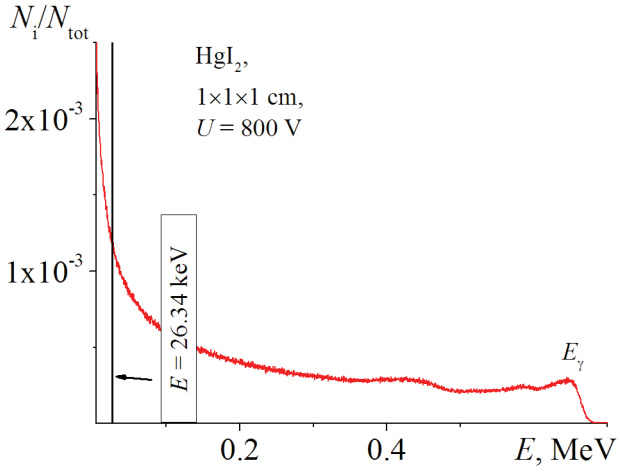


Fig. 5. The change of HgI_2 detector response for lower bias.

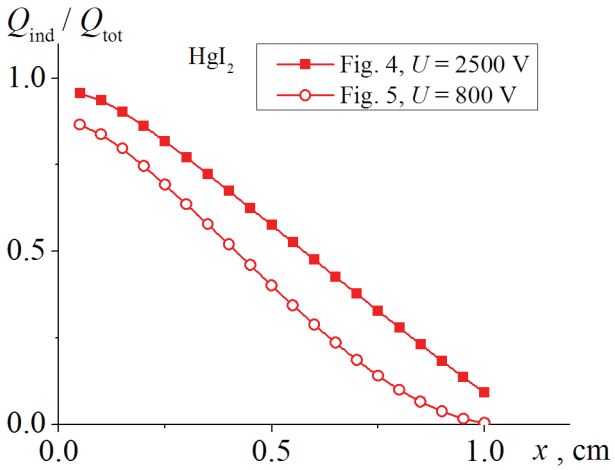


Fig. 6. The change of the charge collection efficiency CCE(x) in the HgI_2 detector.

Calculated sensitivity corresponding to condition of simulation that showed on Fig. 5 is $\delta_5 \approx 1033.4$ pulse/μR and ratio (δ_5/δ_3) is about 0.83. With the noise level increasing the discrimination threshold needs to be specified up to 60 keV and more. As the result the difference between measured sensitivity and maximum possible value of sensitivity can be even worse than mentioned ratio (δ_5/δ_3).

This example presents mediated influence of the defects on SCD sensitivity and problems of recovery of the energy dependence of SCD sensitivity $\delta(E_\gamma)$ using the Monte-Carlo method. The change of value of the internal electric field intensity is one of the ways to make agree between simulation and experiment data. The similar result for this HgI_2 detector can be obtained by changing the ratio between $(\mu\tau)_e$ and $(\mu\tau)_h$. Additional experimental measurements are necessary to choose the variant of matching.

Approximate formulas with several (2 or 3) fit parameters which allow to quickly calculate the sensitivity value $\delta(E_\gamma)$ for the wide gamma-quantum energy range (for example, 0.06…3 MeV) can be useful at the limited set of the experimental data.

RESULTS AND DISCUSSION

This part presents the results of the simulation of the gamma-radiation SCD response functions and the calculation of the $\delta(E_\gamma)$ function. The group of the semiconductor materials which are intensively researched for the past years [22] was chosen for this investigation. For comparison simulation of the cooled germanium detector was run, too. Table 1 contains the parameters of the simulated detectors.

Table 1.

The characteristics of the simulated gamma-radiation detectors

No	Detector	Sizes	$(\mu\tau)_e$, cm^2/V	$(\mu\tau)_h$, cm^2/V	U, V	Refs
1	HgI_2	$25\times25\times2.89$ mm^3	5×10^{-3}	3×10^{-5}	2800	[23]
2	TlBr	7 mm^2 × 1 mm	5×10^{-4}	2×10^{-6}	200	[24]
3	CdZnTe	$6\times6\times3$ mm^3	1.1×10^{-4}	1.3×10^{-5}	300	[15]
4	CdZnTe	$4\times4\times2.5$ mm^3	4×10^{-3}	2×10^{-5}	400	[25]
5	Ge	1000 $mm^2\times13$ mm	1	1	1000	[26]

The intensity of the simulated gamma-quantum flux is the same (10^3 quantum/s) for whole considered energy range between 0.04 and 3 MeV. It is supposed that values of noise characteristics of the simulated measuring channel are like that: equivalent noise charge is 300 e^- (charge units) and leakage current (or dark detector current) is 5 nA. Thus total noise level (detector + measuring channel) is about 400 e^- or less than 2 keV. The discrimination threshold for calculation of the sensitivity has been specified as 26.34 keV because it is proper to set up in the experimental measurements using ^{241}Am source. The shaping time is 1 μs. The dead time of the simulated analog-digital converter is 100 μs.

Fig. 7 shows the results of simulation of the sensitivity dependence $\delta(E_\gamma)$ from the energy of the registered gamma-quanta for CdZnTe detectors no. 3 and 4 (Table 1). Previously it was demonstrated that the simulation data satisfactorily agree with results of the metrological measurements [15]. The comparison between Fig. 2 and Fig. 7 confirms the trend of the $\delta(E_\gamma)$ curves. The smaller volume of detector no. 4 as compared with detector no. 3 is the cause of lower absolute values of its sensitivity $\delta(E_\gamma)$.

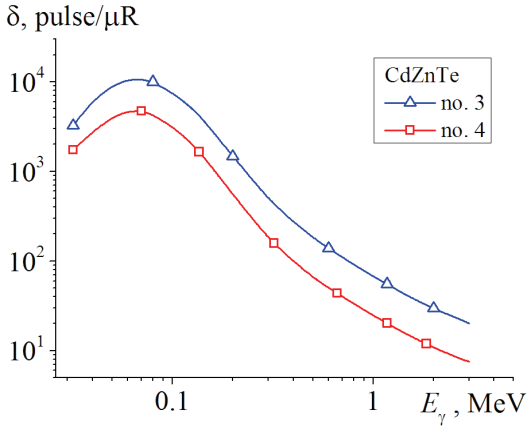


Fig. 7. The dependence of sensitivity vs the energy of registered gamma-quanta for CdZnTe detectors.

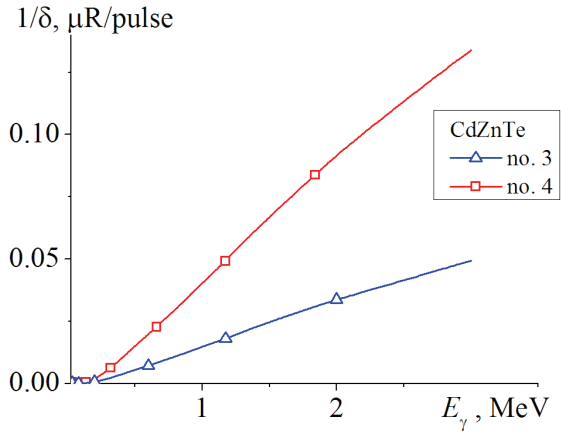


Fig. 8. The dependence $1/\delta = f_0(E_\gamma)$ for CdZnTe detectors.

The analysis of the functional dependence $\delta(E_\gamma)$ for CdZnTe detectors is simplified if the inverse function $1/\delta = f_0(E_\gamma)$ is used. Fig. 8 shows that the functions $1/\delta$ are nearly linear in the energy range E_γ above 0.2 MeV. It allows to suppose that the dependence $\delta(E_\gamma)$ at $E_\gamma \geq 0.2$ MeV can be restored using the function $1/\delta_{fit} = a_0 \times E_\gamma + b_0$. The Table 2 contains the fitting data obtained with the method of least squares at the different initial energies E_0 included in the fitting region.

Data from Table 2 show that the coefficients of the fitting curve are weakly changed even if the nonlinear region between 0.06 and 0.2 MeV is also fitted. Fig. 9 shows the relative difference η between the inverse sensitivity values of CdZnTe detector no. 4 obtained using the simulation data $1/\delta_{simul}$ and using the next expression for linear function $1/\delta_{fit} = a_0 \times E_\gamma + b_0$:

$$\eta = \frac{\frac{1}{\delta_{fit}} - \frac{1}{\delta_{simul}}}{\frac{1}{\delta_{simul}}} \times 100\% . \qquad (2)$$

The difference curves for CdZnTe detector no. 3 do not demonstrate essentially distinctions in comparison with detector no. 4. Fig. 9 shows that the satisfactory fit between the simulation and the fitting data in the energy range E_γ above 0.5 MeV is obtained even if the initial point of fitting specified as $E_0 = 60$ keV. It means that high-energy part of the $\delta(E_\gamma)$ dependence for CdZnTe detectors can be restored with satisfactory accuracy using measurement results with three sources: ^{241}Am (E_γ equals 60 keV), ^{137}Cs (E_γ equals 662 keV), ^{60}Co (doublet 1173 and 1333 keV). Ukrainian national primary standard of the units of exposure dose and exposure dose rate of X- and γ-radiation contains these three sources. Fig. 10 shows the examples of the spectra of ^{137}Cs and ^{60}Co sources calculated for CdZnTe detector no. 3.

Table 2.

The parameters of the linear fitting of $1/\delta(E_\gamma)$ for CdZnTe detectors (Fig. 8)

Initial point, MeV	no. 3		no. 4	
	a_0	b_0	a_0	b_0
0.06	0.0175±0.0002	–0.0024±0.0002	0.0476±0.0005	–0.0064±0.0006
0.1	0.0177±0.0002	–0.0027±0.0002	0.0482±0.0005	–0.0074±0.0006
0.2	0.0180±0.0002	–0.0032±0.0003	0.0489±0.0005	–0.0086±0.0007

The simulation of the spectra of ^{137}Cs and ^{60}Co sources illustrates above mentioned problems of the experimental sensitivity measurement connected with the non-monochromatic of gamma-radiation. Although the relative intensity of low-energy multiplet of ^{137}Cs source centered around 32.2 keV is about 6% (at the same time the intensity of 662-keV line produced by the ^{137}Cs source is 85%) but its contribution in the value of δ can be considerable. Thus, if the discrimination threshold is specified as 26.34 keV that the value of sensitivity of CdZnTe detector no. 3 calculated using the simulation of the ^{137}Cs source (Fig. 10) is 166.1 pulse/μR whereas for the 662-keV monochromatic line sensitivity is 120.4 pulse/μR.

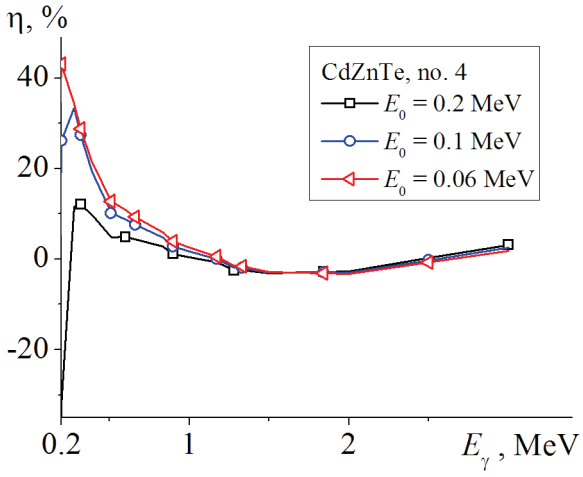


Fig. 9. The difference between the inverse sensitivity values for the simulation and fitting (Fig. 8).

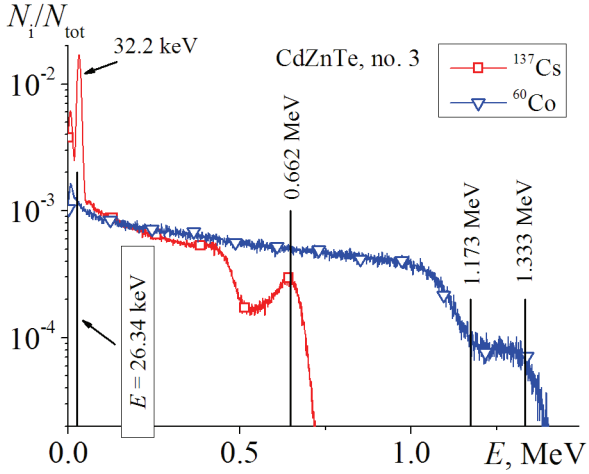


Fig. 10. The calculated spectra of the ^{137}Cs and ^{60}Co sources for CdZnTe detector.

The problem of the nonmonochromaticity for the ^{137}Cs source can be solved using the thin metallic filter absorbed low energy gamma-quanta or increasing the discrimination threshold up to 40–45 keV. However the separation of the neighboring lines with the same intensity is not possible for the ^{60}Co source. The calculated value of sensitivity for the ^{60}Co source is 48.5 pulse/μR (Fig. 10). It corresponds to gamma-quantum energy about 1.28 MeV. The simulation predicts the sensitivity values 55.4 (1173 keV) and 46.8 (1333 keV) pulse/μR for monochromatic lines that correspond to ^{60}Co source. In other words at the experimental measurements of $\delta(E_\gamma)$ the characteristics of the real ^{60}Co source need to be recalculated for the equivalent source of gamma-quanta with energy 1.28 MeV.

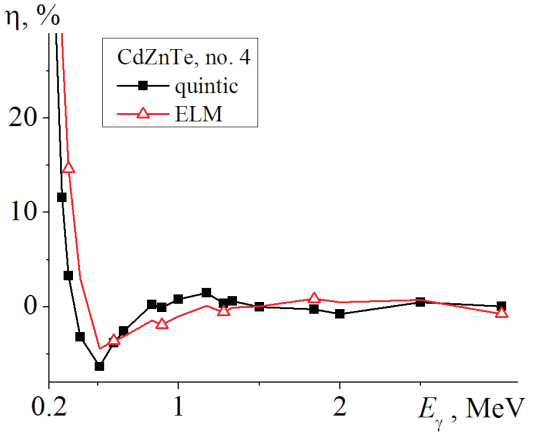


Fig. 11. The difference between inverse sensitivity values for the simulation and different kinds of the fitting.

As Fig. 11 shows the satisfactory approximation $1/\delta = f_0(E_\gamma)$ in the energy range E_γ above 0.2 MeV can be obtained if function $f_0(E_\gamma)$ has either quintic polynomial form or form of

$$\frac{1}{\delta} = \frac{abE_\gamma^{1-c}}{1+bE_\gamma^{1-c}}, \qquad (3)$$

where a, b and c – – the fitting parameters of the extended Langmuir model – ELM.

The number of the experimental points which are necessary for the reliable determination of the polynomial coefficients can exceed the number of the usually accomplished measurements of detector sensitivity. Moreover the difference between the both approximate formulas (the quintic or ELM) and the data of the sensitivity simulation of the CdZnTe detectors in the energy range E_γ below 0.2 MeV is too large. The Fig. 12 shows that power function can satisfactorily fit $1/\delta$ in the energy range between 0.06 and 0.3 MeV. The uniform distribution of the section of fitting between 0.06 and 0.1 MeV by experimental data is desirable for the reliable determination of the power function coefficients. However in practice either one point (60 keV, ^{241}Am) is presented in the energy range between 0.06 and 0.1 MeV [6] or all measurements are grouped

around one or two energies [1, 7].

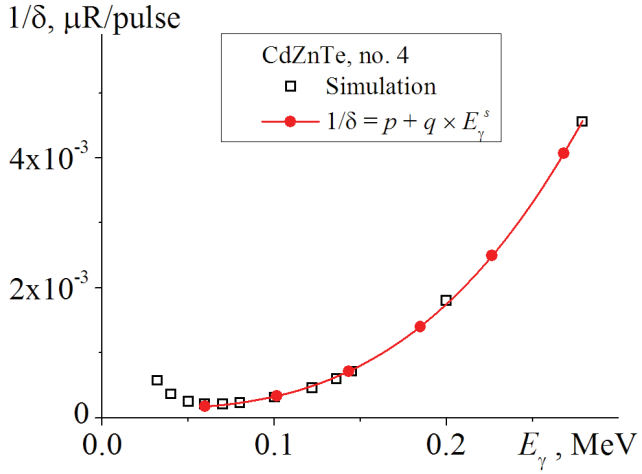


Fig. 12. The fitting of the dependence 1/δ using the power function for CdZnTe detector (p, q, s – fitting parameters).

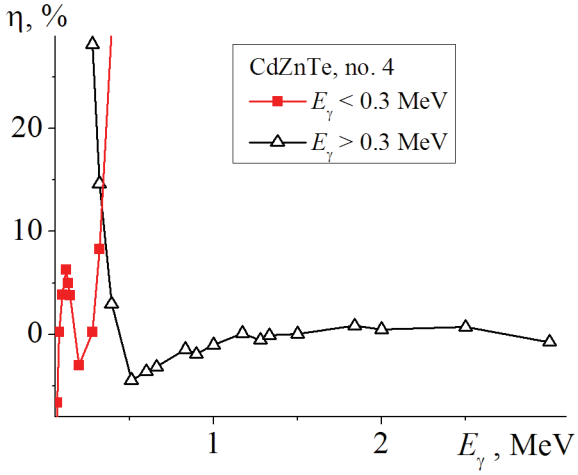


Fig. 13. The difference between the approximate formulas (4) and the Monte-Carlo simulation data for CdZnTe detectors.

As Fig. 12 and Fig. 13 show the satisfactory fit between approximate and simulated values of $1/\delta(E_\gamma)$ in the whole energy range between 0.06 and 3 MeV can be obtained with increasing the number of the points in the energy range E_γ from 0.06 to 0.1 MeV. The maximum error of the approximate formulas for the calculation of $1/\delta(E_\gamma)$ for CdZnTe detectors is found in the energy range E_γ between 0.3 and 0.4 MeV and can exceed up to +10% (Fig. 13). Consequently the maximum error of the calculation of $\delta(E_\gamma)$ using the approximate formulas is –10% in relation to the Monte-Carlo $\delta(E_\gamma)$ simulation data. Thus the obtained detector sensitivity value will be found underestimated.

Consequently for CdZnTe SCD the approximate formulas for the calculation of $\delta(E_\gamma)$ are expressed as

$$\frac{1}{\delta} = \begin{cases} p + qE_\gamma^s, & E_\gamma < 0.3\ \text{MeV, (a)} \\ \dfrac{abE_\gamma^{1-c}}{1 + bE_\gamma^{1-c}}, & E_\gamma > 0.3\ \text{MeV, (b)} \end{cases}. \qquad (4)$$

The maximum difference between $\delta(E_\gamma)$ values calculated using the formulas (4) and the detailed Monte-Carlo simulation data is about 10%.

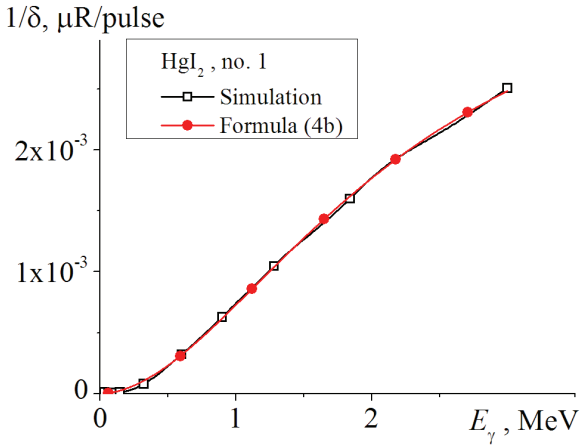


Fig. 14. The $1/\delta$ dependence for HgI_2 detector.

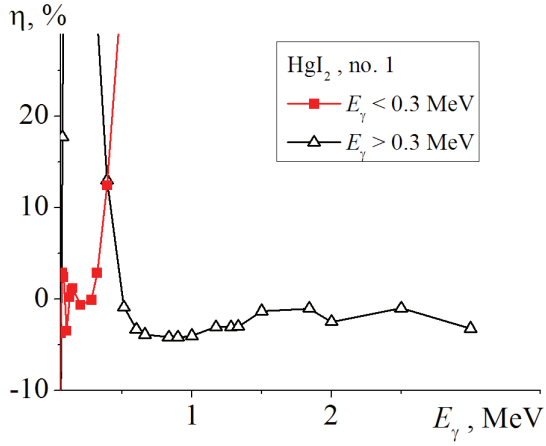


Fig. 15. The difference between the approximate formulas (4) for calculation of $1/\delta$ and the Monte-Carlo simulation data for HgI_2 detector.

The subsequent simulation of the sensitivity $\delta(E_\gamma)$ for other semiconductor materials (HgI_2, TlBr) was run for verification of the universality of formulas (4) obtained for CdZnTe detectors. The Fig. 14 shows the dependence of $1/\delta$ for HgI_2 detector (no. 1, Table 1) and its fitting using the formula (4b). The Fig. 15 shows the difference between the calculation by formulas (4) and the data of the simulation of sensitivity HgI_2 detector in the whole energy range between 0.06 and 3 MeV. Simulation demonstrates that the linear dependence of $1/\delta$ is disturbed for HgI_2 detectors at energy E_γ above 2 MeV (Fig. 14). It means that the method of the reconstruction of the high-energy part of $\delta(E_\gamma)$ using three measurements can not be used for HgI_2 detectors although it has been worked for CdZnTe detectors (Fig. 8). At the same time the difference between the results of the $1/\delta$ calculation used the approximate formulas (4) and the Monte-

Carlo simulation data for HgI_2 detectors (Fig. 15) is similar with that for CdZnTe detectors (Fig. 13). The maximum error of the approximate formulas (4) for HgI_2 detectors also was found in the energy range E_γ between 0.3 and 0.4 MeV and can exceed up to +15%. It is slightly worse than for CdZnTe detectors.

The Fig. 16 shows the 1/δ dependence for TlBr detectors (no. 2, Table 2) in the energy range E_γ below 0.3 MeV and its fitting by the formula (4a). The Fig. 17 presents the full 1/δ dependence and its fitting by the formula (4b). As we can see the 1/δ dependence linearity is absent for TlBr detector at E_γ above 1.5 MeV. Thus the method of the reconstruction of the high-energy part of $\delta(E_\gamma)$ using three measurements can not be used for TlBr detectors, too (similarly HgI_2).

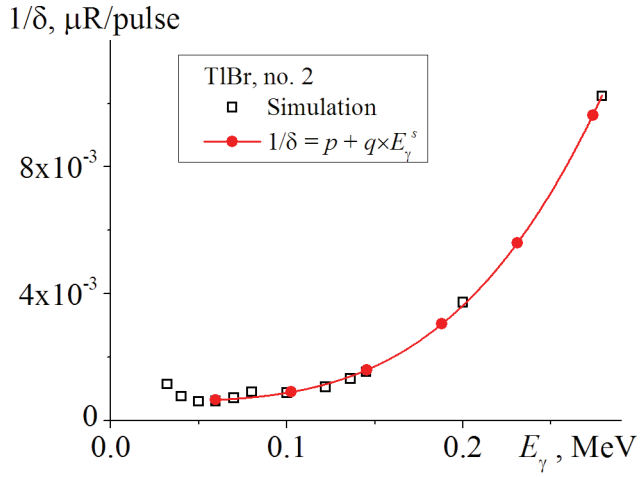


Fig. 16. The 1/δ dependence at E_γ below 0.3 MeV for TlBr detector.

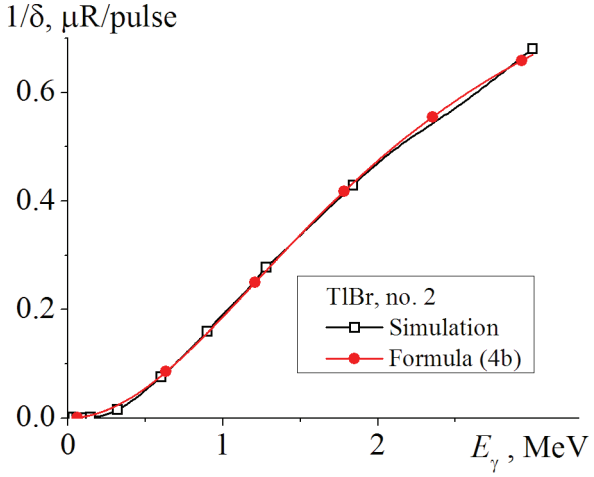


Fig. 17. The total 1/δ dependence for TlBr detector.

The Fig. 18 presents the difference between the 1/δ calculation used the formulas (4) and the data of the TlBr detector simulation in the energy range from 0.06 to 3 MeV. The obtained results show that the more essential difference between the approximate formulas (4) and the detailed Monte-Carlo calculation is typical for TlBr in the gamma-quantum energy range from 0.3 to 0.4 MeV. The maximum error of the 1/δ calculation exceeds up to +25%. Consequently the maximum error of the calculation $\delta(E_\gamma = 0.3\ldots0.4$ MeV) is –25%. Moreover the calculation error $\delta(E_\gamma = 0.07$ MeV) by the formula (4a) exceeds up to about +20% for TlBr detector. It is considerably greater than for CdZnTe (Fig. 13) and HgI_2 (Fig. 15) detectors.

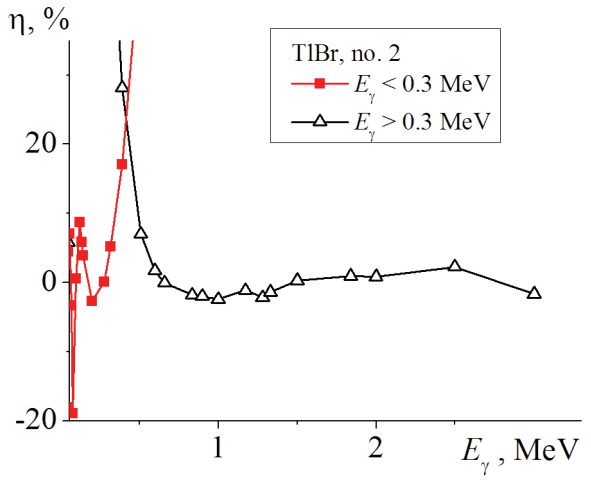


Fig. 18. The difference between the approximate 1/δ calculation with formulas (4) and the Monte-Carlo simulation data for TlBr detector with the thickness of 1 mm.

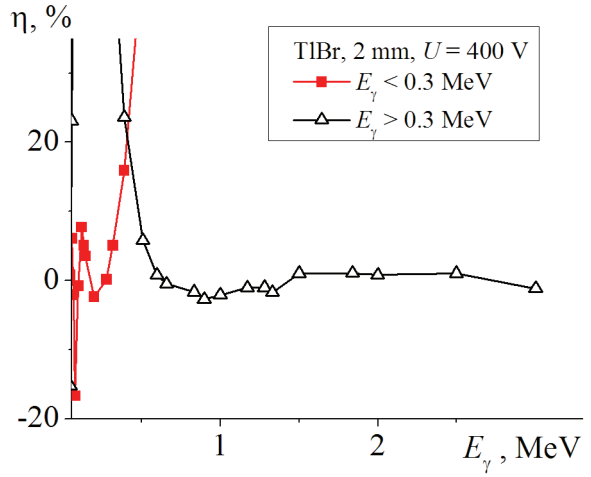


Fig. 19. The difference between the approximate 1/δ calculation with formulas (4) and the Monte-Carlo simulation data for TlBr detector with the thickness of 2 mm.

The simulated TlBr detector has the least thickness among all investigated detectors (Table 1). Thus the simulation of the TlBr detector of 2 mm thickness with bias correspondingly increased up to 400 V was run to find out the reasons of so essential errors. From Fig. 19 it follows that for thicker TlBr detector the approximation error of 1/δ is decreased in the energy range between 0.3 and 0.4 MeV similarly to error of 1/δ for energy E_γ equal 0.07 MeV. However the difference between the approximate formulas and the Monte-Carlo simulation is remained maximum for TlBr detectors in comparison with CdZnTe and HgI_2 detectors.

Sensitivity $\delta(E_\gamma)$ of Ge gamma-radiation detector with characteristics corresponded to the GLP-36360/13P4

detector (ORTEC production [26]) was also calculated in order to compare that with results for detectors based on the wide band-gap semiconductor compounds. The difference between the simulated value of 1/δ and the approximate formulas (4) is minimum among all materials investigated in this work (Fig. 20). The maximum error for Ge detector is about ±6% and it was found in the low energy range (E_γ below 0.2 MeV) in contrast to the room-temperature semiconductor detectors.

Table 3 contains the calculated exponent values of the formulas (4) for all investigated semiconductors. From Table 3 it follows that for wide band-gap semiconductors $\frac{1}{\delta} \sim E_\gamma^{(3...3,5)}$ in the low energy gamma-quantum region. The dependence of 1/δ from E_γ is square-law in this energy range for Ge detector. For wide band-gap semiconductors the sharper form of dependence of 1/δ from E_γ is probably connected with the jump increasing of the cross-section of full gamma-quantum absorption in the energy range between 0.06 and 0.3 MeV (Fig. 1). These jumps occur near the *K*-edge absorption of Hg, Tl, Cd, Te atoms. The binding energy of *K*-electrons in Ge is considerably less (about 11.1 keV) and thus the absorption coefficient changes more smoothly for this semiconductor.

Table 3

The main fit parameters of the formulas (4)

no.	SCD	*s*, (4a)	*c*, (4b)
1	HgI_2	3.075±0.032	–0.855 (±0.034)
2	TlBr	3.45±0.11	–0.96 (±0.05)
3	CdZnTe	2.98±0.08	–0.626 (±0.033)
4	CdZnTe	3.46±0.06	–0.618 (±0.032)
5	Ge	2.07±0.12	–0.367 (±0.019)

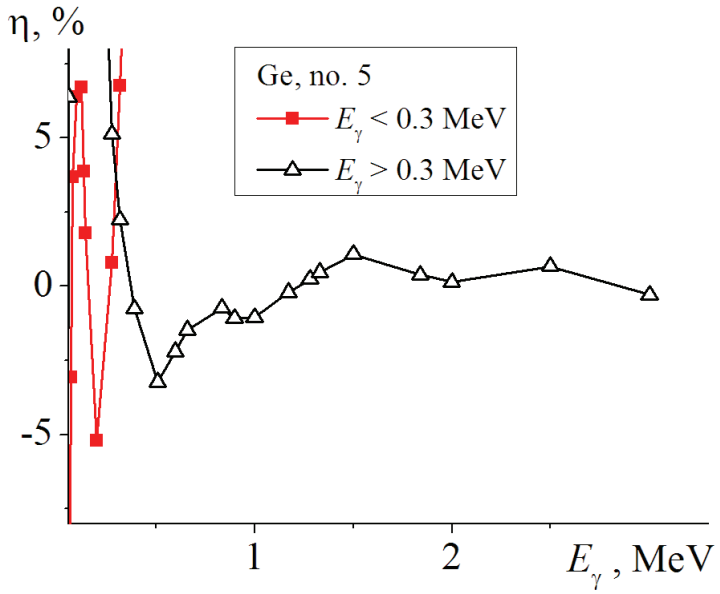


Fig. 20. The difference between the approximate 1/δ calculation formulas (4) and the Monte-Carlo simulation data for Ge detector.

It should be noted that for wide band-gap semiconductors the maximum difference between the fit formulas and the simulation results in the low energy range corresponds to the jumps of the total absorption cross-sections (between 70 and 80 keV).

The obtained formulas (4) are correct for SCD with thickness of more than 1 mm. As Fig. 2 shows the SCD sensitivity value in the gamma-quantum energy range E_γ above 1 MeV is the same order with the noise level due to smaller thicknesses. Consequently the measurement of the sensitivity of the thin SCD in this energy range does not have the practical significance.

CONCLUSIONS

The new approximate formulas that allow to calculate the dependence of the semiconductor detector sensitivity δ(E_γ) from the energy of the registered gamma-quanta in the range between 0.06 and 3 MeV have been obtained. These formulas can be efficient when there is lack of experimental sensitivity measurements for more exact calculation. These approximate formulas can be also used instead of the detailed Monte-Carlo simulation of the δ(E_γ) dependence in the cases when the main control parameters of model (for example, the product of mobility and mean lifetime for electrons and holes and/or the detector internal electric field intensity) can not be determined with accuracy that is necessary for correct reconstruction of the SCD response functions.

It is shown that for the room-temperature detectors the maximum difference between the exact Monte-Carlo simulation and calculation with the approximate formulas is between 10 and 20% depending on the material. The region where maximum difference was found corresponds to the gamma-quantum energy range E_γ between 0.3 and 0.4 MeV. The expected difference is from 2 to 4 times less in the range E_γ below 0.3 MeV and in the range E_γ above 0.4 MeV the expected difference is from 4 to 10 times less.

The obtained approximate formulas are correct for room-temperature semiconductor detectors with thickness of above 1 mm because the sufficiently great value of efficiency of the registration of the gamma-quanta with above 0.5 MeV energy can be received at this thickness range.

Further planned work related to the experimental verification of the obtained approximate formulas.

REFERENCES

1. Demir D., Onder P., Oznuluer T. Performance of CdTe detector in the 13–1333 keV energy range // Radiation Physics and Chemistry. – 2010. – Vol. 79. – P. 1132–1136.
2. Zakharchenko A.A., Khazhmuradov M.A. Issledovanie svojstv poluprovodnikovyh detektorov yadernyh izluchenij metodom Monte-Karlo. ch. 1: Poluprovodnikovye detektory gamma-izlucheniya / Preprint KhFTI. Kharkov, HFTI. - 2011.
3. Sang W., Wei J., Qi Z. et al. Primary study on the contact degradation mechanism of CdZnTe detectors // Nucl. Instr. & Meth. A. – 2004. – Vol. 527. – P. 487–492.
4. Detektory ioniziruiushchih izluchenij poluprovodnikovye. Terminy i opredeleniia: GOST 18177-81. - M.: Izdatel'stvo standartov, 1982. - 20 s.
5. XCOM: Photon cross sections database. NIST Standard Reference Database 8 (XGAM) / M. Berger, J. Hubbell, S. Seltzer, et al. // http://physics.nist.gov/PhysRefData/Xcom/Text/XCOM.html
6. Gorev V.S., Kozhemiakin V.A., Matveev O.A. i dr. Primenenie detektorov na osnove tellurida kadmiia v dozimetrii gamma-izlucheniia // Pribory i tehnika eksperimenta. - 1981. - № 1.- S. 60-64.
7. Zaletin V.M., Krivozubov O.V., Toplin M.A., Fomin V.I. Radiometricheskie i dozimetricheskie harakteristiki HgI_2-detektorov // Atomnaia energiia. - 1987. - T. 63, vyp. 4. - S. 274-277.
8. Akutagawa W., Zanio K. Gamma response of semi-insulating material in the presence of trapping and detrapping // J. Appl. Phys. – 1969. – Vol. 40. – P. 3838–3854.
9. Ruzin A., Nemirovsky Y. Statistical Models for Charge Collection Efficiency and Variance in Semiconductor Spectrometers // J. Appl. Phys. – 1997. – Vol. 82, №. 6. – P. 2754-2758.
10. Hossain A., Xu L., Bolotnikov A.E. et al. Distribution of Te inclusions in a $Cd_{1-x}Zn_xTe$ wafer and their effects on the electrical properties of fabricated devices // Nucl. Instr. & Meth. A. – 2011. – Vol. 652. – P. 146–148.
11. Hossain A., Bolotnikov A., Camarda G. et al. Extended defects in CdZnTe crystals: Effects on device performance // Journal of Crystal Growth. – 2010. – Vol. 312. – P. 1795–1799.
12. Klevkov IU.V., Kolosov S.A., Plotnikov A.F. Transport nositelej zariada v otozhzhennyh krupno- i melkozernistyh polikristallah CdTe // Fizika i tehnika poluprovodnikov. - 2006. – T.40, vyp. 9. - S. 1028-1032.
13. Yang G., Bolotnikov A.E., Camarda G.S. et al. Electric field distribution of cadmium zinc telluride (CZT) detectors / Hard X-Ray, Gamma-Ray, and Neutron Detector Physics XI, Proc. of SPIE. – 2009. – Vol. 7449. - P.74490C-74490C-7.
14. Gerrish V. Polarization and gain in mercuric iodide gamma-ray spectrometers // Nucl. Instr. & Meth. A. – 1992. – Vol. 322. – P. 402-413.
15. Zakharchenko A.A., Verevkin A.A., Kutnij V.E., Rybka A.V., Khazhmuradov M.A. Modelirovanie funkcii otklika CdZnTe detektorov dlia dozimetrii gamma-izlucheniia // Visnik harkivs'kogo natsional'nogo universitetu. Seriia fizichna "Yadra, chastinki, polia". - 2008. - № 832, vyp. 4(40). - S. 71-76.
16. Zakharchenko A.A. Verifikaciia modelej poluprovodnikovyh detektorov gamma-izlucheniia // Visnyk harkivs'kogo natsional'nogo unsversitetu. Seriia fizichna "Yadra, chastinki, polia". – 2011. - №955, vyp. 2(50). - S. 51-59.
17. Zakharchenko A.A., Prokhorenko I.M., Khazhmuradov M.A. Statistical Characteristics of Pulse-Height Spectra of Gamma-Radiation Detectors Based on the Mercuric Compounds / 18th International Workshop on Room-Temperature Semiconductor Detectors (RTSD-2011), 23 – 29 October 2011, Valencia, Spain. – Paper RTSD.S-273.
18. Skrypnyk A.I., Zakharchenko A.A., Khazhmuradov M.A. Comparison of GEANT4 with EGSnrc for simulation of gamma-radiation detectors based on semi-insulating materials // Problems of atomic science and technology, Series: Nuclear Physics Investigations (56). – 2011, № 5. – P. 93–100.
19. Kawrakow I., Mainegra-Hing E., Rogers D. EGSnrcMP, the new multiplatform version of EGSnrc // Med. Phys. – 2004. – Vol. 31. – P. 1731.
20. Baciak J.E., He Z. Spectroscopy on Thick HgI_2 Detectors: A Comparison Between Planar and Pixelated Electrodes // IEEE Transactions on nuclear science. – 2003. – Vol. 50, № 4. – P. 1220–1224.
21. Klimenko I.A., Komar' V.K., Migal' V.P., Nalivajko D.P. Vliianie uprugih polej rostovyh defektov na fotodielektricheskij otklik kristallov $Cd_{1-x}Zn_xTe$ // Fizika i tehnika poluprovodnikov. - 2001. - T. 35, vyp. 2. - S. 139-142.
22. Owens A. Compound Semiconductor Radiation Detectors / Taylor & Francis; 1 edition, 2012. – 567 pages.
23. van den Berg L., Vigil R.D. Fabrication of mercuric iodide radiation detectors // Nucl. Instr. & Meth. A. – 2001. – Vol. 458, №1-2. – P. 148–151.
24. Hitomi K., Kikuchi Y., Shoji T., Ishii K. Improvement of energy resolutions in TlBr detectors // Nucl. Instr. & Meth. A. – 2009. – Vol. 607, №1. – P. 112 –115.
25. Owens A., Bavdaz M., Andersson H. et al. The X-ray response of CdZnTe // Nucl. Instr. & Meth. A. – 2002. – Vol. 484, № 1-3. – P. 242–250.
26. GLP Series Planar HPGe Low-Energy Detector. Product Configuration Guide. / www.ortec-online.com/download/GLP.pdf



Zakharchenko Aleksandr Alekseevich, Ph.D. in physics and mathematics, Senior Researcher, Institute of high-energy physics and nuclear physics of NSC KIPT.
Scientific interest: Monte-Carlo simulation of nuclear radiation interaction with matter, semiconductor physics, dosimetry and nuclear radiation detectors, computer technologies in science research. Author of more than 50 scientific publications (besides conference abstracts).

UDC 621.384.6

DIRECT-ACTION ACCELERATOR BASED ON THE MAGNETRON GUN WITH A SECONDARY-EMISSION CATHODE AND ITS APLICATION IN RADIO-TECHNOLOGIES

A.N. Dovbnya, V.V. Zakutin, N.G. Reshetnyak
Scientific-Prodaction Complex "Accelerator"
National Science Center" Kharkov Institute of Physics and Technology"
Ukraine, 61108, Kharkov, 1, Akademicheskaya St.
E-mail: zakutin@kipt.kharkov.ua
Recieved 15 August 2012, accepted 14 September 2012

Studies have been made into the parameters of the electron beam produced by the accelerator with the secondary-emission cathode magnetron gun as the basis. The experiments were performed in the energy range between 80 and 150 keV with a specific beam power on the target from 5 to 20 J/cm^2, this permitting the use of the beam for irradiating material surfaces. Plane metal samples were subjected to irradiation, and the radiated structure of material surface was examined by metallography methods. Experiments were made to measure the accelerator beam size in both decreasing and increasing magnetic fields; the possibility of irradiating inner and outer of cylindrical surfaces was demonstrated.
KEY WORDS: accelerator, magnetron gun, secondary-emission cathode, electron beam, irradiation, cylindrical surface.

УСКОРИТЕЛЬ ПРЯМОГО ДЕЙСТВИЯ НА ОСНОВЕ МАГНЕТРОННОЙ ПУШКИ С ВТОРИЧНОЭМИССИОННЫМ КАТОДОМ И ЕГО ПРИМЕНЕНИЕ В РАДИАЦИОННЫХ ТЕХНОЛОГИЯХ

А.Н. Довбня, В.В. Закутин, Н.Г. Решетняк
Научно-Исследовательский Комплекс «Ускоритель»
Национальный Научный Центр «Харьковский Физико-Технический Институт»
Украина, 61108, Харьков, 1, ул. Академическая

Изучены параметры электронного пучка ускорителя на основе магнетронной пушки с вторичноэмиссионным катодом в области энергий 80…150 кэВ с удельной мощностью пучка на мишени 5…20 Дж/см^2, что позволило использовать его для облучения поверхности материалов. Проведено облучение поверхности плоских металлических образцов и изучена структура поверхности материала после облучения металлографическими методами. Проведены эксперименты по измерению размеров пучка ускорителя в спадающем и нарастающем магнитных полях и показана возможность облучения внутренней и наружной поверхности цилиндрических областей.
КЛЮЧЕВЫЕ СЛОВА: ускоритель, магнетронная пушка, вторичноэмиссионный катод, электронный пучок, облучение, цилиндрическая поверхность.

ПРИСКОРЮВАЧ ПРЯМОЇ ДІЇ НА ОСНОВІ МАГНЕТРОННОЇ ГАРМАТИ З ВТОРИННОЕМІССІЙНИМ КАТОДОМ ТА ЙОГО ЗАСТОСУВАННЯ В РАДИАЦІЙНИХ ТЕХНОЛОГІЯХ

А.М. Довбня, В.В. Закутін, М.Г. Решетняк
Науково-дослідний Комплекс «Прискорювач»
Національний Науковій Центр «Харківський Фізико-Технічний Інститут»
Україна, 61108, Харків, вул. Академічна

Вивчені параметри електронного пучка прискорювача на основі магнетронної гармати з вторинно-емісійним катодом в діапазоні енергій 80…150 кеВ з питомою потужністю пучка на мішені 5…20 Дж/см^2, що дозволило застосувати його для опромінення поверхні металів. Проведено опромінення поверхні пласких металевих зразків і вивчена структура поверхні матеріалу після опромінення металографічними методами. Проведено експерименти з вимірювання розмірів пучка прискорювача в спадаючому та наростаючому магнітних полях і показано можливість опромінення внутрішній та зовнішній поверхонь циліндричних областей.
КЛЮЧОВІ СЛОВА: прискорювач, магнетронна гармата, вторинно-емісійний катод, електронний пучок, опромінення, циліндрична поверхня.

At present in many countries the beam methods (technologies) for material working with energy fluxes are developed and introduced into the industrial production. Using these methods it is possible to increase the wear resistance, corrosion resistance, fatigue strength, surface polishing of materials etc. For solving such problems one uses extensively the accelerators of intense electron beams with electron energy from 100 to 400 keV [1].

Over the last few years, the work is performed at the NSC KIPT Research Complex "Accelerator" to investigate cold-cathode electron sources operating in the secondary emission mode in crossed electric and magnetic fields [2-4]. Physical processes occurring during beam formation were investigated, with particular attention given to the study of beam current stability, azimuthally homogeneity, beam sizes, the influence of magnetic field components on the current amplitude, the electron bunch formation per voltage pulse, etc. [2,5]. Relying on the previous studies, in 2005 the electron accelerator was created. Parameters of a tubular electron beam from the accelerator [4] have been investigated in the electron energy range from 80 to 150 keV and with pulse duration from ~15 μs. Advantages of the secondary-

© Dovbnya A.N., Zakutin V.V., Reshetnyak N.G., 2012

emission source are as follows: no heating, simple design, ability to work under conditions of technical vacuum (~10^{-6}…10^{-5} Torr), high current density (~50A/cm^2 of the unit of transverse cathode area), cathode emission is not weakened after the air admission. According to evaluations it is generally accepted that the lifetime of cathodes is ~ 100000 hours.

The aims of the present work have been to investigate the electron beam parameters at particle energies between 80 and 150 keV, to modify the surfaces of metals and alloys during their exposure to the electron beam of the accelerator, and also to explore the possibility of the electron beam application for working the internal and external surfaces of cylindrical articles and increasing their corrosion resistance was studied.

ACCELERATOR DESCRIPTION AND RESEARCH TECHNIQUES

The schematic diagram of the accelerator is shown in Fig. 1. The accelerator consists of the following basic units: feeding high-voltage pulsed generator 1, a magnetron gun with secondary-emission cathode C and anode A placed in a vacuum chamber 3, solenoid 4, generating a longitudinal magnetic field, a target device with Faraday cup FC, and computer-aided measurement system 6 for measuring the beam parameters I_b, 2,5 –passed insulators, 7 – control unit. A feed voltage pulse from pulsed oscillator *1* is fed to the cathode of the magnetron gun. In the circuit of the supply pulse generator used is a full battery discharge through the correcting circuit to the step-up transformer, the voltage pulse being formed with the peak surge. Pulsed generator 1 provided the formation of a voltage pulse with an overshoot amplitude of up to 190 kV, an overshoot decay time of ~0.6 μs as for the development of secondary-emission multiplication processes, an amplitude of the flat part of the voltage pulse of up to 150 kV, its length of ~15 μs, and a pulse repetition frequency of (2…10) Hz.

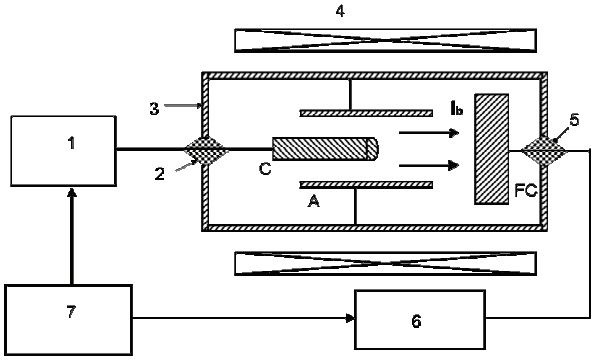


Fig.1. Schematic diagram of the accelerator

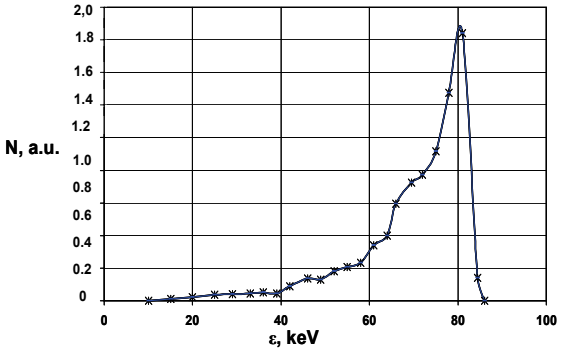


Fig.2. The energy spectrum of the electron beam of the accelerator

The source of electrons is placed in a vacuum chamber 3 with a pressure of ~10^{-6} Torr. The magnetron gun used to generate an electron beam has the following dimensions: the cathode diameter is 40 mm, the cathode length is 85 mm and the inner diameter of the anode is 78 mm, the anode length is 140 mm; the cathode material is copper and the anode material is stainless steel. The principle of operation of the gun is based on the back bombardment of the secondary-emission cathode with the electrons returned by the magnetic field, the formation of an electron cloud near the cathode, and the shaping of a beam [2].

The magnetic field for the generation and transportation of an electron beam is produced by solenoid 4. The amplitude and longitudinal distribution of the magnetic field can be controlled by varying the current magnitude in the sections of the solenoid. During irradiation, the beam current was considerably varied using this effect, as is shown in the Table, which lists the beam parameters upon the irradiation of the targets

Table

Parameters of accelerator

Energies	I, A	W, J/cm^2
50	55	-
60	68	-
80	85	20
100	110	-
120	125	~25

The electron-beam generation bandwidth over the magnetic field was ΔH ~ 300 Oe, which is of great importance for adjusting the accelerator used for technological purposes. Via processing the current and voltage oscillograms, we derived the energy spectrum of the beam (Fig. 2), which shows that ~80% of the beam electrons are in a range of ±7% with a maximum at 0.93eU (U is the cathode voltage).

The target device is placed on the Faraday cup end part which is made of stainless steel, water-cooled, and at a 100mm distance from the gun. The targets to be irradiated were mounted and fastened at the end face.

IRRADIATION OF METAL TARGET FLAT SURFACES

Irradiation has been performed on targets of various metals: steel, stainless steel, Ti, Zr, Zr+1%Nb alloy. The steels under consideration were chosen for surface hardening and zirconium alloys, applied in reactors, for upgrading their strength properties.

The targets were irradiated under similar conditions in one experiment, when a set of 3 -4 samples was fastened at the target device. The beam energy density was varying in different experiments within the range from 5 to 20 J/cm^2. The results obtained [6] have shown that the electron beam with characteristics, being used for metal surface irradiation, can produce appreciable changes in the near-surface layer structure, decrease the grain size, surface fusing, microhardness changes, etc.

Irradiation has been performed on targets of various metals: steel, stainless steel, Ti, Zr, Zr+1%Nb alloy. The steels under consideration were chosen for surface hardening and zirconium alloys, applied in reactors, for upgrading their strength properties.

The targets were irradiated under similar conditions in one experiment, when a set of 3 -4 samples was fastened at the target device. The beam energy density was varying in different experiments within the range from 5 to 20 J/cm^2. The results obtained [6] have shown that the electron beam with characteristics, being used for metal surface irradiation, can produce appreciable changes in the near-surface layer structure, decrease the grain size, surface fusing, microhardness changes, etc.

By irradiating the targets of Zr1%Nb and the energy density of the beam up to W = 20 J/cm^2 leads to the rapid heating of the sample surface to the melting point and, after the completion of the exposure pulse, the heated layer of



a) b) c)

Fig.3. Surface of metal after irradiation.
a) W=20 J/cm^2, mark 300 μm (down on the right)
b) W=20 J/cm^2, mark 30 μm (down on the right)
c) mark 0,5 μm (down)

the material is rapidly cooled. As a consequence of this, the structure and properties of the surface layer change. The modified surface and the interface between the irradiated and unirradiated portions of the sample are shown in Fig. 3a, 3b. The surface differs from the initial surface: cleaner and wider grain boundaries are observed and the grain size hardly changed. By irradiating the targets of stainless steel with a beam current pulse sequence, the nanosized (~100 to 200 nm) formations were obtained at the steel surface (Fig.3c).

The accelerator beam is a circular one, therefore it can be used for annular article irradiation, for example, for modification of collar bushings made from one-piece metal or composed of two layers from different metals [6], and for material surface alloying. Nanosized formations can be used for the research and development of autoemission cathodes and for electron-beam excitation of localized plasmons [7, 8].

IRRADIATION OF THE INNER AND OUTER CYLINDRICAL SURFACES OF THE SAMPLES

Using the accelerator annular electron beam propagating in the magnetic field it is possible to irradiate the internal (in the decreasing field, Fig. 4) or the external (in the increasing field, Fig.6) cylindrical surfaces of tubular samples.

Experiments on the measurement of the sizes of the beam (in the decreasing field, Fig.5c) show, that by during the transportation of the beam in a uniform magnetic field (H~1400 Oe) to a distance of ~100 mm, its diameter is almost unchanged (Fig.5a, curve 2). Further, during the transportation of the beam in a decreasing magnetic field to H ~ 600 Oe, the outer diameter of the beam increases to ~6 cm with a wall thickness of ~4 mm. At a distance of ~240 mm from the edge of the anode of the magnetron gun in a magnetic field of H~300 Oe, the outer diameter of the beam was ~8.5 cm with a wall thickness of 5—6 mm.

Preliminary experiments on the electron beam transport in the copper pipe placed at a distance of ~90 mm from the magnetron gun exit in the decreasing magnetic field were carried out to find optimum conditions for irradiation of the metal pipe internal surface. The copper pipe of 63 mm diameter and 150 mm length (Fig.5b) was composed of 5 rings, each of 30 mm length, the gap between rings from 1,5 to 2 mm. The pipe was placed in the magnetic field produced by a solenoid consisting of 4 sections.

Investigation results show that with ~80 keV electron energy, ~ 70% of beam current are dissipated at the internal pipe surface in the region of the 4th ring (Fig.5a, curve 3) on the ~30 mm length. In the increasing magnetic field

(Fig.5a, curve 1) ~65% of the current is dissipated at 5th ring (Fig.5a, curve 4), the current at the 4th ring decreases by a factor of 5, and, at the same time, the current going onto the central electrode increases by 20%.

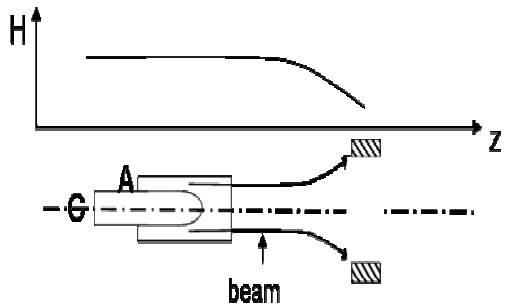


Fig. 4. Scheme of irradiation of the inner cylindrical surface of samples in the decreasing magnetic field

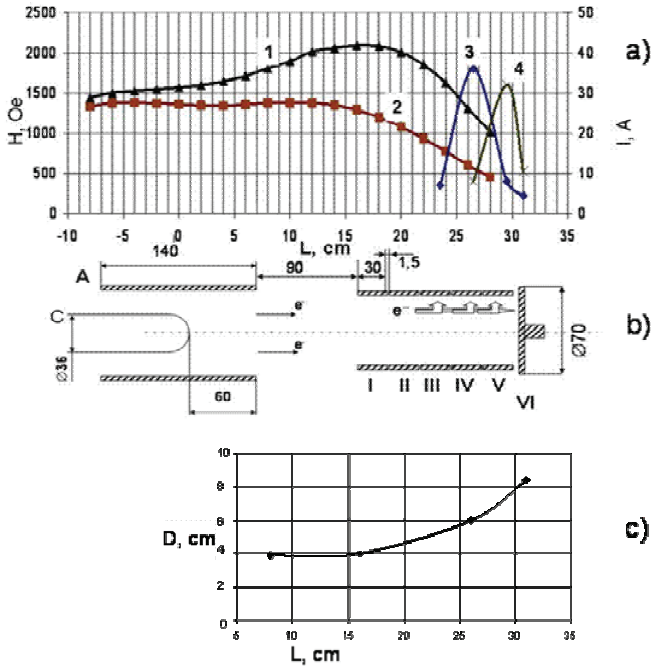


Fig. 5. Experimental results of irradiation of the inner cylindrical surface. a) longitudinal magnetic field distribution in two cases (curves 1,2), current dissipated at rings (curves 3,4) in two cases of longitudinal magnetic field distribution (curves 1,2), b) layout of the metal pipe and gun components, c) diameter of the electron beam D at different distances from the anode of the gun.

To study possibilities for irradiation of the external cylindrical surfaces the experiments have been carried out in which the external and internal beam diameters were measured during the beam transport in the increasing magnetic field.

Scheme of irradiation of the outer cylindrical surface of samples in the increasing magnetic field show on Fig.6. Experiments on measuring the outer of the beam during its transportation in an increasing magnetic field were carried out at a beam energy of ~60 keV and a beam current of ~50 A (Fig. 7). It is evident from the figure that the diameter of the beam decreases and its thickness is also reduced.

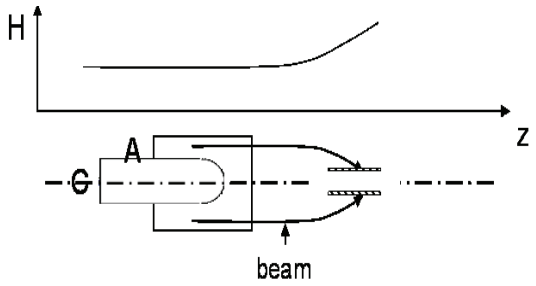


Fig. 6. Scheme of irradiation of the outer cylindrical surface of samples in the increasing magnetic field.

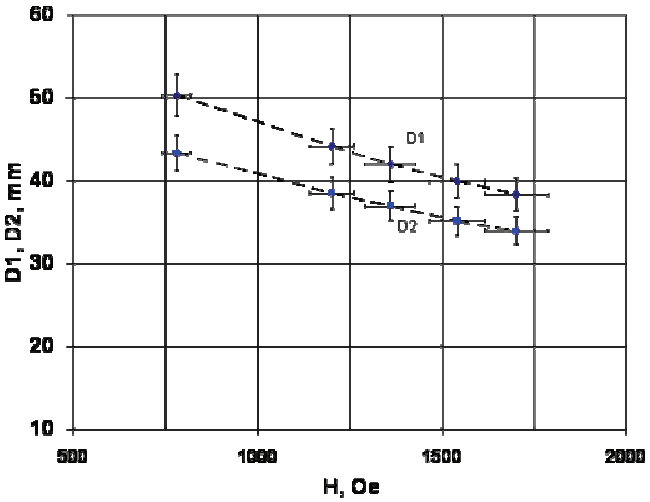


Fig. 7. Dependence of the (D1) outer and (D2) inner diameters of the beam on the amplitude of magnetic field (H) at a distance of 5 cm from the anode.

CONCLUSION

The direct-action accelerator based on the magnetron gun with the secondary-emission cathode can be recommended to use it for the oriented modification of flat and cylindrical surfaces of various metals and alloys, for scientific research and different radiotechnologies.

REFERENCES

1. Engelko V., Mueller G., Andreev A. et al. Pulsed Electron Beam Facilities (GESA) for Surface Treatment / Proceedings of the 10th International Conference on Applied Charged Particle Accelerators in Medicine and Industry (St.-Petersburg, Russia, 2001). - P.412—417.
2. Dovbnya A.N., Zakutin V.V., Reshetnyak N.G. et al. Generation of High-Power Electron Beams in Magnetron Guns with Secondary Emission Cathodes // Zh. Tekh. Fiz. – 2001. – T. 71 (7). – S. 88—91, [Tech. Phys. – 2001. - Vol.46, №7. – P.873.].
3. Dovbnya A.N., Zakutin V.V., Reshetnyak N.G. et al. Investigation of Azimutal Electron-Beam Homogeneity in the Magnetron Gun With a Secondary-Emission Cathode (in Russian) // The Journal of Kharkiv National University, physical series "Nuclei, Particles, Fields". – 2004. - №642. - Iss.3. – P.91—96.
4. Dovbnya A.N., Zakutin V.V., Reshetnyak N.G. et al. The Electron Accelerator Based on the Secondary Emission Source Material - Surface Treatment / Proceedings of the 20th Russian Conference on Charged Particle Accelerators (Novosibirsk, Russia, 2006). - P. 375-377; http://accelconf.web.cern.ch/accelconf/r06/PAPERS/MOLP21.PDF.
5. Dovbnya A.N., Zakutin V.V., Reshetnyak N.G. et al. Investigation of Beam Production in Electron Accelerator With Secondary-Emission Source for Material Surfice Treatment // The Journal of Kharkiv National University, physical series "Nuclei, Particles, Fields".- 2006. - №732. - Iss.2. – P. 96-100.
6. Dovbnya A.N., Lavrinenko S.D., Zakutin V.V. et al. Modification of the Surface of Zirconium and Zr1%Nb Alloy with Electron Beam of Accelerator Based on Magnetron Gun // Vopr. At. Nauki Tekh. – 2011. - №. 2 (97). – P. 39-45.
7. Klimov V.V. Nanoplasmonika // UFN. – 2008. – T.178, №8. – S. 875-880.
8. Dovbnya A.N., Zakutin V.V., Reshetnyak N.G. et al. Electron-Beam Excitation of Localized Plasmons // Proceedings of the 22th International Workshop Charge Particle Accelerators (Alushta, Ukraine, 2011). - P.114.



Dovbnya Anatoliy Nikolaevich, Corresponding Member of the National Academy of Sciences of Ukraine, D.Sc., Professor, Director of the Research Complex "Accelerator" at the National Science Center "Kharkov Institute of Physics and Technology".
Scientific interests: accelerator engineering, nuclear physics, application of accelerated electron beams.



Zakutin Valeriy Viktorovich, Ph.D., Associate professor, a senior research associate of the Research Complex "Accelerator" at the National Science Center "Kharkov Institute of Physics and Technology". Scientific interests: accelerator engineering, nuclear physics, acceleration of electron beams and their application, microwave engineering.



Reshetnyak Nikolay Grigor'evich, Ph.D., Associate professor, senior research associate of the Research Complex "Accelerator" at the National Science Center "Kharkov Institute of Physics and Technology". Scientific interests: accelerator engineering, plasma physics, research of charged particle beams and their application.

PACS: 81.70.-q, 29.17.+w

INTEGRATION OF COMPUTATIONAL METHODS IN SPECTROMETRY OF ELECTRON BEAMS

V.T. Lazurik, V.M. Lazurik, G.F. Popov, Yu.V. Rogov, G.E. Sarukhanian
V.N. Karasin Kharkiv National University
4 Svobody Sq., 61022, Kharkiv, Ukraine
E-mail: popov@univer.kharkov.ua
Received 2 September 2012, accepted 24 September 2012

Investigations related with developments of computer simulation and computational methods for spectrometry of sources irradiation are actual for decision of wide class of scientific tasks into industrial radiation processing. Investigations of influence of electron beam spectrum characteristics on the spatial absorbed dose distributions formation into materials with various atomic numbers were performed. Simulation of spatial distributions of electrons absorbed dose in an irradiated targets was accomplished with the Monte Carlo method by the program ModeRTL. Analysis of numerical experiments results are discussed.
KEY WORDS: computational spectrometry, spectrum electrons, dose distribution, Monte Carlo method, software ModeRTL

ИНТЕГРАЦИЯ ВЫЧИСЛИТЕЛЬНЫХ МЕТОДОВ В СПЕКТРОМЕТРИЮ ЭЛЕКТРОННЫХ ПУЧКОВ

В.Т. Лазурик, В.М. Лазурик, Г.Ф. Попов, Ю.В. Рогов, Г.Э. Саруханян
Харьковский национальный университет им В.Н. Каразина
пл. Свободы 4, 61022 Харьков, Украина

Исследования, направленные на развитие средств компьютерного моделирования и вычислительных методов для спектрометрии источников излучения, являются актуальными для решения широкого класса научных задач в промышленных радиационных технологиях. Проведено исследование влияния спектральных характеристик пучка электронов на формирование распределений поглощенной дозы в материалах с различными атомными номерами. Моделирование пространственных распределений поглощенной дозы электронов в облучаемых мишенях проводилось методом Монте Карло с использованием программы ModeRTL. Обсуждаются результаты численных экспериментов.
КЛЮЧЕВЫЕ СЛОВА: компьютерная спектрометрия, распределение дозы, спектр электронов, метод Монте Карло, программа ModeRTL

ІНТЕГРУВАННЯ ОБЧИСЛЮВАЛЬНИХ МЕТОДІВ У СПЕКТРОМЕТРІЮ ЕЛЕКТРОННИХ ПУЧКІВ

В.Т. Лазурик, В.М. Лазурик, Г.Ф. Попов, Ю.В. Рогов, Г.Е. Саруханян
Харківський національний університет ім. В.Н. Каразіна
пл.Свободи 4, 61022 Харків, Україна

Дослідження, спрямовані на розвиток засобів комп'ютерного моделювання і розрахункових методів для спектрометрії джерел радіаційного випромінювання, являються актуальними для рішення широкого класу задач в промислових радіаційних технологіях. Проведено дослідження впливу спектральних характеристик пучка електронів на формування розподілу поглиненої дози у матеріалах із різними атомними номерами. Моделювання просторового розподілу поглиненої дози електронів в опромінюваних мішенях проводилось методом Монте Карло із використанням програми ModeRTL. Обговорюються результати чисельних експериментів.
КЛЮЧОВІ СЛОВА: комп'ютерна спектрометрія, розподіл дози, спектр електронів, метод Монте Карло, програма ModeRTL

At present electron beam (EB), X-ray and gamma processing are widely used in different industrial radiation technologies, such as sterilization of medical devices, mail sterilization, foodstuff irradiation, advanced composites modification, cross-linking of cables, bulk polymer modification, polymerization of monomers and grafting of monomers onto polymers, tire and rubber pre-cure treatment, decontamination of clinical waste, purification of water and gas wasters and others. The implementation of radiation technology in various fields of industry is accompanied by an increasing number of industrial radiation facilities, expansion of assortment of products treated by ionizing radiation and the development of new methods for radiation processing [1-2]. The usage of new industrial radiation technologies require in increasing of number of controlled variable parameters of process irradiation as well as enhancement of accuracy in determination of these parameters value. In particular it is concerned to monitoring of electron beam energy and spectrum at EB accelerators.

The dosimetric devices and suitable mathematical methods recommended into International Standards for radiation technologies based on EB accelerators allows to obtain only two scalar characteristics for EB spectrum: average energy and most probable energy [3, 4]. Information about influence of an EB energy spread on an absorbed dose distribution formation in an irradiated targets practically is absent. It means, that in the area of radiation processing dosimetry there are the tasks, that are need in developments of new methods for computational dosimetry and spectrometry of ionizing radiation. It should be noted that computational dosimetry and spectrometry do not required

© Lazurik V.T., Lazurik V.M., Popov G.F., Rogov Yu.V., Sarukhanian G.E., 2012

the use of special physical processes or it is difficult realized conditions to performing measurements. These techniques are founded on use of mathematical calculations and special computing methods developed on base of mathematical model of the measurement process for absorbed dose distribution of electrons in an irradiated material.

Investigations related with development of computer simulation and computational methods for spectrometry and dosimetry of powerful sources irradiation are actual for quality control of radiation processing.

The objective of this study was the detailed computer analysis of influence of the EB spectrum on an absorbed dose distribution formation in an irradiated targets. Estimation of uncertainties for method of EB energy control with use of traditional devices such as dosimetric wedge and stack by computational dosimetry method are discussed in the report. Computational dosimetry method suppose the use of computer simulation of radiation-technological process for selected spectrum of electrons.

COMPUTATIONAL APPROACH IN SPECTROMETRY OF ELECTRON BEAMS

International Standards for radiation technologies based on EB accelerators allows to obtain only two scalar characteristics for EB spectrum: E_{av} – average energy and E_p – most probable energy [3, 4]. Uncertainties for an absorbed dose distribution of electrons in the "critical" points of dose map as well as the values of non-uniformity for absorbed dose of electrons when only two scalar characteristics E_{av} and E_p for EB spectrum are controlled should be estimated. "Critical" points of dose map are characterized by locations of the dose minimum (D_{min}) and dose maximum (D_{max}) for the dose map in an irradiated product. Non-uniformity for absorbed dose distribution of electrons in an irradiated product is characterized by relation $DUR=D_{max}/D_{min}$. It is obvious that in general case the reply cannot be obtained.

In practice for determination the spectral characteristics of electron beams the following parameters are used: E_{av}, E_p and energy spread E_w - is the full width of spectrum on the half of maximum. Therefore it is preferable to examine the models of EB spectrum, which use these parameters.

Simplest form, that corresponds to three-parameters function $y(E)$ is triangular form with parameters: E_p, $E_{\min}$ - the value of minimum energy of electrons in an EB spectrum, $E_{\max}$ - the value of maximum energy of electrons in an EB spectrum**.** The parameters E_p, $E_{\min}$, $E_{\max}$ interlinking with E_{av}, E_p, E_w by following equations: $E_{\min}=1.5E_{av}-E_w-0.5E_p$, $E_{\max}=1.5E_{av}+E_w-0.5E_p$. EB spectrum is described by the following formula:

$$y(E)=\begin{cases} h\left(E-E_{\min}\right)/\left(E_p-E_{\min}\right), & E_{\min}<E\le E_p \\ h\left(E-E_{\max}\right)/\left(E_p-E_{\max}\right), & E_p<E<E_{\max} \\ 0, & E\le E_{\min}\vee E\ge E_{\max} \end{cases}$$

where $h=y(E_p)=2/\left(E_{\max}-E_{\min}\right)$ is the maximum function $y(E)$.

EB FACILITY AND SIMULATION MODEL OF RADIATION PROCESSING

Schematic representation of the EB facility used for simulation of the electron depth dose distributions in the heterogeneous target irradiated with scanned EB and on moving conveyor are shown in Figs. 1(a) and (b). The gap between exit window of accelerator and the incident surface of irradiated target is filled with air.

Simulation of EB dose distributions in an irradiated targets was accomplished with the Monte Carlo (MC) method in a 2-dimensional geometrical model with the program ModeRTL [5, 6]. In the program a source of electron beam including spectral characteristics, a scanner, a conveyor line and an irradiated target are considered as uniform self-consistent geometrical and physical models.

The following processes of interaction of electrons with substance and their modeling conceptions were included in the physical model of software ModeRTL:

- electrons lost energy by two basic processes an inelastic collision with atomic electrons and bremsstrahlung;
- inelastic electron collision with atomic electrons lead to excitation and ionization of the atoms along the path of the particles (model of grouping of the transferred energy);
- emission of the secondary electrons (model of the threshold energy);
- electrons participated in elastic collisions with atomic nuclear lead to changes in the electron direction (model of grouping of transferred pulse).

In the default mode of the software ModeRTL, the values of energy cut off and threshold energy of electrons are selected in automatic regimes to provide the necessary space distribution for absorbed dose of electrons in an irradiated target. All physical processes which assure obtaining of results with predetermined accuracy are taken into account at simulation of an absorbed dose distribution of electrons. For example, for EB radiation processing in the energy range of incident electrons from 20 keV to 10 MeV and irradiated materials with atomic number $Z\le 30$, the model uncertainty is less than 5% for calculated dose distribution in the field of the basic EB energy absorption. Software ModeRTL was validated in some benchmarking experiments [5, 6, 7].

The software ModeRTL provides the end-user with: data sets in the graphic and tabular form for an absorbed dose and charge depositions within the target irradiated with a scanned EB; comprehensive comparative analysis of output

data; cognitive visualization of output data; decision of optimization problems with using dynamic and statistical databases; presentation of physical and operational characteristics for radiation processing.

The features of the software ModeRTL are the following: 1. Detailed decomposition of spectral characteristics for irradiation source. 2. Built-in tools for statistical analysis. 3. Built-in tools for uncertainties estimation of results simulation due to uncertainties of input data for radiation facility. 4. Estimation of uncertainties for physical models. 5. Comparison Modulus for visual and a numerical analysis of calculated and experimental data and for decision of optimization tasks in radiation processing.

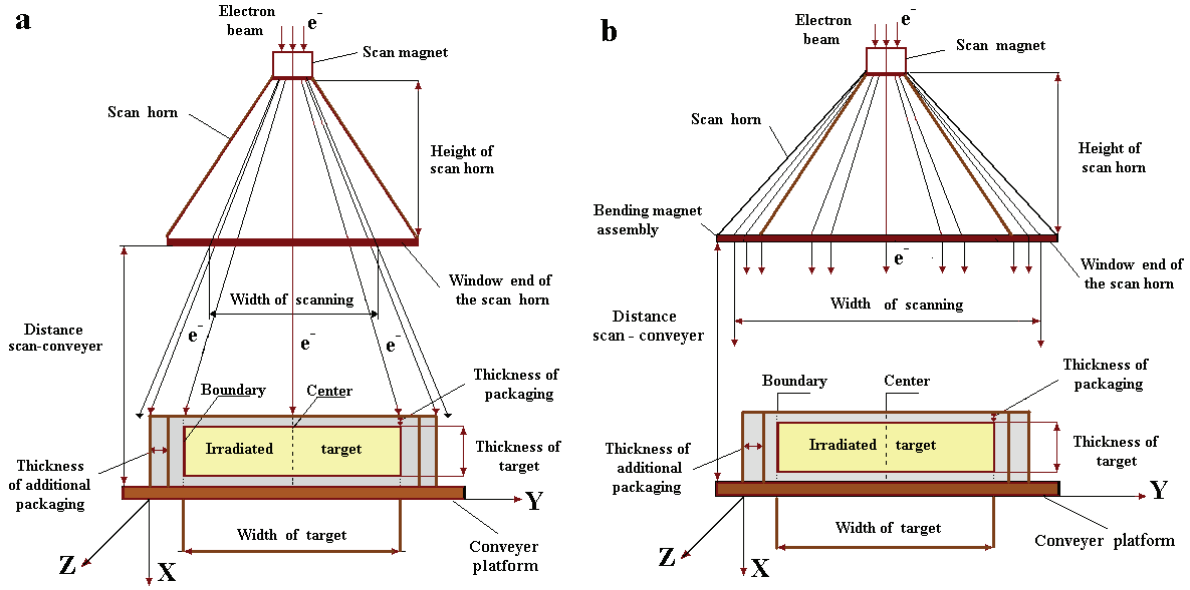


Fig.1. Schemes of EB radiation facility with target and package box placed on moving conveyor.
a) The target irradiated by EB with triangular scanning. b) The target irradiated by EB with non-diverging scanning. Axis X - direction of EB incidence, axis Y - direction of EB scanning, axis Z - direction of conveyer motion.

RESULTS AND DISCUSSIONS

Comparison results of the MC simulation of the absorbed dose distributions (ADD) of electrons in the polyethylene (PE) target irradiated by scanned EB with various energy spread are shown in Fig.2. The flat PE target with density 0.94 g/cm^3 and thickness 4.7cm irradiated with scanned EB from two opposite sides.

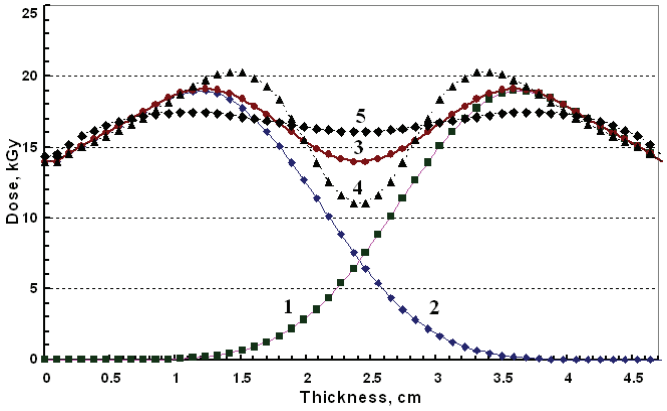


Fig.2. Comparison results: influence of the EB energy spread on absorbed dose distributions of electrons in the PE target. EB average energy -5MeV. Two-sided irradiation. Non-divergent scanned EB. MC simulation.
Curves 1 and 2 – ADDs in the target center irradiated from opposite sides by scanned EB with triangular spectrum. Spectrum parameters: E_{av}= E_p = 5MeV, E_w = 2.5 MeV. Curve 3 – total ADD from curves 1 and 2. Curve 4 - ADD in the target center. Spectrum parameters: E_{av}= E_p = 5MeV, E_w = 0 (mono-energy EB). Curve 5- ADD in the target center. Spectrum parameters: E_{av}= E_p = 5MeV, E_w = 5 MeV.

Analysis of the presented results (Fig.2) have shown that under changing of EB energy spread E_w the values of the ADD of electrons significantly change in the target center and insignificantly change near the entrance surface of EB into target. The target center is the critical area, because in this area the changing of an ADD influenced on the values of dose uniformity ratio DUR=D_{max}/D_{min} and on the optimal target thickness.

The values of relative variation for absorbed dose of electrons in the target center at 2-sided irradiation due to variation of EB spectrum are represented in the Table. MC simulation was performed for process irradiation of target

with optimal thickness by mono-energy EB with $E_w = 0$ and EB with wide triangular spectrum $E_w = E_p$. Calculation was performed at various values of EB energy E_p in the range from 1 to 10 MeV.

Presented results in the Table show that variation of absorbed dose values for EB in the center target at 2-sided irradiation is increased with decreasing of EB energy for materials with small atomic number (PE, Water) and weakly depends for materials with greater atomic numbers (Aluminum). Comparison of the MC simulation results for value variation of the relative absorbed dose ΔD/D for EB in the center of target at 2-sided irradiation of various materials irradiated with various EB energy as function of E_w/E_p value are presented in the Fig.3.

Table

Variation of absorbed dose values for EB in the center target

E_p, MeV / Material	1	2	3	4	5	6	7	8	9	10
	ΔD/D, %									
Polyethylene	30.2	27.9	25.2	21.1	20.1	14.9	14.5	13.3	16.1	11.0
Water	30.5	25.9	28.0	24.7	22.2	22.1	19.4	16.4	17.6	12.6
Aluminum	19.6	21.3	21.8	21.9	20.9	21.9	21.2	21.1	18.6	18.4

Results (Fig.3) show that dependences of the absorbed dose ΔD/D as function of EB energy spread E_w have similar view for various EB energy and atomic numbers of target materials. Therefore, for detection of general regularities, it is interesting to compare obtained dependences at various conditions of normalization. The values of the absorbed dose variations ΔD normalized on the value of maximal deviation for the absorbed dose ΔD_{max} at EB energy $E_w = E_p$, that is (i.e.) when the width of EB spectrum is taken the maximal value, are presented in Fig.4. The values ΔD and ΔD_{max} were calculated in the target center at 2-sided irradiation with EB of various energy.

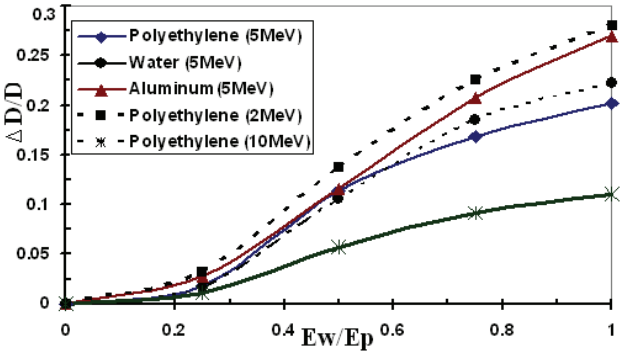


Fig.3. Variation of the relative absorbed dose ΔD/D for EB in the center of target at 2-sided irradiation.

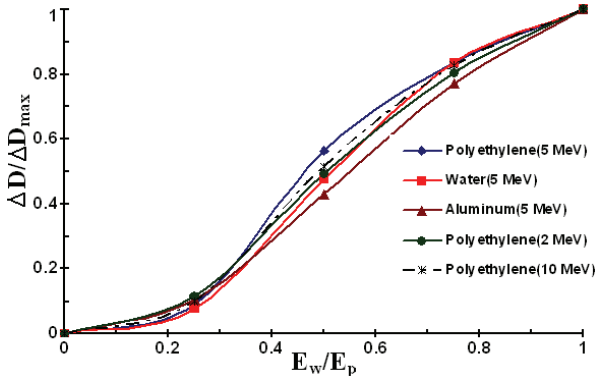


Fig.4. Dependence of the absorbed dose variations ΔD normalized on the value of maximal deviation for the absorbed dose ΔD_{max} as function E_w/E_p value.

As it is seen from Fig.4, the EB absorbed dose distributions into materials with various atomic numbers irradiated with EB of various energy have similar view.

CONCLUSION

Investigations of influence of EB spectrum characteristics on the absorbed dose distribution formation into materials with various atomic numbers irradiated with EB of various energy were performed with use of the computational methods. It was shown, that at 2-sided irradiation of target by EB with variation of EB energy spread the following features were observed:

• under changing of EB energy spread E_w the values of the absorbed dose distribution of electrons significantly change in the target center and insignificantly change near the entrance surface of EB into target.

• variation of absorbed dose values for EB in the center target at 2-sided irradiation is increased with decreasing of EB energy for materials with small atomic number and weakly depends for materials with greater atomic numbers.

• dependences of the absorbed dose ΔD/D as function of EB energy spread E_w have similar view for various EB energies and atomic numbers of target materials.

Results simulations have shown that EB dose map variations can be greater in comparison with predetermined and acceptable in practice uncertainties. This effect can be due to variation of EB energy spread even when controlled EB characteristics such as an average energy and most probable energy are fixed. Therefore, further growth of dosimetry and spectrometry for EB radiation processing related with development of hardware and software for control of the energy spread. In particular, for realization this purpose the development of devices and spectrometry methods on the base of charge deposition registration into multi layer absorber can be used.

REFERENCES

1. International Atomic Energy Agency. Emerging applications of radiation processing. IAEA-TECDOC-1386, Vienna. 2004.
2. International Atomic Energy Agency. Radiation processing: Environmental applications. IAEA-RPEA. 2007.
3. ISO/ASTM Standard 51649. Practice for Dosimetry in an E-Beam Facility for Radiation Processing at Energies between 300 keV and 25 MeV. Annual Book of ASTM Standards. - Vol.12.02. - 2005.
4. ICRU, 1984. Radiation Dosimetry: Electron Beams with Energies between 1 and 50 MeV. Report 35. International Commission on Radiation Units and Measurements, Bethesda, MD, USA. - 1984.
5. Lazurik V.T., Lazurik V.M., Popov G., Rogov Yu. RT-Office for Optimization of Industrial EB and X-Ray Processing // Problems of atomic science and technology. N1. Series: Nuclear Physics Investigation. – 2004. – Vol.43. - P.186-189.
6. Lazurik V.T., Lazurik V.M., Popov G., Rogov Yu. Simulation methods for quality control of radiation technologies. Proceed. of the IAEA Coordination Meeting of the TC RER/8/10 project. Status and prospects of radiation processing in Europe. – 2005. - Warsaw, Poland. – P.141-156.
7. Lazurik V.T., Lazurik V.M., Popov G., Rogov Yu., Zimek.Z. Information System and Software for Quality Control of Radiation Processing / IAEA: Collaborating Center for Radiation Processing and Industrial Dosimetry. - 2011. -Warsaw, Poland. - 232 p.



Valentin Lazurik – D.Sc. of physical and mathematical science, Professor and Dean of Computer Science Faculty at the V.N. Karazin Kharkov National University.
Scientific interests: development of physical models and mathematical methods for simulation of process irradiation into radiation technologies, creation of computer simulation systems for radiation transport through spatially inhomogeneous objects.
He has published three books and more than 250 scientific papers in professional issues



Valentina Lazurik – senior lecturer at the V.N. Karazin Kharkov National University.
Scientific interests: - development of large-scale softwares in the area of processes simulation in radiation physics and in the area of educational measurements.
She has published two books and more than 50 papers in professional issues.



Gennadiy Popov – Ph.D. Leader researcher at the V. N. Karazin Kharkov National University.
Scientific interests: development models for the irradiation process in industrial radiation technologies with real EB, X-ray and Gamma facility. Planning and performing the validation benchmarking experiments by comparison methods of computational against practical dosimetry.
Holder of 12 patents and author one book and more than 100 scientific papers in professional issues.



Yuriy Rogov – Ph.D. Senior researcher at the V. N. Karazin Kharkov National University.
Scientific interests: elaboration of methods for the adequate modeling of interactions of ionizing radiation with real objects; computer modeling of transport radiation through spatial - non-uniform objects.
He has published book and more than 100 scientific papers in professional issues.



Sarukhanian George - postgraduate student of systems and technologies simulation department of computer sciences faculty at the V.N. Karazin Kharkov National University. Scientific interests: development of methods and software for computer simulation of radiation transport through heterogeneous objects. He has published more than 10 scientific papers in professional issues.

UDC 533. 915

STRATIFICATION OF THE POSITIVE COLUMN OF A DC DISCHARGE IN NITROGEN

V.A. Lisovskiy [1,2], V.A. Derevyanko [1], E.P. Artushenko[1], V.D. Yegorenkov [1]
[1] *Kharkov National University*
61022, Kharkov, Svobody Sq., 4, Ukraine
[2] *Scientific Center of Physical Technologies*
61022 Kharkiv, , Svobody Sq., 6, Ukraine
E-mail: lisovskiy@yahoo.com
Received 10 September 2012, accepted 25 September 2012

This paper studies the stratification conditions of the positive column of the dc glow discharge in nitrogen in tubes of various radii. In each discharge tube the striations are observed in closed regions with respect to current and applied voltage values within the limited range of gas pressure values. We revealed that the first striation (counted from the cathode end of the positive column) was clearer expressed and it possessed the maximum thickness. Striation length is weakly dependent on discharge current but it decreases with gas pressure growing. Again the striations with a large order number (counted from the cathode edge of the positive column) possess lesser thickness. We find out that positive column stratification obeys similarity laws well. The extinction curves and striation existence regions registered in different discharge tubes and plotted against the product of gas pressure and inter-electrode distance *pL* coincide. Reduced striation thickness *d*/*R* (striation thickness *d* divided by tube radius *R*) in different tubes also is in good agreement with each other when plotted against *pR*. We observe that the reduced striation thickness obeys the Goldstein-Wehner law $d/R = C/(pR)^m$, the constants for nitrogen being $C = 1.05$ and $m = 0.32$.
KEY WORDS: direct current glow discharge, positive column, striations, nitrogen, low pressure.

СТРАТИФИКАЦИЯ ПОЛОЖИТЕЛЬНОГО СТОЛБА РАЗРЯДА ПОСТОЯННОГО ТОКА В АЗОТЕ

В.А. Лисовский [1,2], В.А. Деревянко [1], Е.П. Артюшенко [1], В.Д. Егоренков [1]
[1] *Харьковский национальный университет*
61022, Харьков, пл. Свободы 4, Украина
[2] *Научный физико-технологический центр*
61022, Харьков, пл. Свободы 6, Украина

В данной работе были исследованы условия стратификации положительного столба тлеющего разряда постоянного тока в азоте в трубках различных радиусов. Показано, что в каждой разрядной трубке страты наблюдаются в замкнутых областях по току и приложенному напряжению в ограниченном диапазоне давлений газа. Получено, что первая (с катодного конца положительного столба) страта ярче выражена и имеет наибольшую длину. Толщина страт слабо зависит от разрядного тока, но уменьшается с ростом давления газа. Также страты с большим порядковым номером (от катодного края положительного столба) имеют меньшую толщину. Показано, что стратификация положительного столба хорошо подчиняется законам подобия. Наблюдается совпадение кривых погасания и областей существования страт, измеренных в различных разрядных трубках и построенных в зависимости от произведения давления газа и расстояния между электродами *pL*. Приведенные толщины страт *d*/*R* (отношение толщины страт *d* к радиусу трубки *R*) в различных трубках также хорошо согласуются друг с другом при построении их в зависимости от *pR*. Показано, что приведенные толщины страт подчиняются закону Гольдштейна-Венера $d/R = C/(pR)^m$, при этом для азота константы $C = 1.05$ и $m = 0.32$.
КЛЮЧЕВЫЕ СЛОВА: тлеющий разряд постоянного тока, положительный столб, страты, азот, низкое давление.

СТРАТИФІКАЦИЯ ПОЗИТИВНОГО СТОВПА РОЗРЯДУ ПОСТІЙНОГО СТРУМУ В АЗОТІ

В.О. Лісовський [1,2], В.О. Дерев'янко [1], К.П. Артюшенко [1], В.Д. Єгоренков [1]
[1] *Харківський національний університет*
61022, Харків, пл. Свободи 4, Україна
[2] *Науковий фізико-технологічний центр*
61022, Харків, пл. Свободи 6, Україна

У цій роботі були досліджені умови стратифікації позитивного стовпа тліючого розряду постійного струму в азоті в трубках різних радіусів. Показано, що в кожній розрядній трубці страти спостерігаються в замкнутих областях по струму і прикладеній напрузі в обмеженому діапазоні тисків газу. Отримано, що перша (з катодного кінця позитивного стовпа) страта яскравіше виражена і має найбільшу довжину. Товщина страт слабо залежить від розрядного струму, але зменшується з ростом тиску газу. Також страти з великим порядковим номером (від катодного краю позитивного стовпа) мають меншу товщину. Показано, що стратифікація позитивного стовпа добре підкоряється законам подібності. Спостерігається збіг кривих згасання і областей існування страт, виміряних в різних розрядних трубках і побудованих в залежності від добутку тиску газу і відстані між електродами *pL*. Наведені товщини страт *d*/*R* (відношення товщини страт *d* до радіуса трубки *R)* в різних трубках також добре узгоджуються один з одним при побудові їх в залежності від *pR*. Показано, що наведені товщини страт підкоряються закону Гольдштейна-Венера $d/R = C/(pR)^m$, при цьому для азоту константи $C = 1.05$ і $m = 0.32$.
КЛЮЧОВІ СЛОВА: тліючий розряд постійного струму, позитивний стовп, страти, азот, низький тиск.

© Lisovskiy V.A., Derevyanko V.A., Artushenko E.P., Yegorenkov V.D., 2012

The dc glow discharge is widely applied in such devices of glow discharge as gas discharge voltage stabilizers (stabilitrons), rectifiers on the ground of glow discharge, as well as gas discharge lasers (neon-helium, carbon dioxide with nitrogen admixture etc) [1]. Positive column stratification lowers the gas discharge laser efficiency therefore it is of considerable interest to study the existence conditions of striations and their characteristics [2-6].

The uniformly glowing positive column under certain conditions is split into striations – consecutive bright and dark regions (layers). In molecular gases they occupy, as a rule, a substantial portion of the positive column whereas in noble gases they are strongly damped or are in a state of constant motion, and their observation is impeded. Standing striations can be seen with a naked eye and they are most easily observed in molecular gases such as hydrogen, nitrogen as well as in mixtures of noble and molecular gases [4,5]. In pure noble gases the steady striations may exist to the anode side of the substantial plasma nonuniformity, e.g. the cathode part of the discharge, a probe with a large negative potential, abrupt tube narrowing; however, their strong damping is observed along the column. An eye cannot observe moving striations because of the large speed of their propagation.

Experimental study and description of standing striations started much earlier than that of moving ones because one did not require special equipment for their observations. Reviews of papers devoted to research into standing and moving striations may be found publications [4,5,7-9]. However, reviews by Nedospasov [7] and Pekarek [8] devoted only little attention to standing striations. At the same time one can observe standing striations in molecular gases in the broad range of discharge current and gas pressure values and they are most clearly expressed.

From the viewpoint of plasma technology it is most important to elucidate the conditions under which the uniform positive column becomes stratified. The authors of paper [6] presented the diagram of various states of plasma discharge in neon showing the existence regions of the uniform and stratified discharges. Papers [10,11] studied the moving striations in nitrogen. Conventionally a positive column of the glow discharge in nitrogen demonstrates standing striations, therefore for observing moving striations an additional electrode was introduced in the column and a weak alternate voltage of a kilohertz range was applied. Authors of papers [10,11] determined the existence regions for every type of striations, their phase and group velocities, dispersion curves (frequency of ionization oscillations against wave number k) and voltage drop across each type of striations depending on discharge current for different nitrogen pressure values.

Klyarfeld [12] dealt mainly with standing striations and concluded that there is no fundamental difference between standing and moving striations — they are the periodic repetitions of the local perturbation in plasma in the direction of the electron drift. Zaitsev [13] studied moving ionization waves and produced them from outside either with an additional internal electrode or through modulation of the discharge current with the alternate voltage of the frequency close to that of the waves.

The authors of paper [14] studied the formation of moving striations in neon in experiment. They found that the striations were formed out of small anode spots usually oscillating with the growing amplitude, increasing in size and then leaving the anode surface. These striations moved with a high speed to the cathode edge of the positive column and then disappeared. The author of paper [15] suggested a refined method with which he determined the value of the critical current (limiting the existence region of striations) in argon and xenon.

In helium, neon and their mixtures the critical current for ionization wave excitation, the dispersion law, the velocity and the waveform and their dependence on gas temperature were studied in experiment in the discharge tubes of 1 to 3 mm in diameter [16]. The authors of paper [17] performed the spatial-temporal probe measurements of plasma parameters in S- and P-striations in neon. Paper [18] proposed a nonlinear model describing the modes of ionization waves in plasma. This model revealed the hysteresis transition between different modes on changing the discharge current. S-, P- and R- striations which may be observed in dc discharge in noble gases at low pressure and small discharge current were studied in paper [19] employing the numerical solution of the Boltzmann kinetic equation.

Authors of paper [20] found out that the layered positive column in molecular gases acquired a macroscopic instability under certain conditions. This instability manifests itself either in a slow spontaneous displacement of the layered positive column to the anode with the velocity order of 1 cm/min, or in slow longitudinal oscillations of the column as a whole. The existence regions of standing as well as moving striations possess a complicated shape. For hydrogen and oxygen they are given, e.g. in paper [8], and for nitrogen they are obtained in [7]. Comparison between the existence regions of standing and moving striations shows that standing striations, as a rule, are observed at lower gas pressure and current values than moving ones.

In noble gases [21] the standing striations in neon exist mainly inside the region free of moving striations (with current values of 1 — 10 mA and pressure values of 0.1 — 1 Torr). In papers [22,23] evanescent standing striations were observed in helium, neon and argon with pressures up to 10^{-2} Torr and currents up to 100 mA.

If you intend to elucidate the nature of standing striations, then a question arises on how possible values of their length d depend on discharge conditions. The length of standing striations usually has the order of the tube radius R and it decreases with current increasing approaching a certain constant value [4]. Also the length of standing striations d decreases on increasing pressure p and decreasing radius R according to the empirical law of Goldstein-Wehner [4,24] $(d/R)\cdot(pR)^m = \text{const}$, where $m < 1$ and it depends on the nature of gas. In noble gases standing striations are usually substantially longer than in molecular gases, their length exceeding several times the tube diameter especially at low pressure. Molecular impurity added to a noble gas makes standing striations the shorter the larger is the impurity

content [25].

Many researchers [12,22,23,26] remark that the striation closest to the cathode somewhat differs from the rest of them being not only the sharpest but also the longest.

Despite a large number of articles devoted to the research into moving and standing striations in the dc discharge, the references lack data on the link between the existence region of striations and the regions of appearance and existence of the discharge itself (its ignition and extinction curves, respectively). Again, the references do not contain a united opinion about the striation shape. For example, in papers [5,26] the first striation (located at the cathode edge of the positive column) shines brighter but its length equals approximately that of subsequent striations (located closer to the anode). However, as was said above, in papers of other researchers [12,22,23] they report that the first striation closest to the cathode is the longest. Still again, the references do not contain detailed information on the behavior of each separate striation against gas pressure and discharge current. Therefore this paper aims at studying extinction curves of the dc discharge in nitrogen, existence regions of standing striations, as well as lengths of separate striations against gas pressure and current.

EXPERIMENTAL CONDITIONS

In order to study the existence conditions and characteristics of striations in the positive column of the dc discharge we employed the discharge chambers shown schematically in Fig.1. Measurements were performed with the tubes of inner radius $R = 4$ mm, 6 mm, 12.5 mm, 27.5 mm and 39.5 mm. We used the discharge devices of similar design. For example, for the tube of radius 27.5 mm the inter-electrode distance was 395 mm. For other tubes the inter-electrode distance also was about 14.4 times larger than the radius.

The studies were performed in nitrogen within the pressure range $p = 0.05 - 0.5$ Torr. The cathode was fed with the dc potential $U_{dc} \le 3000$ V. The resistor of 75 kOhm was switched in series between the cathode and the dc source.

Before measurements we cleaned the cathode surface igniting a glow discharge in nitrogen at the pressure of $p \approx 0.1$ Torr and discharge current of $I_{dc} = 5$ mA during 10 minutes. Under these conditions the ion flux onto the cathode is sufficiently high to remove monolayers of gases, which remained on the cathode surface after mechanical grinding and polishing, but the discharge current is still insufficient for producing cathode spots eroding the cathode surface. We did not employ any external ionization sources for discharge igniting.

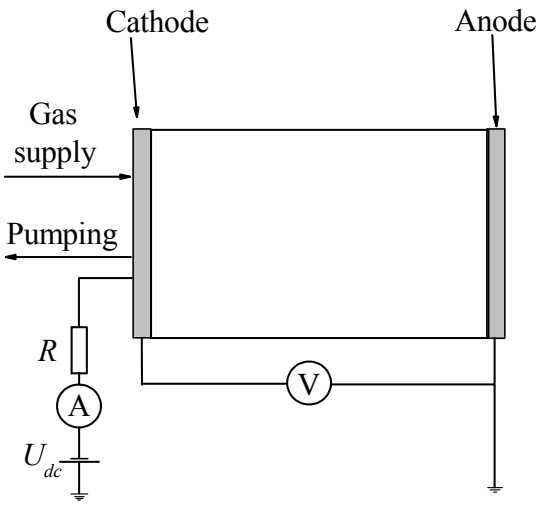


Fig.1. Experimental device setup.

We have taken photos of striations. The obtained images are downloaded to the computer. In order to process them any program can be applied which can separate a rectangular region (Adobe Photoshop, MBizGroup PhotoEditor etc.). If necessary, the images have to be rotated if the discharge tube is located not horizontally but at some small angle. Fig.2 depicts the photo from which you can see how to determine the first striation thickness. As is seen from the photo, it amounts around 9.3 mm. In the same way you can determine the thickness values for the second striation etc which are usually a little thinner and dimmer than the first one, but in this work they are not important. The matter is that near the boundaries of the pressure range you can observe 1-2 striations and further the positive column glow becomes uniform. Therefore it is expedient to deal with only the first striation as the brightest one, long and existing in the broadest range of gas pressure.

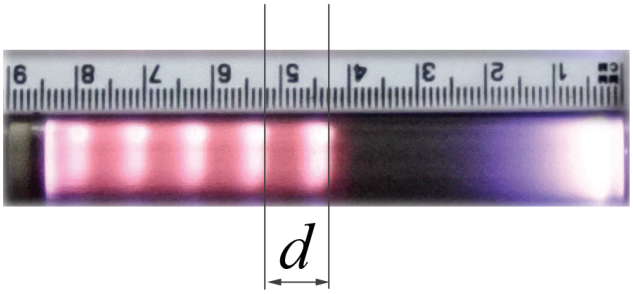


Fig.2. Discharge photo at the nitrogen pressure of $p = 0.6$ Torr and the discharge current of 1.6 mA.
Anode is to the left, and cathode is to the right. d is the first striation thickness. The tube of inner radius $R = 6$ mm.

EXPERIMENTAL RESULTS

The aim of these studied was to clarify the existence conditions for standing striations together with their length for different current and nitrogen pressure values. Fig.3 depicts the discharge extinction curve U_{ext} (the minimum voltage of discharge burning against the product of gas pressure and inter-electrode distance pL) limiting the existence region of standing striations in the glow discharge from below. The voltage U_{high} is the maximum voltage at which the

striations disappear. At the section of the U_{high} curve growing with gas pressure the total length of the cathode sheath, negative glow and dark Faraday space approached the inter-electrode distance and the positive column disappeared. Together with it the striations also disappear because they may be observed only in the positive column. Fig.4 presents the photos of the discharge in the tube of 27.5 mm in radius with a stratified positive column for different current values. At small current values we observe only 2-3 first striations located at the cathode edge of the positive column. The rest of the column seems to be uniform visually. However, on increasing the current almost the total positive column becomes stratified, the striations are readily seen and the column length decreases. And at some maximum values of the voltage U_{high} and current I_{high} the positive column with the striations disappear completely.

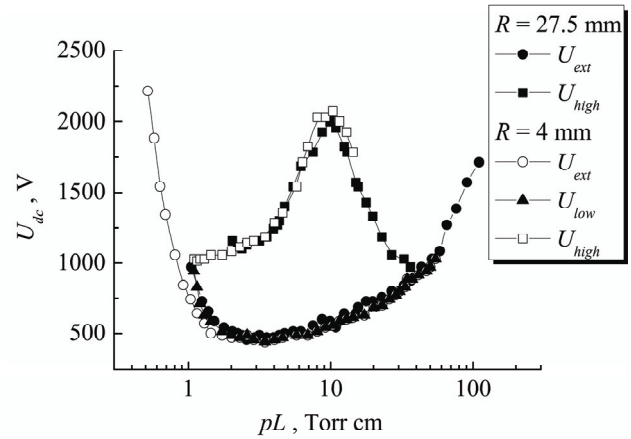


Fig.3. Discharge extinction voltage U_{ext} and maximum voltage of striation existence U_{high} in the tube of 27.5 mm in radius, as well as discharge extinction voltage U_{ext}, minimum and maximum voltage of striation existence U_{low} and U_{high} in the tube of 4 mm in radius against nitrogen pressure.

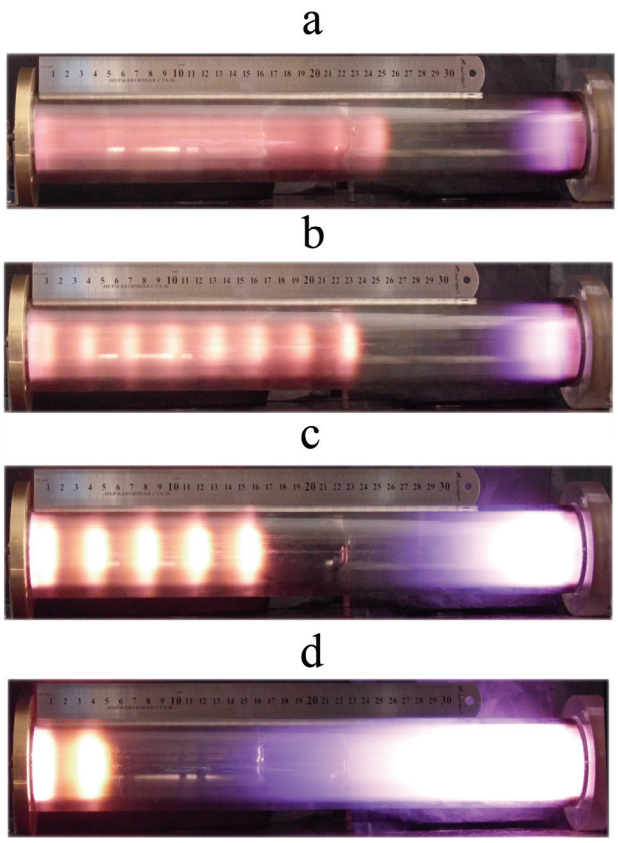


Fig.4. Discharge photos at nitrogen pressure of p = 0.2 Torr and discharge current values:
a) 0.7 mA; b) 1.7 mA; c) 9 mA; d) 29.3 mA.
Anode is to the left, and cathode is to the right.

At the descending section of the curve U_{high} the positive column did not disappear with the current growing but the striations were broadened and the column became uniform. At nitrogen pressure above 1 Torr (for the tube of 27.5 mm in radius) the striations were not observed in the total range of discharge current values studied in the present paper.

As the experiments were performed in geometrically similar tubes then the discharge characteristics had to obey similarity laws. Let us check whether similarity laws apply to a stratified glow discharge.

As we observe in Fig.3, the extinction curves registered for discharge tubes of 27.5 mm and 4 mm in radius and plotted to the scale U_{ext} (pL) actually match each other. The maxima voltage values U_{high} for the striation existence in both tubes also match. It indicates the validity of similarity laws in describing the processes of discharge stratification and extinction. The descending section of the maximum voltage U_{high} in the narrow tube was not registered due to technical reasons because at large gas pressure a strong discharge current flowed through the tube leading to substantial cathode sputtering and discharge chamber heating. However the knowledge of the behavior of this descending section in a wide tube may help us to predict its path for a narrow tube.

Photos in Fig.4 demonstrate that the striation thickness does not remain constant at gas pressure fixed but it experiences changes with the discharge current growth. Fig.5 shows the dependence of the first striation thickness (counted from the cathode end of the positive column) on discharge current at different nitrogen pressure values. The first striation thickness demonstrates a nonuniform pattern with discharge current growth remaining almost constant. The pressure increase leads to the decrease in the first striation thickness.

Photos in Fig.4 also demonstrate that the striations in the positive column do not have the same value because the first of them counting from the column cathode end is thicker and brighter than subsequent ones. The authors of papers [12,22,23,26] also observed that the first striation is the longest one. Fig.6 depicts the striation thickness against its ordinal number (counted from the column cathode end) registered for three different sets of discharge conditions. The figure evidences that the farther is the striation from the cathode end of the positive column the narrower it is. But the striations with large ordinal numbers (N > 4) have approximately equal thickness.

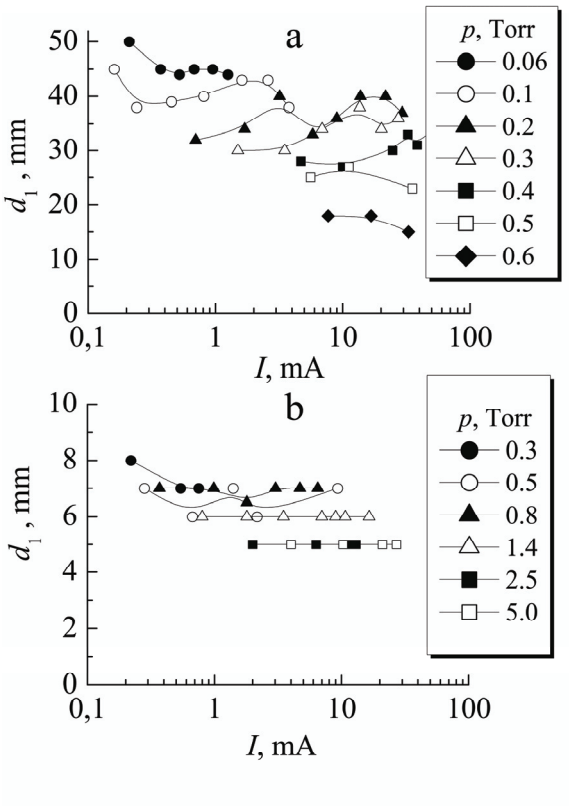


Fig.5. Thickness of the first striation against discharge current at different nitrogen pressure values. Tube radius is 27.5 mm (a) and 4 mm (b).

As follows from Fig.5, the striation thickness experiences little variation with the discharge current increasing. Therefore we averaged the striation thickness value for each fixed gas pressure value. Fig.7 shows the average thickness of the first three striations thus found against nitrogen pressure. In the figure we observe that the average thickness of striations uniformly decreases with gas pressure, the speed of their narrowing with pressure being about equal.

In order to compare between the striation behaviour in the tubes of various radii it is expedient to use a dimensionless (reduced) tube thickness. To this end we divide the striation thickness d by the tube radius R in which the striations were measured. Fig.8 shows in logarithmic scale the reduced average thickness of the first striations against the pR product for all discharge tubes we employed. The figure clearly demonstrates that the striation reduced thickness is well described by the following dependence

$$\frac{d}{R} = \frac{C}{(pR)^m}, \qquad (1)$$

that is called the Goldstein-Wehner law [4, 24]. However we remark that Wehner [24] presented in his paper contradictory data. He approximated his data for the striation reduced thickness (black squares in Fig. 8) with the curve (1) corresponding to the constant values $C = 2$ and $m = 0.32$, though actually the best match between his measured data and formula (1) is observed with the value $C = 0.6$. Our results also are well described with formula (1) but with $C = 1.05$. From axial profiles of discharge glow at different nitrogen pressure values given in paper [5] we determined the thickness of the first striations and also presented it in Fig.8. This figure demonstrates good agreement between the reduced thickness values for the first striations with our results. In the broad range of discharge conditions the thickness of the first striation comprises from one to two radii of the discharge tube. We also determined the thickness of the first striation in nitrogen from the axial profile of the electric field strength measured by Graham [30] (see Fig.12 [30]). The obtained value is also shown in Fig.8 and it is above the results of our work and that of paper [5]. One can see from the description of the experimental conditions given in [30], that Graham employed the mercury manometer therefore the nitrogen in his tube was contaminated with mercury vapour. As the mercury atoms possess a low ionization potential, their presence makes the ionization process easier and makes striations longer. The mercury manometer in [30] was vacuum-sealed without grease and, consequently, organic contamination in nitrogen was absent.

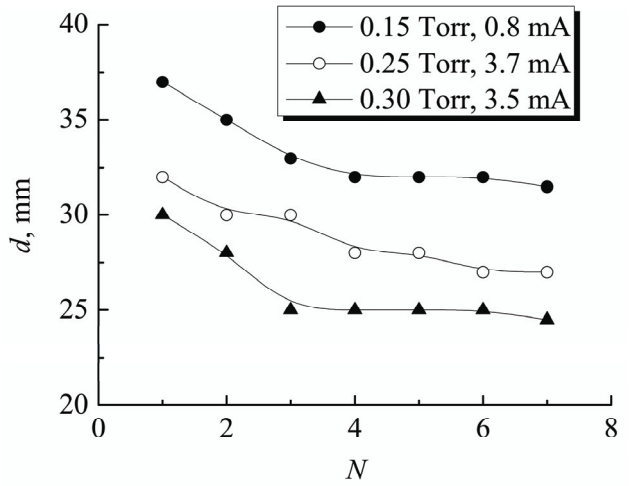


Fig.6. Striation thickness against its ordinal number. Tube radius is 27.5 mm.

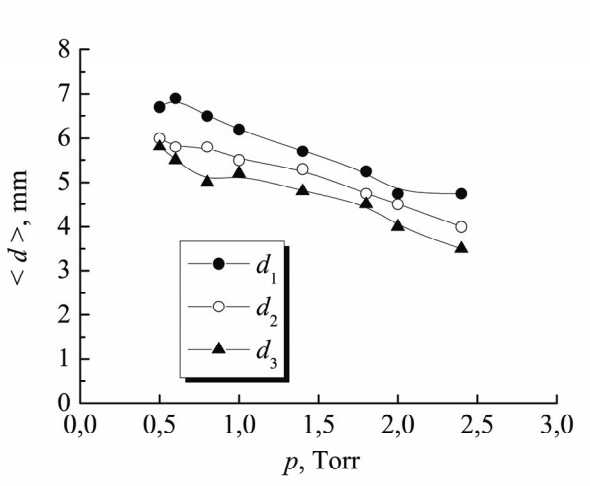


Fig.7. Average thickness of the first three striations against nitrogen pressure. Tube radius is 4 mm.

Note that Wehner made vacuum sealing with cement containing resin and wood oil therefore due to the presence of organic vapour the striation thickness values he had obtained happened to be remarkably lower that in our work and

in paper [5].) The admixture of air does not affect noticeably the applicability of the Goldstein-Wehner law. This can be observed from our results for air presented in Fig.8.

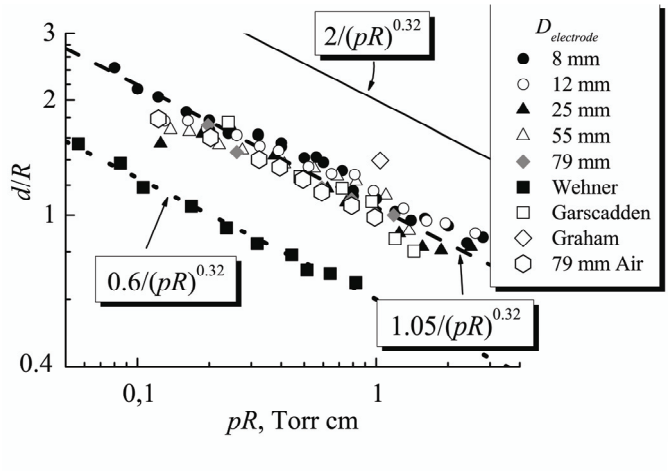


Fig.8. Ratio of averaged thickness of the first striation to tube radius against the product of gas pressure and tube radius.

CONCLUSIONS

This paper clarifies the stratification conditions of the positive column of the dc glow discharge in nitrogen in tubes of radii R = 4 mm, 6 mm, 12.5 mm, 27.5 mm and 39.5 mm. The striations are observed in closed regions with respect to current and applied voltage values within the limited range of gas pressure values. We found that the first striation (counted from the cathode end of the positive column) is clearer expressed and it possesses the maximum thickness. Striation length is weakly dependent on discharge current but it decreases with gas pressure growing. Again the striations with a large order number (from the cathode edge of the positive column) possess lesser thickness.

We found out that positive column stratification obeyed similarity laws well. The extinction curves and striation existence regions registered in different discharge tubes and plotted against the product of gas pressure and inter-electrode distance pL coincide. Reduced striation thicknesses d/R (striation thickness d divided by tube radius R) in different tubes also are in good agreement with each other when plotted against pR.

We observed that the reduced striation thickness obeyed the Goldstein-Wehner law $d/R = C/(pR)^m$, the constants for nitrogen being C = 1.05 and m = 0.32.

REFERENCES

1. Trager F. (Ed.) 2007 *Springer Handbook of Lasers and Optics* (New York: Springer Science + Business Media, LLC)
2. Raizer Y.P. Gas Discharge Physics. – Berlin: Springer, 1991. - 450p.
3. Granovsky V.L. Electric current in gases. - Moscow: Nauka, 1971. - 490p.
4. Francis G. The glow discharge at low pressure // Encyclopedia of Physic, Ed. by Flugge S., Vol. 22 (Gas discharge 2), Berlin: Springer, 1956. – P.53-208.
5. Garscadden A. Ionization Waves in Glow Discharges. // Gaseous Electronics, Ed. by. Hirsh M.N. and Oskam H.J., Vol.1 (Electrical Discharges), New York: Academic Press, 1978. – P.19-64.
6. Pfau S., Rutscher A., Wojaczek K. Das Ähnlichkeitsgesetz für quasineutrale, anisotherme Entladungssäulen // Beitrage Plasmaphys. – 1969. – Vol.9, №4. - P.333-358.
7. Nedospasov A.V. Striations // Soviet Physics Uspekhi. – 1968. – Vol.11, №3. – P.174-187.
8. Pekarek L. Ionization waves (striations) in a discharge plasma // Soviet Physics Uspekhi. – 1968. – Vol.11, No.3. – p. 188-226.
9. Golubovsky Y.B., Kudryavtsev A.A., Nekuchaev V.O., Porokhova I.A., Tsendin L.D. Kinetics of electrons in a nonequilibrium gas discharge plasma. – SPb: St. Petersburg University Publishing. – 2004. – 248 p.
10. Venzke D. Messungen an der geschichteten Niederdruck-Entlandung in Stickstoff // Beitrage Plasmaphys. – 1971. - Vol.11, №2. - P.141-148.
11. Laska L., Exner V.L. Ionization Waves in Nitrogen // Czech. J. Phys. B – 1971. - Vol.21, №2. - P.126-147.
12. Klyarfeld B.N. Formation of striations in a gas discharge // Journal of Experimental and Theoretical Physics. – 1952. - Vol. 22, №1. - P.66-77.
13. Zaitsev A.A. Oscillatory modes and moving layers in the discharge // Reports of USSR Academy of Sciences. - 1952. – Vol. 84, №1. - P.41-44.
14. Coulter J. R. M., Armstrong N. H. K. and Emeleus K. G. Moving Striations and Anode Spots in Neon // Proc. Phys. Soc. – 1960. - Vol. 77, №2. - P.476-482.
15. Sato M. On the critical current of ionisation waves in gas discharges // J. Phys. D: Appl. Phys. – 1982. – Vol.15, №7. – P.1181-1185.
16. Amemiya H. Characteristics of striations of He and Ne plasmas in small-diameter discharge tubes // J. Phys. D: Appl. Phys. - 1984. – Vol. 17, №12. – P. 2387-2398.
17. Golubovskii Yu.B., Kozakov R.V., Wilke C., Behnke J. and Nekutchaev V.O. Oscillations of the positive column plasma due to ionization wave propagation and two-dimensional structure of striations // Plasma Sources Sci. Technol. – 2004. – Vol. 13, №1. – P.135–142.
18. Dinklage A., Bruhn B., Testrich H., and Wilke C. Hysteresis of ionization waves // Physics of Plasmas. – 2008. – Vol.15, №6. – P. 063502.
19. Golubovskii Yu.B., Skoblo A.Yu., Wilke C., Kozakov R.V. and Nekuchaev V.O. Peculiarities of the resonant structure of the electron distribution function in S-, P and R-striations // Plasma Sources Sci. Technol. – 2009. – Vol.18, №4. – P. 045022.
20. Kagan Y.M., Mitrofanov N.K. The energy spectrum of the electrons in a layered column of a glow discharge in hydrogen // Technical Physics. – 1971**.** - Vol. 41, №10. - P.2065-2072.
21. Ruzicka T. The connection between moving and standing striations in a d.c. glow discharge in Ne // Czech. J. Phys. Ser. B. –

1968. - Vol. 18, №7. - P. 928-936.
22. Twiddy N. D. Electron Energy Distributions in Plasmas. III. The Cathode Regions in Helium, Neon and Argon // Proc Roy. Soc. Ser. A. – 1961. - Vol. 262, №1310. - P. 379-394.
23. Twiddy N. D. Electron Energy Distributions in Plasmas. V. A Search for Evidence of a High Anomalous Rate of Energy Exchange between the Electrons of a Low-Pressure Discharge // Proc Roy. Soc. Ser. A. – 1963. - Vol. 275, №1362. - P. 338-356.
24. Wehner F. Schichtabstand und Schichtpotentialdifferenz in der positiven Glimmentladung // Annalen der Physik. – 1910. – Vol.337, №6. – P. 49-85.
25. Zaitsev A. A., Miskinova N. A. On the moving and stationary striations in Ne and Ne-H2 // Radiotekhnika i elektronika. – 1967. - Vol. 12, №7. - P. 1318-1320.
26. Lee D. A., Garscadden A. Standing Striations as Solutions of the Pekarek Equation // Phys. Fluids. – 1972. - Vol. 15, №10. - P. 1826-1830.
27. Schulz G.J., Brown S.C. Microwave Study of Positive Ion Collection by Probe // Phys. Rev. – 1955. – Vol.98, №6. – P. 1642–1649.
28. Zakrzewski Z., Kopiczynski T. Effect of collisions on positive ion collection by a cylindrical Langmuir probe // Plasma Physics. – 1974. – Vol.16. – P. 1195–1198.
29. Tichy M., Sicha M., David P., David T. A Collisional Model of the Positive Ion Collection by a Cylindrical Langmuir probe // Contrib. Plasma Phys. – 1994. – Vol.34, №1. – P. 59–68.
30. Graham W.P. Ueber den Verlauf des Potentialgradienten in Geissler'schen Rohren // Annalen der Physik und Chemie. - 1898. - Vol.64, №1. - P. 49-77.



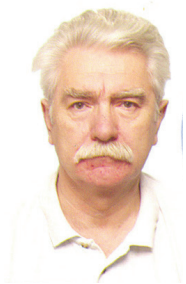
Valeriy A. Lisovskiy - Ph.D. in physics and chemistry of plasmas. From 2001 to 2004, he was at the Ecole Polytechnique, Palaiseau, France, as a post-doctoral research associate. He obtained the Dr. Sc. degree in physics of plasmas from Kharkov National University in 2008. He is currently a Full Professor at Kharkov National University.
His research interests include low-pressure rf, lf, dc, combined and dual-frequency gas discharges, plasma processing, electron transport in gases, plasma sterilization.



Veronika A. Derevyanko (Koval) - graduated from Department of Physics and Technology of V.N. Karazin Kharkov National University in 2010. She is currently a second year Ph.D. student.
Her research interests are in the DC glow discharges, gas breakdown in the long tubes, stratification of the positive column of the dc glow discharge. She is the author and the co-author of 7 papers in the scientific journals.



Ekaterina P. Artushenko - received the B.S. degree in applied physics from Kharkov National University in 2011. She is currently M.S. student.
Her research interests are in the DC glow discharges in electronegative gases, stratification of the positive column of the dc glow discharge in different gases. She is the author and the co-author of 2 papers in the scientific journals.



Vladimir D. Yegorenkov - Dr.Sc. in physics and chemistry. He is currently a Full Professor at Kharkov National University.
His research interests concentrate on studies of physics of fusion plasmas and gas discharge, general physics, lecture demonstration experiments in physics.

UDC 538.945+537.312.62 PACS: 74.72.-h

EFFECT OF HIGH-PRESSURE-INDUCED STRUCTURAL RELAXATION ON EVOLUTION OF THE TEMPERATURE DEPENDENCE PSEUDOGAP IN $HoBa_2Cu_3O_{7-\delta}$ SINGLE CRYSTALS

Z.F. Nazyrov, N.N. Zavgorodnya, R.V. Vovk, K.A. Kotvitskaya
Kharkov National University
4 Svoboda Sq., 61022, Kharkov, Ukraine
email: Ruslan.V.Vovk@univer.kharkov.ua
Received 3 May 2012, accepted 14 September 2012

In present work the influence of high pressure on the conductivity in the basal plane of the oxygen underdoped $HoBa_2Cu_3O_{7-\delta}$ single crystals is investigated. It is found that excess conductivity $\Delta\sigma(T)$ in the $HoBa_2Cu_3O_{7-\delta}$ single crystals over a wide temperature range ($T_c<T<T^*$, where T_c is the critical temperature and T* represents the mean field temperature of the superconducting transition) obeys an exponential temperature dependence. The description of the excess conductivity with $\Delta\sigma\sim(1-T/T^*)exp(\Delta^*_{ab}/T)$ can be interpreted in terms of mean field theory. The temperature dependence pseudogap is satisfactorily described within the framework of the BCS-BEC crossover.
KEY WORDS: excess conductivity, hydrostatic pressure, HoBaCuO single crystals, high-temperature superconductivity, crossover, pseudogap state.

ВПЛИВ ІНДУКОВАНОЇ ВИСОКИМ ТИСКОМ СТРУКТУРНОЇ РЕЛАКСАЦІЇ НА ЕВОЛЮЦІЮ ТЕМПЕРАТУРНОЇ ЗАЛЕЖНОСТІ ПСЕВДОЩІЛИНИ МОНОКРИСТАЛІВ $HoBa_2Cu_3O_{7-\delta}$

З.Ф. Назиров, Н.М. Завгородня, Р.В. Вовк, К.А. Котвицька
Харківський національний університет ім. В.Н. Каразіна
Україна, 61022, м. Харків, пл. Свободи 4

В роботі досліджено вплив високого тиску на провідність в базисній площині ВТНП-монокристалів $HoBa_2Cu_3O_{7-\delta}$ з нестачею кисню. Встановлено, що надлишкова провідність $\Delta\sigma(T)$ монокристалів $HoBa_2Cu_3O_{7-\delta}$ у широкому інтервалі температур $T_c<T<T^*$ підкоряється експоненційній температурній залежності. При цьому описання надлишкової провідності за допомогою співвідношення $\Delta\sigma\sim(1-T/T^*)exp(\Delta^*_{ab}/T)$ може бути інтерпретовано в термінах теорії середнього поля, де Т * представлена, як середньопольова температура надпровідного переходу, а температурна залежність псевдощілини задовільно описується в рамках теорії кросовера БКШ-БЕК.
КЛЮЧОВІ СЛОВА: надлишкова провідність, гідростатичний тиск, монокристали HoBaCuO, високотемпературна надпровідність, кросовер, псевдощілинний стан.

ВЛИЯНИЕ ИНДУЦИРОВАННОЙ ВЫСОКИМ ДАВЛЕНИЕМ СТРУКТУРНОЙ РЕЛАКСАЦИИ НА ЭВОЛЮЦИЮ ТЕМПЕРАТУРНОЙ ЗАВИСИМОСТИ ПСЕВДОЩЕЛИ МОНОКРИСТАЛЛОВ $HoBa_2Cu_3O_{7-\delta}$

З.Ф. Назиров, Н.Н. Завгородняя, Р.В. Вовк, К.А. Котвицкая
Харьковский национальный университет им. В.Н. Каразина
Украина, 61022, г. Харьков-22, пл. Свободы 4

В работе исследовано влияние высокого давления на проводимость в базисной плоскости ВТНП-монокристаллов $HoBa_2Cu_3O_{7-\delta}$ с недостатком кислорода. Установлено, что избыточная проводимость $\Delta\sigma(T)$ монокристаллов $HoBa_2Cu_3O_{7-\delta}$ в широком интервале температур $T_c<T<T^*$ подчиняется экспоненциальной температурной зависимости. При этом описание избыточной проводимости с помощью соотношения $\Delta\sigma\sim(1-T/T^*)exp(\Delta^*_{ab}/T)$ может быть интерпретировано в терминах теории среднего поля, где Т* представлена, как среднеполевая температура сверхпроводящего перехода, а температурная зависимость псевдощели удовлетворительно описывается в рамках теории кроссовера БКШ-БЭК.
КЛЮЧЕВЫЕ СЛОВА: избыточная проводимость, гидростатическое давление, монокристаллы HoBaCuO, высокотемпературная сверхпроводимость, кроссовер, псевдощелевое состояние.

Study of pseudogap anomalies (PG) - a significant decrease in the density of electronic states observed in the phase diagram of underdoped compounds, continues to be one of the most important areas of physics of high temperature superconductivity (HTSC). However, despite the large accumulated literary material, still remain unclear as the nature of origin of PG and questions about its role in the formation of the superconducting state in HTSC. Currently in the literature are discussed extensively two basic scenarios of pseudogap anomalies in HTSC systems. According to the first occurrence of PG associated with short-range order fluctuations of "dielectric" type, for example, antiferromagnetic fluctuations, waves of charge and spin density, etc. [1]. The second scenario allows for the formation of Cooper pairs at temperatures significantly above the critical value T * >> T, followed by the establishment of phase coherence at $T < T_c$ [2,3].

Among the theoretical studies, which supporting the second view, we should note the theory of the crossover from the BCS mechanism to the mechanism of the Bose-Einstein condensation (BEC) [3], which were obtained by the temperature dependence of the pseudogap in the case of weak and strong coupling. In general, these relationships are described by the equation:

© Nazyrov Z.F., Zavgorodnya N.N., Vovk R.V., Kotvitskaya K.A., 2012

$$\Delta(T) = \Delta(0) - \Delta(0)\sqrt{\frac{\pi}{2}}\sqrt{\frac{T}{\Delta(0)}}\exp\left[-\frac{\Delta(0)}{T}\right]\left[1 + erf\left(\sqrt{\frac{\sqrt{x_0^2+1}-1}{T/\Delta(0)}}\right)\right], \quad (1)$$

where $x_0 = \mu/\Delta(0)$ (μ is the chemical potential of the carrier system and $\Delta(0)$ is the value of energy gap at the zero temperature and *erf(x)* is the error function. In the case that of $x_0 \to \infty$ (weak coupling), Eq. (1) becomes:

$$\Delta(T) = \Delta(0) - \Delta(0)\sqrt{2\pi\Delta(0)T}\exp\left[-\frac{\Delta(0)}{T}\right], \quad (2)$$

that is well known in the BCS theory. In the limit of the strong interactions in the three-dimentional case ($x_0 < -1$), Eq. (1) becomes:

$$\Delta(T) = \Delta(0) - \frac{8}{\sqrt{\pi}}\sqrt{-x_0}\left(\frac{\Delta(0)}{T}\right)^{3/2}\exp\left[-\frac{\sqrt{\mu^2+\Delta^2(0)}}{T}\right]. \quad (3)$$

At the same time, as was shown in [2], at a sufficiently high accuracy values $\Delta(T)$ of the pseudogap in a wide temperature range can be determined from the dependency $\rho_{ab}(T)$ (resistivity in the basal plane) at temperatures below a characteristic value T * (temperature the opening of the pseudogap).

The most promising for research on this issue is the connection $ReBa_2Cu_3O_{7-\delta}$ (Re = Y or other rare-earth ion), which is associated with a wide range of variation of their conductive properties and critical parameters by varying the degree of oxygen nonstoichiometry [2] or replacement of components of the component [4]. An important feature of HTSC compounds $ReBa_2Cu_3O_{7-\delta}$ is the ability to implement them in a nonequilibrium state with a certain degree of oxygen deficiency [5,6], which can be induced by external influences, such as temperature [5] or high pressure [6]. This condition is accompanied by processes of redistribution of labile oxygen and structural relaxation, which in turn has a significant impact on electrotransport parameters of the system [5,6]. An important role is played by the replacement of yttrium, rare earth isoelectronic analogamiami it. Of particular interest in this aspect, is replacing yttrium by holmium, which has a large (more than 10 μ_B) magnetic moment [7], which provides connections paramagnetism in its normal state. However, as in the case of other rare earth elements in the implementation of the replacement of Y on paramagnetic ions Re = Ho, Dy doped superconducting properties of oxygen compounds $ReBa_2Cu_3O_{7-\delta}$ with $\delta \le 0.1$, do not change significantly [7]. Apparently this is due to the localization of these ions away from the superconducting planes, which, in turn, prevents the formation of long-range magnetic order. At the same time, we know that in samples of HTSC 1-2-3 system, the oxygen non-stoichiometric composition, rare-earth ion can serve as a sensor which is sensitive to local symmetry of its environment and the distribution of charge density, since they change affects the crystal field forming the electronic structure of the ion [5].

In the absence of a microscopic theory of high temperature superconductivity, of particular importance were the experimental methods to identify the parameters of superconductors, which greatly affect the whole of their physical characteristics in the normal and superconducting state. One of the most important methods in this respect is the use of high pressure [2,6,8]. Analysis of a very extensive study of literary material for PG in the 1-2-3 system shows that to date there are enough small number of papers in which the effect of pressure on the PG mainly in samples close to the stoichiometric composition [8]. However, with this in mind, the most informative is the study of this sample with low oxygen content, because it not only helps to clarify the role and influence of the structural features of the formation of super state, but also allows us to model the leading characteristics and the critical parameters of the superconductor.

The goal of this paper are investigation of the influence of high hydrostatic pressure up to 11 kbar on the different types of conductivity in $HoBa_2Cu_3O_{7-\delta}$ single crystals with oxygen deficient $\delta < 0.35$ and the critical temperature $T_c \approx 67$ K.

EXPERIMENTAL TECHNIQUES

$HoBa_2Cu_3O_{7-\delta}$ single crystals were grown from the flux in a gold crucible using similar technology as for the growth of $YBa_2Cu_3O_{7-\delta}$ single [2,6]. To obtain samples with oxygen concentrations having $\delta \le 0.15$, the crystals were annealed in an oxygen flow at a temperature of 370-410°C for five days. For the resistance measurements the single crystal were selected and had dimensions: 1.7 mm X 1.2 mm X 0.2 mm. In these sample the ***c***-axis was oriented along the smallest dimension. To reduce the oxygen concentration, the crystals were annealed in an oxygen flow at higher temperature range for three to five days. Electric contacts were formed with the standard four-contact scheme by applying silver paste onto the crystal surface and the connection of silver conductor. The resistance in the *ab* plane was measured using the standard method for two opposite directions of a direct current up to 10 mA. The hydrostatic pressure was produced in an autonomous chamber of the piston–cylinder type [2,6] and was measured using a manganin manometer. The temperature measurements were performed using a copper-constantan thermocouple which was mounted at sample level on the outside surface of the chamber. To determine the influence of the structural relaxation, the measurements were made a few days after the pressure application and removal, when the relaxation processes were completed.

RESULTS AND DISCUSSION

Fig. 1 presented the temperature dependence of resistivity measured at the orientation of the transport current **I⊥c** (ρ_{ab}(T)) and different pressures. The application of pressure leads to a decrease in resistivity and an increase in T at $dT_c/dP \approx 0.7$ K·kbar^{-1}, in qualitative agreement with published data [2,6], obtained for samples of $YBa_2Cu_3O_{7-\delta}$ with reduced oxygen content. It is important to note that the decrease in resistivity is not only a result of exposure to hydrostatic pressure, but also in the process of isobaric holding the sample at room temperature immediately after the application of high pressure. For example, in Fig. 1 curves 2 and 3 correspond to dependence, measured immediately after the application of pressure at 4.8 kbar, and also after isobaric sample extracts with the same pressure at room temperature for five days, respectively. It is evident that such exposure leads to an additional decrease in resistivity of about 5%.

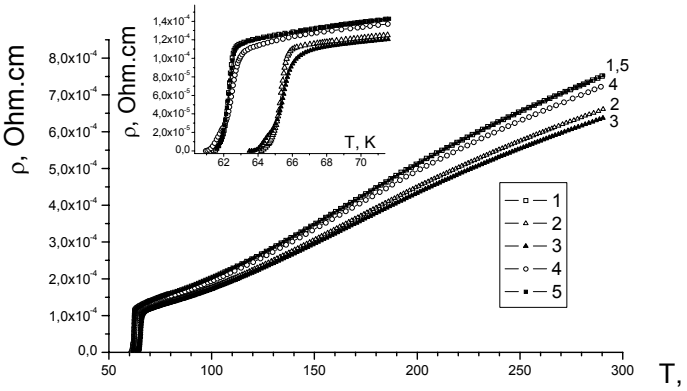


Fig. 1. Temperature dependence of the resistivity ρ_{ab}(T) for $HoBa_2Cu_3O_{7-\delta}$ sample at different pressures.
Curve 1 was obtained prior the application of pressure; curve 2 –was obtained immediately after the application of pressure 4.8 kbar; curve 3 – was measured after keeping the sample in room temperature under pressure 4.8 kbar within a week; curve 4 – was obtained immediately after the removal of pressure and curve 5 – was measured immediately after keeping the sample for three days under zero pressure. The insets show the resistivity transitions to the superconducting phase.

Qualitatively similar behavior of curves ρ_{ab}(T) was observed after removal of high pressure. Thus, in the same figure curves 1 and 4 correspond to dependence, measured before application and immediately after the removal of pressure. Comparison of these curves shows that the measurement results depend significantly on the time of exposure of the sample at room temperature. Thus, immediately after the removal of pressure, the value of the resistivity of the sample at room temperature, the value was approximately 4% lower than measured before application of pressure to continue to relax for about three days to an equilibrium value. After that, the value ρab (290K), saturates, and depending ρ_{ab}(T) is almost completely identical (curve 5) to the original curves (curve 1), measured before the application of high pressure. This indicates that the reversibility of the process.

The application of pressure, also leads to a significant (up to 15 K) expansion of the linear interval of the ρ_{ab}(T) dependence in the region of the higher temperatures. The last one appears to reduce the value of the temperature T*, at which the systematic deviation of experimental points begins downwards from the linear dependence. According to previous work the T* corresponds to the initiation temperature of the PG [1-6]. This will be discussed in more details in what follows.

The abrupt decrease of the ρ_{ab}(T) value, which is observed at temperatures T <T *, indicates the appearance of the so-called excess conductivity $\Delta\sigma$ in the crystal. The temperature dependence of excess conductivity is usually determined from the equation:

$$\Delta\sigma = \sigma - \sigma_0, \quad (4)$$

where $\sigma_0 = \rho_0^{-1} = (A+BT)^{-1}$ is the conductivity obtained from the extrapolation of the linear part to the zero temperature, and $\sigma = \rho^{-1}$ is the experimental value of the conductivity in the normal state. Analysis has shown that the experimental dependence Δσ(T) in the coordinates lnΔσ - 1/T are straight lines in a wide temperature range, which corresponds to the description of the exponential dependence of the form:

$$\Delta\sigma \sim exp(\Delta^*_{ab}/T), \quad (5)$$

where Δ^*_{ab} the value that defines a thermal activated process across the energy gap - the pseudo-gap.

The exponential dependence of $\Delta\sigma(T)$ was also observed earlier, in YBCO samples [2]. In [2] was demonstrated that the description of experimental data can be significantly expanded by introducing the factor $(1-T/T^*)$. The excess conductivity becomes proportional to the superconducting carrier density $n_s \sim (1-T/T^*)$ and inversely proportional to the pairs ~exp(Δ*/*kT*), that are destroyed by thermal motion:

$$\Delta\sigma \sim (1-T/T^*)exp(\Delta^*_{ab}/T), \quad (6)$$

where the temperature interval $T_c < T < T^*$, in which the PG regime exists is defined by the phase of the order parameter that depends on either the oxygen hypostoichiometry or the dopant concentration. Therefore, by using the method [8] we can construct on the experimental curve lnΔσ for the temperature dependence Δ^*_{ab}(T) until the T*.

Fig. 2 shows the temperature dependence of the PG in $\Delta^*(T)/\Delta_{max}$ versus T/T^* coordinates, where Δ_{max} is the Δ* value in the plateau, away from T*, measured under different pressures. The $\Delta^*(T)/\Delta(0)$ versus T/T^* dependence is calculated using Eqs (2), (3) in the mean-field approximation within the context of the BCS–BEC crossover theory [3].

The values of the crossover parameters $\mu/\Delta(0) = 10$ (limit of the BCS) and $\mu/\Delta(0) = -2, -5, -10$ (limit of the BEC) are shown in Fig. 2 as the dotted lines. From this figure it is observed that by increasing the applied pressure there is a shifting of the experimental curves from Eq. (3) (strong coupling) to Eq. (2) (weak coupling). This behaviour is qualitatively similar to the effect of transformation temperature dependence of the pseudogap samples YBCO, observed during the reduction of oxygen non-stoichiometry [2,6]. It is obvious that these correlations in the behaviour of the curves Δ*(T) are not arbitrary. Indeed, as is well known from the literature (see eg. [6]), the application of high pressure to the samples of HTSC 1-2-3 system, as well as decreasing the oxygen content leads to improved conductive properties, which include the increases in the critical temperature and significant reductions of the electrical resistivity.

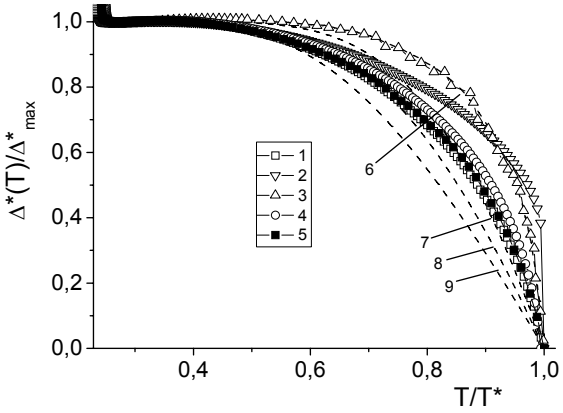


Fig. 2. The temperature dependence of the PG for the $YjBa_2Cu_3O_{7-\delta}$ single crystal, in $\Delta^*(T)/\Delta_{max}$ versus T/T^* coordinates, where Δ_{max} is the Δ* value in the plateau, away from T*.

The numbering of the curves corresponds to the numbers in the Fig. 1. Dotted lines for the $\Delta^*(T)/\Delta(0)$ versus T/T^* dependence were calculated according Eq. (3) for the values of the crossover parameters $\mu/\Delta(0)$=10 (limit of the BCS, curve 6) and $\mu/\Delta(0)$ = -2, -5, -10 (limit of the BEC, curves 7-9).

It should be noted that the structural relaxation is observed in the isobaric holding the sample at room temperature immediately before and after the application of high pressure has a significant influence on the qualitative behavior of the dependences Δ*(T). This shows a comparison of curves 2 and 3 in Fig. 2, corresponding to the dependence of the measured immediately after the application of pressure at 4.8 kbar, and also after isobaric sample extracts with the same pressure at room temperature for five days, respectively. It is evident that the direct application of pressure leads only to a shift from dependence on the experimental curve of the form (3) (2), while retaining some qualitative differences in the behavior of the theoretical and experimental curves. At the same time, after isobaric aging the sample at room temperature, there is almost complete coincidence of these curves.

It is important to note once again that after removing the pressure and the completion of all the relaxation processes, depending $\rho_{ab}(T)$ is almost completely identical to the original curves, measured before the application of high pressure, indicating the reversibility of the process. Thus, given a certain arbitrariness of determining the value of the opening of the pseudogap at T* depending on reject $\rho_{ab}(T)$ from linear behavior, the agreement between experiment and theory in this case can be considered quite satisfactory.

CONCLUSIONS

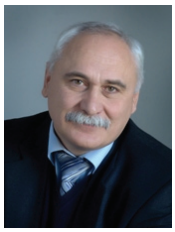
In conclusion, we briefly sum up the main results obtained in this work. The application of high pressure to $HoBa_2Cu_3O_{7-\delta}$ single crystals ($\delta \approx 0.35$) leads to a significant expansion of the interval linear dependence $\rho_{ab}(T)$ and a narrowing of the temperature section of the implementation of the pseudogap regime. In this case excess conductivity obeys an exponential temperature dependence in wide temperature range and temperature dependence of the pseudogap - is satisfactorily described within the framework of the BCS-BEC crossover.

REFERENCIES

1. Sadovskiy M.V. Psevdoshchel' v vysokotemperaturnykh sverkhprovodnikakh // UFN. - 2001. - T.171, №5. - S.539-564.
2. Vovk R. V., Zavgorodniy A. A., Obolenskii M. A., Goulatis I. L., Chroneos A., Pinto Simoes V. M. Influence of high pressure on the temperature-dependence of the pseudo-gap in oxygen deficient $YBa_2Cu_3O_{7-\delta}$ single crystals // Modern Physics Letters B (MPLB) Condensed Matter Physics. – 2010. – Vol.24, №22. – P.2295-2301.
3. Babaev E., Kleinert H. Nonperturbative XY-model approach to strong coupling superconductivity in two and three dimenshions // Phys. Rev. B. - 1999. - Vol.59. - P.12083-12089.
4. Vovk R.V., Obolenskii M.A., Zavgorodniy A.A., Bondarenko A.V., Goulatis I.L., Chroneos A.I. Excess conductivity and pseudo-gap state in YBCO single crystals slightly doped with Al and Pr // J. Mater. Sci: Mater in Electron. - 2007. - Vol.18. - P. 811-815.
5. Vovk R.V., Obolenskii M.A., Zavgorodniy A.A., Goulatis I.L., Beletskii V.I., Chroneos A. Structural relaxation, metal-to-insulator transition and pseudo-gap in oxygen deficient $HoBa_2Cu_3O_{7-\delta}$ single crystals // Physica C. – 2009. – Vol.469. – P.203-206.
6. Vovk R.V., Obolenskii M.A., Zavgorodniy A.A., Bondarenko A.V., Goulatis I.L., Samoilov A.V., Chroneos A.I. Effect of high pressure on the fluctuation conductivity and the charge transfer of $YBa_2Cu_3O_{7-\delta}$ single crystals // Journal of Alloys and Compaunds. – 2008. – Vol.453. - P.69-74.
7. Ginsberg D.M. (ed), Physical properties high temperature superconductors I. – Singapore: Word Scientific, 1989.
8. de Mello E.V.L. et. al. Pressure studies on the pseudogap and critical temperatures of a high-T_c superconductor // Phys. Rev. B. – 2002. – Vol. 66. - P. 092504 (1-4).



Ruslan V. Vovk – D.Sci. in physics and mathematics, Professor in the School of Physics of V.N. Karazin Kharkov National University, Head of the Physics Department at the Ukrainian State Academy of Railway Transport (USART) in Kharkov.
Scientific activities cover a wide range of materials science with the main focus being in high temperature superconductivity and superfluidity. He is author and co-author of more than 150 papers.



Zarif F. Nazyrov - Ph.D. in Physics and Mathematics, Associate Professor, prorector on educational work of V.N. Karazin Kharkov National University.
Scientific interests: Methods of approximate computing, Theory of functions and mathematical physics, Spectral methods for Maxwell's equations in non-stationary problems, Solid State Physics, Superconductivity. He has more than 40 publications of their scientific and educational works in international and domestic trade publications.



Nina N. Zavgorodnyaya - Ph.D. in pedagogics, Associate Professor of "Computer Science and Control Systems" Ukrainian State Academy of Railway Transport, assistant professor of social work and sociology of management of V.N. Karazin Kharkov National University.
Scientific interests: - applied science questions, solid state physics, superconductivity, modeling complex systems, the socialization of the individual. She is co-author over 40 scientific and educational articles and developments.



Claudia A. Kotvitskaya - Senior Lecturer of Physics of the Ukrainian State Academy of Railway Transport.
Scientific Activities - solid state physics. She is co-author of eight articles.

UDC 621.384.6.

THE BASIC SUMMARIES OF WORKING OUT OF RECIRCULATOR SALO MAGNETOOPTICAL SYSTEM

I.S. Guk, S.G. Kononenko, F.A. Peev, A.S. Tarasenko
National Science Centre "Kharkov Institute of Physics and Technology"
Academicheskaja str. 1, Kharkov, Ukraine, 61108
E-mail: guk@kipt.kharkov.ua
Received 30 June 2012, accepted 14 September 2012

Effects of modelling moving an electron beam in the optimised magnetooptical structure recirculator SALO are in-process resulted. Modelling is spent with the account of agency of nonlinear components of a magnetic field of dipole magnets and quadrupole lenses with use of programs TRANSPORT and MAD-X. The gained effects testify to a possibility of a beam production of the given sizes in points of a leading-out and beam acceleration without essential losses along accelerator.
KEY WORDS: electron, recirculator, dipole magnet, quadrupole lens, SALO.

ОСНОВНЫЕ ИТОГИ РАЗРАБОТКИ МАГНИТООПТИЧЕСКОЙ СИСТЕМЫ РЕЦИРКУЛЯТОРА SALO

И.С. Гук, С.Г. Кононенко, Ф.А. Пеев, А.С. Тарасенко
Национальный научный центр «Харьковский физико-технический институт»
ул. Академическая 1, 61108, Харьков, Украина

В работе приведены результаты моделирования движения пучка электронов в оптимизированной магнитооптической структуре рециркулятора SALO. Моделирование проведено с учётом влияния нелинейных компонент магнитного поля дипольных магнитов и квадрупольных линз с использованием программ TRANSPORT и MAD-X. Полученные результаты свидетельствуют о возможности получения пучка заданных размеров в точках вывода и ускорения пучка без существенных потерь вдоль всего ускорителя.
КЛЮЧЕВЫЕ СЛОВА: электрон, рециркулятор, дипольный магнит, квадруполь, SALO.

ОСНОВНІ ПІДСУМКИ РОЗРОБКИ МАГНІТООПТИЧНОЇ СИСТЕМИ РЕЦИРКУЛЯТОРА SALO

І.С. Гук, С.Г. Кононенко, Ф.А. Пеєв, О.С. Тарасенко
ННЦ "Харківський фізико-технічний інститут" НАН України
вул. Академічна 1, 61108, м. Харків, Україна,

У роботі приведені результати моделювання руху пучка електронів в оптимізорованій магнітооптичній структурі рециркулятора SALO. Моделювання проведене з урахуванням впливу нелінійних компонентів магнітного поля дипольних магнітів і квадрупольних лінз із використанням програм TRANSPORT і MAD-X. Отримані результати свідчать про можливості одержання пучка заданих розмірів в точках виводу і прискорення пучка без істотних втрат уздовж усього прискорювача.
КЛЮЧОВІ СЛОВА: електрон, рециркулятор, дипольний магніт, квадруполь, SALO.

Making of major electrophysical facilities usually includes some stages. For developed in NSC KIPT a base accelerating facility on a nuclear physics and a high-energy physics such stages is working out of the perspective program of experiments where the urgency of examinations with electron beams to 1 GeV is displayed, the basic demands to beams are formulated, importance of making on the basis of facility a powerful source of neutrons that will allow to spend a number of applied researches [1, 2] is specified.

On the basis examination of the basic trends in development of the accelerating high technology in the world the select of the plan of the accelerator has been spent, allowing to gain electron beams of the given performances with the account features of its arrangement in existing capital buildings in NSC KIPT [3-7].

At following stage technical requirements to recirculator electromagnetic system basic elements have been formulated and preliminary designs of dipole and quadrupole magnets and all system as a whole [8] are developed. This design has displayed technical possibility embodying of the chosen magnetic structure and has given data for conducting of estimation facility cost. On the other hand, it has determined necessity of the further recirculator structure optimization for unification of magnetic devices and regimes of their operation, and also improvement of performances of output beams.

For support of the continuous regulation of energy on beam lines on an inlet regulating of injection energy has been injected into recirculator accelerating system [9]. Because to the present time the electromagnet with length of poles 100 mm, displayed good performances [10] is designed, made and tested, unification magnets of injection system and magnets of the snake has been spent. For the optimization score it was possible to expel a number of the strong quadrupoles from structure and to diminish fields in quadrupoles of the first and second recycling ring [11]. The General view of modified accelerator magnetic system is presented on Fig. 1.

The main task of this paper is description of the optimized recirculator magnetic system and analysis of beam parameters on an inlet in transportation channels of beams to physical installations. Simulation driving of corpuscles

© Guk I.S., Kononenko S.G., Peev F.A., Tarasenko A.S., 2012

and magnetic structure optimization was carried out by means programs TRANSPORT [12] and MAD X [13] and the methods included in these programs. For deriving of the effects, the most approximate to really implemented in the future facility, used values of effective length of dipole magnets, quadrupole and sextupole field components gained from experimentally measured allocations of fields in magnets, and also models exposition of fields in dipoles and the quadrupoles, widely used in the literature and displayed good coincidence to experimentally measured performances of these magnetic devices [24].

Assuming from features of corpuscles driving at various stages of acceleration and assuming from various designs for the magnetic devices used on these sections, it is convenient to view effects of simulation for system of injection, a gap with accelerating sections, the first turnover of a recycling and the second turnover.

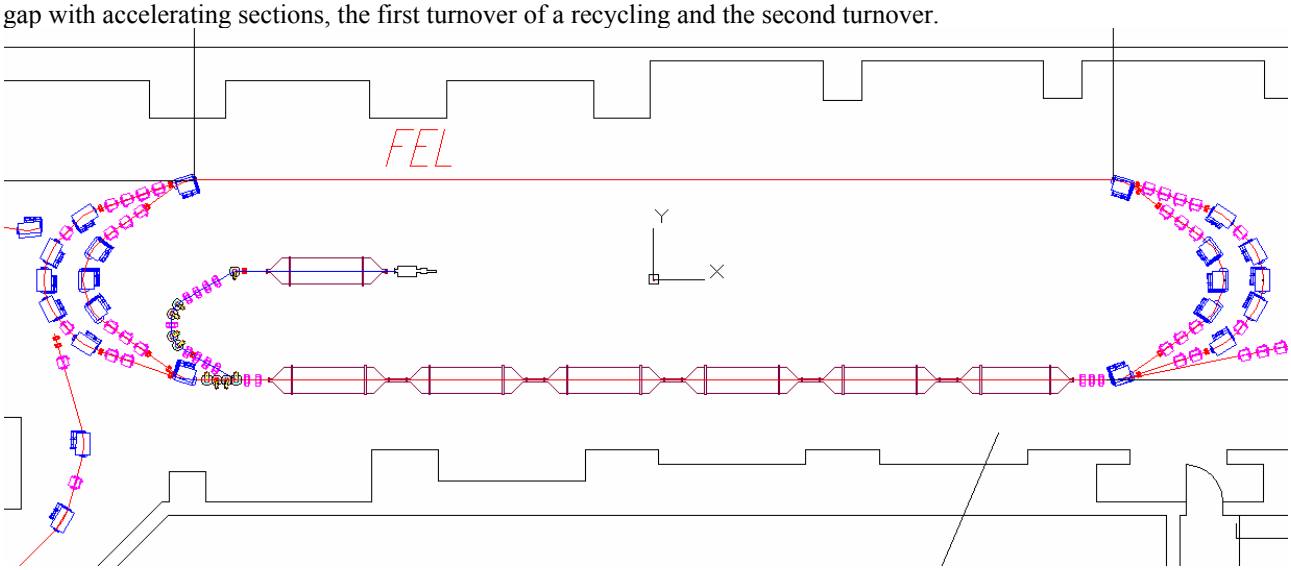


Fig. 1. The General view of recirculator magnetooptical system

RECIRCULATOR ELECTROMAGNETIC SYSTEM DEVICES

As a result of the spent optimization of structure and equipment unification, the recirculator electromagnetic system consists from: dipole magnets system of injection and a snake, quadrupole magnets of system of injection, dipole magnets of the first ring of recirculation, quadrupole magnets of the first ring (they also are used and on the second ring), dipole magnets of the second ring and dipole magnets system of correction.

Dipole magnets (9 copies) injection systems have an s-shaped construction, poles cross-section 100×100 mm, 25 mm distance between poles [10]. Spools windings are executed from a copper wire with heatproof and radioresistance isolation. Cooling of windings is carried out at the expense of air natural circulation. The maximum value of an induction of a field - 0.3 T. The magnet copy is made, the field topography is measured in all effective range of fields. The effective length of a magnet, equal 133, 8 mm, quadrupole and sextupole field components is measured. Maintenance of a pre-production model of a magnet on an exit of technological accelerator "EPOS" within more than one and a half years in the conditions of the strong radiation fields has displayed reliability of a construction and necessary longevity on all prospective expected life.

Quadrupole lenses of injection system [6] (14 copies) are used both on an injection section, and for beam focusing on a section of an arrangement accelerating structures. The maximum value of a field gradient – 6.4 T/m. Diameter of the lens aperture is equal 32 mm. The lens geometrical length is equal 80 mm, settlement effective length - 100 mm. The lens construction is developed on the basis prototype; it is a lot of years operated on electron linacs in NSC KIPT [16]. Cooling of windings air, natural.

10 dipole magnets of electron storage ring EUTERPE [4, 17] are used as dipole magnets of the first ring of recirculation. These magnets have an s-shaped construction with the right-angled poles cross-section 120×480 mm. The positive allowance altitude is equal 25 mm. The magnetic circuit is made of transformer steel leafs, a winding - from the copper tube, chilled by water. The maximum field in a magnet – 1.35 T. Effective length of magnets equal 516 mm. Values of integral sextupole field component along a path of corpuscles [17, 18, 19] which are used in calculations of a path beam driving have been measured also.

28 quadrupole lenses of the first and second turnover of recirculation have been developed and made for ring EUTERPE [4, 17]. The maximum gradient - 15 T/m. The pole length of lens is equal 250 mm, effective length – 274 mm. The radius of the lens aperture is equal 25 mm. The lens yoke is made of a transformer steel. Windings are made of a copper tube and chilled by water.

The design of a dipole magnet of shell-type type is developed for the second ring of recirculation [8]. Cross-section of a pole this magnet equally 120×610 mm, a distance between poles is equal 25 mm. The maximum field of a magnet equally 1.34 T, settlement effective magnet length - 658 mm. The magnet construction guesses manufacture of a yoke from leafs of a transformer steel width 0.35 mm. Windings are supposed to be produced from the copper tube

chilled by water. In total it is necessary to make for a ring 10 magnets.

The construction of the corrector is developed on the basis of the prototype operated on NSC KIPT accelerators [8,16]. The maximum field – 0.02 T, settlement effective length - 100 mm. It has a window construction, is made of a steel, the winding has an air cooling. In total for recirculator it is necessary to make not less than 18 correctors.

SYSTEM OF ELECTRONS INJECTION

As it was already noted [4, 6] acceleration of beams of the polarized and not polarized electrons is supposed in recirculator.

On the given time beams of polarized electrons are actively used in physical experiments on recirculator S-DALINAC in Darmstadt, recirculator CEBAF in Jefferson Laboratory, on microtron MAMI and on accelerator SLAC in Stanford Linear Accelerator Center. Build-up of polarized electron sources typically for all these accelerators [4]. It is longitudinal polarized electrons gain on the basis of a photoeffect from a surface of specially prepared monocrystals of arsenide gallium. These electrons are sped up in a constant electric field to energy 100 KeV and carried to a magnet which gives the chance to spend further beams both polarized, and not polarized electrons on one channel. This channel usually contains the Faraday cup for measuring of a current amount, the Wine filter for regulating of an angle of a spin precession of electrons and Mott polarimeter for measuring magnitude of beam polarization. Further electrons get to accelerating structures, magnetic system and are carried in the experimental halls. No special demands for polarized beams transportation on all facilities are present. The Wine filter allows controlling magnitude of an angle of polarization of electron beams in the experimental halls, canceling an angle of rotation of polarization of the beam, linked with a spin precession of a beam in the course of acceleration. On recirculator SALO there is enough place for disposing of the Wine filter and Mott polarimeter which demand about 1.5 m along an injection line in accelerating section.

Beams parameters of chosen for recirculator prototypes sources of the polarized and not polarized electrons essentially do not differ [4, 6]. But that the not polarized electrons source is supposed to be used in much major number of problems, known measuring of an emittance of this source and design values for different operating modes [14,15] are in-process used for calculations. All reduced values of beam parameters are counted for emittance, equal 1.88 10^{-7} m·rad. The traversal beam cross-section after a gun is presented on Fig. 2.

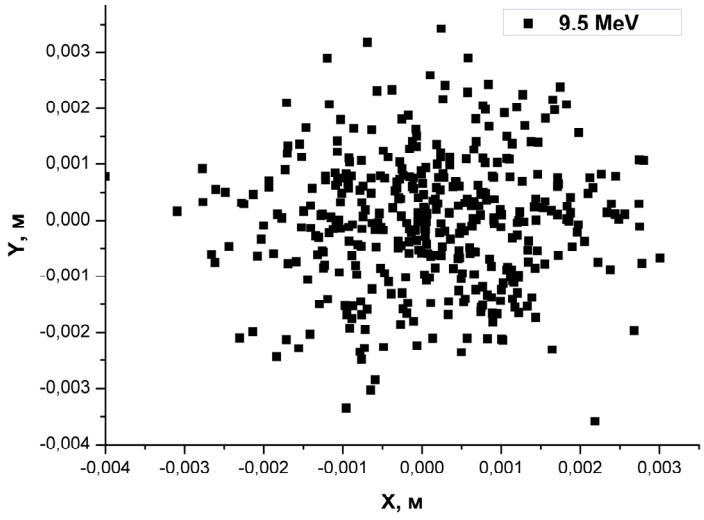


Fig. 2. Traversal cross-section of an injected beam

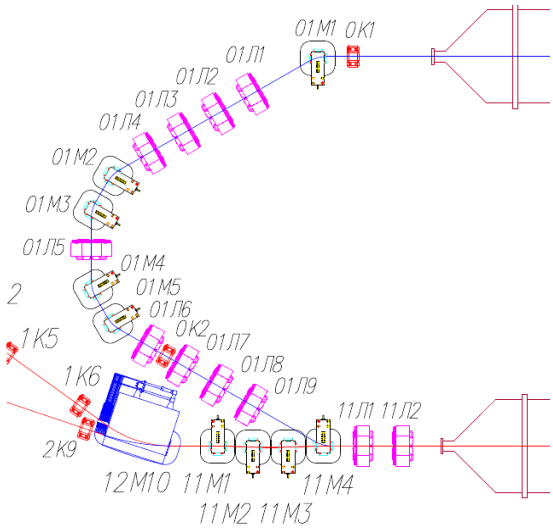


Fig. 3. Structure of the channel beam injection

Electrons are speed up in the accelerating module with superconducting section TESLA to energy 6.66 … 20 MeV after injector and, by means of magnetic system of the transportation presented on Fig. 3, shaped on an entry in the basic accelerating recirculator structure. The traversal cross-section of a beam on an entry in system (a magnet 01M1) is presented on Fig. 4.

The main requirements to the transportation system are isochronism and achromatism. This is achieved by a system consisting of six magnets and 9 quadrupole lenses and the requirement of equality to null elements 1-6, 2-6, 5.6 six-dimensional matrix of transition from the exit of the injection accelerating section up to the entrance to the main accelerating structure [26]. Selection of these requirements was carried out by means of program TRANSPORT [12] and MAD X [13]. Besides, quadrupole lenses of system together with lenses 11Л1, 11Л2 realize traversal focusing of a beam on an entry in the basic accelerator.

Amplitude focusing functions βx, βy and the dispersion function Dx in this area, calculated by the program TRANSPORT [12] and MAD X [13], shown in Fig. 5 and 6.

The envelope of the beam, which represents the maximum deviation from the equilibrium particles orbit, calculated using TRANSPORT [20], is shown in Fig. 7. Obviously, the loss of the beam with dimensions on the path of the injection at the chosen aperture of the magnetic elements will be negligible.

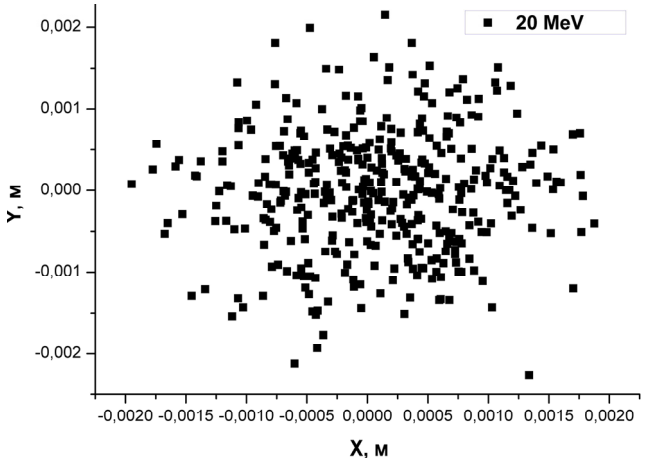


Fig. 4. The cross-section of the injection beam

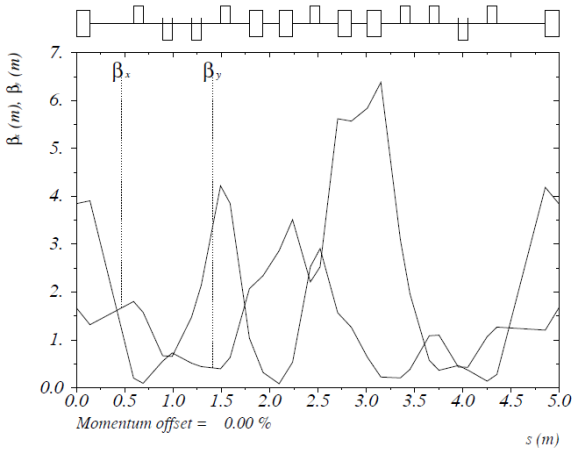


Fig. 5. Focusing functions βx, βy the channel beam injection

The structure of the channel (see Fig. 3) consists of dipole magnets 01M1 - 01M5 and 11M4 dipole magnet, which is part of the snake 11M1 - 11M4. Induction of the field in the magnets in the working range of energies varies from 0.249 to 0.063 T. Quadrupoles 01Л1 – 01Л9 and 11Л1, 11Л2 allow obtaining the necessary achromatism and isochronous system. The maximum value of the gradient in the quadrupole reaches 3.18 T/m. Correctors 0K1, 0K2 can adjust the position of the beam at the entrance of the accelerating section.

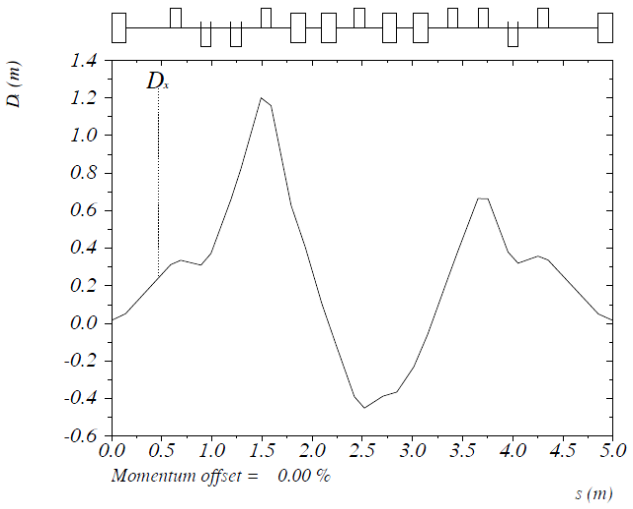


Fig. 6. Dispersion function Dx of the channel of injection

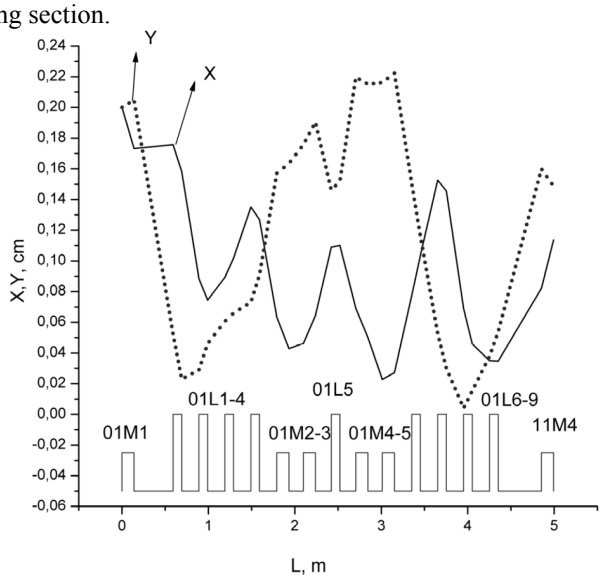


Fig. 7. Beam envelopes on a transportation section

STRAIGHTNESS GAP WITH ACCELERATING STRUCTURE

Snake magnets 11M1 - 11M3 and 11M4 (see Fig. 3, 8), intended to compensate for the effect of the injection field of the 11M4 magnet after the first and the next turns in the first and second ring is located in the straight-line recycling interval length 25.02108 m. Further, in this interval are 6 modules with two superconducting accelerating structures TESLA, allowing to obtain an increase of energy equal to 240 MeV [4]. Calculation of the beam during the passage of the accelerator was carried out under the program MAD-X, which took into account the influence of the transverse defocusing the beam, especially when the injection beam has energy in the energy range 6.67 - 20 MeV. Doublet of quadrupole lenses 11Л1, 11Л2 and triplet-11Л3-11Л5, located before and after the accelerator to compensate defocusing the beam in the accelerating structure and implement its fine-tuning at the entrance to the structure after the first turn without changing modes of magnetic arches of the first and second turn. The maximum gradient is required to perform these procedures does not exceed 4.4 T/m.

The traversal cross-section of a beam on an entry in the accelerator is presented on Fig. 9. On Fig. 10 the cross-section of a beam after acceleration on an entry in the first arch of the first turn of recirculation (a magnet 12M1) is shown.

It is necessary to note, that the specified sizes of a beam correspond to an injector operating mode with average current 1 mA, necessary for implementation operation of the accelerator in the capacity of the driver subcritical assembly [2, 5] and for manufacture isotopes [23]. At this alternative of use of the accelerator it is supposed, that rate of acceleration in superconducting sections equal 10 MeV/m. Really such situation will be already implemented on the accelerating complex ELBE working many years [21, 22] with use of two accelerating modules. At energy spread less

than 0.2 % the beam with such parameters and aggregate power about 140 KW can be transported on tens meters lost-free on a target as it is offered in articles [2,4,5,7], or can be used in a hall of the SP-103 hall for manufacture isotopes of medical appointment [23].

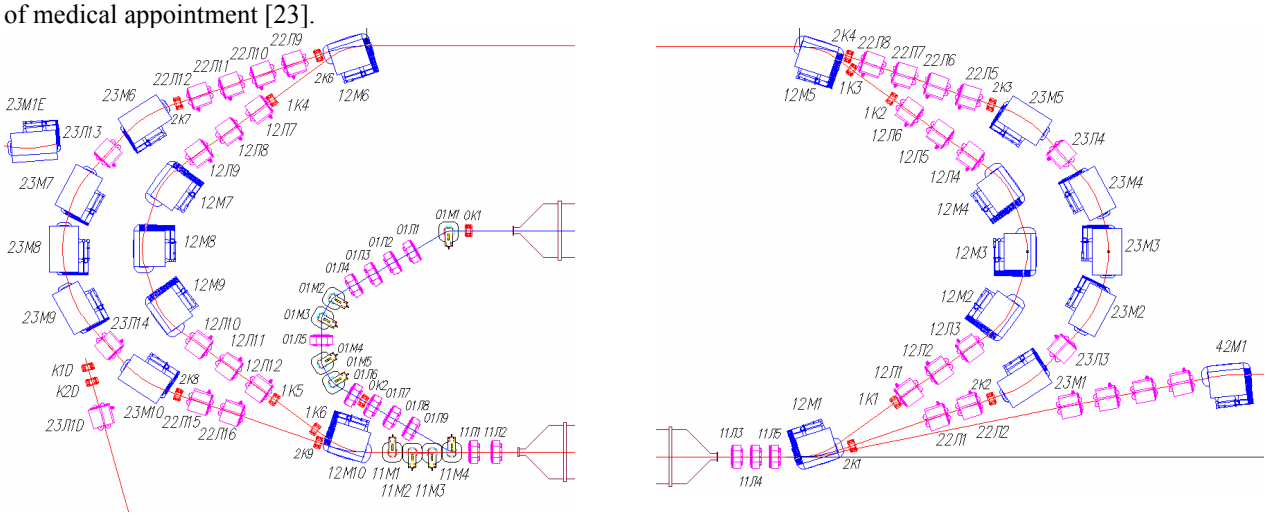


Fig. 8. Structure arches of beam recirculation

We have not detected essential change magnitude of beam losses at emittance magnification in the chosen structure twice.

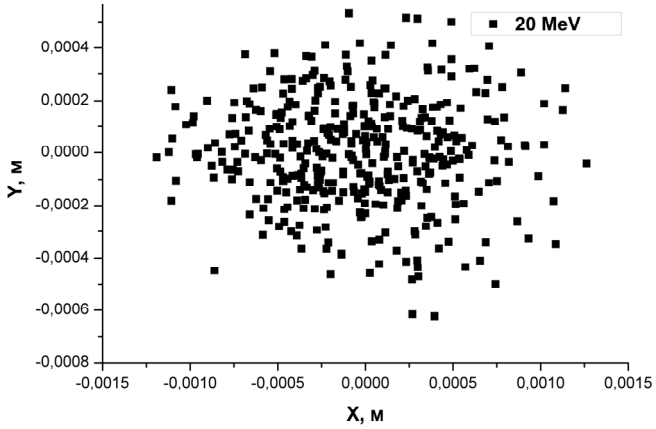


Fig. 9. Beam sizes on an entry in the basic accelerating structure

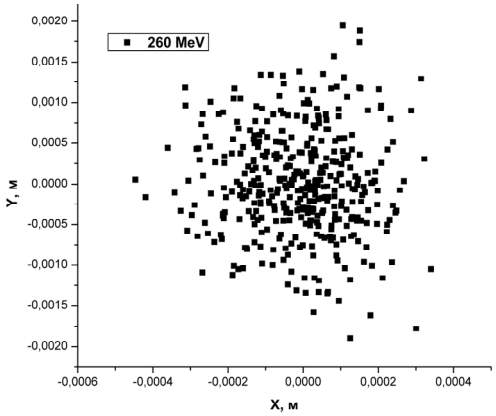


Fig. 10. Beam sizes on an entry in the first arch

The beam current will not exceed 30 μA by recirculator operation on nuclear physics program [25], therefore both the emittance and energies spread of a beam will be less than in a high-current regime. The voltage gradient in the accelerator thus is supposed there will be equal 20 MeV/m.

THE FIRST RING OF RECIRCULATION

The point on an entry in a magnet 12M1 is initial for implementation the first extraction channels of particles from recirculator. First of all, as it has been mentioned above, in a SP-103 hall the direct beam with energy to 260 MeV (140 MeV in a high-current regime) can be received. Besides, at magnet 12M1 turning on, in a hall it is possible to receive the turned beam in the same interval of energies. At partial use of magnets and lenses of the first and second ring of recirculation the beam can be extracted in channels N1-N3 and E, D [25].

The basic demands to sampling of structure and operating modes magnetic devices of arcs the first ring is achromatism, the isochronism and a beam dynamic stability in structure. The length of an equilibrium orbit of a beam was chosen to the multiple wave length of an accelerating field for maintenance of arrival electron bunch in accelerating structure synchronously with an injected beam. The change of path length which is brought in by presence snake of magnets 11M1-11M4 was thus considered. Beam turning angles are equal in all magnets 36°. As a part of the first ring used 10 dipole magnets of storage ring EUTERPE - 12M1-12M10 and 12 quadrupole lenses made for this storage ring - 12Л1-12Л12 (Fig. 1, 8). The maximum field in magnets – 1.02 T, the maximum gradient in lenses – 9.2 T/m.

The rectilinear gap of a ring can be used for free electron laser installation [4]. Studying influence magnetic structure of the laser on beam dynamics in recirculator should become a theme of separate analysis as in magnetic structure of the laser there can be beams the second turn of recirculation with it is essential other energy. The gap does not contain focalizing devices.

Focusing and dispersion functions for the first turn are presented on Fig. 11 and 12.

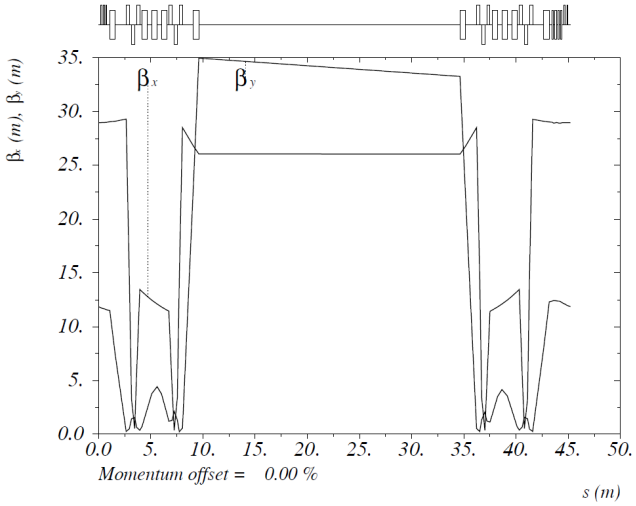


Fig. 11. Focusing functions βx, βy the first ring

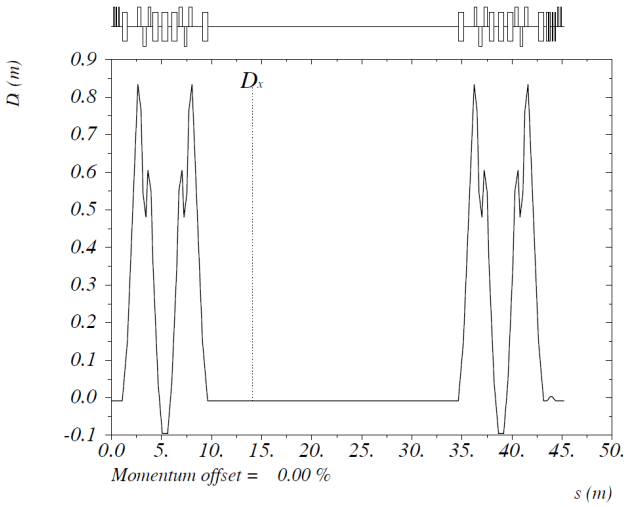


Fig. 12. Dispersion function Dx of the first ring

From the presented data it is visible, that the chosen optimized structure answers the installed measure, and traversal sizes of a beam on all sections of a path equal $\sigma(s) = \sqrt{\varepsilon\beta(s)}$, do not exceed presented on Fig. 10, 13-15.

The traversal beam cross-section on an exit first and on an entry of the second arch is presented on Fig. 13 and 14.

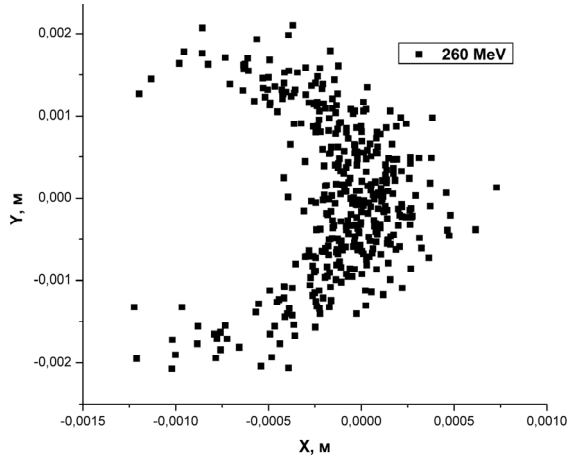


Fig. 13. Beam sizes on 12M5 magnet exit

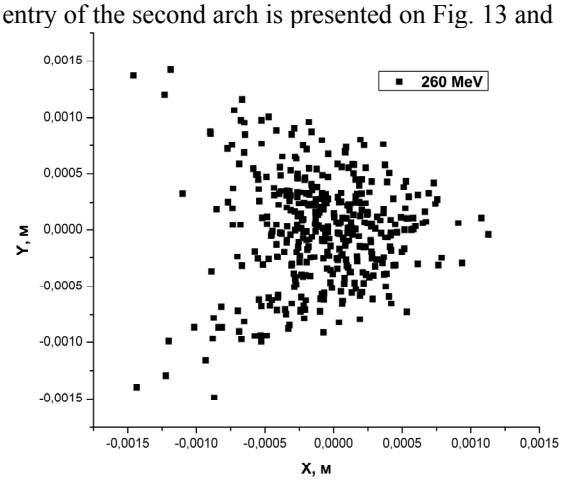


Fig. 14. Beam sizes on an entry in 12M6 magnet

The traversal beam cross-section on an exit of the second arch of the first turn is presented on Fig. 15. Sizes of a beam after double passage of the accelerator (on an entry in a magnet 12M1) are presented on Fig. 16.

The deformation of traversal cross-section of a beam is called by essential change of phase motion of a beam under the influence of nonlinear field component of dipole and quadrupole magnets [24].

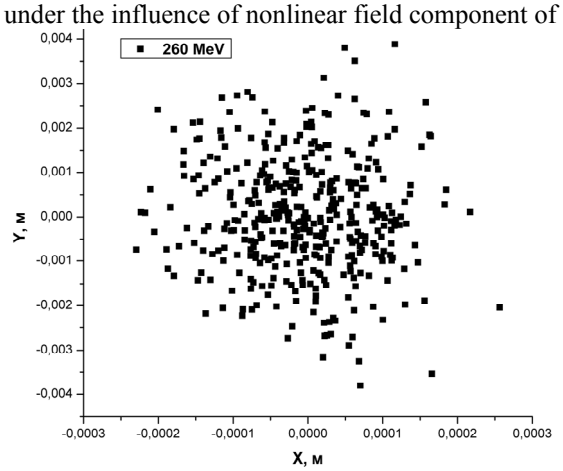


Fig. 15. Beam sizes on 12M10 magnet exit

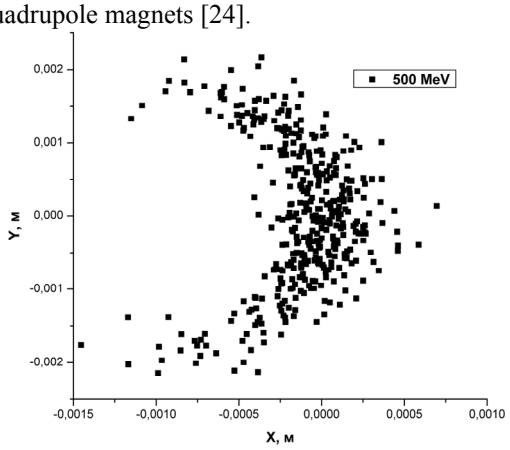


Fig. 16. Beam sizes on an entry in 12M1 magnet

The particles with the maximum energy 500 MeV can be utilize after the first ring of recirculation in SP-103 hall and, with use of dipoles and quadrupoles of the second ring, in channels E and D [25].

THE SECOND RING OF RECIRCULATION

The same demands were made to sampling parameters magnetic system of the second ring of recirculation, as for first, both on geometry, and on optimization of regimes. Characteristic of this ring is lack of a place for disposing quadrupole lenses on a section which is bordering on to the channel of an extraction of particles in SP-103 hall. Such problem has originated that magnets 12M1, 12M5, 12M6 and 12M10 are used as rotary and as parting rings of recirculation and an extraction of particles on the maximum energy. Focusing and dispersion functions for the second turn are presented on Fig. 17, 18.

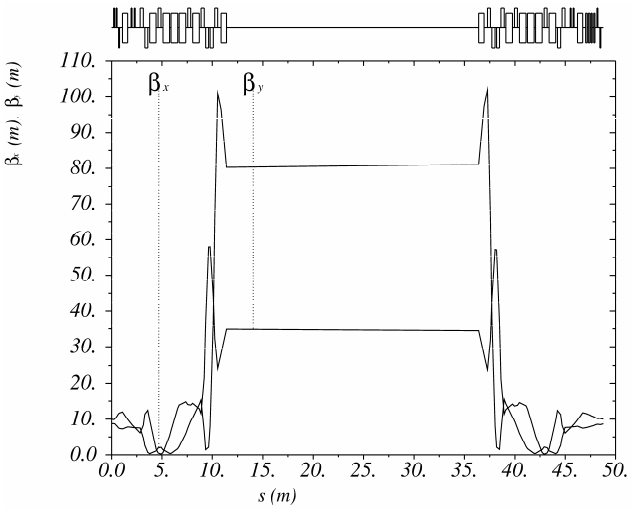


Fig. 17. Focusing functions βx, βy the second ring

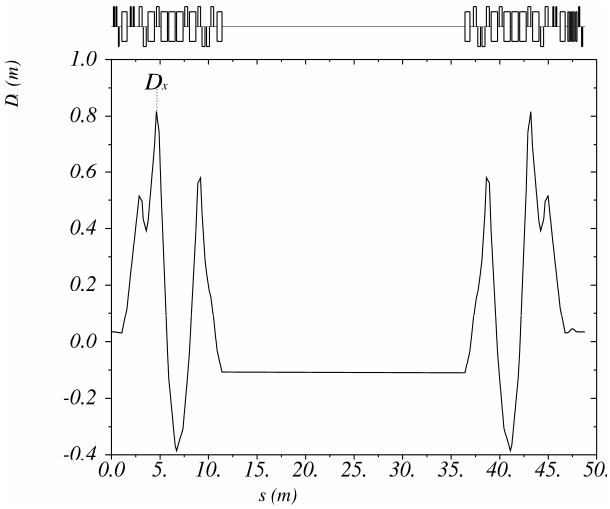


Fig. 18. Dispersion function Dx of the second ring

Traversal beam sizes on 12M5magnet exit, on an entry in magnet 12M6 and on 12M10 magnet exit are presented on Fig. 19-21.

At calculations the sextupole component field of magnets 23M1-23M10 was accepted to the equal magnitude measured for magnets EUTERPE. This magnitude a priori is oversized for the construction of a shell-type dipole magnet, however real magnitude it is impossible to gain because the magnet is not made yet. At sextupole component, equal 0, traversal sizes of a beam in the points figured on Fig. 20, 21 are resulted on Fig. 22, 23. As it is possible to see, it does not lead to an essential dimensional change of a beam size because corpuscles energy essentially major, and the gain is less, than at the first passage of the accelerator.

The beam angle rotation in magnets 23M1-23M10 is equal 28.516º. The maximum value field induction in dipole magnets of this ring attains magnitude 1.25 T and maximum gradient of quadrupole lenses – 15.6 T/m.

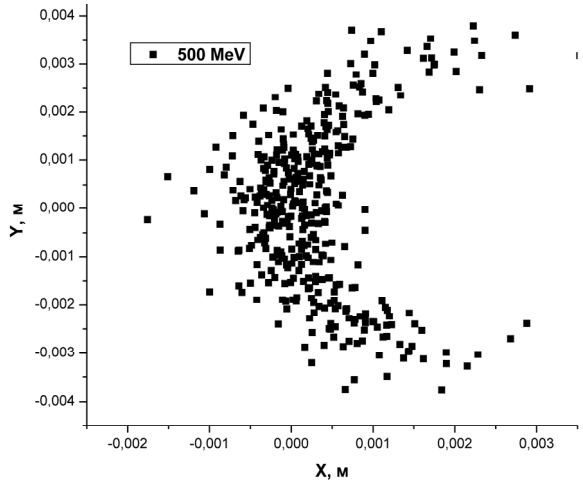


Fig. 19. Beam sizes on the second ring of recirculation (on magnet 12M5 exit)

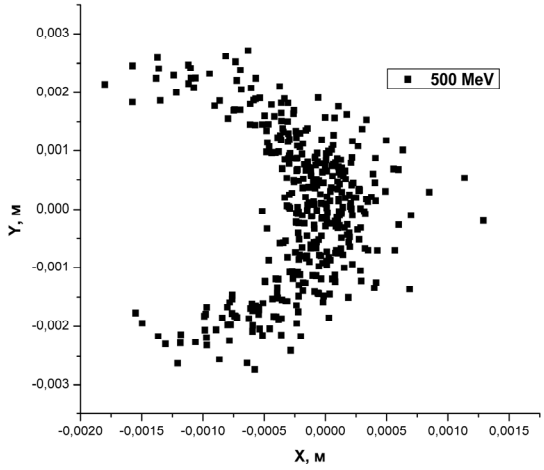


Fig. 20. Beam sizes on the second ring of recirculation (on an entry in 12M6 magnet)

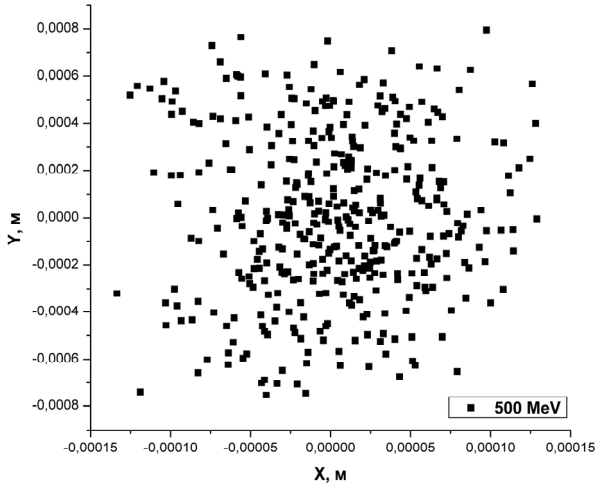


Fig. 21. Beam sizes on the second ring of recirculation (on magnet 12M10 exit)

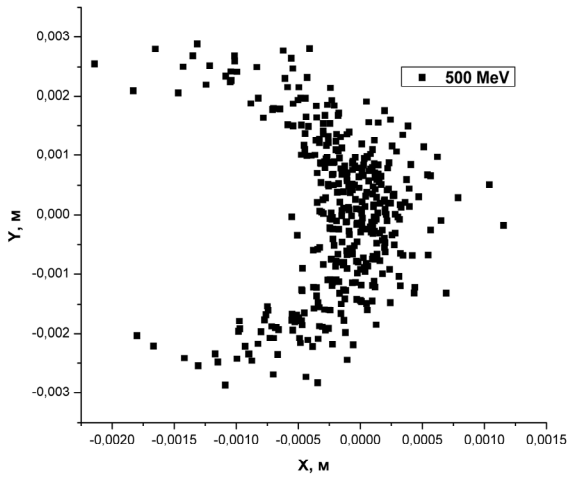


Fig. 22. Beam sizes on the second ring of recirculation (on an entry in 12M6 magnet) with sextupole component equal 0

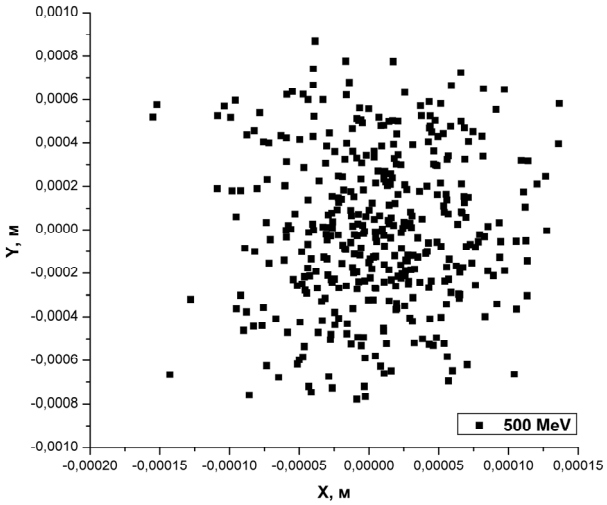


Fig. 23. Beam sizes on the second ring of recirculation (on magnet 12M10 exit) with sextupole component equal 0

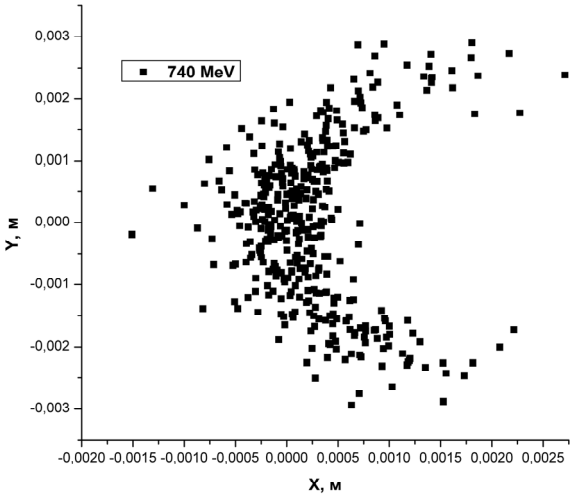


Fig. 24. Beam sizes at the maximum energy on an entry in 12M1 magnet

Traversal beam sizes on an entry in the transportation channel in SP-103 hall are presented on Fig. 24.

CONCLUSION

Optimization of structure and operating modes magnetic devices of recirculator magnetooptical system has allowed gaining the required parameters of electron beam in points leading-out to physical facilities by means of three types of dipole magnets and two types of quadrupole lenses. Nonlinear component fields of dipole and quadrupole lenses work upon traversal beam cross-section, however at shut down sextupole field component of dipole magnets on the second ring of recirculation an essential dimensional change and the beam shape does not occur. The maximum beam sizes along accelerator do not exceed 6 mm; therefore losses of corpuscles at the chosen aperture of magnetic devices will be very small.

REFERENCES

1. Buki A.Y., Ganenko V.B., Korchin A.Yu., Kotljar V.V., Shevchenko N.G. et.al. Fundamental and applied research on Kharkov superconducting electron accelerator on energy up to 730 MeV" (project "SALO"), part 1. – NSC KIPT, Kharkov, 2006. – 116 p.
2. Accelerator Driven Sub-critical Assembly Facility / Proceedings of the Ukraine-USA meeting Ukraine, Kharkiv, February 24-25, 2005. – NSC KIPT, Kharkiv, 2005. – 246 p.
3. Guk I.S., Dovbnya A.N., Kononenko S.G., Tarasenko A.S. Selection of the option of the baseline accelerator facility at NSC-KFTI for research in nuclear and high-energy physics. – Preprint KFTI 2003-3, NSC-KFTI, 2003. – 79 p.
4. Arkatov Yu.M., Dovbnya A.N., Glamazdin A.V., Guk I.S., Kononenko S.G., van der Weil M., Botman J.I.M., Peev F.A., Tarasenko A.S. "SALO" project. – National Science Center Kharkov Institute of Physics Technology, Kharkiv, 2005. – 104 p.
5. Bratchenko M.I., Gann V.V., Guk I.S., Dovbnya A.N., Dyuldya S.V., Kononenko S.G., Peev F.A., Tarasenko A.S., van der Wiel M., Botman J.I.M. Superconducting driver for sub-critical assembly // Proceedings of the International Conference

"Current Problems in Nuclear Physics and Atomic Energy" – Kyiv, Ukraine, 2007. – P. 622 - 632.
6. Dovbnya A.N., Guk I.S., Kononenko S.G., Peev F.A., Tarasenko A.S., Botman J.I.M. Accelerating complex for basic researches in the nuclear physics // Proceedings of the 2-nd International Conference "Current Problems in Nuclear Physics and Atomic Energy", June 9 to June 15, 2008, Kyiv, Ukraine, Kyiv, 2009. – P. 790-795.
7. Dovbnya A.N., Guk I.S., Kononenko S.G., Peev F.A., van der Wiel M., Botman J.I.M. Variants of use superconducting electron accelerator SALO as a driver of subcritical accembly // The Journal of Kharkov National University, physical series "Nuclei, particles, fields". – 2007. - №784. - Issue 4/36/. – P.15-23.
8. Dovbnya A.N., Guk I.S., Kononenko S.G., Koval'ev G.G., Mytsykov A.Y., Peev F.A. Draft design of recirculator SALO magnetic system // The Journal of Kharkov National Univesity, physical series "Nuclei, Particles, Fields". – 2007. – №784. - Issue 4/36/. – P.3 – 14.
9. Guk I.S., Kononenko S.G., Peev F.A., Tarasenko A.S. Magnito-optical system of recirculator SALO with energy over the range 60…740 MeV regulation // VANT, Series "Nuclear Physics Investigations". – 2010. - №3(67). - P. 44-47.
10. Guk I.S., Dovbnya A.N., Kononenko S.G., Lyashchenko V.N., Mytsykov A.Yu., Romas'ko B.P., Tarasenko A.S., Shcherbinin V.A. Dipole Magnet of the Injection System for the SALO Recirculator // Physics of Particles and Nuclei Letters. – 2012. - Vol.9, № 4–5. - P. 410–414.
11. Guk I.S., Dovbnya A.N., Kononenko S.G., Tarasenko A.S., Botman J.I.M. The status of work on designing electron accelerating complex SALO // Problems of atomic science and technology, Series: Nuclear Physics Investigations. - 2010. – №2(53). – P.52-55.
12. Carey D.C., Brown K.L., Rothacker F. Third-Order TRANSPORT with MAD Input A Computer Program for Designing Charged Particle Beam Transport Systems // FERMILAB-Pub-98, 1998. – 310 p.
13. http://mad.home.cern.ch/mad/
14. Teichert J., Arnold A., Büchner A., Büttig H., Janssen D., Justus M., Lehnert U., Michel P., Murcek P., Schurig R., Staats G., Staufenbiel F., Xiang R., Kamps T., Klemz G., Will I., Matheisen A. First operation results of the superconducting photoinjector at ELBE // Proceedings of EPAC08, Genoa, Italy, 2008. – P. 2755-2757.
15. Xiang R., Arnold A., Buettig H., Janssen D., Justus M., Lehnert U., Michel P., Murcek P., Schamlott A., Schneider Ch., Schurig R., Staufenbiel F., Teichert J., Kamps T., Rudolph J., Schenk M., Klemz G., Will I. Running experience of the superconducting rf photoinjector at FZD // Proceedings of FEL2009, Liverpool, UK. – P.488-491.
16. Ayzatsky M.I., Boriskin V.N., Dovbnya A.M., Kushnir V.A., Popenko V.A., Shendrik V.A., Tur Yu.D., Zykov A.I. The NSC KIPT electron linacs - R&D // Problems of atomic science and technology. Series "Nuclear Physics Investigations". - 2003. - №2(33). – P. 19-25.
17. Boling Xi, Botman J.I.M., Timmermans C.J., Hagedoorn H.L. Design study of storage ring EUTERPE // Nucl. Instr. and Meth. – 1992. – Vol.B68. - P. 101.
18. Guk I.S., Dovbnya A.N., Kononenko S.G., Peev F.A., Tarasenko A.S. Aberrations of Magnetooptical System of SALO Recirculator // Physics of Particles and Nuclei Letters. – 2010. - Vol. 7, № 7. - P. 1–4.
19. Boling Xi. Design Studies for the Electron Storage Ring EUTERPE / Thesis (Techn. Univ. Eindhoven), ISBN 90-386-0066-6.
20. Carey D.C., Brown K.L., Rothacker F. Third-Order TRANSPORT with MAD Input A Computer Program for Designing Charged Particle Beam Transport Systems // FERMILAB-Pub-98. – 1998 - 310 p.
21. http://www.fz-rossendorf.de/ http://www.hzdr.de/db/Cms?pNid=584
22. Michel P., Büchner A., Evtushenko P., Gabriel F., Lehnert U., Teichert J., Voigländer J. Comissioning of the ELBE superconducting electron linac // Proceedings of EPAC 2002, Paris, France. – P. 817-818.
23. Guk I.S., Kononenko S.G., Peev F.A. About possibility manufacturing of the diagnostic medical isotope technetium 99M in UKRAINE // The Journal of Kharkov National Univesity, physical series "Nuclei, Particles, Fields". - 2010. - № 916. - Issue 3/47/. – P. 117-126.
24. Guk I.S., Kononenko S.G., Tapasenko A.S. Investigation of the effect of non-linear parameters of dipole and quadrupole magnets on the beam parameters in recirculator SALO // Problems of atomic science and technology. Series "Nuclear Physics Investigations". – 2012. - №3 (79). - P. 137-141.
25. Dovbnja A.N., Ganenko V.B., Guk I.S., Kononenko S.G., Tarasenko A.S. The electron beam lines from SALO recirculator to physical installation // The Journal of Kharkov National Univesity, physical series "Nuclei, Particles, Fields". – 2007. - №784. - Issue 4/36/.- P.74-78.
26. Gavrilov N., Somov S. The equipment for operation with the accelerated beams / Manual – M.: SRNU MIFI, 2010. – 224 p.



Guk Ivan Semenovich, Ph.D., senior scientific researcher NSC KIPT
Scientific interests: framing of large accelerating complexes, beam dynamics in accelerators, synchrotron radiation, powerful sources of neutrons and electrons. The author and the co-author more than 120 papers and 2 books



Kononenko Stanislav Grigor'evich, senior scientific researcher NSC KIPT
Scientific interests: beam dynamics in accelerators, powerful sources of neutrons and electrons
The author and the co-author more than 110 papers and 2 books



Peev Fedor Andreevich, scientific researcher NSC KIPT
Scientific interests: framing of large accelerating complexes, powerful sources of neutrons and electrons
The author and the co-author more than 90 papers and 2 books



Tarasenko Alexander Sergeevich, senior scientific researcher NSC KIPT
Scientific interests: beam dynamics in accelerators, synchrotron radiation, powerful sources of neutrons and electrons
The author and the co-author more than 110 papers and 2 books

UDC 621.039.546

SOLID AND LIQUID WASTE PROCESSING AND REDUCING OF PERSONNEL DOSES

N.A. Azarenkov[1], V.G. Rudychev[1], S.A. Pismenetskiy[1], Y.V. Rudychev[2], P.S. Badzym[3], S.I. Shapar[3], O.V. Vystavna[3]

[1]V.N. Karazin Kharkov National University
Ukraine, Kharkiv, Svobody sq. 4, 61022
[2]National Scientific Center, Kharkov Institute of Physics and Technology
1, Akademicheskaya st., Kharkov, Ukraine, 61108
[3]Kharkov Institute Energoproekt
10-12, Moskovskij pr., Kharkov, Ukraine, 61003
E-mail: rud@pht.univer.kharkov.ua

Received 7 September 2012, revised 11 September 2012, accepted 25 September 2012

In order to minimize the radioactive waste volume at the Ukrainian NPP (nuclear power plants) solid waste is burned and compressed and liquid one evaporated. This dramatically increases their activity as well as their radiation doses during of operation process. In accordance with the ALARA principle the technological solutions that reduce doses to personnel were proposed. First part of the complex built on Zaporozhye NPP consists of processing waste incinerators and pressing facilities. The characteristics of the radiation fields for varying geometries of this facility and isotopic composition of obtained waste was simulated using PENELOPE and GEANT codes. Part of the results was performed using the software packages developed by the authors using point sources method. During operations with burned waste pressed ash the wall thickness of buildings, where equipment is placed is needed, up to 40 cm of concrete. Thickness of the steel technological doors for these premises is required to be of about 12 cm. The alternate design of technological doors (≈ 2cm of steel) by adding special gateway system is to be proposed.
KEY WORDS: radioactive waste, burned radioactive waste, pressed radioactive waste, liquid radioactive waste, radiation doses.

ПЕРЕРАБОТКА ТВЕРДЫХ И ЖИДКИХ ОТХОДОВ И УМЕНЬШЕНИЕ ДОЗ ПЕРСОНАЛА

Н.А. Азаренков[1], В.Г. Рудычев[1], С.А. Письменецкий[1], Е.В. Рудычев[2], П.С. Бадзым[3], С.И. Шапарь[3], Е.В. Выставная[3]

[1]Харьковский национальный университет им. В.Н. Каразина
г. Харьков, 61022 Украина, пл. Свободы, 4
[2]Национальный Научный Центр «Харьковский физико-технический иститут»
ул. Академическая 1, г. Харьков, Украина, 61108
[1]Харьковский институт Энергопроект
г. Харьков, 61003 Украина, пр. Московский 10-12

С целью минимизации объема радиоактивных отходов на украинских АЭС твердые отходы подвергают сжиганию и прессованию, а жидкие – упариванию. Это значительно повышает их удельную активность и дозу облучения в процессе переработки. В соответствии с принципом ALARA были предложены технологические решения, которые сокращают дозы персонала. Первая очередь комплекса, возводимого на Запорожской АЭС, состоит из установок сжигания и прессования отходов. Характеристики радиационных полей для разных геометрий этих установок и изотопного состава принимаемых отходов были рассчитаны с помощью программ PENELOPE и GEANT. Часть результатов была получена с использованием программного обеспечения, разработанного авторами на основе метода точечных источников. При операциях с прессованной золой сожженных отходов толщину стен в помещениях, где эксплуатируется оборудование, потребовалось увеличить до 40 см бетона. Необходимая толщина стальных технологических дверей для этих помещений составляет около 12 см. Предложен альтернативный вариант конструкции технологических дверей (порядка 2 см по стали), который содержит специальное защитное ограждение.
КЛЮЧЕВЫЕ СЛОВА: радиоактивные отходы, сжигаемые радиоактивные отходы, прессуемые радиоактивные отходы, жидкие радиоактивные отходы, дозы излучения.

ПЕРЕРОБКА ТВЕРДИХ І РІДКИХ ВІДХОДІВ ТА ЗМЕНШЕННЯ ДОЗ ПЕРСОНАЛУ

М.А. Азаренков[1], В.Г. Рудичев[1], С.А. Письменецкий[1], Е.В. Рудичев[2], П.С. Бадзим[3], С.І. Шапарь[3], О.В. Виставна[3]

[1]Харківський національний університет ім. В.Н. Каразіна
м. Харків, 61022, пл. Свободи, 4, Україна
[2] Національний науковий центр, «Харківський фізико-технічний інститут»
м. Харків, вул. Академічна, 1
[3]Харківський інститут Енергопроект
м. Харків, 61003 Україна, пр. Московський 10-12

З метою мінімізації об'єму радіоактивних відходів на українських АЕС тверді відходи спалюють і пресують, а рідкі – випаровують. Це значно підвищує їхню питому активність і дозу опромінення в процесі переробки. У відповідності до принципу ALARA було запропоновано технологічні рішення, які зменшують дози персоналу. Перша черга комплексу, який споруджується на Запорізькій АЕС, складається з установок спалювання і пресування відходів. Характеристики радіаційних полів при різних геометріях цих установок і ізотопному складі перероблюваних відходів були розраховані за допомогою програм PENELOPE і GEANT. Частину результатів було отримано за допомогою програмного забезпечення, розробленого

© Azarenkov N.A., Rudychev V.G., Pismenetskiy S.A.,
Rudychev Y.V., Badzym P.S., Shapar S.I., Vystavna O.V., 2012

авторами на основі методу точкових джерел. При операціях із пресованою золою спалених відходів товщину стін у приміщеннях, де експлуатується устаткування, було потрібно збільшити до 40 см бетону. Необхідна товщина стальних технологічних дверей у цих приміщеннях складає 12 см. Запропоновано альтернативний варіант конструкції технологічних дверей (близько 2 см сталі), який передбачає спеціальну захисну огорожу.
КЛЮЧОВІ СЛОВА: радіоактивні відходи, радіоактивні відходи які спалюються, радіоактивні відходи пресуються, рідкі радіоактивні відходи, дози опромінення.

The complex of solid radioactive waste (RW) and liquid radioactive waste (LRW) reprocessing is intended for higher productivity of utilization process of the RW stored at Zaporozhye nuclear power plant (NPP) warehouses and minimization of the amount of RW produced as a result of the RW recycling. The amount of RW produced both in the process of regular operation of a nuclear power plant and during carrying out of any repair work as well as during an accident (any emergency) is considerable enough. In the sequel these volumetric RW are stored at the nuclear power plant (NPP). The problem how to make the waste compact is the matter of topical interest for all the NPP in Ukraine.

As a rule to make solid RW compact they are pressed, and as for combustible waste, they are burned and then pressed. Liquid RW are evaporated, and the combustible, such as oil, for example, are burned. Three units of a complex for RW utilization, namely, units for burning and super-pressing, and also a fragmentation module, are planed to be put into operation at the Zaporozhye NPP. To place the units for burning and super-pressing a special building is under design and the fragmentation module will be disposed in the existing building of the storage site for solid RW. According to the design, in the new building some import processing equipment, delivered under TACIS program, is stipulated to be installed: a burning unit, with productivity of 30 kg/hour; a super-pressing unit, with pressing effort of 150 tons.

The aim of this work is to analyze radiation environment in the premises of RW processing complex both under normal operation of the units, and when any emergency occurred. The layout of the basic burning unit elements is shown on Fig. 1.

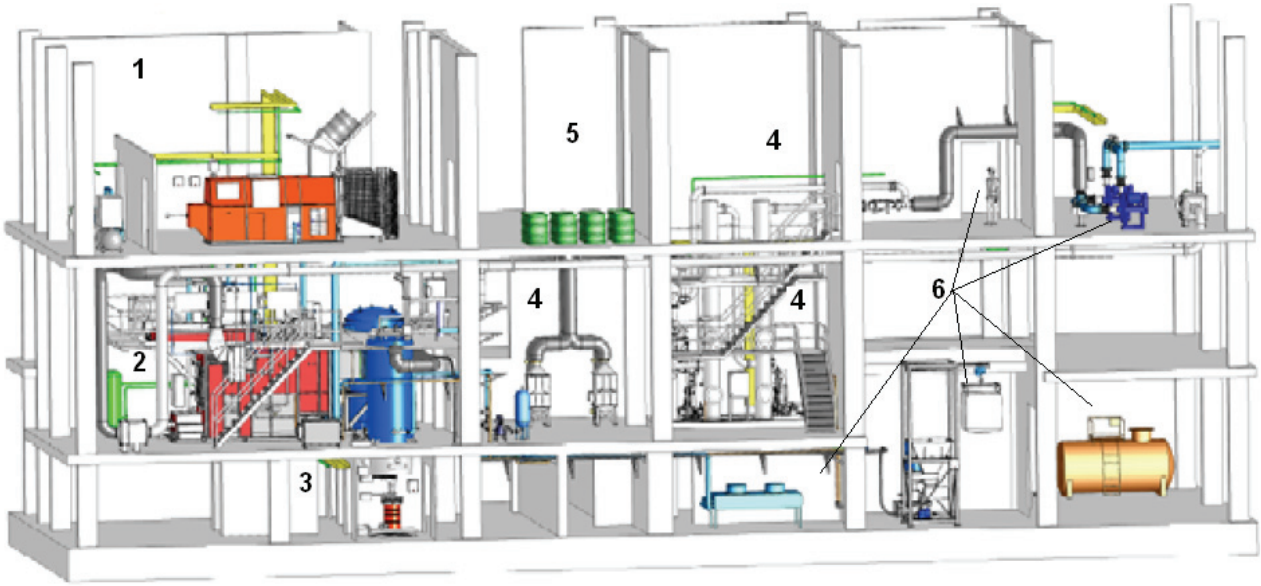


Fig. 1. General layout of the burning unit.
1 – load of RW to be burned, 2 – combustion furnace, 3 – ash unloading; 4 – gas cleaners; 5 – burned RW storage; 6 – service premises.

RADIATIONS CHARACTERISTIC OF RW

Radio nuclide composition of RW and LRW consist of such nuclides: ^{95}Zr, ^{95}Nb, ^{124}Sb, ^{65}Zn, ^{51}Cr, ^{59}Fe, ^{58}Co, ^{110m}Ag, ^{144}Ce, ^{54}Mn, ^{60}Co, ^{134}Cs, ^{137}Cs. Spectrums of gamma radiation for all types of the waste taking into account these nuclides were obtained by SpectrOJAT package [1]. To determine the flow density of beta-particles at the RW exposed surface the total beta-ray spectrums for RW, ash, oil and pressed solid RW were calculated taking into account isotopic composition of the radio nuclides contained in them. The calculation results are given in Fig. 2. The given data show that the radio nuclides contained in oil, generate electrons with high enough energy due to the presence of ^{124}Sb in it. Obtained were used further for estimation of the dose rate in the premises of RW processing complex.

CALCULATION PROCEDURES

The RW processing complex at Zaporozhye NPP includes a combination of ionizing radiation sources of various shape and composition, namely: cylindrical volume radiation sources in the form of steel barrels with volume of 170, 200 and 280 l; solid RW, inside a box with a “glovebox”, packed into packages of 15 kg, which when moving over a

table, take the form of a cylinder with diameter of ~ 45 cm and height of ~3.5 m; the RW, being in a powdery-gaseous state, filling up the cylindrical volumes of a boiler and of a bag filter. The radiation sources as a part of the RW processing complex are exposed radiation sources and represent hybrid beta-gamma emitters.

When calculating the dose rate from the mentioned radiation sources, the following techniques and program codes were used:

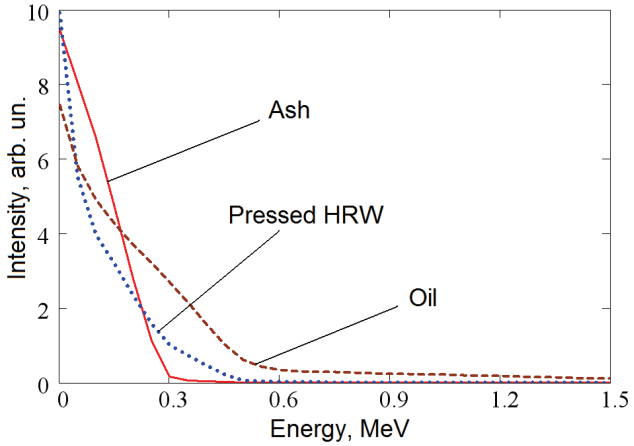


Fig. 2. Spectrums of beta particles of the major in-process RW (ash, pressed solid RW, oil)

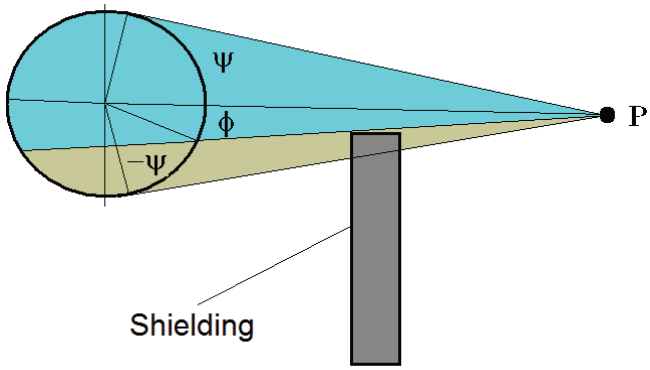


Fig. 3. Geometry of a self-absorbing cylindrical volumetric radiation source with partial shadowing

VOLUME_M – The program complex developed in KhNU, as well as the well known **MicroShield** package based on the method of volumetric or surface integration of point sources, allowing calculating gamma-quantum flows from the sources of different shape provided that some protective constructions are present [2]. Often enough situations occur when a radiation source (RS) is partially shadowed with a protective construction or any other radiation source. In this case the source radiation is divided in two parts: direct radiation and radiation transmitting through the shielding (Fig. 3).

Using **MicroShield** package one cannot calculate a situation like this, but at the same time solution of such problems is possible when using **VOLUME_M** package. During the process of reload and transportation of the RW prepackaged in barrels (solid RW for pressing, ash, briquettes) the barrel may fall down and the radioactive waste may spill out on the floor. The doze rates from the barrel's content spilled out (volume – 170, 200 and 280 l) depend both on the RW composition, and on the shape (the geometrical sizes) of the generated radiation source. For calculation of the dose rate of the spilled out RW (ash, solid RW) different model geometries of radiation sources, such as: a semi-cylinder lying on a surface and hemisphere were used.

EMID Package. EMID program module [3] is based on the use of empirical formulas and algorithms of electrons transport. The package allows calculating various characteristics both of electrons, and of a matter when fast electrons are passing through heterogeneous structures. The package allows to calculate the path range of electrons with different spectral composition in various materials and to determine dose characteristics.

PENELOPE – the program code for carrying out calculations on transport of electrons and gamma-quanta through various objects and mediua [4]. The code is used for calculations of the dose rate provided that protection is heterogeneous. In the given paper some geometrical blocks describing geometry of the radiation sources: barrels, furnaces, «glovebox" , super-pressing device components were created for the PENELOPE package.

SpectrOJAT – a package allowing to calculate spectral composition and intensity of gamma radiation from spent nuclear fuel or any combination of radio-nuclides at any given moment of time [1]. A special feature of the package is feasibility to calculate gamma-quanta spectrum with partition into any arbitrary specified energy intervals. Databases for quantum yields of each radionuclide were generated on the basis of JEF2.2 package [5] with addition of the data from JEF3.2 package [6].

MCNP – the program code developed by Los-Alamos National Laboratory [7] for Department of Energy in the USA. MCNP program is widely used for the analysis of protective shielding in the nuclear industry of the USA. In the present paper the MCNP was used for check and verification of the gained results.

RESULTS OF CALCULATIONS

Calculations of gamma radiation dose rate for the above mentioned radiation sources existing in the devices of the RW processing complex were carried out at different points near them. Ash as well as pressed ash has the greatest specific activity. For the radiation source in the form of cylinder (barrels of 170 and 200 l) dependences of the dose rate on the distance at points laying at semi-height of the cylinder filled with ash whose density is 0.65 g/cm^3, and pressed ash with density of 2.2 g/cm^3, calculated using VOLUME and MCNP packages, are presented in Fig. 4. The dose rate calculated using VOLUME package, exceeds the dose rate, calculated using MCNP package by 5÷10 %. Attention

should be paid to high values of the dose rate near surface of the objects under consideration. For safety improvement during transportation of the barrels filled with ash and any other kinds of the RW on special carts it was offered to install protective shields. The most effective in this case are shields made of lead. In comparison with a steel shield of the same weight (1-cm of Pb and 1.45-cm of Fe) the dose rate behind the shield made of Pb is lower by ≈1.3 times. Fig. 5 presents dependences of the dose rate on the distance in presence of a Pb-shield with thickness of 1 cm for ash, pressed ash as well as for solid RW and liquid RW. For the cases with complex geometry of radiation sources and shielding elements in PENELOPE package a geometrical model was designed and calculations of the dose rate for improvement of biological shielding characteristics were carried out in order not to exceed the norms of radiation safety.

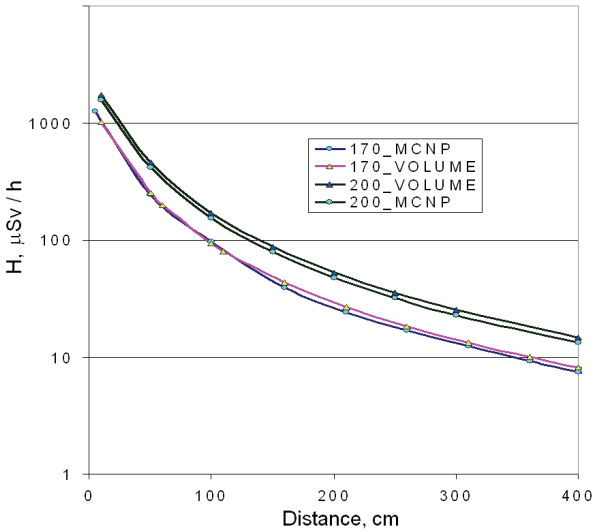


Fig. 4. Dependences of the dose rate on the distance for radiation sources in the form of cylinders (barrels of 170 and 200 l) filled with ash and the pressed ash.

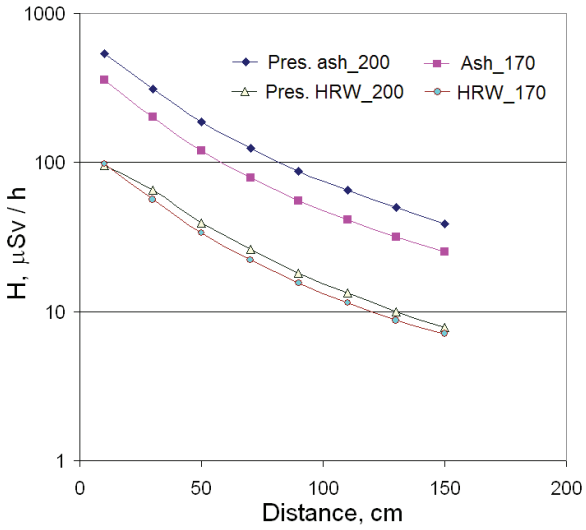


Fig. 5. Dependence of the dose rate from the barrel with ash on the distance in the presence of a 1-cm lead shield.

Fig. 6 illustrates geometrical models and arrangement of detectors (MCNP package) when calculating the dose rate chart from 3 caissons in which the barrels are filled with ash.

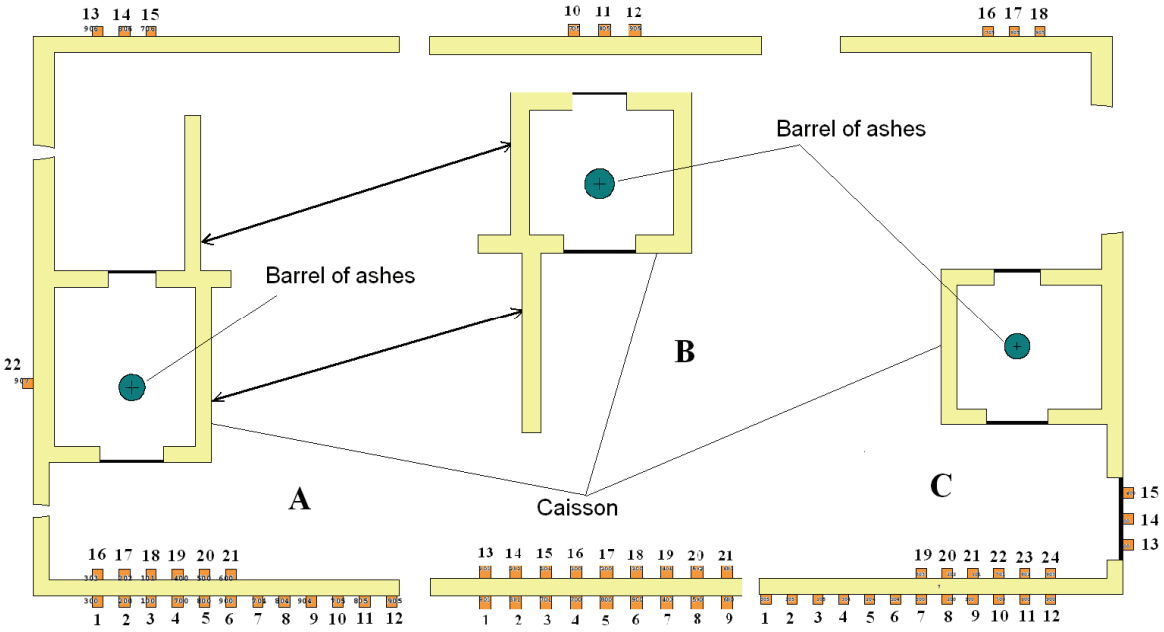


Fig. 6. Geometrical model for calculation of dose rate in the room where the ash channel caissons are placed.

The dose rate from each caisson was calculated, and then the dose loads were added together. As is evident from the data presented in Fig. 4,5 the dose rate, generated by the 1-st container with ash, and especially with the pressed ash, is great enough. This imposes some restrictions on quantity of containers with ash (pressed ash), that are temporarily housed in buffer warehouses with reasonable parameters of biological shielding observed.

Fig. 7 represents distribution of the dose rate from 7 barrels with ash (disposed in a buffer warehouse) behind a

concrete wall whose thickness is 40 cm. Figures on the insulated lines correspond to the dose rate in μZv/h, the sizes in the figures are given in cm. Increase in quantity of the barrels, their arrangement near a wall or decrease of the wall thickness would lead to excess of the admissible dose rate indoors behind the wall of the buffer warehouse.

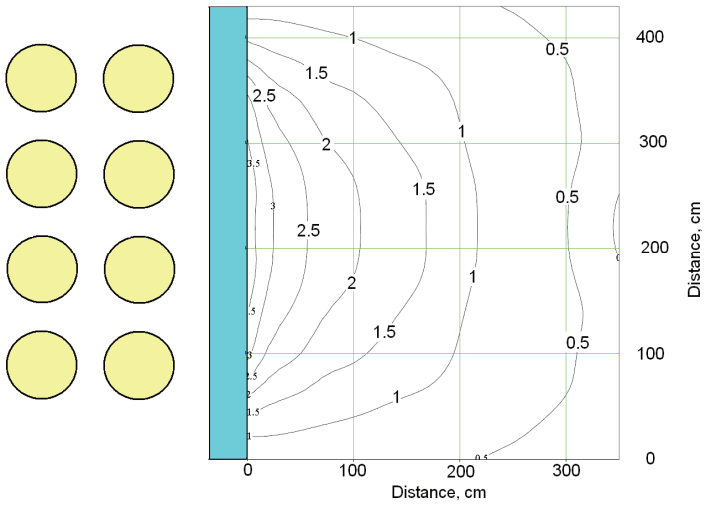


Fig. 7. Distribution of the dose rate from 8 barrels with ash indoors behind a concrete wall with thickness of 40 cm. Figures on insulated lines indicate the dose rate in μZv/h.

According to the norms of radiation safety, a biological shielding in the form of walls (made of concrete), and doors (as a rule made of steel) should bar from exceeding of the dose loads. At thickness of a concrete wall of 40 cm, equivalent thickness of a steel door ≈10÷12 cm as to radiation protection (depends on geometry of radiation sources arrangement).

Using **ALARA** principle**,** we offered to restrict the free access zone by mounting Rabitz fence. The Rabitz fence is mounted at a distance providing non-excess of the dose rate with essential reduction of the doors thickness in the premise containing radiation sources. It should be noted that reduction of the doors thickness would not lead to increase of the personnel body burden due to decrease of time necessary for opening and closing of the doors. Fig. 8 presents the layout of Rabitz fence at the entrance and exit of a premise which houses a pressing device and a buffer warehouse for barrels with ash (the zone of free access is shaded). Taking of such measures would provide the steel doors thickness of ≈1÷2 cm to be sufficient.

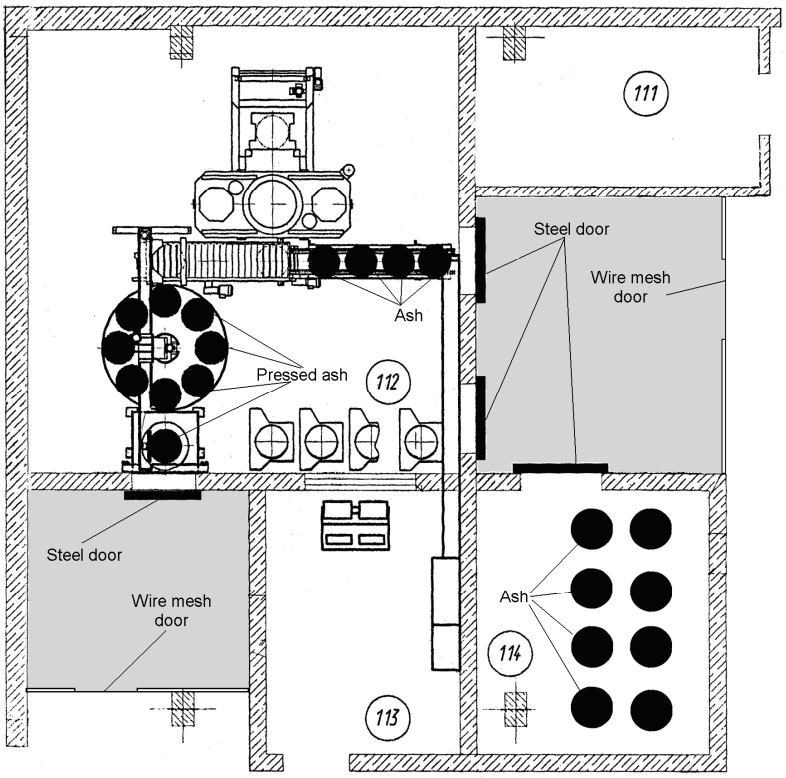


Fig. 8. Layout of Rabitz fence at the entrance and exit of a premise housing a pressing device and of the buffer warehouse for barrels with ash

CONCLUSION

The radiation environment in the premises of the RW processing complex both under normal operation of the units, and when any emergency occurred was analyzed. The design characteristics of the mentioned units specified by their manufacturers, as well as operative norms and rules in Ukraine on the RW treatment were taken as the initial data for the paper.

1. For radiation sources of complex geometry and isotopic composition **VOLUME_M** package, allowing to calculate protective properties and dose loads in real problems, was modified.
2. It was shown that when processing RW, treatment of such waste demands application of special accident control measures (protective shields) because of essential increase of the RW specific activity.
3. Some measures for improving safety of the personnel work in the premises where the radiation sources are disposed were offered. That allows essential improvement of the biological shielding design, in particular, reducing thickness of the doors between premises.

REFERENCES

1. Pismenetskiy S., Rudychev V., Rudychev Y., Tutunik O. Analysis of external radiation RW cylindrical volume // The Journal of Kharkiv National University, physical series "Nuclei, Particles, Fields. – 2008. –Vol. 808. - Issue. 2(38). - P.53-60.
2. Pismenetskiy S., Pyshkin V., Rudychev V., Rudychev Y. Spectral characteristics of VVER-1000 spent nuclear fuel which is intended for a dry storage keeping // The Journal of Kharkiv National University, physical series "Nuclei, Particles, Fields. – 2007. –Vol. 784. - Issue. 4(36). - P.109-114.
3. Lazurik V.T., Tabata T., Lazurik V.M. Database for Electron-Material Interactions // Rad. Phys. & Chem. – 2001. –Vol. 60. -P. 161-162.
4. Baro J., Sempau J., Salvat F., Fernandez-Varea J. PENELOPE: an algorithm for Monte Carlo simulation of the penetration and energy loss of electrons and positrons in matter // Nucl. Instr. & Meth. – 1995. - Vol. B100. - P.31-46.
5. JEF-2.2 Radioactive Decay Data, OECD Nuclear Energy Agency, JEF Report 13, 1994.
6. Nichols Assessment and evaluation of decay data for EAF – 1999/2000, UKNSF(99). - P.130.
7. MCNP^{TM} – A General Monte Carlo N-Particle Transport Code, Los Alamos National Laboratory Report LA-12625-M, Version 4B, Ed. by J. Briesmeister**. -** Los Alamos, New Mexico, 1997. – 736 p.

UDC 548.1:533.9

NUCLEAR GAMMA-RESONANCE OBSERVATION IN CONDITIONS OF COMBINED LINEAR AND TRANSVERSE DOPPLER SHIFTS AND FEATURES OF RELATIVISTIC THEORY

V.G. Kirichenko[1], O.V. Kovalenko[1], T.A. Kovalenko[1], Yu.I. Gofman[2]

[1]*Kharkov National KarazinUniversity, High Technology Institute*
31 Kurchatov St., Kharkov, 61108, Ukraine
E-mail: val_kir48@mail.ru
[2]*Jerusalem College of Technology, Department of Applied Physics*
P.O. B. 16031, Jerusalem 91160, Israel
E-mail: gofman@jct.ac.il
Received 21 June 2012, accepted 25 September 2012

We consider the problem of nuclear gamma-resonance observation and the effects of displacement energy gamma rays in conditions of combined linear and quadratic Doppler effect. The main result of this experiment was concluded in the possibility of realization of second order Doppler shift observation in the range of the combined shits with help of commutation electronic schemes for coherent transverse and linear shifts. This gives simplifications in experimental procedure. We reached the values of minimum measurable linear velocity of about 10^{-5}mm/s· pulse using the isotope Sn^{119}. It confirms the real possibilities of measurement method Doppler shift using the Mossbauer effect to determine the maximum acceleration and the prospects for development of such researchers.
KEY WORDS: Nuclear gamma resonance, linear and quadratic Doppler effect, the scheme of registration, the shift of the spectrum, extended theory of relativity, maximal acceleration

НАБЛЮДЕНИЕ ЯДЕРНОГО ГАММА-РЕЗОНАНСА В УСЛОВИЯХ КОМБИНИРОВАННОГО ЛИНЕЙНОГО И ПОПЕРЕЧНОГО ДОПЛЕРОВСКИХ СДВИГОВ И ОСОБЕННОСТИ ТЕОРИИ ОТНОСИТЕЛЬНОСТИ

В.Г. Кириченко[1], О.В. Коваленко[1], Т.А. Коваленко[1], Ю.И. Гофман

[1]*Харьковский национальный университет имени В.Н. Каразина, Институт высоких технологий*
61108, г. Харьков, пр. Курчатова, 31
[2]*Иерусалимский технологический институт - Махон Лев, Отделение прикладной физики*
п.я. 16031, Иерусалим 91160, Израиль

Рассмотрена проблема наблюдения ядерного гамма-резонанса и смещение энергии гамма-излучения в условиях комбинированного линейного и квадратичного эффекта Доплера. Основной результат этого эксперимента заключается в возможности реализации наблюдения доплеровского сдвига второго порядка с помощью электронных схем коммутации для когерентных поперечных и линейных сдвигов. Это упрощает проведение эксперимента. Мы достигли с помощью изотопа Sn^{119} минимально измеримого значения линейной скорости около 10^{-5} мм/с·имп. Это подтверждает реальные возможности метода измерения доплеровского сдвига с помощью эффекта Мессбауэра для определения максимального ускорения и перспективы для развития таких исследований.
КЛЮЧЕВЫЕ СЛОВА: ядерный гамма-резонанс, линейный и квадратичный эффект Доплера, схема регистрации, смещение спектра, расширенная теория относительности, максимальное ускорение

ОСОБЛИВОСТІ СПОСТЕРЕЖЕННЯ ЯДЕРНОГО ГАММА-РЕЗОНАНСУ ОБЕРТОВИХ ОБ'ЄКТІВ ТА РОЗШИРЕНА ТЕОРІЯ ВІДНОСНОСТІ

В.Г. Кіріченко[1], О.В. Коваленко[1], Т.О. Коваленко[1], Ю.Й. Гофман[2]

Харківський національний університет імені В.Н. Каразіна, Інститут високих технологій
61108, м. Харків, пр. Курчатова, 31
[2]*Єрусалимський технологічний інститут - Махон Лев, Відділення прикладної фізики*
п.с. 16031, Єрусалим 91160, Ізраїль

Розглянуто проблема спостереження ядерного гамма-резонансу і зсув енергії гамма-випромінювання в умовах комбінованого лінійного і квадратичного ефекту Доплера. Основний результат цього експерименту полягає в можливості реалізації спостереження доплерівського зсуву другого порядку за допомогою електронних схем комутації для когерентних поперечних і лінійних зрушень. Це спрощує проведення експерименту. Ми досягли за допомогою ізотопу Sn^{119} мінімально вимірного значення лінійної швидкості близько 10^{-5} мм/с·імп. Це підтверджує реальні можливості методу вимірювання доплерівського зсуву за допомогою ефекту Мессбауера для визначення максимального прискорення і перспективи для розвитку таких досліджень.
КЛЮЧОВІ СЛОВА: ядерний гамма-резонанс, лінійний і квадратичний ефект Доплера, схема реєстрації, зсув спектра, розширена теорія відносності, максимальне прискорення

Some fundamental problems of physics such, as gravitational red shift, Planck mass l_m and Planck length l_p, acceleration of particle to ultrahigh energies corresponded to wave length $\lambda \sim l_p$, expansion of the universe and many others solved and can be solved by using Doppler effect. As well known, Doppler effect is the dependence of wave frequency from velocity of observer or analyzer relative to its source. Doppler effect is widely used in astronomy to measure radial velocities of stars and galaxies, temperature measurement in plasma physics and astronomy, Doppler

© Kirichenko V.G., Kovalenko O.V., Kovalenko T.A., Gofman Yu.I., 2012

radars, medical imaging, flow measurements and many other applications [1, 2].

In recent years, scientific and technical interest to the problem of monitoring and implementation of the Doppler effect in the Mössbauer spectroscopy was renewed. This is due both to the possible use of the Mossbauer effect in the technique of detection of small shifts, angles, speeds and acceleration for implementation of the Mossbauer effect in solving the fundamental physics problems of space – time: the unit of length, the anisotropy of space, the stability of the temporal and spatial intervals, minimum and maximum velocities and accelerations.

For effective using of the unique resolution of the nuclear gamma-resonance known as Mossbauer effect [3] is necessary to create new methods of observation. Application of the nuclear gamma - resonance for the experimental verification theory of relativity and theory of gravity is based on minimum ratio $\Delta E/E$ ($\Delta E = \Gamma$ - line width and E - the energy of gamma - quanta) which values reaches $3.1 \cdot 10^{-13}$ and $5.2 \cdot 10^{-16}$ for the isotopes Fe^{57} and Zn^{67} respectively, and on the rare possibility of using for it's observation combined linear and quadratic Doppler effect. This made it possible to verify the presence of the gravitational red shift on Earth [3] with accuracy to within 1%, to test the central field of the Schwarzschild equation [4-8]. It is noted that in nuclear gamma - resonance experiments it is necessary to use more accurate measure of linear and quadratic Doppler effect. This method should include the improvement devices of measurement and control the speed and acceleration of moving objects in space, which have previously created gyroscopic device based on the Mossbauer Effect [9-11].

An important application of the Mössbauer effect in modern physics is an experimental verification of the extended theory of relativity (ETR). It obtained from the new approach to the analysis of relativistic effects which is based on the symmetry of space-time, the isotropy of the space and principle of relativity [12,13]. This approach explains existence of the limit speed of light from fundamental properties of space-time, in particular. ETR predicts the existence of a maximal acceleration [14]. This is fundamentally new relativistic phenomenon, which relates the special and general relativity, requires a careful verification. Evaluation of maximum acceleration $a = (1.006 \pm 0.063) \cdot 10^{19}$ m/s², was given in [14] from experimental date [7]. But it requires repetition and new types of experiments with the use of modern high-precision experimental techniques, of course. A maximum acceleration effect is more shows at high values of accelerations, thus**.** It expect or very high force or very small masses or both together. Analysis of the acceleration for different physical phenomena in cosmology, nuclear physics and other areas of modern physics show that the greatest acceleration observed in collisions of nuclear particles [15], in particular.

The aim of this study is to improve the accuracy of nuclear gamma-resonance observation and the effects of displacement energy gamma rays in conditions of combined linear and quadratic Doppler effect in physical systems related with moving and rotating objects.

EXPERIMENTAL RESEARCH METHOD

For alternative to [16, 17] the source of the Mossbauer isotope Sn^{119}gamma - rays was used the nuclei Sn^{119} in $CaSn^{119m}O_3$ matrix. The refined wavelength with energy 23.87 keV is $\lambda =$ [18]. The scheme of observation of combined linear and transverse Doppler shifts is given on Fig. 1.

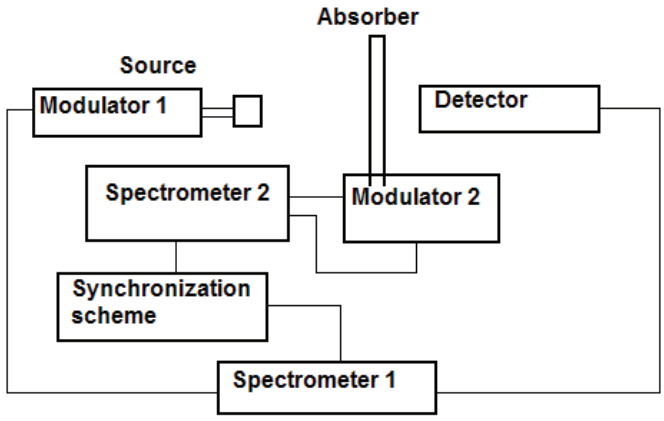


Fig. 1. The scheme of combined linear and transverse Doppler shifts observation

This scheme was realized the synchronous motion of the source Sn^{119}gamma – rays (linear Doppler shift) and absorber SnO_2 (transverse Doppler shift). It was very simple and gives the time interval of synchronization with accuracy 10^{-4} s.

Operation of the scheme is to the synchronization of the radial and transverse motion of the source and absorber in the same spatial plane. The ability to change the angle between the axes of the source and absorber is provided. This can be used to study the effects of anisotropy. The number of studies to measure the second order Doppler shifts using the Mossbauer isotope $Sn^{119}$is small. This is because the line width is much greater than that of the isotope Fe^{57}. On the other hand, the observation of the Mossbauer effect on Sn^{119} is less sensitive to vibrations. Previously it was shown that at the measurement of small linear and angular displacements of objects the cross Doppler effect with the Mössbauer technique obstacles arise first of all due to the vibrations, the pulses, disturbance of the strict orientation of objects in space, the inhomogeneous distribution of resonant nuclei on the surface of the object.

RESULTS AND DISCUSSION

Traditionally, the experimentally measured value of the isomer shift of the absorption line or scattering relative to the standard is the resultant of two shifts: the shift determined by the electron density distribution δ_{chim} and the shift

determined by the rms velocity fluctuations of the nuclei δ_{temp}:

$$\delta_{is} = \delta_{chim} + \delta_{temp}. \quad (1)$$

Determination of second order Doppler shifts was carried out by measuring δ_{temp}. According to the Einstein model of solids for δ_{temp} the following expression can be obtained:

$$\delta_{TEMП} = \frac{3}{4}\frac{\hbar\omega_E}{M_C} cth\left(\frac{\hbar\omega_E}{2kT}\right). \quad (2)$$

Values ω_E, in turn, can be determined from the temperature dependence of the effect probability

$$\frac{R}{\hbar\omega_E}\left[cth\left(\frac{\hbar\omega_E}{2kT_2}\right) - cth\left(\frac{\hbar\omega_E}{2kT_1}\right)\right] - \ln\frac{f_{T_1}}{f_{T_2}} = 0\,. \quad (3)$$

The calculation results suggest that the observed increase δ_{iz} with decreasing temperature fully explained by the second order Doppler effect. And besides this shift of the spectra in the direction of positive values of the Doppler radial velocity does not depend on the type of the Mössbauer isotope, because it does not include the nuclear characteristics, unlike to the shift defined by electron density.

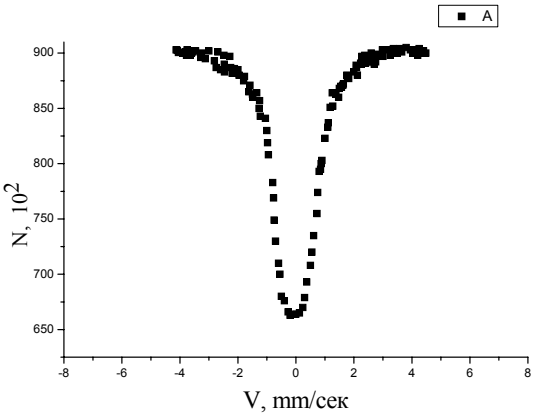


Fig. 2. Mossbauer spectrum of SnO_2

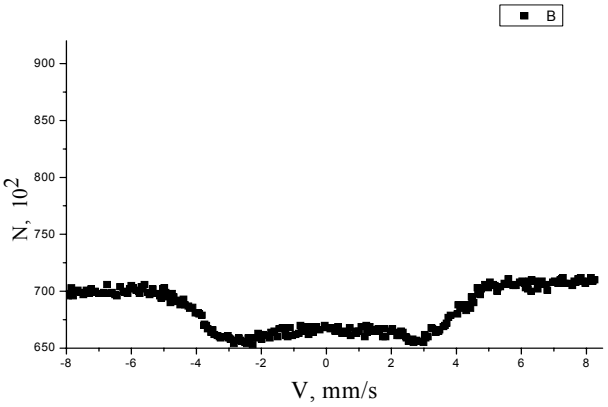


Fig. 3. Mossbauer spectrum of SnO_2 under influence transverse motion

We try to show that in our case, spectral shift toward positive values Doppler of radial velocity is observed under the transverse motion of the absorber. It is shown the spectrum of the initial absorber SnO_2 at absence of transverse motion (Fig. 2). The splitting of a single line of SnO_2 and the formation of an asymmetric doublet spectrum with very weak asymmetry (Fig. 3) is observed at synchronization with an accuracy of up to 10^{-4}s a linear shift required for the registration of the spectrum and the transverse motion.

In our case the source and absorber, characterized by single lines of emission and absorption were used. The dependence of the resonant transmission of gamma rays from linear radial Doppler velocity (spectra on Fig. 2, 3) under the parameter X = Aω for the determination of small displacements was obtained, where the A – amplitude ω – frequency of transverse motion.

The Doppler shift energy of gamma - rays for the laboratory coordinate system, i.e. the frequency υ of γ – rays, is given by:

$$\nu = \nu_0\left(1 + \frac{\vartheta}{c}\cos\alpha - \frac{1}{2}\frac{\vartheta^2}{c^2}\right). \quad (4)$$

Here ν_0 - frequency of γ - rays for fixed relative to each other the source and absorber, α - the angle between the recording γ - rays and the velocity vector of the relative motion of the source or sink, υ - the relative velocity of source on to the absorber. Usually in the expression (4) it is necessary to take the instantaneous values $\vec{V}(t)$.

It is necessary to search for ways to effectively eliminate its influence on the instrument readings. In addition to measuring the linear velocity and displacement by nuclear gamma - resonance it is possible to carry out measurement and control of transverse velocities and accelerations.

It were built dependences of the velocities of linear displacement of the number recruited in each point of the pulse and had a trend line (Fig. 5,6) for a more complete analysis of the asymmetry of the weak positive (velocity in Fig. 3) and the negative part of the spectrum.

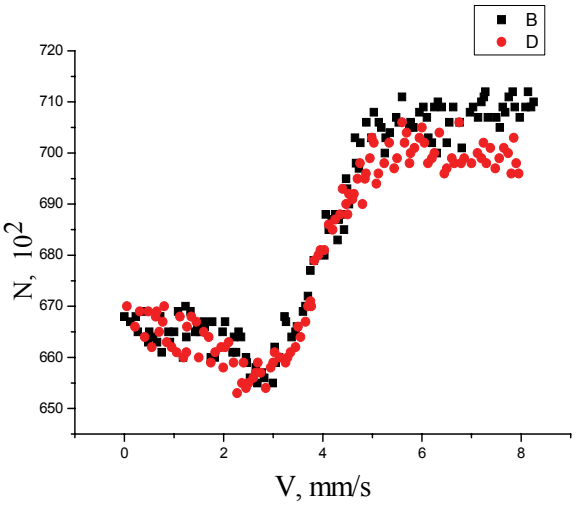


Fig. 4. Slow asymmetry of Mossbauer spectrum of SnO_2 under influence transverse motion

Linear dependences (Fig. 3,4) allow us to evaluate the achieved accuracy of spectrum shift in the transverse displacement, which is standard value of 0.01 mm/s under normal conditions reached maximal accuracy evaluation is 10^{-5} mm/s·pulse at measurement accuracy of the resonance transmission. Shift of the right side of the spectrum relative to the left side is $3 \cdot 10^{-5}$. This is due to the use of an isotope with a broad emission line, which eliminates the advantages of insensitivity to vibrations.

The main result of this experiment was concluded in the possibility of realization of second order Doppler shift observation in the range of the combined shits with help of commutation electronic schemes for coherent transverse and linear shifts. This gives simplifications in experimental procedure.

As example the values of the contributions from the second order Doppler shift for Fe^{57} nuclei are small and approximately equal to 0.00005 mm/s [16].

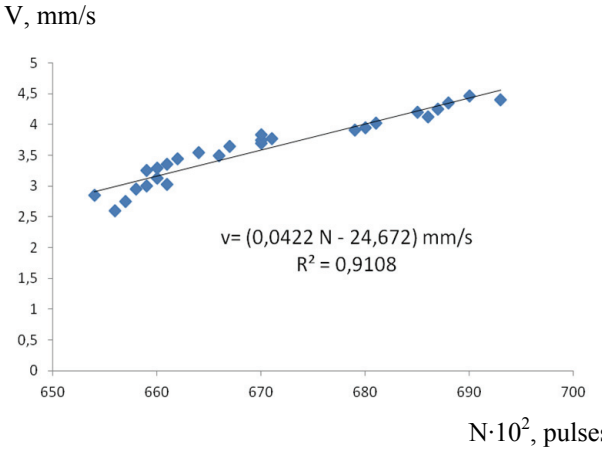


Fig. 5. Dependence of the linear Doppler velocity of the number of pulses on the most steep part of the resonance curve in the negative part of the spectrum (Fig. 3,4)

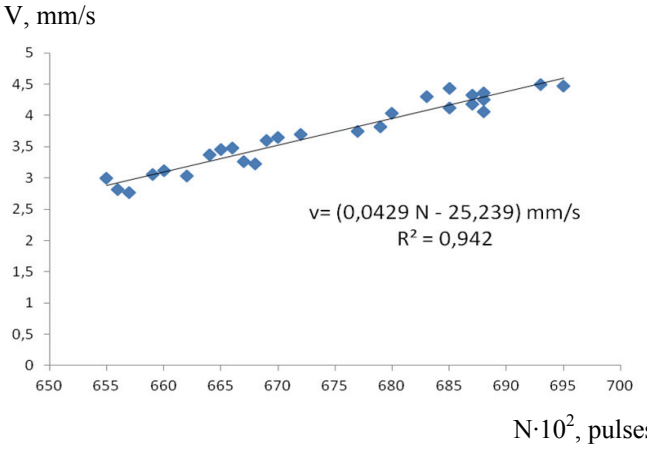


Fig. 6. Dependence of the linear Doppler velocity of the number of pulses on the most steep part of the resonance curve of the positive part of the spectrum (Fig. 3,4)

The maximum high accuracy of electromagnetic irradiation frequency measurement using Mossbauer effect allows to test of one of the consequences of general relativity -"transverse Doppler effect" [16]. As shown [12] in the ERT Doppler shift between inertial system K' and accelerated system $\tilde{K}$ moving together is determined by the coefficient (1 - a/A) due to the acceleration $\tilde{K}$ relatively K'. Evaluation of maximum acceleration a = (1.006 ± 0.063) 10^{19} m/s², using experimental data [5] was carried out. Such a significant acceleration it is possible to reach at modern experimental installations, at particular, at CERN's the muon storage ring [17].

CONCLUSIONS

The main result of this experiment was concluded in the possibility of realization of second order Doppler shift observation in the range of the combined shits with help of commutation electronic schemes for coherent transverse and linear shifts. This gives simplifications in experimental procedure. We reached the values of minimum measurable linear velocity of about 10^{-}mm/s· pulse using the isotope Sn^{119}. It confirms the real possibilities of measurement method Doppler shift using the Mössbauer effect to determine the maximum acceleration and the prospects for development of such researchers.

REFERENCES

1. Evans D.H., McDicken, W.N. Doppler Ultrasound (Second ed.). - New York: John Wiley and Sons, 2000.
2. Qingchong L. Doppler measurement and compensation in mobile satellite communications systems / Military Communications Conference Proceedings, MILCOM. – 1999. - Vol.1. – P. 316–320.
3. Mössbauer R.L. Kernresonanzfluoreszenz von Gammastrahlung in Ir^{191} // Zeitschrift für Physik. – 1958. – Vol.A 151 (2). – P.124–143.
4. Pound R.V., Rebka Jr.G.A. Gravitational Red-Shift in Nuclear Resonance // Physical Review Letters. - 1959. – Vol.3 (9). – P.439–441.

5. Pound R.V., Rebka Jr.G.A. Apparent weight of photons // Physical Review Letters. - 1960. Vol.4 (7). – P.337–341.
6. Pound R.V., Snider J.L. Effect of Gravity on Nuclear Resonance // Physical Review Letters. - 1964. – Vol.13 (18). – P.539-540.
7. Kündig W. Measurement of the Transverse Doppler effect in an Accelerated System // Phys.Rev. - 1963. - Vol.129, №6. - P.2371-2375.
8. Smorodinskiy Ya.A. Effekt Mössbauera i teoriya otnositel'nosti // UFN. - 1963. - T. LXXIX. - T.4. - S.590-598.
9. Kirichenko V.G., Chekin V.V. Sposob izmereniya uglovoy skorosti / A.S. SSSR, №782501. - 1980. - 6s. Zayavka №2683000. prioritet 4.11.78, zaregistrirov. 25.07.80.
10. Chekin V.V., Kirichenko V.G., Rogov V.S., Kharchenko A.V. Izmerenie malykh uglovykh smeshcheniy s pomoshch'yu effekta Messbauera / Dep. TsNII "Rumb" 25.02.80. "Parus-330". - 1980. - V.4.-12s.
11. Kirichenko V.G., Chekin V.V. Vliyanie poperechnogo dvizheniya na parametry messbauerovskoy linii // Zavodskaya laboratoriya. - 1980. - T.46, №7. - S.608-610.
12. Friedman Y., Gofman Yu. Why Does the Geometric Product Simplify the Equations of Physics // Int. J. Theoretical Physics. - 2002. - Vol.41, № 10. - P.1841-1855.
13. Friedman Y., Gofman Yu. Relativistic Linear Space-Time Transformations Based on Symmetry // Foundations of Physics. – 2002. - Vol. 32. - Iss. 11. - P.1717-1736.
14. Friedman Y., Gofman Yu. A new relativistic kinematics of accelerated systems // Phys. Scr. - 2010. – Vol.82. – P. 015004.
15. Gofman Yu. Maximal acceleration and the physical phenomena in extreme condition // Bull. Isr. Phys. Soc. – 2007. – Vol. 53. – P.175.
16. Kirichenko V.G., Kovalenko O.V., Leonov V.N., Kovalenko T.A., Gofman Yu.I. The nuclear gamma-resonance in research of gravitation and relativistic uniformly accelerated motion. Detecting of Mössbauer spectra of rotating objects // The Journal of Kharkov National University, Physical series "Nuclei, Particles, Fields". – 2011. - №955. – Vyp. 2/50/. - S. 15-23.
17. Gofman Yu.I., Kovalenko O.V., Kovalenko T.A., Leonov V.N. The features of nuclear gamma-resonance observation of rotating objects and extended relativistic theory // The Journal of Kharkov National University, Physical series "Nuclei, Particles, Fields". – 2011. – №979. - Vyp. 4/52/. - S.78-81.
18. Lucht M. The Wavelength of the 14.4 keV Mössbauer Radiation in ^{57}Fe : A Novel Length Standard For Atomic Scales. Dissertation zur Erlangung des Doktorgrades des Fachbereichs Physik der Universitat Hamburg, Hamburg, 2005. – 104s.



Kirichenko Valerij Grigir'evitch - Associate Professor of Department of Material Reactor Building and Physical Technology
Research interests: Solid State Physics, Hyperfine Interactions, Mössbauer Effect, Phase Transformations, Surface Science, Low Temperature Physics, Nuclear and Nano Materials.
Scientific Publications: Three books, three review papers and about 300 scientific and methodological publications.



Kovalenko Olga Vladimirovna - graduate student at Kharkov National University named V.N. Karazin.
Research interests: solid state physics, magnetooptics, hyperfine interactions. She is author of 39 publications.



Kovalenko Tat'yana Aleksandrovna - research associate at the Kharkov National University named V.N. Karazin.
Research interests: solid state physics, radiation material science. She is author of more than 20 publications.



Gofman Yuriy - Ph.D., lecturer, Department of Applied Physics, Jerusalem College of Technology, Jerusalem, Israel, laureate of honorary award for the development of science and hi-tech in Jerusalem "Jerusalem on Rise" (2009).
Field of interest: radiation damage and radiation technology of materials, modern physics.

UDC 53.092; 538.93; 542.61

FORMATION OF ASSOCIATES FROM NANOSIZED COMPLEXES OF URANIUM IN THE WATER - SUPERCRITICAL CARBON DIOXIDE SYSTEM

B.V. Borts[1)], S.F. Skoromnaya[1)], V.I. Tkachenko[1, 2)]
[1)] *National Science Center "Kharkov Institute of Physics and Technology"*
1, Akademicheskaya St., 61108, Kharkov, Ukraine
[2)] *V.N. Karazin Kharkov National University*
4, Svobody Sq., 61022, Kharkov, Ukraine
E-mail: tkachenko@kipt.kharkov.ua
Received 16 July 2012, accepted 5 September 2012

The paper describes the results from studies into the role of water in the formation of associates from nanosized complexes of uranium in a supercritical carbon dioxide (SC CO_2) medium. It has been demonstrated experimentally that water in the SC CO_2 exists in the form of microdrops. It is found that at a pressure of 10 MPa and a temperature of 40°C the $UO_2(NO_3)_2 \cdot 2(C_4H_9O)_3PO$ complex may take on hydrophilic properties. The conclusion is made that in that event the mentioned complex would concentrate in water microdrops. The concentration of the complex in water microdrops gives rise to the formation of associates, the size of which is determined by microdrop dimensions.
KEY WORDS: supercritical carbon dioxide, supercritical fluid extraction, uranium, water, tributyl phosphate.

ФОРМИРОВАНИЕ АССОЦИАТОВ ИЗ НАНОРАЗМЕРНЫХ КОМПЛЕКСОВ УРАНА В ДВУХФАЗНОЙ СИСТЕМЕ ВОДА - СВЕРХКРИТИЧЕСКИЙ ДИОКСИД УГЛЕРОДА

Б.В. Борц[1)], С.Ф. Скоромная[1)], В.И. Ткаченко[1, 2)]
[1)] *ННЦ "Харьковский физико-технический институт"*
г. Харьков, 61108, ул. Академическая, 1, Украина
[2)] *Харьковский национальный университет имени В.Н. Каразина*
г. Харьков, 61022, пл. Свободы, 4, Украина
Приведены результате исследования роли воды в образовании ассоциатов из наноразмерных комплексов урана в среде СК CO_2. Экспериментально показано, что вода в СК CO_2 существует в виде микрокапель. Отмечено, что при давлении 10 МПа и температуре 40 °С комплекс $UO_2(NO_3)_2 \cdot 2(C_4H_9O)_3PO$ может приобретать гидрофильные свойства. Сделан вывод о том, что вследствие приобретения этим комплексом гидрофильных свойств он будет концентрироваться в микрокаплях воды. Концентрирование комплекса в микрокаплях воды приводит к образованию в системе ассоциатов, размер которых определяется размером микрокапель.
КЛЮЧЕВЫЕ СЛОВА: сверхкритический углекислый газ, сверхкритическая флюидная экстракция, уран, вода, трибутилфосфат.

УТВОРЕННЯ АССОЦИАТІВ ІЗ НАНОРОЗМІРНИХ КОМПЛЕКСІВ УРАНУ В СИСТЕМІ ВОДА - НАДКРИТИЧНИЙ ДІОКСИД ВУГЛЕЦЮ

Б.В. Борц[1)], С.Ф. Скоромна[1)], В.І. Ткаченко[1, 2)]
[1)] *ННЦ "Харківський фізико-технічний інститут"*
м. Харків, 61108, вул. Академічна, 1, Україна
[2)] *Харківський національний університет імені В.Н. Каразіна*
м. Харків, 61022, м. Свободи, 4, Україна
Наведено результаті дослідження ролі води в утворенні асоціатів з наноразмірних комплексів урану в середовищі НК CO_2. Експериментально показано, що вода в НК CO_2 існує у вигляді мікрокрапель. Відзначено, що при тиску 10 МПа й температурі 40 °С комплекс $UO_2(NO_3)_2 \cdot 2(C_4H_9O)_3PO$ може придбавати гідрофільні властивості. Зроблено висновок про те, що внаслідок придбання цим комплексом гідрофільних властивостей він буде концентруватися в мікрокраплях води. Концентрування комплексу в мікрокраплях води приводить до утворення в системі асоціатів, розмір яких визначається розміром мікрокрапель.
КЛЮЧОВІ СЛОВА: надкритичний вуглекислий газ, надкритична флюїдна екстракція, уран, вода, трибутілфосфат.

Among vital issues in the development of nuclear-power engineering are the nuclear fuel production as well as the reprocessing of spent nuclear fuel (SNF) and uranium industry wastes. However, the advance in this respect is hindered by a number of factors such as the exhaust of raw-material resources base, environmental degradation of uranium industrial estates, and low economic indicators of traditional methods of uranium fuel production and reprocessing due to large quantities of liquid radioactive wastes. Therefore, the elaboration of new, ecologically safe technologies, which would be helpful in avoiding the mentioned problems or in solving them in a new way, is one of the most important tasks of nuclear-power engineering.

Currently, supercritical fluid technologies (SCFT) of extraction are finding increasing use in various spheres of industrial production, e.g., in pharmaceutics; in fat-and-oil, chemical industries; in coal conversion and petroleum refining. Along with the mentioned applications, the SCFT hold a particular position in SNF and uranium industry waste reprocessing, and also, in the processes of deactivation and selective extraction of actinides [1, 2]. At that, preference is given to supercritical carbon dioxide (SC CO_2) as an extractant, because it appears a most economical and ecofriendly solvent as compared to those employed in traditional chemical processes. The SC CO_2 is harmless and is noted for its low critical temperature and pressure values, this being of

© Borts B.V., Skoromnaya S.F., Tkachenko V.I., 2012

undeniable advantage. Besides, the technology under discussion makes it possible [3]:
- to reduce considerably the volume of secondary liquid radioactive wastes;
- to give up the use of inflammable, toxic or expensive solvents;
- to carry out pre-separation of extractable compounds at the extraction stage due to an essential change in the solving power of SC CO_2 at insignificant variations in the extractor temperature and pressure;
- to decrease corrosion load on the equipment elements;
- to use water-insoluble selective reagents;
- to reduce essentially the process flow scheme and operating areas of radiochemical facilities.

The presence of small water portions is known to improve the extraction efficiency. It has been demonstrated in [2] that the presence of water is the necessary condition for SC CO_2 extraction of metals. It has been established by experiments that in the absence of water the process of metal extraction is not observed at all. An increase in the quantity of water added up to a certain limit leads to an increase in the efficiency of SC CO_2 extraction of metals. A further increase in the quantity of water added exerts practically no effect on the extraction efficiency.

In [4], it has been shown by theory and experiment that, as in [2], with an increase in the quantity of water the extraction efficiency increases up to a certain peak level. However, after that, as the quantity of added water increases, the extraction efficiency drops. In the opinion of the authors of [4], this drop in the extraction efficiency is due to the following two reasons:
- the existence of water solubility limit in SC CO_2;
- competition between the uranium complex and pure water on their dissolving in a restricted volume of SC CO_2.

Though in recent years an array of experimental data has been obtained about the influence of water on the extraction efficiency of uranium complexes (e.g., see refs. [1-3]), some aspects of the problem still remain unclear. Among them, we should mention, first of all, a clear understanding of the structure of the resulting uranyl nitrate+tributyl phosphate (TBP) complex, the description of possible ways of associate formation [5] from nanosized complexes of uranium in the SC CO_2 medium in the presence of microquantities of water, and also, the determination of the form and size of the associates.

Despite the fact that the authors of refs. [6, 7] have analyzed the processes of micelle formation during supercritical fluid extraction of uranium, as well as the processes of spontaneous formation of associates in the SC CO_2 medium during uranium extraction from SNF, their substantiations are not based on a common ground, i.e., the phenomena of micelle formation and associate formation were analyzed as separate processes.

Therefore, the objectives of the present work are to analyze the parameters of a nanosized uranyl nitrate+TBP complex; to describe possible ways of associate formation from nanosized complexes of uranium in the SC CO_2 medium in the presence of microquantities of water; and to determine the form and size of the associates from a unified standpoint.

EXPERIMENTAL STUDIES ON PHASE STATES IN THE TWO-PHASE WATER-SC CO_2 SYSTEM

The determining influence of the presence of water on the extraction process has been indicated in [2, 4]. Previously, there were reports in the scientific literature about some peculiarities of water solubility in supercritical carbon dioxide (e.g., see [8, 9]). For all that we have made a series of experiments to investigate the phenomenon at the SFE-U facility [4] (modification of SCFE-1 [10]).

From the experimental data reported in [4] it follows that in the pressure range under study (7 to 17 MPa) at a temperature of 40°C the mole fraction of water dissolved in SC CO_2 is practically constant and makes about 0.0054.

So, at a given temperature the supercritical fluid can dissolve only a certain quantity of water, i.e., the supercritical fluid is characterized by the water solubility limit. The excess water remains on a filter paper, and thus cannot participate in the SFE-CO_2 process.

Laser diffractometry

Along with the evaluation of water solubility in SC CO_2, the phase state of water dissolved in SC CO_2 was also analyzed.

In-situ measurements have been carried out to investigate the phase state of water in SC CO_2 using the SFE-U facility, where at outlet from the reactor, 48.13 cm^3 in volume, there is an optical high-pressure cell (HPC) with sapphire windows. After the extraction has been made, the eluent was discharged into the HPC for investigating its state by optical methods such as laser light diffractometry and optical microscopy. The cell design is shown in Fig. 1.

The water-phase laser diffraction was investigated in accordance with the scheme presented in Fig. 2. The cell was placed in the holder with the outside surface of the HPC sapphire window perpendicular to the laser beam at a distance of no less than 0.5 m from the laser exit aperture. The screen was removed from the cell at the distance L=3.3 m. Along the perimeter of the screen there were two mutually perpendicular rules with 0.5 cm divisions, intended for evaluating the dimensions of diffraction pattern elements.

The spectral range of single-crystalline sapphire window transparency lies within 280 to 1200 nm. The sapphire windows are 10.0 mm in diameter and 6.0 mm in thickness. The windows in the cell are sealed in such a way as to exclude the sapphire-metal contact and to prevent their mechanical failure. Ceramic heaters and a chromel-alumel thermocouple are fastened to the side walls of the cell. The temperature of the cell is maintained with a control device in the range from room temperature to 50°C to an accuracy of ±1°C. The cell casing is made from stainless steel and is rated for pressures up to 20 MPa. The cell volume is 1.57 cm^3.

The optical path length of the cell could be varied from 0.1 mm up to 21.0 mm. This could be attained by introducing additional 3.0 mm thick glasses and positioning them at the sapphire window facing the laser beam source.

In the course of experimentation it was established that the water phase in SC CO_2 existed in the form of microdrops. Their dimensions were evaluated from diffraction patterns obtained when passing red laser beam through

the optical HPC. The occurrence of diffraction patterns at laser beam scattering by water microdrops in SC CO_2 is due to the fact that the refraction indices of water and SC CO_2 are different. As is known, the diffractional lattices are formed even in a transparent liquid or gas, where the refraction index is changed by travelling or standing ultrasonic waves [11].

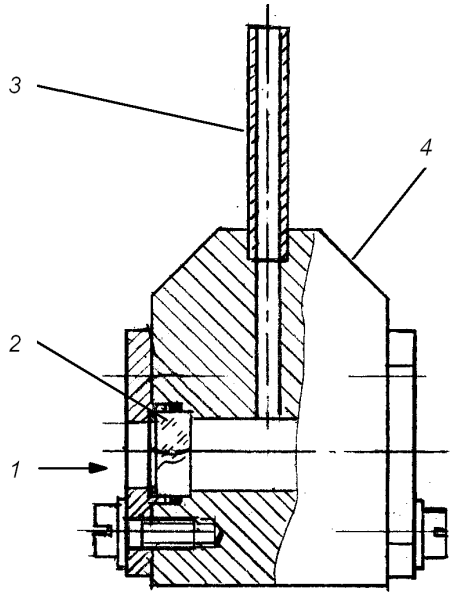


Fig. 1. Design of the optical high-pressure cell.
1- optical channel; 2 – sapphire window; 3 – inlet/outlet connection; 4 – casing

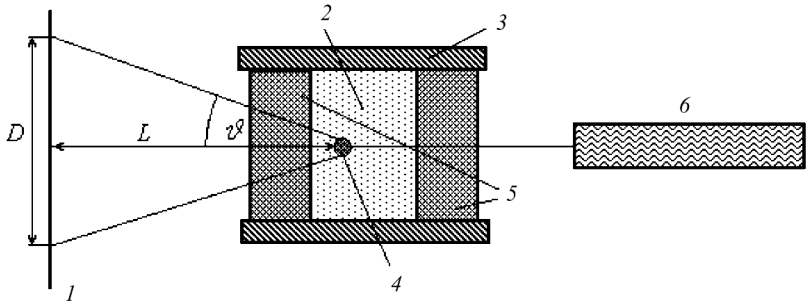


Fig. 2. Diagram of diffraction pattern formation at laser beam scattering by the water microdrops.
1 – screen; 2 – SC CO_2; 3 – HPC metal casing; 4 – water drop of diameter d; 5 - sapphire windows; 6 – laser beam source.

The HPC contents were investigated using the diffraction patterns induced by the scattered laser radiation. A red laser diode-based pointer of < 1 mW power that generates radiation in the wavelength range $\lambda = 655.7 \pm 2.5$ nm was used as a laser beam source.

Water-phase laser diffractometry experiments were performed in the following order.

A filter paper, soaked in 0.5 ml of distilled water, was placed in the SFE-U reactor. According to the quality certificate, the original water content in carbon dioxide at standard conditions (pressure 101.3 kPa, temperature 20°C) was less than 0.076 g/m^3. The estimates show that at pressures up to 16.0 MPa the proper water content in CO_2 was considerably less than the quantity of water taken up on the filter paper. On attaining the required reactor pressure and after the 5 min dwell time, a part of the fluid was forwarded through the inlet/outlet connection (see Fig. 1) to the optical HPC. The cell fluid with the water solved in it was examined with the red laser. The laser radiation that passed through the cell was directed onto the screen (see Fig. 2). The time-varying diffraction pattern, obtained at a definite pressure, was being shot with a video camera for 5 min. The obtained video was split into separate shots, which represented static diffraction patterns comprising the information on water drop sizes in SC CO_2.

Figure 3 shows one of the images of the static diffraction pattern for the 6.0 mm optical path to the HPC (to reduce the optical path length, 5 glasses were used) at CO_2 pressure of 10.0 MPa and a temperature of 40°C.

Based on a series of the resulting static diffraction patterns, it can be assumed that certain microquantities of water in SC CO_2 form water droplets, which present spherical particles of diameter *d* (water drops) distributed in a supercritical fluid. In the pressure range from 8.0 MPa to 16.0 MPa at a temperature of 40°C, in accordance with the phase diagram of CO_2 [12], the weight of water microdrops is greater than the weight of the fluid forced out by the microdrops. For this reason, the microdrops like small shots in oil slowly settle down under the action of gravity, and simultaneously move in convective streams (these being due to the temperature gradient) with changing their position in space. Since the medium is optically transparent, all particles being on the optical path in the cell can be considered as the ones being in the same virtual plane *P*. In this case, the analysis of the above-given diffraction pattern is similar to the analysis of diffraction patterns from a two-dimensional grating.

We now describe the experimentally observed evolution of diffraction patterns at laser radiation scattering by water microdrops in the SC CO_2.

With a red laser, the diffraction pattern image on the screen generally represents slowly moving light spots. At certain instants of time the microparticles in the SC CO_2 may be distributed randomly in the virtual plane *P* and give diffraction patterns, from which one can evaluate the average size of water microdrops in the SC CO_2.

Let us estimate the water drop size for the diffraction pattern shown in Fig. 3. Here, the laser beam of oval shape (major diameter 3 mm, minor diameter 2 mm), escaping from the source 6 (Fig. 2) is scattered by the water drops

located in the virtual plane *P*. From experimental observations it follows that the laser spot area is great in comparison with the water drop size. Therefore, the influence of the laser radiation spot limitation on the diffraction pattern is neglected.

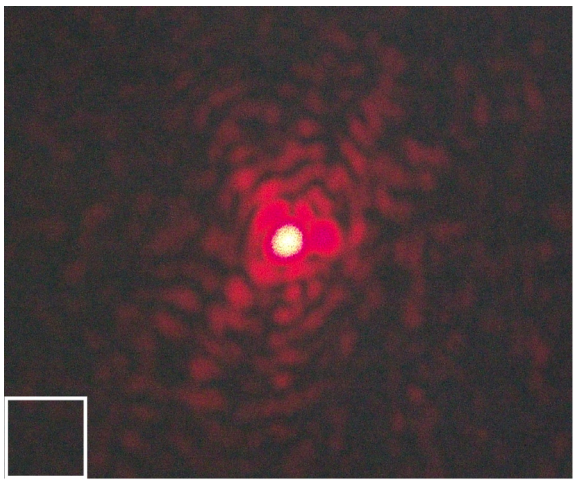


Fig. 3. Image of the static diffraction pattern at a pressure of 10.0 MPa and the 6.0 mm optical path in the HPC.
A white square contour in the left bottom corner with a lateral length of 10.0 mm is given for evaluating the diffraction pattern element dimensions.

The superposition of different quantities of water microdrops, which are projected onto the plane *P* on the principle of belonging to one and the same laser beam, will create an inhomogeneously illuminated surface, i.e., at the greatest quantities of water drops give the highest intensity of illumination, and at the least quantities - the lowest illumination. In the ideal case, the regions of maximum illuminance correspond to concentric superposition of water drops, while the lowest-illumination regions correspond to the absence of this superposition. So, laser radiation should scatter on the plane with randomly arranged circles of diameter *d*, where *d* is the diameter of spherical water drop projection onto the plane *P*. In this case, the diffraction pattern must look like a bright circle at the center, surrounded by a sequence of dark and light rings [13]. The bright circle at the center has an angular radius $\vartheta \simeq \frac{D}{2L} = 1,22\frac{\lambda}{d}$. Hence, one would think that this provides a simple evaluation of the water drop size as $d = 2,44\frac{\lambda L}{D}$. In actual fact, at the periphery of Fig. 3 one can see rows of spots that form a certain quantity of radial rays, about 12 to 14 in number. This fact is the evidence that diffraction occurs not on randomly arranged circles, but on their pileup forming a rectilinear polygon with *n* sides. At that, it is known that the number of rays is always even, i.e., 2*n* [14]. Reasoning from this, we determine the average *d* value. For the purpose, we assume that, at least, two inscribed circular projections of water drops fall on one side of the polygon (a greater number of them smoothes-off the angles and makes the rays disappear). Then, by setting the perimeter of the bright circle in the diffraction pattern (Fig. 3) equal to the polygon perimeter with inscribed 2*n* circles of diameter *d* we find the average drop size:

$$d \simeq 2,44\pi\frac{\lambda L}{2nD} \qquad (1)$$

Substituting the experimental data into expression (1), we evaluate the average size as $d = 45 \div 50$ μm.

Optical micrometry evaluation of water microdrop dimensions

To verify the results obtained by the laser methods, we have also examined the eluent discharged into the HPC, using a 32-power optical microscope. In this case, instead of the microscope slide we placed the HPC in such a way that the sapphire window area should be orthogonal to the microscope-head optical axis. For the analysis of water phase state, an oblique flare with a wide light beam was used provided that the light source should not get into the field of viewing, and the eluent was against a dark background.

As a result of direct optical observations it has been established that the water dissolved in the SC CO_2 at a pressure of 10 MPa and a temperature of 40°C exists in the form of microdrops. According to optical microscope measurements the diameter of these microdrops was estimated to be 55±3 μm.

So, the experimental investigation into the existence of phases in the two-phase water-SC CO_2 system has demonstrated that the water is characterized by the limit of solubility in the SC CO_2, i.e., the molar fraction of dissolved water is constant with an increase in pressure.

The water in the SC CO_2 exists in the form of microdrops, the diameter of which, for example, at a pressure of 10 MPa and a temperature of 40°C is found to be about 50 μm. It is evident that the droplet diameter decreases with an increase in pressure.

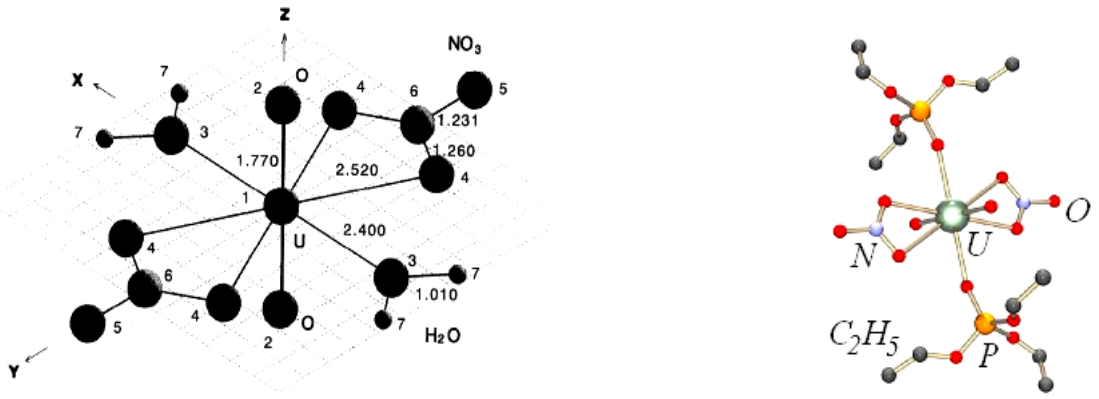
ANALYSIS OF THE PARAMETERS OF NANOSIZED URANIUM COMPLEXES AND THEIR SOLUBILITY IN WATER. FORMATION OF ASSOCIATES

For an understanding of the kinetics of uranium extraction to the SC CO_2 medium it is necessary to decide the following issues: to determine the structure of the resulting uranyl nitrate+TBP (uranyl nitrate+$(C_4H_9O)_3PO$) complex, and to describe possible ways of associate formation from that sort of complexes.

In spite of the existence of a sufficient number of publications on the matter (e.g., see [15, 16]), the problems still

remain to be solved.

Thus, it has been shown in [15, 16] that the HNO_3+TBP complex efficiently extracts uranium to the SC CO_2 medium. The complex reacts with uranium oxide to form the $UO_2(NO_3)_2 \cdot 2TBP$ compound, which is extracted to the SC CO_2. Figure 4 and Table give the structure and the values of coupling parameters of the complexes formed by uranyl nitrate with water and triethyl phosphate (TEP), respectively [17].



a) b)

Fig. 4. Schematic diagrams of complex structures
a) $UO_2(NO_3)_2 \cdot 2H_2O$, b) $UO_2(NO_3)_2 \cdot 2TEP$ [17, 18]

As it follows from Fig. 4, two water molecules from dehydrate of uranyl nitrate (on the left) are replaced by two TEP ($C_6H_{15}O_4P$) molecules (on the right). In the $UO_2(NO_3)_2 \cdot 2TEP$ complex the two TEP molecules freely rotate and can take up any conformation, while the interatomic spacing between U and O atoms (just as for the P=O coupling) is harmonically fixed to the equilibrium distance.

Table

Geometrical characteristics of the $UO_2(NO_3)_2 \cdot 2TBP$ complex, [15-20].

Complex	$r_{U=O}$ (Å)	r_{U-O2NO} (Å)	r_{U-L} (Å)	Θ_{U-O-P} (deg)
$UO_2(NO_3)_2 \cdot 2H_2O$	1.77	2.52	2.40	–
$UO_2(NO_3)_2 \cdot 2TMP$	1.78	2.53	2.36	161±7
$UO_2(NO_3)_2 \cdot 2TBP$	1.78	2.54	2.41	172±10

It is known that TBP shows a relatively low solubility in the aqueous phase [21]. It represents a compound ether of phosphoric acid and butanol, which can hydrolyze, for example, in acidic medium. In acidic aqueous solutions there occurs breaking of carbon-to-oxygen bonds of TBP with gradual abstraction of butanol molecules and formation of dibutyl phosphate (DBP), monobutyl phosphate (MBP) and, eventually, phosphoric acid. It should be noted that MBP forms with uranium the compound, which shows a strong aqueous phase affinity. The ratio of the formed DBP and MBP is approximately 10:1. The hydrolysis reactions occur in both aqueous and organic phases. The rate of TBP hydrolysis appreciably increases with increase in temperature. For example, as temperature rises from 25 to 40°C, the rate of DBP formation increases by a factor of 5, and with a rise up to 75°C – by a factor of 25.

So, based on the structure of the resulting complex and the temperature conditions of the experiment (40°C), it is believed that the $UO_2(NO_3)_2 \cdot 2TBP$ complex can hydrolyze, i.e., may take on diphilic (one TBP molecule of the complex forms the MBP molecule) or fully hydrophilic properties (two TBP molecules of the complex are transformed into the MBP molecule). In this case, because the complex takes on hydrophilic properties in the SC CO_2 medium comprising water microdrops dissolved in it, the complex will concentrate in the aqueous phase to form supramolecular assemblies [5]. The last ones represent polymolecular associates resulting from spontaneous association of uranium complexes into a specific phase, in our situation, the water microdrop (inverted water micelle [1]).

This concentration apparently leads to the formation of associates in the system, the size of which is determined by the size of water microdrops, and the way of assembling of nanosized complexes still remains to be elucidated. It is evident that the water microdrop represents a microreactor, where the extraction processes occur. A detailed investigation of the structure and properties of these microreactors is of importance for understanding the nature of current processes, and this in total should contribute towards the improved extraction of uranium complexes efficiency into the SC CO_2 medium.

CONCLUSIONS

In summary, as a result of studies of the role of water in the formation of associates from nanosized complexes of uranium in a supercritical carbon dioxide (SC CO_2) medium, it has been established that at given temperature the water exists in the form of microdrops, the diameter of which makes, for example, at a pressure of 10 MPa and a temperature of 40°C, about 50 μm.

It has been noted that at a pressure of 10 MPa and a temperature of 40°C the nanosized $UO_2(NO_3)_2 \cdot 2TBP$ complex can take on hydrophilic properties.

As a result of taking on hydrophilic properties, the $UO_2(NO_3)_2 \cdot 2TBP$ complex will concentrate in water microdrops.

The concentration of the complex in water microdrops leads to the formation of associates in the system, the associate size being determined by the size of water microdrops.

REFERENCES

1. Shadrin A.Yu., Murzin A.A., Babain V.A. Osobennosti ehkstraktsii kationov metallov rastvorami kompleksonov v sverkhkriticheskom i zhidkom diokside ugleroda // Sverkhkriticheskie Flyuidy: teoriya i praktika. – 2007. - Vol. 2, № 3. - P. 57-66.
2. Shadrin A.Yu. Ehkstraktsiya aktinoidov rastvorami kompleksonov v sverkhkriticheskom i zhidkom diokside ugleroda / Trudy Radievogo Instituta im. V.G. Khlopina. – 2007. - Vol. XII. - P.20-43.
3. Revenko U.A., Kudinov K.G., Podoynitsin S.V., Starchenko V.A., Shadrin A.Yu. Pererabotka OYaT s ispol'zovaniem ehkstraktsii sub- i sverkhkriticheskimi gazami // Tret'ya Rossyiskaya konferentsiya po radiokhimii. Radiokhimiya-2000: GUP NPO "Radievyi institut im. V.G. Khlopina", SPb. Tezisy dokladov. St-Petersburg, 28 November - 1 December, 2000. - 278p.
4. Borts B.V., Kazarinov U.G., Sirenko S.A., Skoromnaya S.F., Tkachenko V.I. Vliyanie vody na effektivnost' sverkhkriticheskoi CO_2 ehkstraktsii urana iz prirodnykh mineralov // The Journal of Kharkiv National University, physical series "Nuclei, Particles, Fields". - 2012, № 1001. - Iss. 2(54). - P.125 – 134.
5. Stid Dj.V., Atvud Dj.L. Supramolekulyarnaya himiya. - M.: Akademkniga, 2007. - 898p.
6. Borts B.V., Kazarinov Y.G., Shakhova P.V., Skoromnaya S.F., Tkachenko V.I. Micelle Formation Phenomena in the Process of Uranium Supercritical Fluid Extraction // Proc. of XIX International Conference on Physics of Radiation Phenomena and Radiation Materials Science (06-11 September, 2010, Alushta, Crimea, Ukraine). - P.164-165.
7. Borts B.V., Kazarinov Y.G., Shakhova P.V., Skoromnaya S.F., Tkachenko V.I. Self-assembling associate formation in supercritical carbon dioxide medium under conditions of uranium extraction process // Proc. of XIX International Conference on Physics of Radiation Phenomena and Radiation Materials Science (06-11 September, 2010, Alushta, Crimea, Ukraine). - P. 166-167.
8. Sabirzyanov A.N., Il'in A.P., Akhunov A.R., Gumerov F.M. Solubility of Water in Supercritical Carbon Dioxide // High Temperature. – 2002. – Vol.40, № 2. - P. 203-206.
9. King M.B., Mubarak A., Kim J.D., Bott T. R. The Mutual Solubilities of Water with Supercritical and Liquid Carbon Dioxide // Journal of Supercritical Fluids. – 1992. - № 5. - P. 296-302.
10. Aleksandrov A.N., Tkachenko V.I., Ulesov A.V., Korenskaya I.M., Moskvitin A.V., Skoromnaya S.F., Zaginailov V.G. Issledovanie sverkhkriticheskoi ehkstraktsii i fraktsionirovaniya lipifilnykh izvlecheniy iz prirodnogo aromaticheskogo syr'ya // Ehkotekhnologii i resursosberezhenie. – 2008. - № 2. - P. 38-43.
11. Gorelik G.S. Kolebaniya i volny. - M.: Izdatel'stvo fiziko-matematicheskoi literatury, 1959. - 572 p.
12. Pichugin A.A., Tarasov V.V. Supercritical extraction and prospects for the creation of new waste-free products //Russian Chemical Reviews. – 1991. – Vol.60 (11). - P. 1249 – 1254.
13. Landsberg G.S. Optika. /Uchebnoe posobie dlya VUZov. 6-e izd., stereot. – M.: Fizmatlit, 2003. - 848 p.
14. Zommerfeld A. Optika. – M.:Izdatel'stvo inostrannoi literatury, 1953. - 486 p.
15. Sawada K., Uruga K., Koyama T., Shimada T., Mori Y., Enokida Y., Yamamoto I. Stoichiometric relation for extraction of uranium from UO_2 powder using TBP complex with HNO_3 and H_2O in supercritical CO_2 //Journal of Nuclear Science and Technology. – 2005. - Vol. 42, №. 3. - P. 301-304.
16. Sawada K., Enokida Y., Kamiya M., Koyama T., Aoki K. Distribution Coefficients of U(VI), Nitric Acid and FP Elements in Extractions from Concentrated Aqueous Solutions of Nitrates by 30% Tri-n-butylphosphate Solution //Journal of Nuclear Science and Technology. – 2009. – Vol. 46. – Issue 1. – p.83-89.
17. Jayasinghe M. A dissertation submitted to the Division of Graduated Studies and Research of the University of Cincinnati; in partial fulfillment of the requirement for the degree of Ph.D. in the dep. of physics of the College of Art and Sciences. - 2007.- P. 85-95. Electronic Resources.
18. Hirata M., Monjyushirob H., Sekinec R., Onoed J., Nakamatsue H., Mukoyamae T., Adachif H., Takeuchid K. Valence electronic structure of uranyl nitrate $UO_2(NO_3)_2 \cdot 2H_2O$ //Journal of Electron Spectr. and Rel. Phenomena. – 1997. - Vol 83, issue 1. - P. 59-64.
19. Oda Y., Koyama T., Funasaka H. Structural study of uranyl (VI) nitrate complexes: $[UO_2(NO_3)_2(H2O)_2]$ and $[UO_2(NO_3)_2TMP_2]$ by ab initio molecular orbital calculation. Int. Conf. Scientific research. 24-26 October, 2000, Atalante, P.2.04.
20. Auwer C.D., Charbonnel M.C., Presson M.T., Madic C., Guillaumont R. Xas study of actinide solvent extraction compounds. ii: $UO_2(NO_3)_2(L)_2$ (with L=tri-isobutylphosphate, tri-n-butylphosphate, trimethylphosphate and triphenylphosphate). //Polyhedron. – 1998. - Vol 17, № 25. - P. 4507-4517.
21. Gromov B.V. et al. Khimicheskaya tekhnologiya obluchennogo yadernogo topliva: Uchebnik dlya VUZov. B.V. Gromov, V.I. Savelev, V.B. Shevchenko. — M.: Ehnergoatomizdat, 1983. - 352 p.



Tkachenko Victor Ivanovich - D.Sc. in physics and mathematics. Currently working as a Director of Science & Production Establishment "Renewable Energy Sources & Sustainable Technologies" National Science Center "Kharkov Institute of Physics & Technology" and a Head of the Department of Physics of Innovative Energy & Technology & Ecology of V.N. Karazin Kharkov National University. His research interests are in the plasma physics, plasma electronics, solid state physics, hydromechanics and nonlinear physics, alternative energy, supercritical fluid extraction. He is the author and the co-author more than 200 scientific publications, 8 patents.



Borts Boris Victorovich - Ph.D. of technical science, head of laboratory of new technology of National Science Center “Kharkov Institute of Physics and Technology”. The area of his scientific interests: welding of heterogeneous materials in solid phase, production of composite materials, hydrogen power, physico-chemical processes during the direct production of electric power. He is an author and co-author of more than 84 scientific papers, 16 inventions and patents.



Skoromnaya Stella Fedorovna graduated from physics and technology department of V.N. Karazin Kharkov National University in 2009. She is a third year graduate student. Her research interests are in the alternative energy, supercritical fluid extraction, nonlinear physics. She is the author and the co-author of 24 scientific publications and 2 patents.

UDC 530.1(075.8)

ONCE AGAIN ABOUT ADVANTAGES OF THE NEW METHOD OF ELECTROMAGNETIC ISOTOPES SEPARATION

Yu.A. Kirochkin[1], A.Yu. Kirochkin[2]
[1]*Kharkov National University named V.N. Karazin*
61022, Kharkov, Svobody Sq., 4
[2]*National Civil Defence University of Ukraine*
61023, Kharkov, Chernyshevskogo street, 94
E-mail: kira_the_pooh@mail.ru
Received 3 June 2012, accepted 5 September 2012

The advantage of the new method of electromagnetic isotopes separation in the crossed electric and magnetic fields in comparison with an ordinary method with the presence of only magnetic field is shown in the paper. It is also shown that the theory of ordinary method of isotopes separation in the magnetic field of linear current, written in article of Bardakov V.M. etc. in ZTF, 2010, Vol. 80, No. 10, pp. 115-119, is built wrong.
KEY WORDS: electromagnetic field, isotope, separation, current, trajectory

ЕЩЕ РАЗ О ПРЕИМУЩЕСТВАХ НОВОГО МЕТОДА ЭЛЕКТРОМАГНИТНОГО РАЗДЕЛЕНИЯ ИЗОТОПОВ

Ю.А. Кирочкин[1], А.Ю. Кирочкин[2]
[1]*Харьковский национальный университет им. В.Н. Каразина*
61022, Харьков, пл. Свободы, 4
[2]*Национальный университет гражданской защиты Украины*
61023, Харьков, ул. Чернышевского, 94
В работе показано преимущество нового метода электромагнитного разделения изотопов в скрещенных электрическом и магнитном полях по сравнению с обычным методом при наличии только магнитного поля. Также показано, что теория обычного метода разделения изотопов в магнитном поле линейного тока, изложенная в работе Бардакова В.М. и др. в ЖТФ, 2010, Т. 80, Вып. 10, С. 115-119, построена неверно.
КЛЮЧЕВЫЕ СЛОВА: электромагнитное поле, изотоп, разделение, ток, траектория

ЩЕ РАЗ ПРО ПЕРЕВАГИ НОВОГО МЕТОДА ЕЛЕКТРОМАГНІТНОГО РОЗДІЛЕННЯ ІЗОТОПІВ

Ю.О. Кірочкін[1], О.Ю. Кірочкін[2]
[1]*Харківський національний університет ім. В.Н. Каразіна*
61022, Харків, пл. Свободи, 4
[2]*Національний університет цивільного захисту України*
61023, Харків, вул. Чернишевського, 94
В роботі показана перевага нового метода електромагнітного розділення ізотопів у схрещених електричному та магнітному полях у порівнянні зі звичайним методом при наявності тільки магнітного поля. Також показано, що теорія звичайного метода розділення ізотопів у магнітному полі лінійного струму, викладена у роботі Бардакова В.М. та ін. у ЖТФ, 2010, Т. 80, Вип. 10, С. 115-119, побудована невірно.
КЛЮЧОВІ СЛОВА: електромагнітне поле, ізотоп, розділення, струм, траєкторія

Two works [1, 2] devoted to the theoretical research of a new method of electromagnetic separation of isotopes moving in constant electromagnetic field of a cylindrical capacitor and a linear current flowing along its axis (nonzero fields strengths H_α and E_r are inversely proportional to the distance r from the capacitor axis z; r, α and z are the cylindrical coordinate system) offered by the group of the Kharkov scientists (also including authors [1, 2]) that were published in 2007 year. In papers [1, 2] expressions for isotopes trajectories in the form of rather simple single integrals, which numeral integration enabled to present trajectories graphically and ipso facto to determine the experimental setup basic parameters, are obtained.

RESULTS AND DISCUSSION

On the face of it there can be a question: but isn't it simpler to separate isotopes in the same setup under only the magnetic field H_α (i.e. by $E_r = 0$)? In works [1, 2] this special case was not examined in detail. Authors considered that this, maybe, old method (further denoted M_O) is considerably worse than the new one (further denoted M_N). This assertion is easily proved by a limiting process $E_r \to 0$ (or $\eta = \dfrac{cE_r}{H_\alpha v_0} \to 0$) in isotopes path equations obtained within the bounds of M_N. Supposing $\eta = 0$ in the formulas (19-22) of [1], one obtain the isotope path equation in $\zeta\xi$ plane ($\zeta = \dfrac{z}{a}$, $\xi = \dfrac{r}{a}$, a is a distance of isotopes source from an axis)

© Kirochkin Yu.A., Kirochkin A.Yu., 2012

$$\zeta(\xi) = -\kappa(1+\delta_z)\mathrm{e}^{\kappa(1+\delta_z)} \int\limits_{-\frac{\pi}{2}}^{\arcsin\left[\frac{\ln\xi}{\kappa(1+\delta_z)}-1\right]} d\theta \sin\theta\, \mathrm{e}^{\kappa(1+\delta_z)\sin\theta},\ 1 \le \xi \le \mathrm{e}^{2\kappa(1+\delta_z)}, \quad (1)$$

where $\kappa = \dfrac{mc^2 v_0}{2qJ}$, J is a linear current strength, m and q are isotope mass and charge, $\vec{v}_0 = \vec{e}_z v_0(1+\delta_z)$ is initial velocity of an isotope emitted from the source, $\delta_z = \dfrac{\delta v_z}{v_0}$, δv_z is the fluctuation of the initial velocity, and $|\delta_z| << 1$, $\xi_0 = 1$, and $\zeta_0 = 0$ are isotopes source coordinates, $\xi_2 = \mathrm{e}^{2\kappa(1+\delta_z)}$ is an isotope turning point transverse coordinate at its motion in the line of r growth, $\xi_z = \mathrm{e}^{\kappa(1+\delta_z)}$ is an isotope turning point transverse coordinate at its motion in the line of z growth (see [1] (13), (18)).

Using (1), one graphs trajectories of lithium isotopes and heavy in comparison with them uranium isotopes at the same parameters with M_N and assume $a = 3$ cm.

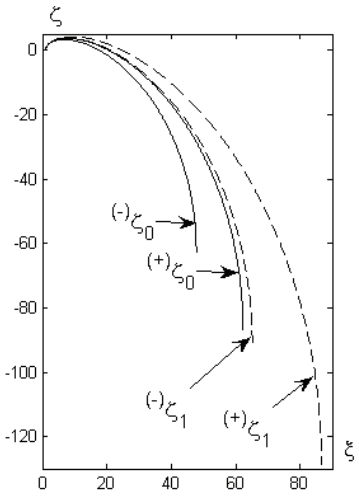


Fig. 1. Lithium isotopes trajectories

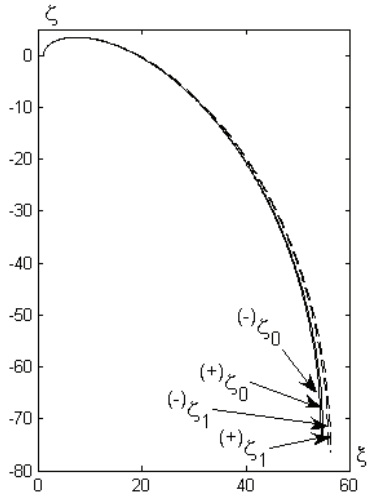


Fig. 2. Uranium isotopes trajectories

Graphs are built at the following parameters values:

^{6}Li: $\kappa = \kappa_0 = 2$; $\delta = 0{,}033$; curve ${}^{(-)}\zeta_0(\xi)$ at $\delta_z = -\delta$, curve ${}^{(+)}\zeta_0(\xi)$ at $\delta_z = +\delta$;

^{7}Li: $\kappa = \kappa_1 = \sqrt{\dfrac{m_1}{m_0}}\kappa_0 = 2{,}16$; $\delta = 0{,}033$; curve ${}^{(-)}\zeta_1(\xi)$ at $\delta_z = -\delta$, curve ${}^{(+)}\zeta_1(\xi)$ at $\delta_z = +\delta$;

^{235}U: $\kappa = \kappa_0 = 2$; $\delta = 9{,}03 \cdot 10^{-4}$; curve ${}^{(-)}\zeta_0(\xi)$ at $\delta_z = -\delta$, curve ${}^{(+)}\zeta_0(\xi)$ at $\delta_z = +\delta$;

^{238}U: $\kappa = \kappa_1 = \sqrt{\dfrac{m_1}{m_0}}\kappa_0 = 2{,}01277$; $\delta = 9{,}03 \cdot 10^{-4}$; curve ${}^{(-)}\zeta_1(\xi)$ at $\delta_z = -\delta$, curve ${}^{(+)}\zeta_1(\xi)$ at $\delta_z = +\delta$.

From a Fig. 1 we find that maximal transversal distance between the beams of separated lithium isotopes is $\Delta r_{10} = {}^{(-)}r_1 - {}^{(+)}r_0 = 2a = 6$ cm, longitudinal size of chamber $\Delta z = 90a = 270$ cm, chamber radius $R_{II} = 70a = 210$ cm. As it is obvious from a Fig. 2 approximately the same dimensions turn out at the uranium isotopes separation (only the distance between beams is half). Comparison with the proper dimensions in M_N leads to an essential difference in the setup transversal dimensions: in M_O a setup radius must be about 2 m, and in M_N ~20 cm. This is one of essential advantages of M_N. Moreover, M_N setup can be used for the decision of other physical problems (mass-spectrometer creation, electromagnetic traps etc.).

One notices that in M_O maximum distance between separated isotopes at its motion in radial direction is approximately equal to the difference of its turning points coordinates, each of which depends on the value of its own κ and is determined by formula (1)

$$ {}^{(+)}r = a\,\mathrm{e}^{2\kappa(1+\delta_z)}.$$

By this formula the minimum transversal setup radius, decreasing with κ decrease, is determined. However maximum transversal distance Δr_{10} between separated beams decreases with κ_1 and κ_0 decrease that reduces separation efficiency. As is obvious from expression for κ, it can be decreased either due to J growth, and it is difficult at the already large values of J (in a fig. 1 and 2 $J = 5$ kA) or due to isotopes initial velocity decreasing, that is not desirable

(in opinion of experimenters; in the fig. 1 $v_{01} \sim 4 \cdot 10^6$ cm/s, in the fig. 2 $v_{01} \sim 1{,}5 \cdot 10^6$ cm/s). Thus, M_N is much better than M_O!

Now about remarks on work [3] which describes the isotopes separation on M_O. Authors of this work did not give expression for the ion trajectory, limited with the remark that this problem «analytically cannot be solved and the ion trajectory can be found only by numerical calculations». But this assertion is refuted with the above mentioned expression (1) with the use of which the isotopes trajectories, presented on a fig. 1 and 2, are right built. For description of isotopes separation the authors of work [3] used equation (2) from this work as basic, which in the previous paragraph of that article is written in physically more transparent form

$$v_z = v_{z0} - u \ln \frac{r}{r_0} = u \left(\frac{v_{z0}}{u} - \ln \frac{r}{r_0} \right),$$

or, passing to our notations, one obtains

$$\frac{d\zeta}{dt} = \frac{v_{0z}}{\kappa a} \left(\kappa - \ln \frac{r}{a} \right), \quad \kappa = \frac{v_{0z}}{u} = \frac{mc^2 v_{0z}}{2Jq}.$$

It's easy to see that this equation determines the isotope turning point transversal coordinate at its motion along an axis z (without taking in account δ_z), namely $\xi_z \equiv \frac{r_z}{a} = \mathrm{e}^{\kappa}$, i.e. $v_z > 0$ at $\xi < \xi_z$, $v_z = 0$ at $\xi = \xi_z$ and $v_z < 0$ at $\xi > \xi_z$. Because, according to our calculations, isotope turning point transversal coordinate at its motion in the line of r growth equal to $\xi_2 = \mathrm{e}^{2\kappa}$ is greater than ξ_z then an isotope will not perform radial oscillations (see fig. 1 and 2), as authors of work [3] assert. As it is obvious from a fig. 1 and 2, isotopes separation near a coordinate ξ_z is insignificantly in comparison with a separation near a coordinate ξ_2, therefore separation theory M_O near a coordinate ξ_z, offered by the authors of work [3], does not have practical application. One can notice that work [3], as well as our work [1], is published in ZTF, however there are no references on our works there [3].

CONCLUSIONS

Definite advantage of new method of isotopes separation in the magnetic field of constant linear current flowing along the axis of cylindrical capacitor – separation chamber and the electrostatic field of the same cylindrical capacitor in comparison with the isotopes separation method in the same setup in the absence of the electrostatic field, whereupon the second (old) method is found practically inapplicable. Moreover, errors done in the process of construction and validation of the second (old) method of isotopes separation are found.

REFERENCES

1. Kirochkin Yu.A., Kirochkin A.Yu. Theoretical investigation of the possibility of isotope separation during motion of charged particles in the electromagnetic field of a cylindrical capacitor and a linear current flowing along its axis // Technical Physics. – 2007. - Vol. 52, №10. - P. 1336–1344. (Original Russian text published in Zhurnal Tekhnicheskoi Fiziki. – 2007. - Vol. 77, № 10. – P. 89–96).
2. Kirochkin Yu.A., Kirochkin A.Yu. Dvizhenie relyativistskikh zaryadov v postoyannom elektromagnitnom pole tsilindricheskogo kondensatora i lineynogo toka, tekushchego vdol' ego osi // The Journal of Kharkiv National University, physical series "Nuclei, Particles, Fields". – 2007. – № 784. – Vyp. 4/36/. – S. 113-116.
3. Bardakov V.M., Kichigin G.N., Strokin N.A., Tsaregorodtsev E.O. Plazmoopticheskaya mass-separatsiya izotopov v magnitnom pole lineynogo toka // Zhurnal tekhnicheskoy fiziki. – 2010. – T. 80. – Vyp. 10. – S. 115-119.



Kirochkin Yuri Alexeyevich, associate professor of the department of theoretical nuclear physics and mathematics of Karazin KNU
Research interests are in electrodynamics



Kirochkin Alexei Yuriyevich, scientific researcher of research laboratory of emergency monitoring of NCDUU
Research interests are in emergency monitoring, electrodynamics

UDC 004.7:519.2

HIGH-SPEED COMMUNICATION NETWORKS CHAOTIC BEHAVIOR ANALYSIS OF DATA SYSTEMS

A.V. Karpukhin, I.N. Kudryavtsev, A.V. Borisov, D.I. Gritsiv
V.N. Karazin Kharkiv National University
Svobody Sq. 4, 61022, Kharkiv. Ukraine
E-mail: kav-102@yandex.ru, arkaim77@mail.ru, dgritsiv@gmail.com
Received 7 June 2012, accepted 4 September 2012

Chaos and self-similarity are the state-of-the-art problems in various areas of modern science and technology, thus network systems are not exception from this rule. Increasing number of various network protocols, applications and services leads to the fact that network traffic becomes more complex and unpredictable. It has been shown that phenomenon of self-similarity is caused by the properties of network traffic whose origin is the behavior of TCP protocol. And all this properties became more significant with appearing of the high-speed data transmission technologies. Finally this behavior leads to congestion in network and packet losses as the result of it. But even modern congestion control mechanisms handle such kind of situations quite unfair. For example, as shown by W. Feng et al., TCP Reno loss rate exceeds 5% in a heavily congested network. So it's easy to calculate that over a Gigabit Ethernet link such loss rate translates into a loss of over 50 Mb/s. Obviously this level of loss rate is unacceptable. However models that describe behavior of information systems sufficiently and give a possibility for scientists to apply all set of classical methods of chaos theory and analyze particular nonlinear dynamical system have not been offered so far. Phase portraits of the studied system were built and Lyapunov exponents for different values of the basic system parameters were calculated. In the present paper a new approach in analysis of the packet switching networks behavior with TCP protocol is proposed. These networks are analyzed as nonlinear dynamical systems that show chaotic properties at a certain value of parameters.
KEY WORDS: self-similarity, network traffic, chaos, packet loss, quality of service, TCP/IP.

ИЗУЧЕНИЕ ХАОТИЧЕСКОГО ПОВЕДЕНИЯ ВЫСОКОСКОРОСТНЫХ СЕТЕЙ СВЯЗИ ИФОРМАЦИОННЫХ СИСТЕМ

А.В. Карпухин, И.Н. Кудрявцев, А.В. Борисов, Д.И. Грицив
Харьковский национальный университет имени В.Н. Каразина
пл. Свободы 4, 61022, Харьков, Украина

Проблема самоподобия в различных областях науки и техники интересовала исследователей давно. Появление и широкое распространение компьютерных сетей, а также увеличение количества разнообразных сетевых услуг привело к тому, что сетевой трафик стал более сложным и непредсказуемым. Особенно сильно эти свойства стали проявляться с появлением технологий высокоскоростной передачи данных. Это связано с тем, что одним из основных показателей качества (QoS) работы сетей с пакетной передачей является количество потерянных пакетов. Потеря пакетов приводит к дополнительной нагрузке на сеть и, в конечном счете, к «заторам». При больших скоростях передачи данных потери пакетов, выражающиеся в долях процента, приводят к значительным потерям информации. В многочисленных работах, посвященных исследованию сетевого трафика, было показано, что указанные выше явления связаны со свойствами самоподобия трафика, основной причиной которого является поведение протокола TCP. Однако до сих пор не были предложены модели, адекватно описывающие поведение систем связи информационных систем, позволяющие применить весь арсенал классических методов анализа нелинейных динамических систем. В работе предлагается новый подход к анализу поведения сетей связи информационных систем с протоколом TCP – рассмотрение их как нелинейных динамических систем, проявляющих хаотические свойства при определенных значениях параметров. Построены фазовые портреты исследуемой системы, рассчитаны показатели Ляпунова для различных значений основных параметров системы. Предложены рекомендации по проектированию и эксплуатации высокоскоростных оптических сетей связи информационных систем.
КЛЮЧЕВЫЕ СЛОВА: самоподобие, сетевой трафик, хаос, потери пакетов, качество обслуживания, TCP/IP.

ВИВЧЕННЯ ХАОТИЧНОЇ ПОВЕДІНКИ ВИСОКОШВИДКІСНИХ МЕРЕЖ ЗВ'ЯЗКУ ІНФОРМАЦІЙНИХ СИСТЕМ

О.В. Карпухін, І.М. Кудрявцев, О.В. Борисов, Д.І. Гриців
Харківський національний університет імені В.Н. Каразіна
м. Свободи 4, 61022 Харків, Україна

Проблема самоподоби в різних областях науки та техніки цікавила дослідників давно. Поява та широке розповсюдження комп'ютерних мереж, а також зріст кількості різноманітних послуг привело до того, що мережевий трафік став більш складним і непередбачуваним. Особливо сильно ці властивості стали проявлятися з появою технологій високошвидкісної передачі даних. Це пов'язано з тим, що одним із основних показників якості (QoS) роботи мережі з пакетною передачею даних є кількість втрачених пакетів. Втрата пакетів призводить до додаткового навантаження на мережу і зрештою до «заторів». При великих швидкостях передачі даних втрата пакетів, що виражається в долях відсотка сприяє значним стратам інформації. В багаточисленних роботах, присвячених дослідженню мереженого трафіка було показано, що вказані вище явища пов'язані з властивостями самоподібного трафіка, основною причиною якого є поведінка протоколу TCP. Проте до сіх пір не були запропоновані моделі, які б адекватно описували поведінку систем зв'язку інформаційних систем, що дозволили б застосувати весь арсенал класичних методів аналізу нелінійних динамічних систем. В роботі пропонується новий підхід щодо аналізу поведінки мереж зв'яку інформаційних систем з протоколом TCP – розгляд їх як нелінійних

© Karpukhin A.V., Kudryavtsev I.N., Borisov A.V., Gritsiv D.I., 2012

динамічних систем, що проявляють хаотичні властивості за наявності визначених значень параметрів. Побудовані фазові портрети досліджуваної системи, розраховані показники Ляпунова для різних значень основних параметрів системи. Запропоновані рекомендації щодо проектування та експлуатації високошвидкісних оптичних мереж зв'язку інформаційних систем.
КЛЮЧОВІ СЛОВА: самоподоба, мережений трафік, хаос, втрата пакетів, якість обслуговування, TCP/IP.

For a long time the problem of self-similarity was interesting for researchers in different fields of science and engineering (hydrology, geophysics, biophysics, biology, financial economics) (an extensive enough bibliography is contained in [1]). Network traffic has become more complex and unpredictable because of appearance and wide propagation of computer networks and growth of different network services. Especially with appearance of high-speed data transmission technologies these qualities have shown up themselves strongly. It is connected with one of the major network work characteristics (QoS) with packet transmission is a number of lost packets. The loss of packets leads to additional load on any network and congestions in the final analysis. The high-speed data transmission loss of packets expressed in percentage leads to considerable loss of data. And even the bandwidth increasing of network affects on the improvement of its work poorly.

For the first time applying the conception of self-similarity for telecommunication systems was proposed by B. Malderbrot [2].

In the following numerous studies dedicated to the network traffic research has been shown all the above mentioned phenomena are connected with self-similarity traffic properties.

For the last 10-15 years a great amount of studies has been dedicated to the self-similarity network traffic problem. They can be divided into two large groups symbolically. The first group and the most extensive one includes the studies which the authors analyze the network traffic and define its statistic characteristics. The data analyzing source is either a full-scale experiment (for instance [3]) or modeling by means of application software (for instance ns [4], OPNET [5]).

To the second group related the studies (unfortunately they are not numerous) in which the data system is considered to be the dynamic one where self-similarity is an inner property of the system itself [6].

The goal of the given article is to consider the data communication networks with TCP protocol as non-linear dynamic systems which show some chaotic properties under certain parameter values and a new approach to behavior analysis of such systems is proposed.

THE CAUSES OF THE NETWORK TRAFFIC SELF-SIMILARITY

Most researchers believe that TCP is the main reason of traffic self-similarity (the basic transport Internet protocol). To understand the influence of TCP protocol on the network traffic self-similarity is to describe the TCP operation algorithm in general terms [7,8,9].

TCP is a service directed to the connection which ensures reliable (in accurate sequence) delivery of byte flow. Releasing applications from necessity "to worry" about missed or reordered data. It includes the control mechanism which ensures that a sender doesn't overfill the recipient buffer and the congestion control mechanism tries to prevent the oversized data volume injection in network (which leads to the loss of packets). While the window size of the data flow control is static, the congestion window size is changing during long time in compliance with the network status. There are several modifications of the TCP protocol implementation (Reno, Vegas, Tahoe). Obviously, the most widespread is TCP Reno [10].

The TCP Reno congestion control mechanism is composed of two phases: (1) slow start and (2) congestion avoidance. At the slow start phase the congestion window size increases exponentially (i.e. it doubles every time when the sender transmits the amount of bytes successfully which is equal to the current congestion window size in network) until doesn't emerge the timeout which means the loss of packets. At that moment the Threshold value is set in an amount of a half the window. TCP Reno restarts the congestion window size to one packet and returns at the slow start phase increasing the congestion window exponentially to the value of Threshold. When threshold reached TCP Reno enters the avoidance congestion phase in which the congestion window is increased by one packet each time as the sender transmits content of window successfully in network. When a packet is lost during the avoidance congestion phase TCP Reno attempts the same actions as when a packet is lost during slow start phase.

Here and now TCP Reno implements fast retransmit as well and it carries out the fast recovery mechanism for both the congestion avoidance phase and the slow start phase. If the sender receives three double ACK (an indication that some packet had been lost but subsequent packets were received) then the sender will retransmit a lost packet immediately (fast retransmit) instead of carrying out a timeout situation waiting acknowledgement (ACK) of the lost packet. Since subsequent packets were received the network congestion is considered to be less serious than if all packets were lost. And the sender just decreases its congestion window by half and returns at the avoidance congestion phase repeatedly evading the slow start phase again.

TCP Vegas introduces the new congestion control mechanism which tries to prevent them and it doesn't react to appeared congestions. When the congestion window size increases then expected transmission rate (ER) increases as well. But if actual transmission rate (AR) remains the same it will mean that the available bandwidth is poor to provide transmission rate ER. Hence any extension of the congestion window size will result in overfilling the router buffer in the bottleneck gateway. TCP Vegas tries to detect this phenomenon and avoid congestion in the router bottleneck

gateway adjusting the congestion window size and consequently ER adapting for the available bandwidth. TCP Vegas defines two threshold values α and β for the congestion avoidance phase to regulate the congestion window in a proper way. The third threshold value γ is defined for crossing between the congestion avoidance phase and the slow start phase. Conceptually, $\alpha = 1$ means that TCP Vegas tries to keep at least one packet from each flow located in a queue of the router while $\beta = 3$ keeps three packets maximum. In consideration of Diff = ER – AR Vegas increases the congestion window linearly during the next RTT (Round Trip Time) if Diff $< \alpha$. When Diff $> \beta$ then Vegas decreases the congestion window linearly during the next RTT otherwise the congestion window stays invariable. The parameter γ can be considered as "initial" value when TCP Vegas enters its congestion avoidance phase. To improve more TCP characteristics Floyd and the others proposed to use RED routers (Random Early Detection) [12] to detect incipient congestion. The RED routers support weighed mean lengths of a queue. While the weighed mean length of a queue stays below minimum threshold ($\min th$), all packets remain in a queue. When the weighed mean length of a queue exceeds ($\min th$) packets will be skipped (lost) with probability P. And when the weighed mean length of a queue exceeds maximum threshold ($\max th$), still arriving packets will be lost.

In recent years several new modifications of TCP protocol have been proposed. There are Binary Increase Control TCP (BIC-TCP), CUBIC TCP, Westwood TCP (TCPW), Parallel TCP Reno (P-TCP), Scalable TCP (S-TCP), Fast TCP, HighSpeed TCP(HS-TCP), HighSpeed TCP Low Priority (HSTCP-LP), Hamilton TCP (H-TCP), Yet Another Highspeed TCP(YeAH-TCP), Africa TCP, Compound TCP etc.

Almost all of them are based on well-known old TCP versions and they differ from each other various congestion avoidance means. To be more precise they are based on different ways of detecting the packets loss occurrence fact which means appearance of congestion. Various formulas for cwnd (congestion window) calculation are used in different modifications.

ESSENCE AND RELEVANCE OF THE PROBLEM

To study congestions arising in computer networks and avoidance methods is the very topical question at modern stage of the computer network development. New technologies such as GRID and distributed calculations are appearing and they transmit quite great amount of data via network. Videoconferences and applications for transferring voice represent more and more tough quality of service (QoS) requirements. The Internet network is developing and at the same time an amount of users is increasing as well. Hence growth of the transfer traffic capacity which compounds about 7500-1200 PBytes per month at the end of 2009. All these factors are precondition for appearing congestions in computer networks.

Well studied and tested methods of the theory of chances are suitable for describing and preventing network congestions. Also the Internet architecture of protocols places certain limitations. For example competitive TCP flows and all plurality of transport protocols used in computer networks don't know anything about each other but various models of the congestion control in TCP and other protocols should coexist in harmony. If one of implementations turns out to be more aggressive than the others then it will use a major part of the bandwidth which can prevent from the data transmission in "adjacent" connections. At the same time unnecessary conservatism of an algorithm will have a negative impact on the general protocol performance.

THE TEST BED

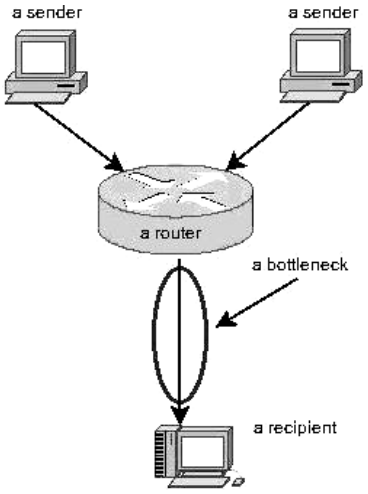


Fig. 1. The model network topology

It has been used the discretely temporal simulator with source code NS-3 (Network Simulator 3) in the present work for investigating TCP flows. NS-3 gives a researcher the class set which can be used and modified. Thus it is possible to simulate the wide range of protocols and processes occurring in computer networks. Also the simulator makes possible to model processes in real time and integrate it with the test bed making this a part of modeling network etc. The NS-3 simulator includes the great amount of tests for all components which guarantees veracity obtained results. The model of TCP/IP network has been created by means of the given simulator where all hosts connected with a router by the point-to-point connection type (Fig. 1). The work of the application has been simulated in sender hosts sending data with permanent bitrate to the host recipient where the application worked and received data from the both type of hosts. The data generation rate of senders (C_f), the delay (d_b) and the bandwidth of pipes in the bottleneck and also the delay and the bandwidth of pipes in host senders were varied specifying particular parameters for each numerical experiment. The type Drop Tail Queue (Q_s) queue size also was varied in the router network interface connected with the recipient.

The receiving host window (rwnd) was made very large deliberately to make limiting factor the only value of the congestion window (cwnd).

Obviously in such network the congestion state will be occurred when total rate sending data from the sender host

exceeds the bandwidth of the recipient channel. Therewith the key parameters affecting on congestion appearance are C_f, d_b, C_b, and Q_s because sender hosts have sufficient bandwidth and low delay and it won't affect on the congestion control algorithm by TCP protocol. There will be shown the values only these parameters in the further description of numerical experiments.

THE BEHAVIOR STUDYING METHODOLOGY OF TCP PROTOCOL

The variables number characterizing state of the given system is very large even in such simple system with two TCP connections. But it can be chosen a suitable section of the phase space by force of proper selection these variables. The magnitude of congestion window has been chosen because it affects on the data transmission rate directly.

It was tracking an alteration of each TCP flow cwnd values from the sender to the recipient during the work simulation process of two TCP-connections. A new value and a time moment were recorded into the file for each cnwd value variation when this alteration happened. Finally two time sequences specifying the step-type function which contains cwnd dependence of time have been obtained for two hosts (as cwnd value is stored in memory all the time and it changes at fixed time moments).

But there is not enough cwnd dependence of time for studying given process in details. The problem lies in the fact that the congestion window value is just a projection of the full set of system variables. Therewith the cwnd(t) function is not continuous. The second problem is that the congestion window value doesn't make possible to draw a conclusion about system status in details starting from the certain time moment.

In this work it has been proposed to use averaging over N values of the time sequence $\left[x_t, x_{t-\sigma\cdot t}, x_{t-2\sigma\cdot t}, \ldots\right]$ as easy measured characteristic of complex systems and showed that it can be used for recovery of the hidden multidimentional trajectories. The given method applied to the congestion window values (cwnd) leads to the relations [6]:

$$x[i] = \frac{1}{N}\sum_{j=1}^{N} cwnd_x[i-j], \qquad (1)$$

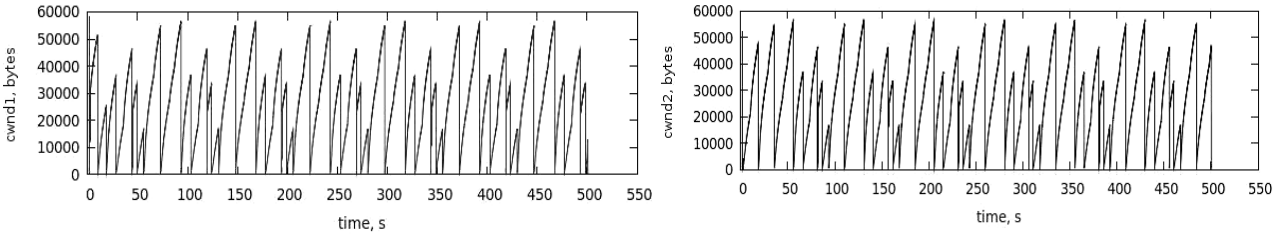
$$y[i] = \frac{1}{N}\sum_{j=1}^{N} cwnd_y[i-j].$$

Two TCP flows are indicated as x and y here. The N quantity is responsible for a scale of averaging and the more N the more hidden dimensions of the system can be recovered.

In this case cwnd(t) functions are different for hosts and only moments of changing values this function are fixed. Therefore to apply mentioned above method and to plot a phase portrait means to get the congestion window values at the same moments of time.

THE PHASE PORTRAIT

Such system seems to be easy enough and it shows quite difficult behaviour under certain parameters of the test bed. Specifically the graphics of cwnd(t) dependence if C_f =5Mbps, d_b=10ms, C_b=5Mbps, Q_s=20 packets[1] and more hard mode under Q_s=2 packets are mentioned below. Regular beating can be noticed in the both plots. And each TCP flow takes an advantage one over another by turns at the particular time intervals.

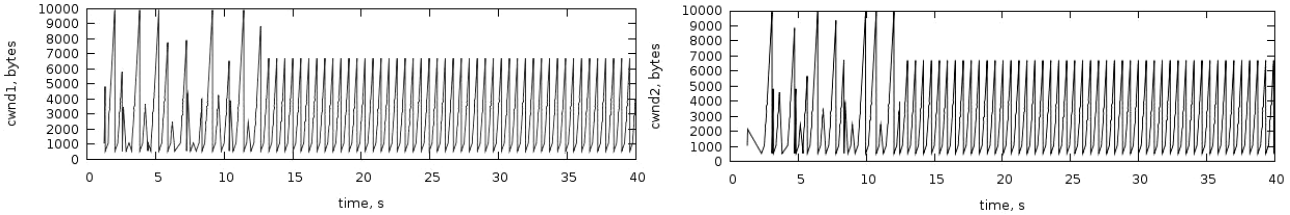


a) b)

Fig. 2. The congestion window dependence of time
a) the first TCP-flow under C_f =5Mbps, d_b=10ms, C_b=5Mbps, Q_s=20,
b) the second TCP-flow under C_f =5Mbps, d_b=10ms, C_b=5Mbps, Q_s=20

According to described algorithm in the previous section the associating phase portraits are obtained by data processing and displayed respectively in the Fig. 2-3. In case of N=2000 and d_t=10 ms the phase portraits are shown in the Fig. 4-5.

[1] 1 packet = 536 bytes, in all conducted numerical experiments



a) b)

Fig. 3. The congestion window dependence of time
a) the first TCP-flow under C_f =5Mbps, d_b=10ms, C_b=5Mbps, Q_s=2
b) the second TCP-flow under C_f =5Mbps, d_b=10ms, C_b=5Mbps, Q_s=2

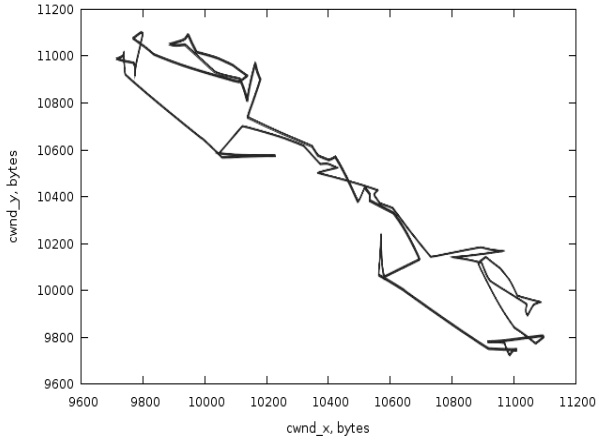


Fig. 4. The phase portrait
under C_f =5Mbps, d_b=10ms, C_b=5Mbps, Q_s=20
(the regime initialization transient process was removed)

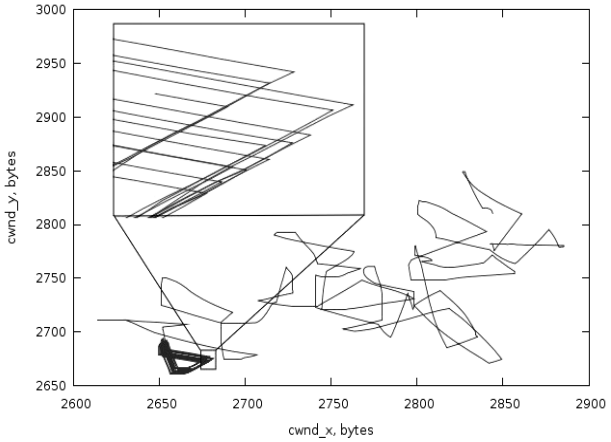


Fig. 5. The phase portrait
under C_f =5Mbps, d_b=10ms, C_b=5Mbps, Q_s=2
The cycle section was scaled up to make possible to see its complex structure.

As can be seen the phase trajectories shape the limit cycle which has a quite delicate structure. And this trajectory is pretty steady because an image point after little "roaming" begins to describe the same closed trajectory in process of TCP flows start time changing relatively one another. For comparison data and the phase portrait are stated below when senders don't overfill the recipient pipe. In other words there is no congestion (Fig. 6 and Fig. 7). In this case the cwnd value of both hosts increases indefinitely as expected and there is no any anomalies in the phase portrait.

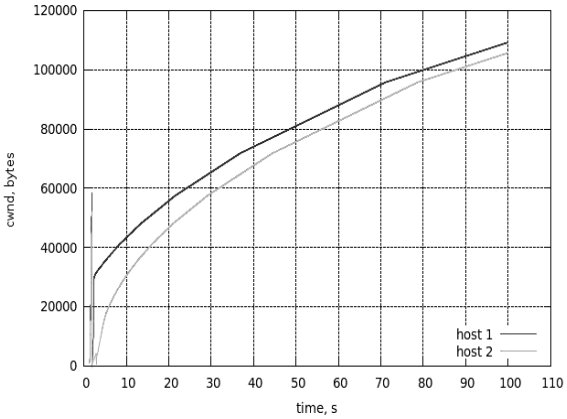


Fig. 6. The congestion window dependence of time
under C_f =2Mbps, d_b=10ms, C_b=5Mbps, Q_s=100 (there is no congestion)

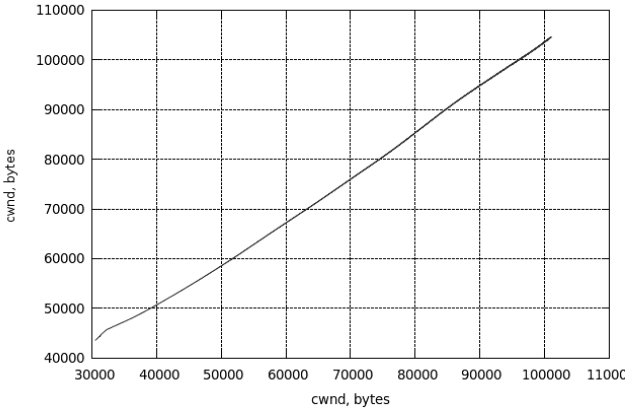


Fig. 7. The phase portrait
under C_f =2Mbps, d_b=10ms, C_b=5Mbps, Q_s=100

THE MAXIMUM LYAPUNOV EXPONENT

Phase portraits are useful not only to show the dynamic system status. If you have a phase portrait you will be able to calculate a maximum Lyapunov [2] exponent λ. It's the quantity which is able to characterize the recession rate of close trajectories and usually its positive value is considered to be an indicator of the system chaotic behaviour.

However to graph the system phase portrait is possible only in a few cases. When one adds a new sender into the

[2] For example using Benettin's algorithm [15]

simulated network then the analyzed phase space dimensionality will increase by one and to analyze obtained data will be more complicated. Apart from the phase space visualization is possible if its dimensionality is fewer than 4.

Thus it is necessary to have the instrument which allows obtained data to be tested aside from a number of available TCP sessions. For this purpose the utility package TISEAN has been chosen [16]. It is intended for analysis of time series and based on the theory of nonlinear deterministic dynamic systems or the chaos theory. TISEAN is represented to be an implementation of the theory chaos algorithms. However these algorithms don't give "simple" answers to questions taking into account the research field newness where hasty utilization of algorithms can bring to incorrect, unclear or false results. Therefore for instance asking the question about attractor dimensionality it can't be given the finite numerical answer. Instead of this it will be computed the correlated sum which can be analyzed by other utility package. A researcher is responsible for correct interpretation of work results.

The utility lyap_k from TISEAN package has been used for calculating the maximum Lyapunov exponent. The result of its work is the data set which represents the logarithm coefficient of trajectories recession dependence of time $S(\varepsilon, m, \Delta n)$ [17], it is computed in the following way:

$$S(\varepsilon, m, \Delta n) = \frac{1}{N}\sum_{n_0=1}^{N} \ln\left(\frac{1}{\left|U(s_{n_0})\right|}\times \sum_{S_n \subset U(s_{n_0})} \left(s_{n_0+\Delta n} - s_{n+\Delta n}\right(\right), \tag{2}$$

where ε is neighbourhood of S_{n_0} point, m is dimensionality of the phase space, Δn is time, and $U\left(S_{n_0}\right)$ – neighbourhood of the point S_{n_0} with diameter ε.

In the given algorithm the point S_{n_0} is chosen in the phase space and its "neighbours" remote from S_{n_0} within ε distance are marked. Then average distance to all the "neighbours" is calculated as a function of passed Δn time. Thus at the time moment $n_0 + \Delta n$ (plus a logarithm of the initial state) a logarithm of average distance is some effective rapidity of trajectories recession during Δn time. All fluctuations have been averaged out under repetition described steps for quite large amount n_0 values. If $S(\varepsilon, m, \Delta n)$ quantity shows linear increase with the same slope in the reasonable range of ε values then slope ratio approximating this part of the line can be considered to be roughly equal to the maximum Lyapunov exponent.

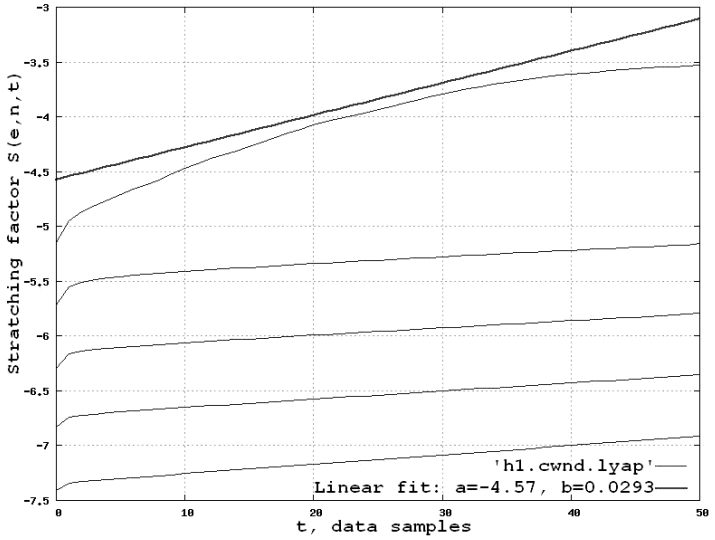


Fig. 8. The Lyapunov exponent calculation
(Q_s=20: λ ~ 0.029)

The results obtained after processing and visualization cwnd(t) time series are represented here and they have been brought into accordance with Fig. 4,5 and 7 (take a look at Fig. 8 − 10) with the aid of lyap_k utility. The curves $S(\varepsilon, m, \Delta n)$ for five different ε values and the line $y = a + bx$ approximating linear section of these curves are pictured in the figures. Thus b value equals to the maximum Lyapunov exponent numerically.

The data obtained in process of the network work simulation in the absence of congestion have been analyzed. In this case as expected if λ < 0 such system doesn't show chaotic behaviour proceeding from experiment definition as can be seen in the graph.

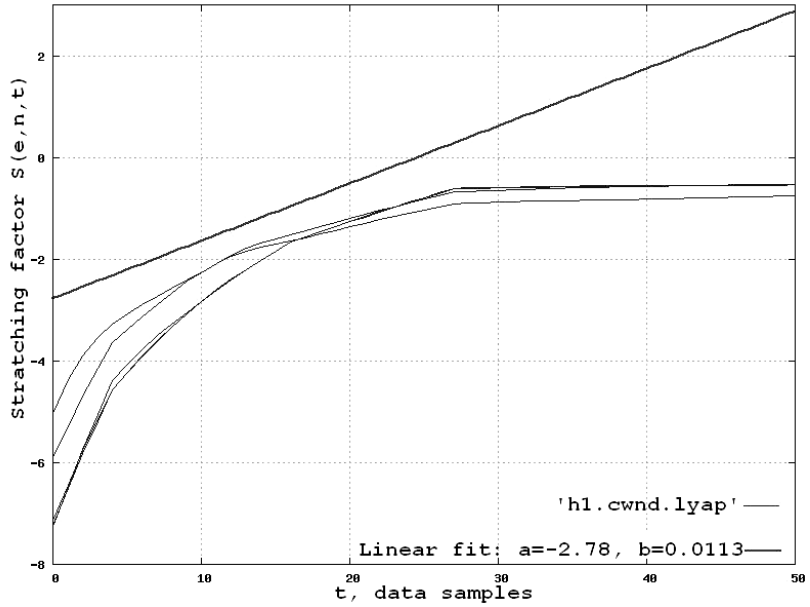


Fig. 9. The Lyapunov exponent calculation
(Q_s=2: $\lambda \sim 0.113$)

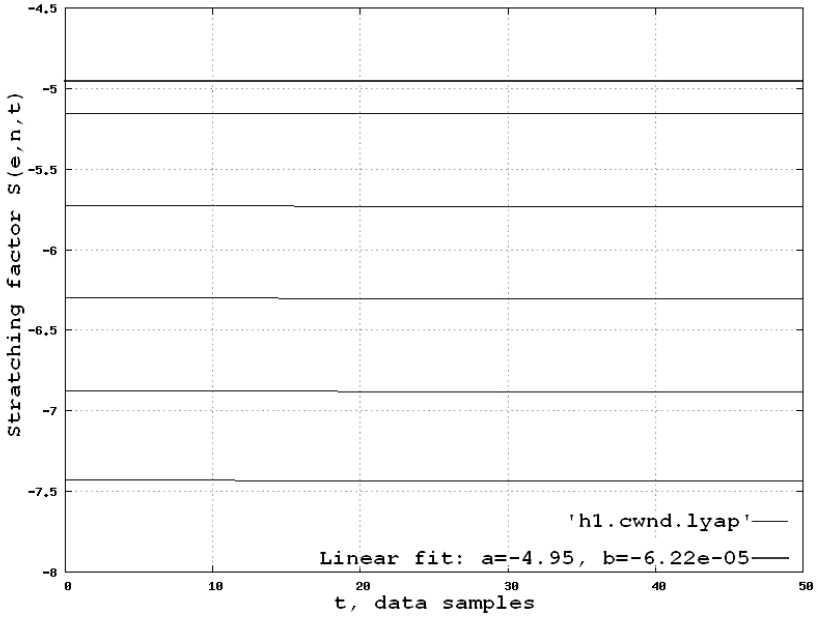


Fig. 10. The Lyapunov exponent calculation
C_f =2Mbps, d_b=10ms, C_b=5Mbps, Q_s=100:
$\lambda \sim$ -0.00006 means absence of chaos

THE CONCLUSIONS AND FURTHER RESEARCH DIRECTIONS

The carried out research makes possible to conclude that the router buffer size is one of the key parameters influencing on TCP protocol work.

According to our reckoning the further way consists of describing communication networks of data systems using the TCP protocol as nonlinear dynamic systems. In this case there is a possibility to apply all the classical methods set of behavior analysis such systems developed by Poincare, Lyapunov, Birkhoff. It concerns with qualitative analysis of the dynamic system behavior in the phase space which gives an opportunity to define all possible system motion (work) modes and to detect parameter values that cause undesirable chaotic phenomena (the loss of packets, performance decreasing) In the first place these questions are topical for the ISP (Internet providers) who unfortunately don't pay proper attention to them. Obviously to solve the problem of congestions and the loss of packets is not possible on a global scale the whole of Internet network in connection with inability to redesign the whole network in virtue of technical and economical reasons.

However it is possible to give some recommendations to design (and further exploitation) for the limited in scale networks (even large enough) that allows negative phenomena of chaotization to be minimized.

REFERENCES

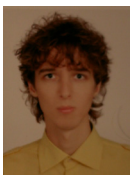
1. Willinger W., Taqqu M.S., Erramilli A. A bibliographical guide to self-similar traffic and performance modeling for modern high-speed networks // Stochastic Networks: Theory and Applications, Royal Statistical Society Lecture Notes Series. – 1996. – Vol. 4. – P. 339 - 366.
2. Mandelbrot B.B. Self-similar error clusters in communications systems and the concept of conditional systems and the concept of conditional stationarity // IEEE Transactions on Communications Technology. – 1965. – Vol. 13, issue 1. – P. 71 - 90.
3. Leland W.E., Taqqu M.S., Willinger W., and Wilson D.V. On the self-similarnature of ethernet traffic // IEEE/ACM Transactions of Networking. – 1994. – Vol. 2, issue 1. – P.1 - 15.
4. Floys F., Simulator tests [Online resource]. – 1995. – Access mode: ftp://ftp.ee.lbl.gov/papers/simtests.ps.Z, NS is available at http://www-nrg.ee.lbl.gov/.
5. Zhu C., Yang O.W.W., Aweya J., Oullete M., Montuno D.Y. A comparison of active queue management algorithms using the OPNET Modeler // IEEE Communication Magazine. – 2002. – Vol. 40, issue 6. – P. 158 - 167.
6. Veres A, Boda V. The chaotic nature of TCP congestion control // In Proc. IEEEINFOCOM. – 2000. – P. 1715 - 1723.
7. Feng W., Tinnakornsrisuphap P. The failure of TCP in High-Performance Computational Grids // In Proceedings of International Conference on Parallel Processing (ICPP'00). – 2000. – Article №. 37.
8. Feng W., Tinnakornsrisuphap P. The Adverse Impact of the TCP Congestion-Control Mechanism in Distributed Systems // In Proceedings ICPP'00 of International Conference on Parallel Processing. –2000. – P. 299 - 306.
9. Nagle J. RFC896-Congestion control in IP/TCP internetworks. – 1984.
10. Jacobson V. Congestion Avoidance and Control // In Proceedings of the SIGCOMM'88 Symposium. – 1988. – Vol. 18, issue 4. – P. 314 - 332.
11. Brakmo L., Peterson L. TCPVegas: End to End Congestion Avoidance on a Global Internet // IEEE Journal of Selected Areas in Communications. – 1995. – Vol. 13, issue 8. – P. 1465 - 1480.
12. Floyd S. and Jacobson V. Random Early Detection Gateways for Congestion Avoidance // IEEE/ACM Transactions on Networking. – 1993. – Vol. 1, issue 4. – P. 397 - 413.
13. Simulator NS-3 and concomitant documentation [Online resource]. – Access mode: http://nsnam.org.
14. Packard N.H., Crutchfield J.P., Farmer J.D. and Shaw R.S. Geometry from a Time Series // Physical Review Letters. – 1980. – Vol. 45. – P. 712 - 716.
15. Benettin G., Galgani L., Giorgilli A., Strelcyn J.M. Lyapunov characteristic exponents for smooth Dynamical systems; a method for computing all of them. Part 1: Theory; Part 2: Numerical application // Meccanica. –1980. – Vol. 15. – P. 9 - 30.
16. Hegger R., Kantz H., Schreiber T. The package of TISEAN programs and concomitant documentation [Online resource]. – Access mode: http://www.mpipks-dresden.mpg.de/~tisean/.
17. Hegger R., Kantz H., Schreiber T. Practical implementation of nonlinear time series methods: The TISEAN package // Chaos. – 1999. – Vol. 9, issue 2. – P. 413 - 435.



Karpukhin Aleksandr Vladimirovich – PhD (Technology), an associate professor of The Chair of Information Technologies in Physical and Power Systems of V.N. Karazin Kharkiv National University.
Scientific interests: studying methodology of non-linear dynamic systems with small-scale nonlinearity and large-scale one.



Kudryavtsev Igor Nikolaevich – PhD (Physics and Mathematics), an associate professor of The Chair of Physics of Alternative Energy Technologies and Ecology of V.N. Karazin Kharkiv National University.
Scientific interests: research of chaotic phenomena for data system networks with TCP protocol.



Borisov Aleksandr Viktorovich – a graduating student of V.N. Karazin Kharkiv National University.
Scientific interests: computer simulation of chaotic phenomena for data system networks with TCP protocol.



Gritsiv Dmitry Igorevich – a postgraduate student of V.N. Karazin Kharkiv National University.
Scientific interests: computer simulation of chaotic phenomena for data system networks with TCP protocol.